CONNECTIONS TO MEMBRANE TRAFFICKING WHERE YOU LEAST EXPECT THEM: DISEASES, DYNAMICS, DIET AND DISTANCE

EDITED BY: Rachel Susan Kraut, Guillaume Thibault, Sarita Hebbar and Elisabeth Knust

PUBLISHED IN: Frontiers in Cell and Developmental Biology and Frontiers in Physiology

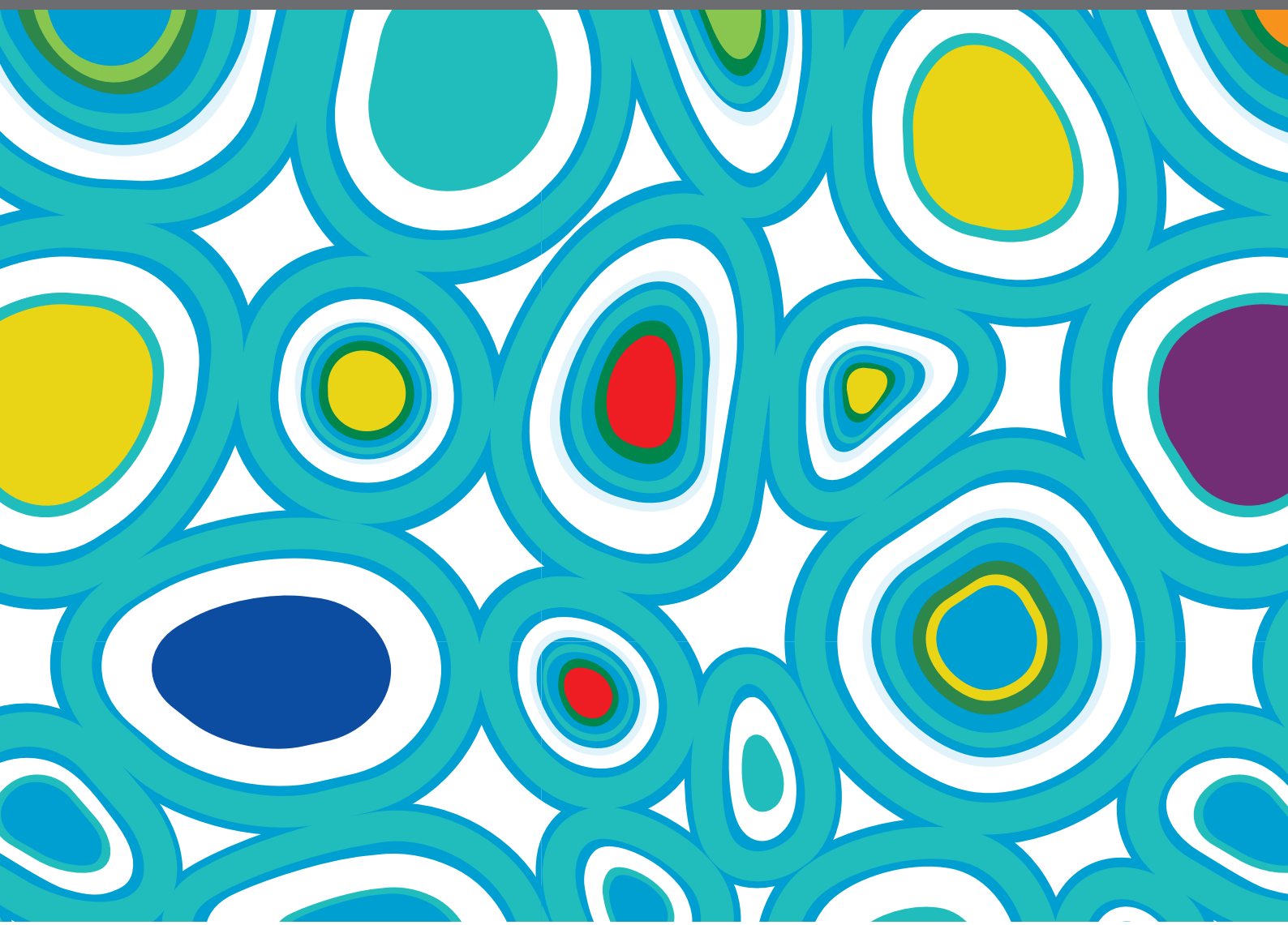

frontiers Research Topics

frontiers

ISSN 1664-8714
ISBN 978-2-88963-429-3
DOI 10.3389/978-2-88963-429-3

About Frontiers

Frontiers is more than just an open-access publisher of scholarly articles: it is a pioneering approach to the world of academia, radically improving the way scholarly research is managed. The grand vision of Frontiers is a world where all people have an equal opportunity to seek, share and generate knowledge. Frontiers provides immediate and permanent online open access to all its publications, but this alone is not enough to realize our grand goals.

Frontiers Journal Series

The Frontiers Journal Series is a multi-tier and interdisciplinary set of open-access, online journals, promising a paradigm shift from the current review, selection and dissemination processes in academic publishing. All Frontiers journals are driven by researchers for researchers; therefore, they constitute a service to the scholarly community. At the same time, the Frontiers Journal Series operates on a revolutionary invention, the tiered publishing system, initially addressing specific communities of scholars, and gradually climbing up to broader public understanding, thus serving the interests of the lay society, too.

Dedication to Quality

Each Frontiers article is a landmark of the highest quality, thanks to genuinely collaborative interactions between authors and review editors, who include some of the world's best academicians. Research must be certified by peers before entering a stream of knowledge that may eventually reach the public - and shape society; therefore, Frontiers only applies the most rigorous and unbiased reviews.
Frontiers revolutionizes research publishing by freely delivering the most outstanding research, evaluated with no bias from both the academic and social point of view. By applying the most advanced information technologies, Frontiers is catapulting scholarly publishing into a new generation.

What are Frontiers Research Topics?

Frontiers Research Topics are very popular trademarks of the Frontiers Journals Series: they are collections of at least ten articles, all centered on a particular subject. With their unique mix of varied contributions from Original Research to Review Articles, Frontiers Research Topics unify the most influential researchers, the latest key findings and historical advances in a hot research area! Find out more on how to host your own Frontiers Research Topic or contribute to one as an author by contacting the Frontiers Editorial Office: researchtopics@frontiersin.org

CONNECTIONS TO MEMBRANE TRAFFICKING WHERE YOU LEAST EXPECT THEM: DISEASES, DYNAMICS, DIET AND DISTANCE

Topic Editors:
Rachel Susan Kraut, Max Planck Institute of Molecular Cell Biology and Genetics (MPI-CBG), Germany
Guillaume Thibault, Nanyang Technological University, Singapore
Sarita Hebbar, Max Planck Institute of Molecular Cell Biology and Genetics (MPI-CBG), Germany
Elisabeth Knust, Max Planck Institute of Molecular Cell Biology and Genetics (MPI-CBG), Germany

Citation: Kraut, R. S., Thibault, G., Hebbar, S., Knust, E., eds. (2020). Connections to Membrane Trafficking Where You Least Expect Them: Diseases, Dynamics, Diet and Distance. Lausanne: Frontiers Media SA. doi: 10.3389/978-2-88963-429-3

Table of Contents

frontiers in Cell and Developmental Biology

EDITORIAL
published: 06 December 2019
doi: 10.3389/fcell.2019.00327

Editorial: Connections to Membrane Trafficking Where You Least Expect Them: Diseases, Dynamics, Diet and Distance

Sarita Hebbar[1], Elisabeth Knust[1], Guillaume Thibault[2,3] and Rachel Susan Kraut[1]**

[1] Max Planck Institute of Molecular Cell Biology and Genetics, Dresden, Germany, [2] Lipid Regulation and Cell Stress Research Group, School of Biological Sciences, Nanyang Technological University, Singapore, Singapore, [3] Institute of Molecular and Cell Biology, A*STAR, Singapore, Singapore

Keywords: vesicles, membrane traffic, lipids, membrane dynamics, disease models

Editorial on the Research Topic

Connections to Membrane Trafficking Where You Least Expect Them: Diseases, Dynamics, Diet and Distance

OPEN ACCESS

Edited and reviewed by:
Vladimir Lupashin, University of Arkansas for Medical Sciences, United States

****Correspondence:***
Guillaume Thibault
thibault@ntu.edu.sg
Rachel Susan Kraut
rkraut1000@googlemail.com

Specialty section:
This article was submitted to Membrane Traffic, a section of the journal Frontiers in Cell and Developmental Biology

Received: *18 October 2019*
Accepted: *26 November 2019*
Published: *06 December 2019*

Citation:
Hebbar S, Knust E, Thibault G and Kraut RS (2019) Editorial: Connections to Membrane Trafficking Where You Least Expect Them: Diseases, Dynamics, Diet and Distance. Front. Cell Dev. Biol. 7:327. doi: 10.3389/fcell.2019.00327

Membranous compartments within cells form not only an aesthetically interesting, dynamical three-dimensional structure—they also present a conundrum: how do these exotic vesicular, tubular, and pancake-like shapes meld into each other and communicate, yet maintain distinct identities and morphologies, in addition to steering the trafficking and precise targeting of their cargoes? How are their shapes, compositions, and positions in the cell controlled—all of which seem to be of prime importance to their functions? Perhaps most mysteriously of all, how does vesicle trafficking impinge upon spatially (and conceptually) distant downstream processes such as morphology and metabolism?

Defects in membrane trafficking can be disastrous for the cell and for the organism. Diseases as diverse as Parkinson's, diabetes, metabolic syndrome, and cancer are known to have at least some causal component, if not a central origin, related to vesicle trafficking and/or lipid metabolic control. An expanding array of possible causes and consequences of faulty trafficking among vesicular compartments is being cataloged, with ever more surprising connections being discovered.

Vesicular organelles were once thought to function as more or less independent entities, but cellular processes demand an interplay between different compartments. One way in which different membrane-bound compartments interact is via physical contact. Although previously underappreciated, now with the help of the newest wave of high-resolution imaging techniques, vesicular organelles have been observed in the act of intimate contact and lipid exchange. Endoplasmic reticulum (ER)-mitochondrial contacts were an early example of such conduits of transport, but now nearly all possible pairings have been witnessed and their purposes described. The review by Joshi and Cohen in this collection comprehensively summarizes the links between two intracellular metabolic hubs: lipid droplets (LD) and peroxisomes. LD and peroxisomes are tethered by interactions between spastin and ABCD1, but this review further elaborates on how these two compartments are also linked by their common origin in the same ER sub-domains.

Interaction of membrane-bound compartments also comes into play in the degradation of toxic, misfolded, or otherwise harmful proteins. For example, autophagy-based degradation is almost entirely dependent on the prerequisite of membrane transfer/contact starting from its biogenesis. Two research papers in this collection investigate the mechanisms underlying the relevance of membrane bound processes in degradation of protein and metabolite build-up (Jacomin et al.; Sim et al.).

Other functions mediated by vesicular membranes are less obvious. For example, one area that will surely break into this realm of research in a big way is the influence of metabolic factors like diet and oxidative stress. Several papers in this issue deal with this topic: Trautenberg et al. also related elements of the diet to potentially protective or degenerative intracellular signaling pathways, the relevant lipid cues derived from stationary *S. cerevisiae* activating Akt/PKB isoforms through the accumulation of PIP_3.

One of the ways in which dietary lipids could affect trafficking is by changing the deformability and bending of membranes. This is a likely scenario, since dietary lipids alter the composition of cellular membranes, after a long journey through the digestive system and metabolism (Clandinin et al., 1983). Differences in physical and biochemical structure in turn affect both vesiculation (Pinot et al., 2014), and susceptibility to ROS-induced peroxidation. In pursuit of understanding the physical effects that could mediate these changes, Tyler et al. examined the effects of cis vs. trans fatty acids on the properties of membranes using X-ray diffraction and membrane fluctuation analysis.

Among the topics in this collection, we encounter innovative methods that are used in different model organisms to approach aspects of ROS- and free-radical mediated damage to neurons. For example, Jacomin et al. apply X-ray synchrotron spectromicroscopy for the first time to study the effects of age and autophagy on iron accumulation in the fly brain. Age, autophagy, and iron are factors associated with degeneration, partly via oxidative stress arising from non-degraded mitochondria or the damage done by the catalysis of free radical reactions. The use of this unconventional approach enabled the authors to flag Fe-S complexes in mitochondria, rather than total levels of Fe in the brain, as a likely culprit. Beaudoin-Chabot et al. whose study similarly dealt with the effects of oxidative stress-inducing conditions showed, by feeding deuterated polyunsaturated fatty acids (dPUFAs) to *C. elegans* worms, that this diet could protect the animals against the deleterious effects of peroxidated lipids, extending the lifespan. The mechanism they propose helps to solve the long-standing problem of why antioxidants are frustratingly ineffective in combating degenerative conditions. In an overview of the involvement of another stress- and degeneration-related phenomenon, ER stress, Chadwick and Lajoie describe its interplay with lipids, autophagy, and aging, touching on many of the factors mentioned above.

Membrane biophysics and dynamics are important determinants of vesicular behavior and have accordingly been a subject of keen interest. Many questions concern the influence of lipid composition, curvature, and specific lipid species on membrane dynamics, and how these either control or are controlled by membrane sub-domains. For instance, lipid mediators are surely involved in the corralling of receptors into an array of specific domains at the plasma membrane surface, which in turn affect endocytic uptake, and thus function. Phenomena like this are described by Busto and Wedlich-Söldner in their review of the domain segregation of nutrient transporters in yeast.

In addition to lateral segregation of different classes of membrane lipids influencing endocytic budding, the sorting of particular signaling species, like phosphatidic acid (PA), to different membrane locales can also regulate intracellular membrane transport and the activities of associated proteins. Thakur et al., provide a cell biological, analytical, and biochemical perspective on PA structure, metabolism, and its segregation into distinct functional pools. Interestingly this segregation is crucial for the signaling functioning of PA with consequences for tissue development, health, and physiology.

There is a vast diversity of lipid species in eukaryotes (Wenk, 2010). How this diversity contributes to specific membrane trafficking routes is unanswered. Corollary to this is the question of how the spatial distribution of the lipid species in the different membrane-bound compartments is achieved, especially (i) within organelles and (ii) when they exchange membranes during transport.

Another recurring theme in the collection is the surprising role of adaptors or accessory proteins in different vesicular systems (see Lurick et al., 2018 for review) in neuronal morphology, e.g., early-to-late endocytic trafficking and autophagy: Harish et al., for example show that dMon1, a Rab7 exchange factor involved in conversion of early to late endosomes in the fly, puts the brakes on dendritic branching of neurons. This was mediated, not as expected, through "passive" interference with lysosomal trafficking, but rather through a Rab11 recycling pathway at the membrane. Sim et al. used live primary neurons, also in the fly, to show that a BEACH domain protein, known previously only as a Rab11-interacting autophagic adaptor, not only actively moves around between early and late autophagic vesicles depending on the stressor (starvation or protein aggregates) but when overexpressed greatly increases the numbers of mature autophagosomes. Coincidentally, like dMon1, the protein was originally identified because of an effect on neuronal branching patterns (Kraut et al., 2001). Here, we repeatedly see trafficking systems regulated by Rab proteins and their adaptors or associates, that also control morphological processes, seemingly far away from the vesicular events themselves. These reports together with the literature open new questions on the role of guanine nucleotide exchange factors (GEFs) in trafficking. What are the different guanine nucleotide exchange factors (GEFs) and GTPase-activating proteins (GAPS) that coordinate different transport routes? How their perturbation affects cargo and the transport routes? Is this specific to cell-types?

The questions abound—as do the methods and model systems used to address these. An exciting sampling of some of these

will be presented in this Research Topic on connections to membrane trafficking.

AUTHOR CONTRIBUTIONS

All authors listed have made a substantial, direct and intellectual contribution to the work, and approved it for publication.

ACKNOWLEDGMENTS

We thank all contributing authors and reviewers for their support to the Research Topic. GT gratefully acknowledges support from Singapore Ministry of Education Academic Research Fund Tier 2 (MOE2018-T 2-1-002).

REFERENCES

Clandinin, M. T., Foot, M., and Robson, L. (1983). Plasma membrane: can its structure and function be modulated by dietary fat? *Comp. Biochem. Physiol. B* 76, 335–339. doi: 10.1016/0305-0491(83)90079-2

Kraut, R., Menon, K., and Zinn, K. (2001). A gain-of-function screen for genes controlling motor axon guidance and synaptogenesis in Drosophila. *Curr. Biol.* 11, 417–430. doi: 10.1016/s0960-9822(01)00124-5

Lurick, A., Kummel, D., and Ungermann, C. (2018). Multisubunit tethers in membrane fusion. *Curr. Biol.* 28, R417–R420. doi: 10.1016/j.cub.2017.12.012

Pinot, M., Vanni, S., Pagnotta, S., Lacas-Gervais, S., Payet, L. A., Ferreira, T., et al. (2014). Lipid cell biology. Polyunsaturated phospholipids facilitate membrane deformation and fission by endocytic proteins. *Science* 345, 693–697. doi: 10.1126/science.1255288

Wenk, M. R. (2010). Lipidomics: new tools and applications. *Cell* 143, 888–895. doi: 10.1016/j.cell.2010.11.033

Conflict of Interest: The authors declare that the research was conducted in the absence of any commercial or financial relationships that could be construed as a potential conflict of interest.

frontiers in Cell and Developmental Biology

MINI REVIEW
published: 21 May 2019
doi: 10.3389/fcell.2019.00084

Endoplasmic Reticulum Stress Coping Mechanisms and Lifespan Regulation in Health and Diseases

*Sarah R. Chadwick and Patrick Lajoie**

Department of Anatomy and Cell Biology, The University of Western Ontario, London, ON, Canada

Multiple factors lead to proteostatic perturbations, often resulting in the aberrant accumulation of toxic misfolded proteins. Cells, from yeast to humans, can respond to sudden accumulation of secretory proteins within the endoplasmic reticulum (ER) through pathways such as the Unfolded Protein Response (UPR). The ability of cells to adapt the ER folding environment to the misfolded protein burden ultimately dictates cell fate. The aging process is a particularly important modifier of the proteostasis network; as cells age, both their ability to maintain this balance in protein folding/degradation and their ability to respond to insults in these pathways can break down, a common element of age-related diseases (including neurodegenerative diseases). ER stress coping mechanisms are central to lifespan regulation under both normal and disease states. In this review, we give a brief overview of the role of ER stress response pathways in age-dependent neurodegeneration.

Keywords: endoplasm reticulum stress, aging, neurodegeneration, unfolded protein response, proteostasis

OPEN ACCESS

Edited by:
Guillaume Thibault,
Nanyang Technological University, Singapore

Reviewed by:
Jesse C. Hay,
University of Montana, United States
Marcelo Ehrlich,
Tel Aviv University, Israel

***Correspondence:**
Patrick Lajoie
plajoie3@uwo.ca

Specialty section:
This article was submitted to Membrane Traffic, a section of the journal Frontiers in Cell and Developmental Biology

Received: *05 March 2019*
Accepted: *03 May 2019*
Published: *21 May 2019*

Citation:
Chadwick SR and Lajoie P (2019) Endoplasmic Reticulum Stress Coping Mechanisms and Lifespan Regulation in Health and Diseases. Front. Cell Dev. Biol. 7:84. doi: 10.3389/fcell.2019.00084

INTRODUCTION

Protein homeostasis (or proteostasis) is the sum of cellular processes involving protein transcription, translation, folding, and degradation (Balch et al., 2008). In order for a cell to remain functional and capable of adapting to changing biochemical and environmental signals, proteostasis must remain uncompromised (Ben-Zvi et al., 2009). Protein folding is particularly important for cellular processes, as the final conformation of a folded protein is essential to its function. Cellular membrane dynamics are a pivotal aspect of protein folding; adaptations in the ER membrane's composition and size are required to maintain proteostasis, and proper protein folding, in turn, is required to maintain this membrane integrity (Hou and Taubert, 2014).

Under normal circumstances, proteins destined for the secretory pathway are translated directly into the ER via ribosomes embedded in the ER membrane, bound by chaperone proteins, folded, and then packaged into vesicles for secretion (Novick et al., 1981). This includes proteins destined for the plasma membrane, such as membrane-linked receptors, or secreted factors released into the extracellular environment. In some cases, however, this pathway can go awry; proteins may become misfolded or unfolded in the ER, and unable to be recovered by the protein quality control machinery. In this instance, the improperly folded protein is targeted for degradation, exported into the cytosol, and degraded by a proteasome (Werner et al., 1996). Again, however, this process is imperfect. Some environmental, cellular, or molecular factors can cause disruptions in this pathway, preventing the proper turnover of misfolded or unfolded proteins, potentially leading to their

accumulation and aggregation. This generates a cellular condition known as ER stress (Friedlander et al., 2000; Walter and Ron, 2011; Karagöz et al., 2019).

Endoplasmic reticulum stress and the failure to correctly fold proteins are associated with loss of protein function and cell death (Zinszner et al., 1998; Hetz et al., 2006; Upton et al., 2012). To avoid this, the cell resolves misfolded protein stress via two major stress response pathways: the heat shock response (HSR) (Verghese et al., 2012), which handles misfolded proteins in the cytoplasm, and the unfolded protein response (UPR), which takes place in the ER (Kohno et al., 1993; Cox and Walter, 1996; Liu and Chang, 2008). These protein quality control mechanisms are essential for maintaining the function and integrity of cellular processes. When perturbed, they can lead to whole-cell dysfunction and toxicity (Ruis and Schüller, 1995; Voellmy, 2004). Under normal conditions, both lead to resolution of the cellular stress caused by the presence of misfolded proteins. In some cases, such as in several misfolded protein-associated diseases (Yoshida, 2007; Torres et al., 2015), these stress response pathways themselves can become impaired. This leads to further accumulation of misfolded proteins, which in turn causes further UPR or HSR impairment (Delépine et al., 2000; Zhang et al., 2002). Misfolded protein aggregates have also been shown to bind and sequester machinery important for degrading misfolded proteins via ER-associated degradation (ERAD), a protein quality-control mechanism which recognizes unfolded or misfolded proteins synthesized in the ER (Lippincott-Schwartz et al., 1988; McCracken and Brodsky, 1996). This ERAD impairment induces further stress in the ER and causes induction of the UPR. Proteostatic dysfunction essentially leads to a vicious cycle of increasing ER stress, protein accumulation, and stress response impairment.

The UPR is a complicated signaling pathway which works to resolve ER stress and allow protein synthesis and folding to continue and has been shown to interact with multiple cellular pathways and processes to do so, including (but not limited to) those occurring in the ER (Welihinda et al., 1999; Travers et al., 2000; Walter and Ron, 2011; Snapp, 2012). It has also been shown to be impacted by several seemingly unrelated external influences, including aging and lipid metabolism, and dysfunction in this pathway has been linked with shortened cellular lifespan and cell death (Jazwinski, 2002; Hou et al., 2014; Labunskyy et al., 2014). Because of this, the study of the molecular mechanisms behind ER stress and the UPR is essential to the understanding of how protein homeostasis impacts the entire cell and its processes, including response to stressors, aging, and cell death.

ACTIVATION OF THE UNFOLDED PROTEIN RESPONSE

As previously mentioned, the UPR is a stress response pathway specifically activated in response to ER stress, which is a condition that can be generated by things such as small molecules, environmental factors, or the accumulation of misfolded proteins in the ER (Welihinda et al., 1999). The UPR is activated when ER stress sensors embedded in the ER membrane detect the stressors and respond. Interestingly, the ultimate function of the UPR depends on the degree of activation and the length of time before the stress is resolved (Rutkowski et al., 2006; Rutkowski and Kaufman, 2007; Vidal and Hetz, 2012). It is primarily an adaptive response, which rescues cells from ER stress, but prolonged ER stress or high amplitude of UPR signaling causes the response to become maladaptive. In these circumstances, the UPR can activate alternate signaling pathways that result in apoptosis (Hetz et al., 2006; Rutkowski et al., 2006; Lin et al., 2007; Upton et al., 2012; Lu et al., 2014; Hetz and Papa, 2018).

In mammals, three distinct ER stress sensors exist: inositol requiring kinase 1 (IRE1) (Sidrauski and Walter, 1997; Yoshida et al., 2001; Calfon et al., 2002), double-stranded RNA-activated protein kinase like endoplasmic reticulum kinase (PERK) (Harding et al., 2000), and activating transcription factor 6 (ATF6) (Yoshida et al., 1998). When the UPR is activated, ER chaperone proteins (such as BIP) dissociate from these sensors, allowing their activation which in turn activates downstream signaling pathways (Welihinda et al., 1999; Shen et al., 2002; Ma and Hendershot, 2004; Pincus et al., 2010). Effector proteins from each of the three pathways bind to UPR response element (UPRE) sequences in gene promoters. A cell may activate over 400 UPR target genes involved in responding to ER stress, such as chaperone proteins, ribosome biogenesis genes, ERAD effectors, and genes to expand the ER lumen (Welihinda et al., 1999; Ma and Hendershot, 2004; Aragón et al., 2009). Upregulation of such genes contributes to adapt the ER folding environment to the new misfolded protein burden.

Despite its name, the UPR can be activated by stresses unrelated to misfolded or unfolded proteins. In addition to increased misfolded protein burden, ER stress can be induced by environmental factors; glucose deprivation/caloric restriction, for example, has been shown to mildly induce ER stress (Kaeberlein et al., 2005; Goldberg et al., 2009). Lipid concentration and composition in cells or in the extracellular environment have also been shown to significantly impact ER stress and UPR induction (Pineau et al., 2009; Promlek et al., 2011; Thibault et al., 2012). There is evidence to suggest that the UPR sensors IRE1 and PERK can detect perturbations of ER membrane lipid composition, independently of their luminal sensing domains, through their transmembrane domain (Promlek et al., 2011; Volmer et al., 2013; Kono et al., 2017). Other studies have also shown that the UPR is highly involved in responding to perturbation of lipid homeostasis (Thibault et al., 2012) and controls lipid synthesis and ER membrane proliferation in response to various cell stresses (Bernales et al., 2006; Schuck et al., 2009). Thus, UPR activation in the absence of unfolded proteins, via perturbation in the lipid composition of ER membrane, represents another regulatory mechanism (Promlek et al., 2011; Lajoie et al., 2012; Snapp, 2012; Volmer et al., 2013; Volmer and Ron, 2015) which may be important for UPR activation in ER stress-associated diseases.

Macroautophagy (henceforth, "autophagy") is another protein quality control process which relies heavily upon functional membrane dynamics and proper membrane lipid composition. It is a non-specific maintenance process by which protein aggregates and damaged, defective, or aging cellular contents

and organelles are transported to the lysosome for degradation (Klionsky and Emr, 2000; Mizushima, 2007; Glick et al., 2010). The membrane around the cargo destined for degradation by autophagy, the autophagosome, is derived from the ER membrane [with apparent contributions from the mitochondrial and plasma membranes (Nascimbeni et al., 2017)], wherein autophagic cargo are degraded by lysosomal hydrolases (Dunn, 1990). Autophagy occurs at a basal level in cells, but can be strongly induced by nutrient deprivation due to autophagy's role in nutrient conservation and starvation adaptation, using bulk degradation to replenish amino acid availability for other cellular functions (Munafó and Colombo, 2001; Mizushima, 2007). ER stress has been shown to trigger autophagy, indicating parallel proteostatic responses to ER stress in the form of the UPR and autophagy (Bernales et al., 2006; Yorimitsu et al., 2006; Vidal and Hetz, 2012; Hou and Taubert, 2014). Importantly, activation of autophagy has been shown to be important for maintenance of proteostasis and lifespan regulation in multiple organisms and experimental models (Meléndez et al., 2003; Alvers et al., 2009a; Lee et al., 2012; Carroll et al., 2013).

ER STRESS AND AGING

Aging has been shown to modulate some of the factors leading to ER stress. It is an important modifier of the proteostasis network, meaning that aging cells may have altered capacity to properly carry out protein transcription, translation, folding, and degradation (Naidoo, 2009; Brown and Naidoo, 2012; **Figure 1**). Aging cells have been shown to have decreased total levels of a number of ER proteins, including protein chaperones (such as PDI, BIP, etc.) which normally supervise and ensure proper protein folding, and assist in targeting misfolded proteins for degradation (Paz Gavilán et al., 2006; Hussain and Ramaiah, 2007; Naidoo et al., 2008). This usually prevents the accumulation and aggregation of misfolded proteins and prevents them from having toxic effects on the cell. In addition, the limited chaperones that are still present in the aging ER appear to be impaired. This is possibly due to an increased rate of oxidation of these chaperones in aged cells, leading to structural changes and consequently decreased function (van der Vlies et al., 2003; Snapp et al., 2006; Naidoo et al., 2008). For example, both BIP ATPase activity and PDI enzymatic function have been shown to be significantly decreased in aged mouse livers (Nuss et al., 2008), and similar results have been seen in a number of other models as well, such as aged mouse cerebral cortex (Naidoo et al., 2008). Other components of UPR signaling have also shown to be reduced during aging. PERK mRNA, for example, has been shown to be reduced in aged rat hippocampi, indicating less efficient UPR signaling (Paz Gavilán et al., 2006).

Aging also appears to alter the threshold at which the UPR switches from the adaptive pathway to the apoptotic pathway, which is perhaps related to the changes to proteostasis previously mentioned. When PERK signaling is decreased during aging, for example, there is evidence of an increase in GADD34 expression, which helps remove the translational block that occurs through PERK phosphorylating eIF2. This allows the expression of pro-apoptotic proteins, such as CHOP (Brown and Naidoo, 2012). CHOP has been shown to be increased with stress during aging and at baseline in aged muscular tissue in rats (Hussain and Ramaiah, 2007; Naidoo et al., 2008; Baehr et al., 2016); caspase-12 is also increased with stress in aged cells, but not during stress in younger cells (Paz Gavilán et al., 2006). The apoptotic protein JNK (which is activated by IRE1 during prolonged UPR signaling) is also upregulated during aging, as are JNK kinases that phosphorylate other apoptotic transcription factors such as ATF-2 and c-Jun (Hussain and Ramaiah, 2007; Brown and Naidoo, 2012). Calcium-mediated cell death pathways are also altered during aging. Aging has been linked to increased calcium flux between the ER and mitochondria, and consequently increased exposure to reactive oxygen species and sensitivity to cell death in the case of mitochondrial calcium overload (Fernandez-Sanz et al., 2014; Calvo-Rodríguez et al., 2016; Madreiter-Sokolowski et al., 2019). These factors, in turn, lead to a decreased threshold for the activation of calcium-mediated apoptosis. This aging-related decrease in adaptive UPR signaling and increase in apoptotic signaling may account for the apparent sensitivity of aged cells to ER stress, and the increased rate of cell death amongst stressed cells when aged (Rutkowski et al., 2006; Lu et al., 2014; Tay et al., 2014). Autophagy has also been shown to become less efficient at clearing damaged organelles and misfolded proteins during aging in yeast (as well as other models), and lifespan extension has been demonstrated when autophagy is heavily induced (Zhang and Cuervo, 2008; Alvers et al., 2009b; Caramés et al., 2010; Koga and Cuervo, 2011; Martinez-Lopez et al., 2015).

ER STRESS AND AGE-DEPENDENT HUMAN DISEASES

Aging is a common risk factor for a number of protein misfolding diseases, including several neurodegenerative diseases (Martínez et al., 2017), a number of which have links to UPR function as described in the previous section. While not all aging-related diseases are directly linked to breakdown of UPR signaling, this breakdown may still contribute to disease pathogeneses. For example, type 2 diabetes is known to develop more frequently due to both obesity and aging, with the two factors often coexisting in patients (Ozcan et al., 2004). As aging has also been linked to the decreases in UPR effector proteins associated with diabetes and insulin resistance, these results suggest that aging-related UPR defects may be linked to these diseases as well. Obesity and insulin resistance are also linked to heart disease and atherosclerosis, both of which increase in prevalence with age and have also been linked to ER stress and the UPR (Han et al., 2006). Huntington's disease (HD), Parkinson's disease, and Alzheimer's disease have been clearly and repeatedly linked to UPR dysfunction which increases with age, thus increasing disease severity (Vidal and Hetz, 2012; Carroll et al., 2013). Though the three diseases have different causative genes, they all share misfolded protein accumulation and aggregation as part of their pathology, leading

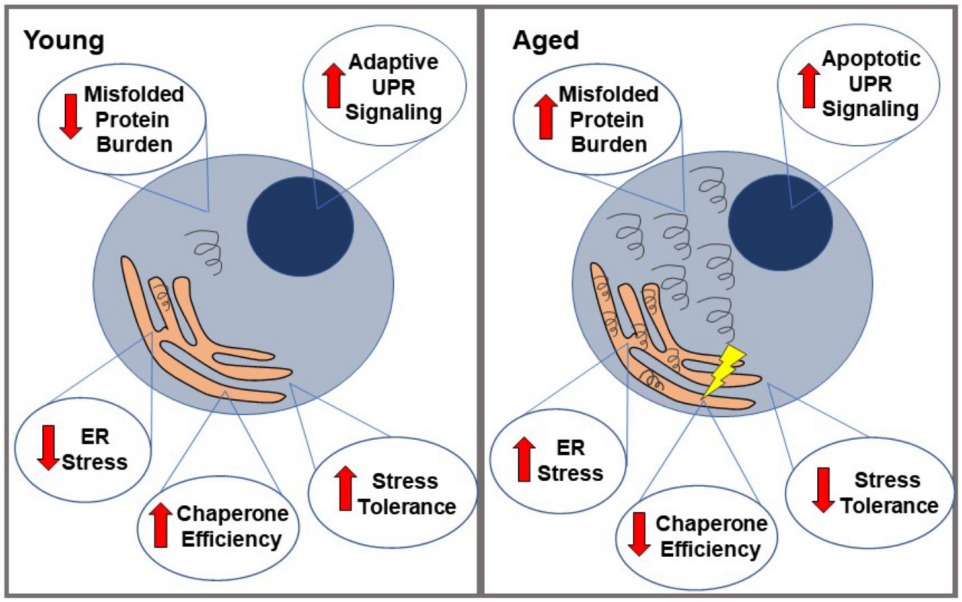

FIGURE 1 | Proteostatic changes in aged vs. young cells. When faced with misfolded proteins, young cells demonstrate relatively low ER stress, high chaperone efficiency and stress tolerance, and primarily adaptive UPR signaling. This generally leads to a resolution of the misfolded proteins and therefore, ER stress. In contrast, aged cells are more likely to accumulate these misfolded proteins (partially due to loss of chaperone protein efficiency), leading to a state of ER stress, which they are less able to resolve. Their lower stress tolerance eventually leads to a relative increase in apoptotic UPR signaling over adaptive, ultimately causing cell death.

to impaired proteostasis and ER stress responses, and then cellular toxicity.

In Alzheimer's disease, for example, tau neurofibrillary tangles and amyloid-β plaques accumulate in neurons and lead to neurodegeneration (Lee et al., 2010). Studies have shown that cells with these protein aggregates have high UPR induction identified through high levels of phosphorylated eIF2α, PERK, and IRE1 (Hoozemans et al., 2005, 2009; Gerakis and Hetz, 2018a,b). This has been identified in early stages of protein accumulation and linked to later stage neurodegeneration, suggesting an early beneficial role for the UPR that may later become maladaptive (Hoozemans et al., 2009). Indeed, as cells age, the UPR's capacity to cope with the misfolded protein load decreases in an fly model of Alzheimer's disease; decreased signaling through the IRE1 branch of the UPR has been identified in this model, leading to decreased misfolded protein clearance (Marcora et al., 2017). Similar findings have also been reported in spinal cord tissue from patients with sporadic Amyotrophic Lateral Sclerosis (ALS) (Atkin et al., 2008). Enhancing UPR signaling and/or reducing ER stress through genetic and pharmacological modulation of UPR effectors such as eIF2α, PERK, XBP1, ATF4, and heat shock proteins have all been shown to have positive effects on various models of ALS (Hetz et al., 2009; Saxena et al., 2009; Castillo et al., 2013; Matus et al., 2013; Saxena et al., 2013; Jiang et al., 2014; Wang et al., 2014a,b; Das et al., 2015; Vieira et al., 2015; Nagy et al., 2016). Huntington's disease is another neurodegenerative disease which is characterized by the accumulation of misfolded huntingtin protein, which undergoes abnormal expansion of a segment of polyQ repeats (Penney et al., 1997). Longer polyQ tracts are associated with earlier onset and more severe symptoms (Macdonald, 1993), and are also more prone to aggregation and are associated with a higher degree of UPR induction but a lower degree of HSR induction (Martindale et al., 1998; Chafekar and Duennwald, 2012). These aggregates have also been shown to cause ER stress and impaired ERAD due to sequestration of ERAD machinery, leading to UPR hyperactivation (Duennwald and Lindquist, 2008; Lajoie and Snapp, 2011; Leitman et al., 2013; Jiang et al., 2016). In agreement with dysregulated UPR in HD, restoration of "normal" XBP1 and PERK activity has been shown to improve disease phenotypes in both cell and animal models (Vidal et al., 2011, 2012; Leitman et al., 2014; Rivas et al., 2015). Importantly, activation of ER stress pathways has been detected in post-mortem patient samples (Carnemolla et al., 2009). Similarly, UPR has been associated with the onset of Parkinson's disease (Mercado et al., 2016). Accumulation of α-synuclein has been shown to block ER to Golgi trafficking and consequently activate the UPR in both yeast and humans (Cooper et al., 2006; Heman-Ackah et al., 2017). PERK inhibition showed positive effects in a mouse model of Parkinson's disease (Celardo et al., 2016; Mercado et al., 2018). In Parkinson's disease, misfolded proteins accumulate in the substantia nigra region of the brain, leading to loss of dopaminergic neurons in this region. Similar to the studies performed on Alzheimer's disease, it has been shown that the UPR is highly activated in these areas and that this UPR activation may be causally linked to the neurodegeneration seen in this disease (Hoozemans et al., 2007). ER stress is therefore a common determinant of multiple neurodegenerative diseases.

Thus, targeting the UPR has emerged as an attractive therapeutic approach these disorders (Rivas et al., 2015; Valenzuela et al., 2016).

CONCLUSION

As more connections are drawn between ER proteostasis and aging, it becomes clear that these interactions reach much further than previously thought – from neurodegeneration to temperature adaptation, and from simple model organisms like yeast up to higher mammals. Future research on these fields (individually and as a whole) will hopefully address some yet-unanswered questions on how and why these connections exist. For example, could age-related changes in membrane composition and fluidity explain age-related increases in UPR signaling? What advantage would be conferred to the cell by UPR stress-sensing proteins responding to changes in membrane lipids as well as ER stress? What other cellular functions and pathways intersect with these processes, in both baseline and stressed/aged states? In all likelihood, there is not one single cause for the breakdown of ER homeostasis during aging, but instead a combination of factors contributes to overall increased sensitivity to ER stress. Increased misfolded protein accumulation, decreased effectiveness of the adaptive UPR, and an altered threshold for apoptotic UPR signaling likely all play a role (Naidoo et al., 2008; Brown and Naidoo, 2012; Madreiter-Sokolowski et al., 2019). Finally, ER stress sensitivity is not only dictated by the amplitude of the UPR response but also by upregulation of a specific set of target genes required to adapt the ER folding environment for a given stress-causing situation (Thibault et al., 2011). Therefore, the question of what categories of UPR target genes define the aging UPR is a crucial one that needs to be addressed. As technology and research methods advance and our understanding of these areas improves, this future research will likely have important implications for basic science and therapeutic approaches to human diseases.

AUTHOR CONTRIBUTIONS

PL and SC wrote the manuscript. SC generated the figure.

FUNDING

This work was supported by a grant from the Canadian Institutes for Health Research (MOP-137041). SC is the recipient of an Ontario Graduate Scholarship.

REFERENCES

Alvers, A. L., Fishwick, L. K., Wood, M. S., Hu, D., Chung, H. S., Dunn, W. A., et al. (2009a). Autophagy and amino acid homeostasis are required for chronological longevity in *Saccharomyces cerevisiae*. *Aging Cell* 8, 353–369. doi: 10.1111/j.1474-9726.2009.00469.x

Alvers, A. L., Wood, M. S., Hu, D., Kaywell, A. C., Dunn, W. A., and Aris, J. P. (2009b). Autophagy is required for extension of yeast chronological life span by rapamycin. *Autophagy* 5, 847–849. doi: 10.4161/auto.8824

Aragón, T., van Anken, E., Pincus, D., Serafimova, I. M., Korennykh, A. V., Rubio, C. A., et al. (2009). Messenger RNA targeting to endoplasmic reticulum stress signalling sites. *Nature* 457, 736–740. doi: 10.1038/nature07641

Atkin, J. D., Farg, M. A., Walker, A. K., McLean, C., Tomas, D., and Horne, M. K. (2008). Endoplasmic reticulum stress and induction of the unfolded protein response in human sporadic amyotrophic lateral sclerosis. *Neurobiol. Dis.* 30, 400–407. doi: 10.1016/j.nbd.2008.02.009

Baehr, L. M., West, D. W. D., Marcotte, G., Marshall, A. G., De Sousa, L. G., Baar, K., et al. (2016). Age-related deficits in skeletal muscle recovery following disuse are associated with neuromuscular junction instability and ER stress, not impaired protein synthesis. *Aging* 8, 127–146. doi: 10.18632/aging.100879

Balch, W. E., Morimoto, R. I., Dillin, A., and Kelly, J. W. (2008). Adapting proteostasis for disease intervention. *Science* 319, 916–919. doi: 10.1126/science.1141448

Ben-Zvi, A., Miller, E. A., and Morimoto, R. I. (2009). Collapse of proteostasis represents an early molecular event in *Caenorhabditis elegans* aging. *Proc. Natl. Acad. Sci. U.S.A.* 106, 14914–14919. doi: 10.1073/pnas.0902882106

Bernales, S., McDonald, K. L., and Walter, P. (2006). Autophagy counterbalances endoplasmic reticulum expansion during the unfolded protein response. *PLoS Biol.* 4:e423. doi: 10.1371/journal.pbio.0040423

Brown, M. K., and Naidoo, N. (2012). The endoplasmic reticulum stress response in aging and age-related diseases. *Front. Physiol.* 3:263. doi: 10.3389/fphys.2012.00263

Calfon, M., Zeng, H., Urano, F., Till, J. H., Hubbard, S. R., Harding, H. P., et al. (2002). IRE1 couples endoplasmic reticulum load to secretory capacity by processing the XBP-1 mRNA. *Nature* 415, 92–96. doi: 10.1038/415092a

Calvo-Rodríguez, M., García-Durillo, M., Villalobos, C., and Núñez, L. (2016). In vitro aging promotes endoplasmic reticulum (ER)-mitochondria Ca2+ cross talk and loss of store-operated Ca2+ entry (SOCE) in rat hippocampal neurons. *Biochim. Biophys. Acta* 1863, 2637–2649. doi: 10.1016/j.bbamcr.2016.08.001

Caramés, B., Taniguchi, N., Otsuki, S., Blanco, F. J., and Lotz, M. (2010). Autophagy is a protective mechanism in normal cartilage, and its aging-related loss is linked with cell death and osteoarthritis. *Arthritis Rheum.* 62, 791–801. doi: 10.1002/art.27305

Carnemolla, A., Fossale, E., Agostoni, E., Michelazzi, S., Calligaris, R., De Maso, L., et al. (2009). Rrs1 is involved in endoplasmic reticulum stress response in Huntington disease. *J. Biol. Chem.* 284, 18167–18173. doi: 10.1074/jbc.M109.018325

Carroll, B., Hewitt, G., and Korolchuk, V. I. (2013). Autophagy and ageing: implications for age-related neurodegenerative diseases. *Essays Biochem.* 55, 119–131. doi: 10.1042/bse0550119

Castillo, K., Nassif, M., Valenzuela, V., Rojas, F., Matus, S., Mercado, G., et al. (2013). Trehalose delays the progression of amyotrophic lateral sclerosis by enhancing autophagy in motoneurons. *Autophagy* 9, 1308–1320. doi: 10.4161/auto.25188

Celardo, I., Costa, A. C., Lehmann, S., Jones, C., Wood, N., Mencacci, N. E., et al. (2016). Mitofusin-mediated ER stress triggers neurodegeneration in PINK1/Parkin models of Parkinson's disease. *Cell Death Dis.* 7:e2271. doi: 10.1038/cddis.2016.173

Chafekar, S. M., and Duennwald, M. L. (2012). Impaired heat shock response in cells expressing full-length polyglutamine-expanded huntingtin. *PLoS One* 7:e37929. doi: 10.1371/journal.pone.0037929

Cooper, A. A., Gitler, A. D., Cashikar, A., Haynes, C. M., Hill, K. J., Bhullar, B., et al. (2006). Alpha-synuclein blocks ER-Golgi traffic and Rab1 rescues neuron loss in Parkinson's models. *Science* 313, 324–328. doi: 10.1126/science.1129462

Cox, J. S., and Walter, P. (1996). A novel mechanism for regulating activity of a transcription factor that controls the unfolded protein response. *Cell* 87, 391–404. doi: 10.1016/s0092-8674(00)81360-4

Das, I., Krzyzosiak, A., Schneider, K., Wrabetz, L., Antonio, M. D., Barry, N., et al. (2015). Preventing proteostasis diseases by selective inhibition of a phosphatase regulatory subunit. *Science* 348, 239–242. doi: 10.1126/science.aaa4484

Delépine, M., Nicolino, M., Barrett, T., Golamaully, M., Lathrop, G. M., and Julier, C. (2000). EIF2AK3, encoding translation initiation factor 2-alpha kinase 3, is mutated in patients with Wolcott-Rallison syndrome. *Nat. Genet.* 25, 406–409. doi: 10.1038/78085

Duennwald, M. L., and Lindquist, S. (2008). Impaired ERAD and ER stress are early and specific events in polyglutamine toxicity. *Genes Dev.* 22, 3308–3319. doi: 10.1101/gad.1673408

Dunn, W. A. (1990). Studies on the mechanisms of autophagy: maturation of the autophagic vacuole. *J. Cell Biol.* 110, 1935–1945. doi: 10.1083/jcb.110.6.1935

Fernandez-Sanz, C., Ruiz-Meana, M., Miro-Casas, E., Nuñez, E., Castellano, J., Loureiro, M., et al. (2014). Defective sarcoplasmic reticulum-mitochondria calcium exchange in aged mouse myocardium. *Cell Death Dis.* 5:e1573. doi: 10.1038/cddis.2014.526

Friedlander, R., Jarosch, E., Urban, J., Volkwein, C., and Sommer, T. (2000). A regulatory link between ER-associated protein degradation and the unfolded-protein response. *Nat. Cell Biol.* 2, 379–384. doi: 10.1038/35017001

Gerakis, Y., and Hetz, C. (2018a). A decay of the adaptive capacity of the unfolded protein response exacerbates Alzheimer's disease. *Neurobiol. Aging* 63, 162–164. doi: 10.1016/j.neurobiolaging.2017.09.012

Gerakis, Y., and Hetz, C. (2018b). Emerging roles of ER stress in the etiology and pathogenesis of Alzheimer's disease. *FEBS J.* 285, 995–1011. doi: 10.1111/febs.14332

Glick, D., Barth, S., and Macleod, K. F. (2010). Autophagy: cellular and molecular mechanisms. *J. Pathol.* 221, 3–12. doi: 10.1002/path.2697

Goldberg, A. A., Bourque, S. D., Kyryakov, P., Gregg, C., Boukh-Viner, T., Beach, A., et al. (2009). Effect of calorie restriction on the metabolic history of chronologically aging yeast. *Exp. Gerontol.* 44, 555–571. doi: 10.1016/j.exger.2009.06.001

Han, S., Liang, C.-P., DeVries-Seimon, T., Ranalletta, M., Welch, C. L., Collins-Fletcher, K., et al. (2006). Macrophage insulin receptor deficiency increases ER stress-induced apoptosis and necrotic core formation in advanced atherosclerotic lesions. *Cell Metab.* 3, 257–266. doi: 10.1016/j.cmet.2006.02.008

Harding, H. P., Novoa, I., Zhang, Y., Zeng, H., Wek, R., Schapira, M., et al. (2000). Regulated translation initiation controls stress-induced gene expression in mammalian cells. *Mol. Cell* 6, 1099–1108. doi: 10.1016/s1097-2765(00)00108-8

Heman-Ackah, S. M., Manzano, R., Hoozemans, J. J. M., Scheper, W., Flynn, R., Haerty, W., et al. (2017). Alpha-synuclein induces the unfolded protein response in Parkinson's disease SNCA triplication iPSC-derived neurons. *Hum. Mol. Genet.* 26, 4441–4450. doi: 10.1093/hmg/ddx331

Hetz, C., Bernasconi, P., Fisher, J., Lee, A.-H., Bassik, M. C., Antonsson, B., et al. (2006). Proapoptotic BAX and BAK modulate the unfolded protein response by a direct interaction with IRE1alpha. *Science* 312, 572–576. doi: 10.1126/science.1123480

Hetz, C., and Papa, F. R. (2018). The unfolded protein response and cell fate control. *Mol. Cell* 69, 169–181. doi: 10.1016/j.molcel.2017.06.017

Hetz, C., Thielen, P., Matus, S., Nassif, M., Court, F., Kiffin, R., et al. (2009). XBP-1 deficiency in the nervous system protects against amyotrophic lateral sclerosis by increasing autophagy. *Genes Dev.* 23, 2294–2306. doi: 10.1101/gad.1830709

Hoozemans, J. J. M., van Haastert, E. S., Eikelenboom, P., de Vos, R. A. I., Rozemuller, J. M., and Scheper, W. (2007). Activation of the unfolded protein response in Parkinson's disease. *Biochem. Biophys. Res. Commun.* 354, 707–711. doi: 10.1016/j.bbrc.2007.01.043

Hoozemans, J. J. M., van Haastert, E. S., Nijholt, D. A. T., Rozemuller, A. J. M., Eikelenboom, P., and Scheper, W. (2009). The unfolded protein response is activated in pretangle neurons in Alzheimer's disease hippocampus. *Am. J. Pathol.* 174, 1241–1251. doi: 10.2353/ajpath.2009.080814

Hoozemans, J. J. M., Veerhuis, R., Van Haastert, E. S., Rozemuller, J. M., Baas, F., Eikelenboom, P., et al. (2005). The unfolded protein response is activated in Alzheimer's disease. *Acta Neuropathol.* 110, 165–172.

Hou, N. S., Gutschmidt, A., Choi, D. Y., Pather, K., Shi, X., Watts, J. L., et al. (2014). Activation of the endoplasmic reticulum unfolded protein response by lipid disequilibrium without disturbed proteostasis in vivo. *Proc. Natl. Acad. Sci. U.S.A.* 111, E2271–E2280. doi: 10.1073/pnas.1318262111

Hou, N. S., and Taubert, S. (2014). Membrane lipids and the endoplasmic reticulum unfolded protein response: an interesting relationship. *Worm* 3:e962405. doi: 10.4161/21624046.2014.962405

Hussain, S. G., and Ramaiah, K. V. A. (2007). Reduced eIF2alpha phosphorylation and increased proapoptotic proteins in aging. *Biochem. Biophys. Res. Commun.* 355, 365–370. doi: 10.1016/j.bbrc.2007.01.156

Jazwinski, S. M. (2002). Growing old: metabolic control and yeast aging. *Annu. Rev. Microbiol.* 56, 769–792. doi: 10.1146/annurev.micro.56.012302.160830

Jiang, H. Q., Ren, M., Jiang, H. Z., Wang, J., Zhang, J., Yin, X., et al. (2014). Guanabenz delays the onset of disease symptoms, extends lifespan, improves motor performance and attenuates motor neuron loss in the SOD1 G93A mouse model of amyotrophic lateral sclerosis. *Neuroscience* 277, 132–138. doi: 10.1016/j.neuroscience.2014.03.047

Jiang, Y., Chadwick, S. R., and Lajoie, P. (2016). Endoplasmic reticulum stress: the cause and solution to Huntington's disease? *Brain Res.* 1648, 650–657. doi: 10.1016/j.brainres.2016.03.034

Kaeberlein, M., Hu, D., Kerr, E. O., Tsuchiya, M., Westman, E. A., Dang, N., et al. (2005). Increased life span due to calorie restriction in respiratory-deficient yeast. *PLoS Genet.* 1:e69. doi: 10.1371/journal.pgen.0010069

Karagöz, G. E., Acosta-Alvear, D., and Walter, P. (2019). The unfolded protein response: detecting and responding to fluctuations in the protein-folding capacity of the endoplasmic reticulum. *Cold Spring Harb. Perspect. Biol.* [Epub ahead of print].

Klionsky, D. J., and Emr, S. D. (2000). Autophagy as a regulated pathway of cellular degradation. *Science* 290, 1717–1721. doi: 10.1126/science.290.5497.1717

Koga, H., and Cuervo, A. M. (2011). Chaperone-mediated autophagy dysfunction in the pathogenesis of neurodegeneration. *Neurobiol. Dis.* 43, 29–37. doi: 10.1016/j.nbd.2010.07.006

Kohno, K., Normington, K., Sambrook, J., Gething, M. J., and Mori, K. (1993). The promoter region of the yeast KAR2 (BiP) gene contains a regulatory domain that responds to the presence of unfolded proteins in the endoplasmic reticulum. *Mol. Cell. Biol.* 13, 877–890. doi: 10.1128/MCB.13.2.877

Kono, N., Amin-Wetzel, N., and Ron, D. (2017). Generic membrane-spanning features endow IRE1α with responsiveness to membrane aberrancy. *Mol. Biol. Cell* 28, 2318–2332. doi: 10.1091/mbc.e17-03-0144

Labunskyy, V. M., Gerashchenko, M. V., Delaney, J. R., Kaya, A., Kennedy, B. K., Kaeberlein, M., et al. (2014). Lifespan extension conferred by endoplasmic reticulum secretory pathway deficiency requires induction of the unfolded protein response. *PLoS Genet.* 10:e1004019. doi: 10.1371/journal.pgen.1004019

Lajoie, P., Moir, R. D., Willis, I. M., and Snapp, E. L. (2012). Kar2p availability defines distinct forms of endoplasmic reticulum stress in living cells. *Mol. Biol. Cell* 23, 955–964. doi: 10.1091/mbc.E11-12-0995

Lajoie, P., and Snapp, E. L. (2011). Changes in BiP availability reveal hypersensitivity to acute endoplasmic reticulum stress in cells expressing mutant huntingtin. *J. Cell Sci.* 124, 3332–3343. doi: 10.1242/jcs.087510

Lee, H., Noh, J.-Y., Oh, Y., Kim, Y., Chang, J.-W., Chung, C.-W., et al. (2012). IRE1 plays an essential role in ER stress-mediated aggregation of mutant huntingtin via the inhibition of autophagy flux. *Hum. Mol. Genet.* 21, 101–114. doi: 10.1093/hmg/ddr445

Lee, J. H., Won, S. M., Suh, J., Son, S. J., Moon, G. J., Park, U. J., et al. (2010). Induction of the unfolded protein response and cell death pathway in Alzheimer's disease, but not in aged Tg2576 mice. *Exp. Mol. Med.* 42, 386–394. doi: 10.3858/emm.2010.42.5.040

Leitman, J., Barak, B., Benyair, R., Shenkman, M., Ashery, U., Hartl, F. U., et al. (2014). ER stress-induced eIF2-alpha phosphorylation underlies sensitivity of striatal neurons to pathogenic huntingtin. *PLoS One* 9:e90803. doi: 10.1371/journal.pone.0090803

Leitman, J., Ulrich Hartl, F., and Lederkremer, G. Z. (2013). Soluble forms of polyQ-expanded huntingtin rather than large aggregates cause endoplasmic reticulum stress. *Nat. Commun.* 4:2753. doi: 10.1038/ncomms3753

Lin, J. H., Li, H., Yasumura, D., Cohen, H. R., Zhang, C., Panning, B., et al. (2007). IRE1 signaling affects cell fate during the unfolded protein response. *Science* 318, 944–949. doi: 10.1126/science.1146361

Lippincott-Schwartz, J., Bonifacino, J. S., Yuan, L. C., and Klausner, R. D. (1988). Degradation from the endoplasmic reticulum: disposing of newly synthesized proteins. *Cell* 54, 209–220. doi: 10.1016/0092-8674(88)90553-3

Liu, Y., and Chang, A. (2008). Heat shock response relieves ER stress. *EMBO J.* 27, 1049–1059. doi: 10.1038/emboj.2008.42

Lu, M., Lawrence, D. A., Marsters, S., Acosta-Alvear, D., Kimmig, P., Mendez, A. S., et al. (2014). Opposing unfolded-protein-response signals converge on

death receptor 5 to control apoptosis. *Science* 345, 98–101. doi: 10.1126/science.1254312

Ma, Y., and Hendershot, L. M. (2004). ER chaperone functions during normal and stress conditions. *J. Chem. Neuroanat.* 28, 51–65. doi: 10.1016/j.jchemneu.2003.08.007

Macdonald, M. (1993). A novel gene containing a trinucleotide repeat that is expanded and unstable on Huntington's disease chromosomes. *Cell* 72, 971–983. doi: 10.1016/0092-8674(93)90585-E

Madreiter-Sokolowski, C. T., Waldeck-Weiermair, M., Bourguignon, M.-P., Villeneuve, N., Gottschalk, B., Klec, C., et al. (2019). Enhanced inter-compartmental Ca2+ flux modulates mitochondrial metabolism and apoptotic threshold during aging. *Redox Biol.* 20, 458–466. doi: 10.1016/j.redox.2018.11.003

Marcora, M. S., Belfiori-Carrasco, L. F., Bocai, N. I., Morelli, L., and Castaño, E. M. (2017). Amyloid-β42 clearance and neuroprotection mediated by X-box binding protein 1 signaling decline with aging in the *Drosophila* brain. *Neurobiol. Aging* 60, 57–70. doi: 10.1016/j.neurobiolaging.2017.08.012

Martindale, D., Hackam, A., Wieczorek, A., Ellerby, L., Wellington, C., McCutcheon, K., et al. (1998). Length of huntingtin and its polyglutamine tract influences localization and frequency of intracellular aggregates. *Nat. Genet.* 18, 150–154. doi: 10.1038/ng0298-150

Martínez, G., Duran-Aniotz, C., Cabral-Miranda, F., Vivar, J. P., and Hetz, C. (2017). Endoplasmic reticulum proteostasis impairment in aging. *Aging Cell* 16, 615–623. doi: 10.1111/acel.12599

Martinez-Lopez, N., Athonvarangkul, D., and Singh, R. (2015). Autophagy and aging. *Adv. Exp. Med. Biol.* 847, 73–87. doi: 10.1007/978-1-4939-2404-2_3

Matus, S., Lopez, E., Valenzuela, V., Nassif, M., and Hetz, C. (2013). Functional contribution of the transcription factor ATF4 to the pathogenesis of amyotrophic lateral sclerosis. *PLoS One* 8:e66672. doi: 10.1371/journal.pone.0066672

McCracken, A. A., and Brodsky, J. L. (1996). Assembly of ER-associated protein degradation in vitro: dependence on cytosol, calnexin, and ATP. *J. Cell Biol.* 132, 291–298. doi: 10.1083/jcb.132.3.291

Meléndez, A., Tallóczy, Z., Seaman, M., Eskelinen, E.-L., Hall, D. H., and Levine, B. (2003). Autophagy genes are essential for dauer development and life-span extension in *C. elegans*. *Science* 301, 1387–1391. doi: 10.1126/science.1087782

Mercado, G., Castillo, V., Soto, P., López, N., Axten, J. M., Sardi, S. P., et al. (2018). Targeting PERK signaling with the small molecule GSK2606414 prevents neurodegeneration in a model of Parkinson's disease. *Neurobiol. Dis.* 112, 136–148. doi: 10.1016/j.nbd.2018.01.004

Mercado, G., Castillo, V., Soto, P., and Sidhu, A. (2016). ER stress and Parkinson's disease: pathological inputs that converge into the secretory pathway. *Brain Res.* 1648, 626–632. doi: 10.1016/j.brainres.2016.04.042

Mizushima, N. (2007). Autophagy: process and function. *Genes Dev.* 21, 2861–2873. doi: 10.1101/gad.1599207

Munafó, D. B., and Colombo, M. I. (2001). A novel assay to study autophagy: regulation of autophagosome vacuole size by amino acid deprivation. *J. Cell Sci.* 114, 3619–3629.

Nagy, M., Fenton, W. A., Li, D., Furtak, K., and Horwich, A. L. (2016). Extended survival of misfolded G85R SOD1-linked ALS mice by transgenic expression of chaperone Hsp110. *Proc. Natl. Acad. Sci. U.S.A.* 113, 5424–5428. doi: 10.1073/pnas.1604885113

Naidoo, N. (2009). ER and aging-Protein folding and the ER stress response. *Ageing Res. Rev.* 8, 150–159. doi: 10.1016/j.arr.2009.03.001

Naidoo, N., Ferber, M., Master, M., Zhu, Y., and Pack, A. I. (2008). Aging impairs the unfolded protein response to sleep deprivation and leads to proapoptotic signaling. *J. Neurosci.* 28, 6539–6548. doi: 10.1523/JNEUROSCI.5685-07.2008

Nascimbeni, A. C., Giordano, F., Dupont, N., Grasso, D., Vaccaro, M. I., Codogno, P., et al. (2017). ER-plasma membrane contact sites contribute to autophagosome biogenesis by regulation of local PI3P synthesis. *EMBO J.* 36, 2018–2033. doi: 10.15252/embj.201797006

Novick, P., Ferro, S., and Schekman, R. (1981). Order of events in the yeast secretory pathway. *Cell* 25, 461–469. doi: 10.1016/0092-8674(81)90064-7

Nuss, J. E., Choksi, K. B., DeFord, J. H., and Papaconstantinou, J. (2008). Decreased enzyme activities of chaperones PDI and BiP in aged mouse livers. *Biochem. Biophys. Res. Commun.* 365, 355–361. doi: 10.1016/j.bbrc.2007.10.194

Ozcan, U., Cao, Q., Yilmaz, E., Lee, A.-H., Iwakoshi, N. N., Ozdelen, E., et al. (2004). Endoplasmic reticulum stress links obesity, insulin action, and type 2 diabetes. *Science* 306, 457–461. doi: 10.1126/science.1103160

Paz Gavilán, M., Vela, J., Castaño, A., Ramos, B., del Río, J. C., Vitorica, J., et al. (2006). Cellular environment facilitates protein accumulation in aged rat hippocampus. *Neurobiol. Aging* 27, 973–982. doi: 10.1016/j.neurobiolaging.2005.05.010

Penney, J. B., Vonsattel, J. P., MacDonald, M. E., Gusella, J. F., and Myers, R. H. (1997). CAG repeat number governs the development rate of pathology in Huntington's disease. *Ann. Neurol.* 41, 689–692. doi: 10.1002/ana.410410521

Pincus, D., Chevalier, M. W., Aragón, T., van Anken, E., Vidal, S. E., El-Samad, H., et al. (2010). BiP binding to the ER-stress sensor Ire1 tunes the homeostatic behavior of the unfolded protein response. *PLoS Biol.* 8:e1000415. doi: 10.1371/journal.pbio.1000415

Pineau, L., Colas, J., Dupont, S., Beney, L., Fleurat-Lessard, P., Berjeaud, J.-M., et al. (2009). Lipid-induced ER stress: synergistic effects of sterols and saturated fatty acids. *Traffic* 10, 673–690. doi: 10.1111/j.1600-0854.2009.00903.x

Promlek, T., Ishiwata-Kimata, Y., Shido, M., Sakuramoto, M., Kohno, K., and Kimata, Y. (2011). Membrane aberrancy and unfolded proteins activate the endoplasmic reticulum stress sensor Ire1 in different ways. *Mol. Biol. Cell* 22, 3520–3532. doi: 10.1091/mbc.E11-04-0295

Rivas, A., Vidal, R. L., and Hetz, C. (2015). Targeting the unfolded protein response for disease intervention. *Expert Opin. Ther. Targets* 19, 1203–1218. doi: 10.1517/14728222.2015.1053869

Ruis, H., and Schüller, C. (1995). Stress signaling in yeast. *Bioessays* 17, 959–965. doi: 10.1002/bies.950171109

Rutkowski, D. T., Arnold, S. M., Miller, C. N., Wu, J., Li, J., Gunnison, K. M., et al. (2006). Adaptation to ER stress is mediated by differential stabilities of pro-survival and pro-apoptotic mRNAs and proteins. *PLoS Biol.* 4:e374. doi: 10.1371/journal.pbio.0040374

Rutkowski, D. T., and Kaufman, R. J. (2007). That which does not kill me makes me stronger: adapting to chronic ER stress. *Trends Biochem. Sci.* 32, 469–476. doi: 10.1016/j.tibs.2007.09.003

Saxena, S., Cabuy, E., and Caroni, P. (2009). A role for motoneuron subtype-selective ER stress in disease manifestations of FALS mice. *Nat. Neurosci.* 12, 627–636. doi: 10.1038/nn.2297

Saxena, S., Roselli, F., Singh, K., Leptien, K., Julien, J.-P., Gros-Louis, F., et al. (2013). Neuroprotection through excitability and mTOR required in ALS motoneurons to delay disease and extend survival. *Neuron* 80, 80–96. doi: 10.1016/j.neuron.2013.07.027

Schuck, S., Prinz, W. A., Thorn, K. S., Voss, C., and Walter, P. (2009). Membrane expansion alleviates endoplasmic reticulum stress independently of the unfolded protein response. *J. Cell Biol.* 187, 525–536. doi: 10.1083/jcb.200907074

Shen, J., Chen, X., Hendershot, L., and Prywes, R. (2002). ER stress regulation of ATF6 localization by dissociation of BiP/GRP78 binding and unmasking of Golgi localization signals. *Dev. Cell* 3, 99–111. doi: 10.1016/s1534-5807(02)00203-4

Sidrauski, C., and Walter, P. (1997). The transmembrane kinase Ire1p is a site-specific endonuclease that initiates mRNA splicing in the unfolded protein response. *Cell* 90, 1031–1039. doi: 10.1016/s0092-8674(00)80369-4

Snapp, E. L. (2012). Unfolded protein responses with or without unfolded proteins? *Cells* 1, 926–950. doi: 10.3390/cells1040926

Snapp, E. L., Sharma, A., Lippincott-Schwartz, J., and Hegde, R. S. (2006). Monitoring chaperone engagement of substrates in the endoplasmic reticulum of live cells. *Proc. Natl. Acad. Sci. U.S.A.* 103, 6536–6541. doi: 10.1073/pnas.0510657103

Tay, K. H., Luan, Q., Croft, A., Jiang, C. C., Jin, L., Zhang, X. D., et al. (2014). Sustained IRE1 and ATF6 signaling is important for survival of melanoma cells undergoing ER stress. *Cell. Signal.* 26, 287–294. doi: 10.1016/j.cellsig.2013.11.008

Thibault, G., Ismail, N., and Ng, D. T. W. (2011). The unfolded protein response supports cellular robustness as a broad-spectrum compensatory pathway. *Proc. Natl. Acad. Sci. U.S.A.* 108, 20597–20602. doi: 10.1073/pnas.1117184109

Thibault, G., Shui, G., Kim, W., McAlister, G. C., Ismail, N., Gygi, S. P., et al. (2012). The membrane stress response buffers lethal effects of lipid disequilibrium

by reprogramming the protein homeostasis network. *Mol. Cell* 48, 16–27. doi: 10.1016/j.molcel.2012.08.016

Torres, M., Matamala, J. M., Duran-Aniotz, C., Cornejo, V. H., Foley, A., and Hetz, C. (2015). ER stress signaling and neurodegeneration: at the intersection between Alzheimer's disease and Prion-related disorders. *Virus Res.* 207, 69–75. doi: 10.1016/j.virusres.2014.12.018

Travers, K. J., Patil, C. K., Wodicka, L., Lockhart, D. J., Weissman, J. S., and Walter, P. (2000). Functional and genomic analyses reveal an essential coordination between the unfolded protein response and ER-associated degradation. *Cell* 101, 249–258. doi: 10.1016/s0092-8674(00)80835-1

Upton, J.-P., Wang, L., Han, D., Wang, E. S., Huskey, N. E., Lim, L., et al. (2012). IRE1α cleaves select microRNAs during ER stress to derepress translation of proapoptotic Caspase-2. *Science* 338, 818–822. doi: 10.1126/science.1226191

Valenzuela, V., Martínez, G., Duran-Aniotz, C., and Hetz, C. (2016). Gene therapy to target ER stress in brain diseases. *Brain Res.* 1648, 561–570. doi: 10.1016/j.brainres.2016.04.064

van der Vlies, D., Woudenberg, J., and Post, J. A. (2003). Protein oxidation in aging: endoplasmic reticulum as a target. *Amino Acids* 25, 397–407. doi: 10.1007/s00726-003-0025-9

Verghese, J., Abrams, J., Wang, Y., and Morano, K. A. (2012). Biology of the heat shock response and protein chaperones: budding yeast (*Saccharomyces cerevisiae*) as a model system. *Microbiol. Mol. Biol. Rev.* 76, 115–158. doi: 10.1128/mmbr.05018-11

Vidal, R., Caballero, B., Couve, A., and Hetz, C. (2011). Converging pathways in the occurrence of endoplasmic reticulum (ER) stress in Huntington's disease. *Curr. Mol. Med.* 11, 1–12. doi: 10.2174/156652411794474419

Vidal, R. L., Figueroa, A., Court, F. A., Thielen, P., Molina, C., Wirth, C., et al. (2012). Targeting the UPR transcription factor XBP1 protects against Huntington's disease through the regulation of FoxO1 and autophagy. *Hum. Mol. Genet.* 21, 2245–2262. doi: 10.1093/hmg/dds040

Vidal, R. L., and Hetz, C. (2012). Crosstalk between the UPR and autophagy pathway contributes to handling cellular stress in neurodegenerative disease. *Autophagy* 8, 970–972. doi: 10.4161/auto.20139

Vieira, F. G., Ping, Q., Moreno, A. J., Kidd, J. D., Thompson, K., Jiang, B., et al. (2015). Guanabenz treatment accelerates disease in a mutant SOD1 mouse model of ALS. *PLoS One* 10:e0135570. doi: 10.1371/journal.pone.0135570

Voellmy, R. (2004). *Transcriptional Regulation of the Metazoan Stress Protein Response*. Amsterdam: Elsevier, 143–185.

Volmer, R., and Ron, D. (2015). Lipid-dependent regulation of the unfolded protein response. *Curr. Opin. Cell Biol.* 33, 67–73. doi: 10.1016/j.ceb.2014.12.002

Volmer, R., van der Ploeg, K., and Ron, D. (2013). Membrane lipid saturation activates endoplasmic reticulum unfolded protein response transducers through their transmembrane domains. *Proc. Natl. Acad. Sci. U.S.A.* 110, 4628–4633. doi: 10.1073/pnas.1217611110

Walter, P., and Ron, D. (2011). The unfolded protein response: from stress pathway to homeostatic regulation. *Science* 334, 1081–1086. doi: 10.1126/science.1209038

Wang, L., Popko, B., and Roos, R. P. (2014a). An enhanced integrated stress response ameliorates mutant SOD1-induced ALS. *Hum. Mol. Genet.* 23, 2629–2638. doi: 10.1093/hmg/ddt658

Wang, L., Popko, B., Tixier, E., and Roos, R. P. (2014b). Guanabenz, which enhances the unfolded protein response, ameliorates mutant SOD1-induced amyotrophic lateral sclerosis. *Neurobiol. Dis.* 71, 317–324. doi: 10.1016/j.nbd.2014.08.010

Welihinda, A. A., Tirasophon, W., and Kaufman, R. J. (1999). The cellular response to protein misfolding in the endoplasmic reticulum. *Gene Expr* 7, 293–300.

Werner, E. D., Brodsky, J. L., and McCracken, A. A. (1996). Proteasome-dependent endoplasmic reticulum-associated protein degradation: an unconventional route to a familiar fate. *Proc. Natl. Acad. Sci. U.S.A.* 93, 13797–13801. doi: 10.1073/pnas.93.24.13797

Yorimitsu, T., Nair, U., Yang, Z., and Klionsky, D. J. (2006). Endoplasmic reticulum stress triggers autophagy. *J. Biol. Chem.* 281, 30299–30304. doi: 10.1074/jbc.M607007200

Yoshida, H. (2007). ER stress and diseases. *FEBS J.* 274, 630–658. doi: 10.1111/j.1742-4658.2007.05639.x

Yoshida, H., Haze, K., Yanagi, H., Yura, T., and Mori, K. (1998). Identification of the cis-acting endoplasmic reticulum stress response element responsible for transcriptional induction of mammalian glucose-regulated proteins. Involvement of basic leucine zipper transcription factors. *J. Biol. Chem.* 273, 33741–33749. doi: 10.1074/jbc.273.50.33741

Yoshida, H., Matsui, T., Yamamoto, A., Okada, T., and Mori, K. (2001). XBP1 mRNA is induced by ATF6 and spliced by IRE1 in response to ER stress to produce a highly active transcription factor. *Cell* 107, 881–891. doi: 10.1016/s0092-8674(01)00611-0

Zhang, C., and Cuervo, A. M. (2008). Restoration of chaperone-mediated autophagy in aging liver improves cellular maintenance and hepatic function. *Nat. Med.* 14, 959–965. doi: 10.1038/nm.1851

Zhang, P., McGrath, B., Li, S., Frank, A., Zambito, F., Reinert, J., et al. (2002). The PERK eukaryotic initiation factor 2 alpha kinase is required for the development of the skeletal system, postnatal growth, and the function and viability of the pancreas. *Mol. Cell Biol.* 22, 3864–3874. doi: 10.1128/mcb.22.11.3864-3874.2002

Zinszner, H., Kuroda, M., Wang, X., Batchvarova, N., Lightfoot, R. T., Remotti, H., et al. (1998). CHOP is implicated in programmed cell death in response to impaired function of the endoplasmic reticulum. *Genes Dev.* 12, 982–995. doi: 10.1101/gad.12.7.982

Conflict of Interest Statement: The authors declare that the research was conducted in the absence of any commercial or financial relationships that could be construed as a potential conflict of interest.

frontiers in Physiology

BRIEF RESEARCH REPORT
published: 28 May 2019
doi: 10.3389/fphys.2019.00641

Deuterated Polyunsaturated Fatty Acids Reduce Oxidative Stress and Extend the Lifespan of *C. elegans*

*Caroline Beaudoin-Chabot[1], Lei Wang[1†], Alexey V. Smarun[2], Dragoslav Vidović[3], Mikhail S. Shchepinov[2] and Guillaume Thibault[1]**

[1] School of Biological Sciences, Nanyang Technological University, Singapore, Singapore, [2] Retrotope Inc., Los Altos, CA, United States, [3] School of Chemistry, Monash University, Melbourne, VIC, Australia

OPEN ACCESS

Edited by:
Mauricio Antonio Retamal, Universidad del Desarrollo, Chile

Reviewed by:
Andrey Y. Abramov, University College London, United Kingdom
Manuel Torres, Lipopharma Therapeutics, Spain
Leonardo R. Silveira, Campinas State University, Brazil

***Correspondence:**
Guillaume Thibault
thibault@ntu.edu.sg

†Present address:
Lei Wang, Department of Physiology and Biophysics, Miller School of Medicine, University of Miami, Miami, FL, United States

Specialty section:
This article was submitted to Membrane Physiology and Membrane Biophysics, a section of the journal Frontiers in Physiology

Received: *10 March 2019*
Accepted: *06 May 2019*
Published: *28 May 2019*

Citation:
Beaudoin-Chabot C, Wang L, Smarun AV, Vidović D, Shchepinov MS and Thibault G (2019) Deuterated Polyunsaturated Fatty Acids Reduce Oxidative Stress and Extend the Lifespan of C. elegans. Front. Physiol. 10:641. doi: 10.3389/fphys.2019.00641

Chemically reinforced essential fatty acids (FAs) promise to fight numerous age-related diseases including Alzheimer's, Friedreich's ataxia and other neurological conditions. The reinforcement is achieved by substituting the atoms of hydrogen at the bis-allylic methylene of these essential FAs with the isotope deuterium. This substitution leads to a significantly slower oxidation due to the kinetic isotope effect, inhibiting membrane damage. The approach has the advantage of preventing the harmful accumulation of reactive oxygen species (ROS) by inhibiting the propagation of lipid peroxidation while antioxidants potentially neutralize beneficial oxidative species. Here, we developed a model system to mimic the human dietary requirement of omega-3 in *Caenorhabditis elegans* to study the role of deuterated polyunsaturated fatty acids (D-PUFAs). Deuterated trilinolenin [D-TG(54:9)] was sufficient to prevent the accumulation of lipid peroxides and to reduce the accumulation or ROS. Moreover, D-TG(54:9) significantly extended the lifespan of worms under normal and oxidative stress conditions. These findings demonstrate that D-PUFAs can be used as a food supplement to decelerate the aging process, resulting in extended lifespan.

Keywords: polyunsaturated fatty acid (PUFA), deuterated fatty acid, oxidative stress, lipid peroxidation, lifespan, *C. elegans*, essential fatty acids, linolenic acid

INTRODUCTION

Sensitive to oxidative damage, the brain consumes around 20% of oxygen despite making only 2% of body weight. The brain is rich in polyunsaturated fatty acids (PUFAs) and oxygen in the lipid bilayer is particularly high reaching millimolar levels (Subczynski and Hyde, 1983). This tissue requires large quantity of ATP to maintain intracellular ion homeostasis resulting in high oxygen uptake. Iron also accumulates in the brain becoming problematic in late-life by catalyzing free radical reactions (Zecca et al., 2004). As the brain produces more mitochondria-generated superoxide compared to skeletal muscle, neuron produces more reactive oxygen species (ROS) with low levels of endogenous antioxidants (Malinska et al., 2009). As a result, the brain spends a quarter of its energy to maintain and repair lipid membranes damaged from ROS (Brenna and Carlson, 2014). Several studies demonstrated that blocking the production of lipid peroxides can be beneficial to prevent the development of Alzheimer's disease (AD), Parkinson's disease, and Huntington's disease (Huang et al., 1999; Lee et al., 2011; Reed, 2011; Gandhi et al., 2012; Shichiri, 2014; Deas et al., 2016).

Senescence is a major cause of age-related diseases, correlating with an accumulation of ROS (McHugh and Gil, 2018). Enhanced formation of ROS oxidizes lipids to generate peroxides and aldehydes. Unlike short-lived ROS, these lipid peroxidation (LPO) products can produce damage throughout the cell due to their non-radical nature. Thus, lipid peroxidation is also strongly linked to aging and the accumulation of LPO products has been observed in AD, Parkinson's disease, stroke, rheumatic arthritis, and cancer (Davies and Guo, 2014; Shichiri, 2014). However, clinical studies on the efficiency of antioxidants for these age-associated diseases have been disappointing.

The rate liming step of PUFA autoxidation is an ROS-driven hydrogen abstraction off a bis-allylic (between double bounds) methylene group, which is followed quickly by a series of transformations, generating toxic end-products (Shchepinov, 2007). During the nineties, there was a prominent research interest in dietary antioxidants generating hope as potential agent to slow aging and to prevent the development of ROS-related diseases. Disappointing results emerged from the studies conducted in humans (Moller and Loft, 2002). Thus, it appeared that human cells generate a certain amount of beneficial free radicals, playing important roles in cellular functions (Halliwell, 2011; Sena and Chandel, 2012; Yan, 2014). A balance of antioxidants and ROS must be kept *in vivo*, and supplementation of dietary antioxidants might compromise this critical equilibrium (Sies et al., 2017). This may be due to several reasons, including (1) the near-saturating amount of antioxidants already present in living cells and the stochastic nature of the ROS-inflicted damage, (2) the importance of ROS in cell signaling and hormetic upregulation of protective mechanisms, (3) the pro-oxidant nature of some antioxidants such as vitamin E, and (4) the non-radical nature of PUFA peroxidation products, which can no longer be quenched with most antioxidants (Shchepinov, 2011).

Mitochondrial membranes are rich in cardiolipin, predominantly containing linoleic acid (LA) and α-linolenic acid (ALA) FAs (Paradies et al., 2002; **Figure 1A**). Thus, as PUFAs are essential nutrients in human, supplementing a diet with deuterated bis-allylic methylenes could represent the most promising approach to fight against ROS-initiated attacks leading to alleviate the influence of aging and age-associated diseases on human life. In *Saccharomyces cerevisiae*, deuterated PUFAs (D-PUFAs) have been shown to reduce oxidative stress (Hill et al., 2011) by protecting mitochondria against ROS (Andreyev et al., 2015). In addition, D-PUFA prevented lipid peroxidation in primary co-cultures of neurons and astrocytes (Angelova et al., 2015) and in Friedreich ataxia model system (Cotticelli et al., 2013). More recently, D-PUFAs significantly ameliorated performance in cognitive and memory tests using the AD mouse model *Aldh2*$^{-/-}$ (Elharram et al., 2017). This recent finding suggests that D-PUFAs might be sufficient to reduce the generation of AD-induced lipid peroxidation and to prevent the cognitive decline in AD. In human, a recent randomized clinical trial has been conducted, demonstrating the safety and potential protective effect against Friedreich's ataxia (Zesiewicz et al., 2018). Friedreich's ataxia is a neurodegenerative disease associated with an increase of oxidative stress (Ventura et al., 2009). More than a decade ago, supplementing the diet with D-PUFAs was predicted to delay aging (Shchepinov, 2007). However, there is still no study reporting the role of D-PUFAs in modulating lifespan.

In this study, we characterized the role of D-PUFAs against ROS in the multicellular model organism *C. elegans*. This organism was recently reported to be sensitive to deuterated lysine (5,5-D_2-lysine) which strongly affected its development (Korneenko et al., 2017). To mimic the dietary requirement of omega-3 in human, we selected the omega-3 fatty acid desaturase *fat-1*(*loss-of-function*; *lof*) mutant worm which is also sensitive to the oxidative stress agent paraquat. Triglyceride with three omega-3 PUFAs, trilinolenin [TG(54:9)], was sufficient to induce lipid peroxidation while deuterated TG(54:9) [D-TG(54:9)] was protective. D-TG(54:9) reduced the oxidative stress response in addition of significantly extending the lifespan of *fat-1*(*lof*) under normal and oxidative stress conditions. These findings demonstrate that D-TG(54:9) is adequate to prevent the propagation of ROS-induced molecular damages resulting in a significant extension of lifespan.

MATERIALS AND METHODS

Statistics

Error bars indicate standard error of the mean (SEM), calculated from at least three biological replicates, unless otherwise indicated. *P*-values were calculated using one-way ANOVA with Tukey's test or log-rank test for lifespan, unless otherwise indicated and reported as *P*-values. All statistical tests were performed using GraphPad Prism 7 software.

C. elegans Strains, Bacterial Strains, and Food Additive

All strains were grown at 20°C using standard *C. elegans* methods as previously described (Koh et al., 2018). Nematode growth media (NGM) agar plates were seeded with *Escherichia coli* strain OP50 for normal growth. *C. elegans* strains wild type N2, *fat-1*(*bx24*), *mev-1*(*tk22*), *gst-4p::GFP::NLS*(*cl2166*), *sod-3p::GFP*(*cf1553*) and bacteria strains *OP50* were gifted from the *Caenorhaditis* Genetics Center. Trilinolenin [TG(54:9)] was obtained from Nu-Chek Prep and deuterated at bis-allylic position as previously described (Smarun et al., 2017) to obtained a mixture of 76% deuterated TG(54:9) [D-TG(54:9)]. Lipids were stored into an atmosphere of argon to prevent lipid oxidation. Lipids were freshly dissolved in PBS buffer (137 mM NaCl, 10 mM phosphate, 2.7 mM KCl, pH 7.4) containing 0.1% Triton X-100 or kept at −80°C for later use prior to supplementing NGM agar plate as previously described (Deline et al., 2013). Butylated hydroxytoluene (BHT) and paraquat (PQ) were obtained from Sigma and Acros Organics, respectively.

Lifespan Assays

Lifespan assays were performed at 20°C as previously described (Apfeld and Kenyon, 1999). Synchronized animals were transferred to NGM plates containing 0.2 mM BHT, 1 mM

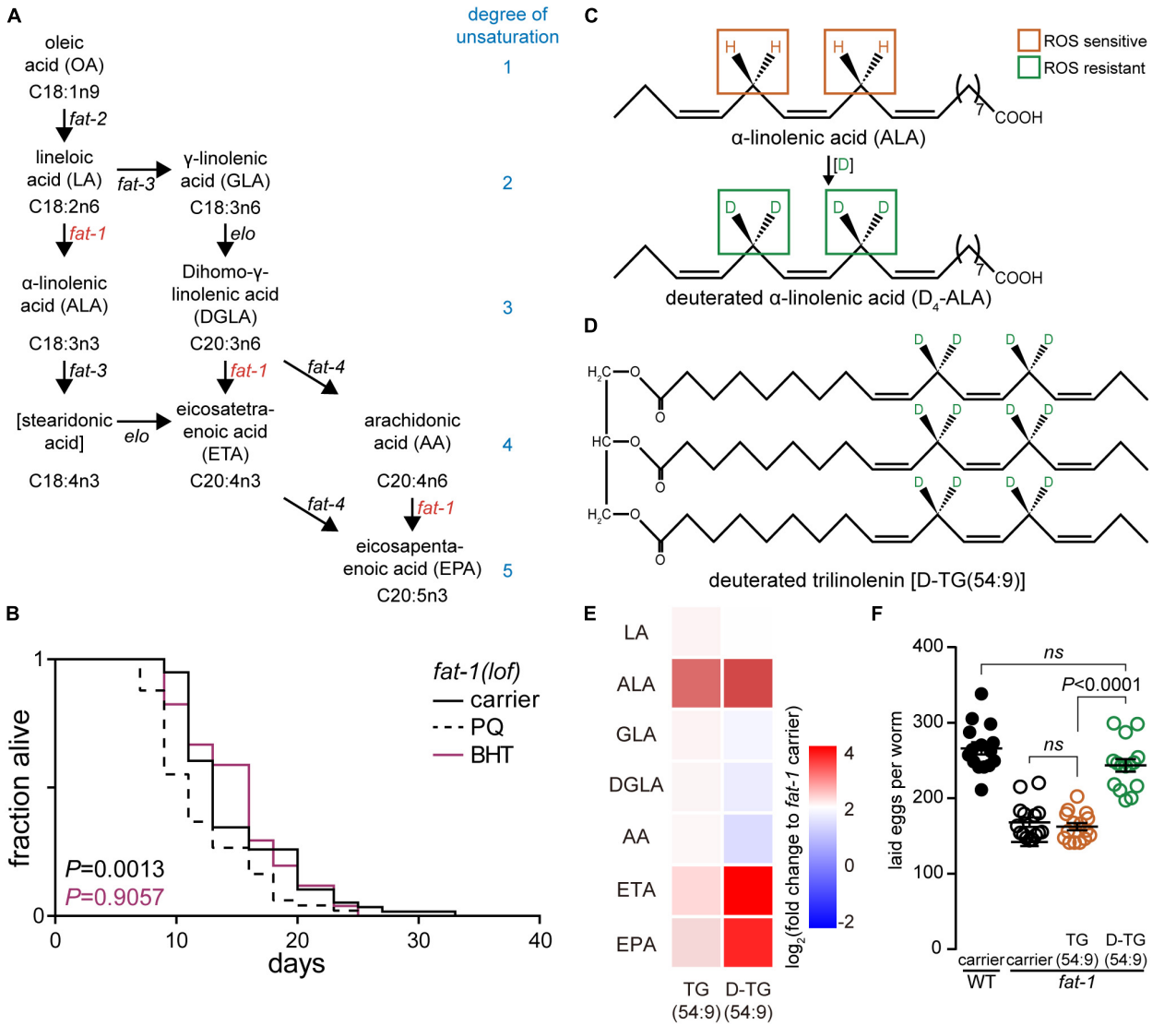

FIGURE 1 | Deuterated trilinolenin rescues *fat-1* infertility phenotype. **(A)** Polyunsaturated fatty acid (PUFA) biosynthesis in *C. elegans*. Key enzymes *fat-1* and *fat-2* are highlighted in red. Adapted from Shmookler Reis et al. (2011). **(B)** Lifespan assay of *fat-1*(*lof*) subjected to carrier, 0.2 mM butylated hydroxytoluene (BHT), or 1 mM PQ. Log-rank test to carrier. **(C)** α-linolenic acid (ALA) is susceptible to oxidation attacks while deuterated ALA (D4-ALA) is protected. **(D)** Schematic representation of deuterated trilinolenin [D-TG(54:9)]. **(E)** Heat map of PUFAs extracted in *fat-1*(*lof*) supplemented with carrier, 0.48 mM trilinolenin [TG(54:9)] or 0.48 mM deuterated trilinolenin [D-TG(54:9)]. **(F)** Number of laid eggs per worm of WT and *fat-1*(*lof*) animals treated as in **(E)**.

paraquat (PQ), 0.48 mM TG(54:9), or 0.48 mM D-TG(54:9), when indicated. Pyrimidine analog 5-fluoro-2'-deoxyuridine (FUdR, Sigma; St. Louis) was added at 50 μM to pre-fertile young adult worms to prevent development of progeny. Adults were scored manually as dead or alive every 2–3 day. Nematodes which ceased pharyngeal pumping and had no respond to gentle stimulation were recorded as dead. Those worms that were male, crawled off the plate or non-natural death were censored.

Lipid Analysis

Synchronized L1 animals were transferred to NGM plates containing 0.48 mM TG(54:9), 0.48 mM D-TG(54:9) or carrier. Approximately 10,000 L4 to young adult worms were harvested and washed thoroughly with M9 buffer and lyophilised overnight (Vertis, Warminster, PA, United States). FAs were esterified to fatty acid methyl esters (FAME) with 300 μl of 1.25 M HCl-methanol for 1 h at 80°C. FAMEs were extracted three times with 1 ml of hexane. Combined extracts were dried under nitrogen, resuspended in 100 μl hexane. FAMEs were separated by gas chromatography with flame ionization detector (GC-FID; GC-2014; Shimadzu, Kyoto, Japan) using an ULBON HR-SS-10 50 m × 0.25 mm column (Shinwa, Tokyo, Japan). Supelco 37 component FAME mix was used to identify corresponding FAs (Sigma-Aldrich, St. Louis, MO, United States). Data was normalized

using internal standard pentadecanoic acid (C15:0) and worm dry weight.

TBARS Assay

Synchronized L1 mev-1 mutants were transferred to NGM plates containing 0.1 mM BHT, 0.48 mM TG(54:9), 0.48 mM D-TG(54:9) or carrier for 54 h, after which they were transferred on supplemented plates with 8 mM paraquat when indicated for 24 h. Approximately 1,000 L4 to adult worms were harvested and washed thoroughly with M9 buffer, resuspended in 300 µl RIPA buffer (50 mM Tris–HCL pH7.5, 150 mM NaCl, 2 mM EDTA, 1% NP-40, 0.1% SDS), lysed with 1 mm silica beads by bead beating. Protein concentration was carried out using the Bicinchoninic Acid (BCA) Protein Assays kit following manufacturer's protocol (Sigma; St. Louis). Assays for lipid peroxidation, using the thiobarbituric acid reactive substrate (TBARS) kit were performed following manufacturer's protocol (Cayman Chemical).

BODIPY-C11 Lipid Peroxidation Reporter Assay

Synchronized L1 mev-1 animals were transferred to NGM plates containing 0.1 mM BHT, 0.48 mM TG(54:9), 0.48 mM D-TG(54:9) or carrier and supplemented with 5 mM paraquat when indicated. L4 to young adult worms were transferred to 10 µM BODIPY 581/591 undecanoic acid (BODIPY$^{581-591}$-C11) solution and stained for 30 min and washed three times with M9. Images were captured using confocal fluorescence microscope Zeiss LSM 710 microscope with a 20 × objective (Carl Zeiss MicroImaging). Oxidized and non-oxidized BODIPY$^{581-591}$-C11 were excited at 488 and 568 and images were collected from emission at 530(30) and 590(30) nm, respectively. Fluorescence signal ratio of oxidized to non-oxidized BODIPY was normalized to carrier.

Fluorescence Microscopy

Synchronized L1 *gst-4p::GFP* or *sod-3p::GFP* worms were transferred to NGM plates containing 0.48 mM TG(54:9), 0.48 mM D-TG(54:9) or carrier and supplemented with 5 mM paraquat when indicated. To quantify GFP signal, worms were immobilized with 25 mM tetramisole and mounted on 2% agarose pad. Images were captured using Zeiss Axiovert 200 M fluorescence microscope with a 20 × objective. Images were stitched, and total fluorescence were quantified using Fiji ImageJ software.

Egg Counting Assay

Synchronized L1 WT and *fat-1*(*lof*) animals were transferred to NGM plates containing 0.48 mM TG(54:9), or 0.48 mM D-TG(54:9) and supplemented with 5 µM 5-fluoro-2'-deoxyuridine (FUdR, Sigma; St. Louis) to facilitate the counting of the eggs. The fertility of the worms was scored by counting eggs on day 5 and 6 after the transfer of the adults to a new plate.

RESULTS

Worm Lacking *fat-1* as a Model to Mimic Human Dietary Needs of Omega-3

In human, FAs lineloic acid (LA; omega-6) and α-linolenic acid (ALA; omega-3) are essentials (MacLean et al., 2004). In contrast, *C. elegans* synthesize both LA and ALA consequently we selected omega-3 fatty acid desaturase *fat-1*(*loss-of-function*; *lof*) mutant animal to mimic the human dietary requirement of ALA (Watts and Browse, 2002; **Figure 1A**). We tested different ROS agents including paraquat (PQ) and 95% oxygen (data not shown). Paraquat is reduced into radical from the mitochondrial leaking electrons to induce the production of superoxide radicals such as superoxide anion radical ($O_2^{\bullet-}$).

TABLE 1 | Lifespan analysis.

Strains	Treatment*	Mean lifespan ± SEM (days)	75%	% change to control	Number of animals	*P*-values versus carrier	Figure
fat-1(*lof*)	carrier	14.8 ± 0.7	19		58/60		**Figure 1C**
	PQ	11.7 ± 0.6	13	−21	55/60	0.0002	
	BHT	15.1 ± 0.6	18	+3	51/60	0.9057	
fat-1(*lof*)	TG(54:9)	19.6 ± 0.6	21		59/60		**Figure 4A**
	D-TG(54:9)	21.4 ± 0.6	23	+9**	56/60	0.0230**	
fat-1(*lof*)	carrier + PQ	11.7 ± 0.6	13	0	55/60		**Figure 4B**
	TG(54:9) + PQ	13.3 ± 0.8	18	+14	55/60	0.5070	
	D-TG(54:9) + PQ	16.7 ± 1.0	18	+43	42/60	0.0001	
fat-1(*lof*)	carrier	25.6 ± 0.8	29		58/60		biological replicates for **Figure 1C**
	PQ	22.9 ± 0.9	25	−10	48/60	0.0725	
	BHT	23.7 ± 0.9	27	−8	50/60	0.1952	
fat-1(*lof*)	TG(54:9)	12.5 ± 0.6	16		42/60		biological replicates for **Figure 4A**
	D-TG(54:9)	16.4 ± 0.7	18	+31**	47/60	<0.0001**	

*BHT, 0.2 mM butylated hydroxytoluene; PQ, 1 mM paraquat; TG(54:9), 0.48 mM trilinolenin; D-TG(54:9), 0.48 mM deuterated trilinolenin.
**compared to TG(54:9) treatment.

In turn, hydroperoxyl radicals $HO_2^{\bullet}$ modify PUFAs through oxidative damage in a chain-propagation fashion (Bielski et al., 1983; De Grey, 2002). As low levels of oxidative stress has been reported to increase the lifespan of *C. elegans* (Wei and Kenyon, 2016) while high levels decrease lifespan (Schaar et al., 2015), we carried out a lifespan assay with *fat-1*(*lof*) worms. As expected, high concentration of 1 mM paraquat significantly reduced the lifespan of *fat-1*(*lof*) worms compared to carrier (**Figure 1B** and **Table 1**). This result indicates that *fat-1*(*lof*) worms are sensitive to the production of ROS by the toxic level of paraquat. We also subjected *fat-1*(*lof*) worms to the antioxidant BHT but the lifespan was unchanged compared to carrier. This result suggests that *fat-1*(*lof*) basal level of ROS is not harmful and neutralising ROS further with antioxidant does not influence *fat-1*(*lof*) longevity.

Trilinolenin Aggravates *fat-1(lof)* Infertility Phenotype

The protective effect of D-PUFAs against ROS has been demonstrated in yeast (Hill et al., 2011; Cotticelli et al., 2013; Andreyev et al., 2015), in primary co-cultures of neurons and astrocytes (Angelova et al., 2015) as well as in AD mouse model *Aldh2*$^{-/-}$ (Elharram et al., 2017) by supplementing the media with deuterated LA or ALA (**Figure 1C**; Hill et al., 2011; Cotticelli et al., 2013; Andreyev et al., 2015). We generated deuterated ALA from trilinolenin [TG(54:9)] to obtain deuterated trilinolenin [D-TG(54:9)] as triglycerides reflect human intake mainly consisting of esterified FAs (**Figure 1D**). The replacement of hydrogen by deuterium at the potential four bis-allylic CH_2 group between the two double bonds was effective at 97.5% (data not shown) using our recently reported site-specific deuteration

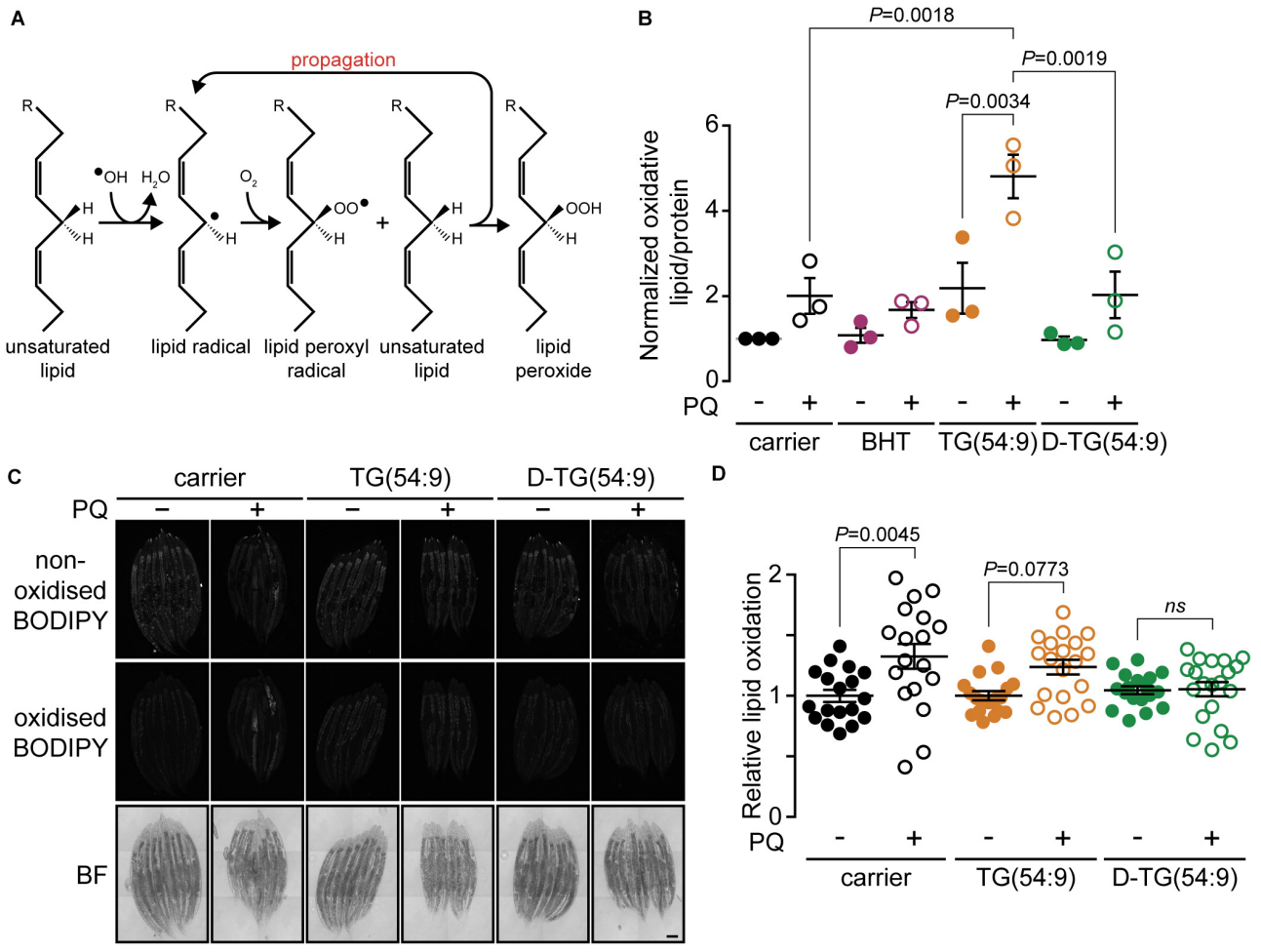

FIGURE 2 | Trilinolenin is sufficient to induce lipid peroxidation while deuterated trilinolenin is protective. **(A)** Schematic representation of lipid peroxidation. **(B)** Normalized oxidized lipids of *mev-1*(*lof*) worms fed OP50 supplemented with carrier, 0.1 mM BHT, 0.48 mM trilinolenin [TG(54:9)] or 0.48 mM deuterated trilinolenin [D-TG(54:9)] and subjected to 8 mM paraquat (PQ) when indicated. **(C)** Representative confocal fluorescence images of *mev-1*(*lof*) worms fed OP50 supplemented with carrier, 0.48 mM trilinolenin [TG(54:9)] or 0.48 mM deuterated trilinolenin [D-TG(54:9)] and subjected to 5 mM paraquat (PQ) when indicated. Scale bar, 100 μm. **(D)** Quantification of oxidized to non-oxidized BODIPY581/591-C11 from **(C)**.

of polyunsaturated alkenes method (Smarun et al., 2017). To ensure that *C. elegans* ingests and metabolizes D-TG(54:9) as well as non-deuterated TG(54:9), we fed L1 larvae *fat-1*(*lof*) mutant with standard diet on NGM plates supplemented with 0.48 mM TG(54:9), D-TG(54:9), or the carrier (0.1% Triton X-100 in PBS). *C. elegans* is typically fed *E. coli* OP50 bacteria in which PUFAs are naturally absent but can be easily incorporated if supplemented to the media (Webster et al., 2013). Worms were harvested at stage larva 4 (L4)/young adult and lyophilized. Dried worms were subjected to derivatisation with hydrogen chloride in methanol to generate FAME. FAMEs were extracted with hexane and separated on GC-FID using a capillary column (Ulbon HR-SS-10). We observed a significant accumulation of eicosatetraenoic acid (ETA) and eicosapentaenoic acid (EPA) in *fat-1*(*lof*) fed D-TG(54:9) while the other changes were statistically non-significant compared to carrier (**Figure 1E**). This result indicates that deuterated α-linolenic acid is metabolized by *C. elegans* as a precursor to synthesize PUFAs with higher degrees of unsaturation.

Next, we asked if D-TG(54:9) is toxic to *fat-1*(*lof*) mutant by measuring its fertility which is diminished by ROS (Alcantar-Fernandez et al., 2018). As Δ9 fatty acid desaturases *fat-6*;*fat-7* double mutant exhibits lower fertility (Brock et al., 2007), we monitored the number of laid eggs in wild-type (WT, N2) and *fat-1*(*lof*) mutant with standard diet on NGM plates supplemented with 0.48 mM TG(54:9), D-TG(54:9), or the carrier. On carrier, *fat-1*(*lof*) mutant laid a significant lower amount of eggs compared to WT (**Figure 1F**). Similarly, *fat-1*(*lof*) mutant, fed TG(54:9), laid a similar amount of eggs per worm compared to *fat-1*(*lof*) mutant on carrier. To our surprise, *fat-1*(*lof*) mutant, fed D-TG(54:9), laid a similar amount of eggs per worm compared to WT. This result suggests that D-TG(54:9) promotes fertility in *fat-1*(*lof*) mutant while TG(54:9) might promote lipid peroxidation.

Trilinolenin Is Sufficient to Induce Lipid Peroxidation While Deuterated Trilinolenin Is Protective Upon Oxidative Stress

As PUFAs contribute to the generation of oxidative stress through the propagation of lipid peroxide (Porter et al., 1995; Yin et al., 2011; **Figure 2A**), we hypothesized that TG(54:9) will intensify paraquat-induced lipid peroxidation. Lipid peroxidation was monitored by measuring thiobarbituric acid reactive substances (TBARS) (Lagman et al., 2015) in lipid peroxidation-sensitive *mev-1*(*lof*) mutant worms (Labuschagne et al., 2013). The protein MEV-1 is the homolog of succinate dehydrogenase cytochrome

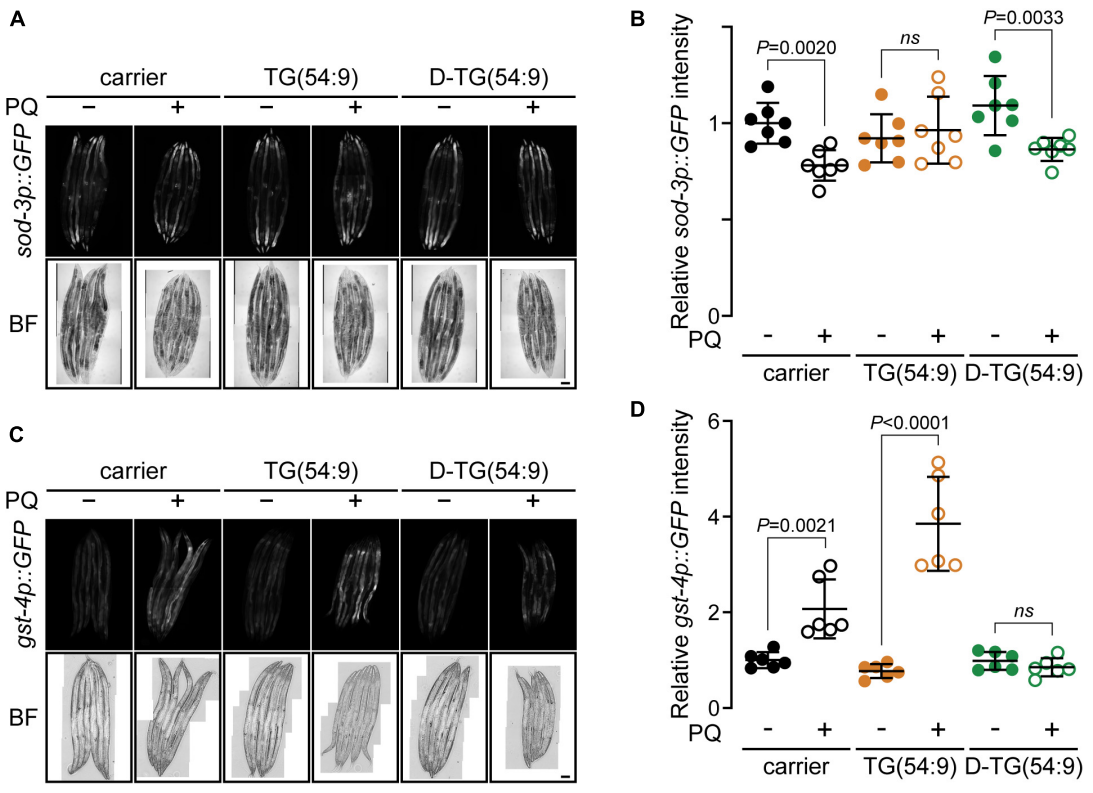

FIGURE 3 | Deuterated trilinolenin reduces oxidative stress response. **(A)** Representative confocal fluorescence images of *sod-3p::GFP* transgenic worms fed OP50 supplemented with carrier, trilinolenin [TG(54:9)] or deuterated trilinolenin [D-TG(54:9)] and subjected to 5 mM paraquat (PQ) when indicated. Scale bar, 100 μm. **(B)** Quantification of A. **(C)** Representative confocal fluorescence images of *gst-4p::GFP::NLS* transgenic worms treated as in A fed OP50 supplemented with carrier, trilinolenin [TG(54:9)] or deuterated trilinolenin [D-TG(54:9)] and subjected to 5 mM paraquat (PQ) when indicated. Scale bar, 100 μm. **(D)** Quantification of C.

b560 subunit of the mitochondrial respiratory chain complex II (Ishii et al., 1998). Synchronized L1 *mev-1*(*lof*) mutants were grown on NGM plates seeded with bacteria supplemented with carrier, BHT, TG(54:9), or D-TG(54:9). Subsequently, L4/young adult *mev-1*(*lof*) mutants were exposed to 24 h of paraquat. Paraquat alone was insufficient to significantly increase the accumulation of lipid peroxide compared to carrier alone (**Figure 2B**). On the other hand, *mev-1*(*lof*) mutants grown on TG(54:9) and subjected to paraquat exhibited a dramatic increase in lipid peroxides compared to paraquat alone and to TG(54:9) in the absence of paraquat. This result reinforces the role of PUFAs in catalyzing the propagation of ROS through lipid peroxidation (Yang et al., 2016). D-TG(54:9) was sufficient to prevent the propagation of paraquat-induced ROS through lipid peroxidation. This result indicates that D-PUFAs, in the form of triacylglycerol, are resistant to ROS and thus preventing further cellular damages.

To further assess the role of D-TG(54:9) in preventing the formation of lipid peroxides, we monitored *in vivo* fluorescence of the sensor BODIPY$^{581/591}$ undecanoic acid (BODIPY$^{581/591}$-C11). The sensor emission peak shifts from 590 to 510 nm when the polyunsaturated butadienyl domain is oxidized (Naguib, 1998; Aldini et al., 2001). *mev-1*(*lof*) mutants were grown and treated as for the TBARS assay. In contrast to the TBARS assay, paraquat alone was sufficient to significantly induce lipid peroxidation (**Figures 2C,D**). This suggests that BODIPY$^{581/591}$-C11 is more sensitive than the TBARS assay to monitor lipid peroxidation in *C. elegans* as previously reported in different cell types (Dominguez-Rebolledo et al., 2010). In contrast to the TBARS assay, TG(54:9) combined with paraquat did not induce lipid peroxidation further compared to paraquat alone in *mev-1*(*lof*) mutants. D-TG(54:9) was sufficient to protect *mev-1*(*lof*) mutants against paraquat-induced lipid peroxidation. As the BODIPY-C11 lipid peroxidation reporter assay yielded small differences, BODIPY possibly failed to be incorporated evenly through the animal and perhaps not sufficiently where most of lipid peroxidation occurs. Together with the TBARS assay, these results demonstrate that D-PUFA is sufficient to prevent lipid peroxidation in *C. elegans*.

Deuterated Trilinolenin Reduces Oxidative Stress Response

To further assess the role of D-TG(54:9) in preventing the propagation of lipid peroxide, we monitored the oxidative stress response *in vivo*. We monitored the expression of the reporter protein GFP under the promotor *sod-3* (*sod-3p::GFP*) (Xu and Kim, 2012). SOD-3 is a mitochondrial superoxide dismutase which has been reported to increase transcriptionally as a result of oxidative stress (An and Blackwell, 2003). These worms were grown and treated as per the TBARS assay. No significant increase in the expression of *sod-3p::GFP* was observed across the different conditions (**Figures 3A,B**). As this assay was inconclusive, we used the transgenic worm expressing GFP tagged with a nuclear localisation signal under the promotor *gst-4* (*gst-4p::GFP::NLS*) (Paek et al., 2012). GST-4 is a glutathione S-transferase protein that responds to oxidative stress by an increase at the transcription and translational levels (Link and Johnson, 2002). Glutathione S-transferases protect cells against lipid peroxidation (Yang et al., 2001). *gst-4p::GFP::NLS* worms were grown with triacylglycerol and paraquat as per the TBARS assay. The expression of *gst-4p::GFP::NLS* was significantly increased in the presence of paraquat and further increase with the addition of TG(54:9) (**Figures 3C,D**). On the other hand, no significant change in GFP expression was observed in animals fed D-TG(54:9) in the absence or the presence of paraquat. Consistent with the TBARS assay, these findings further demonstrate that TG(54:9) is harmful by exponentially propagating paraquat-induced ROS while D-TG(54:9) exhibit a strong protective effect.

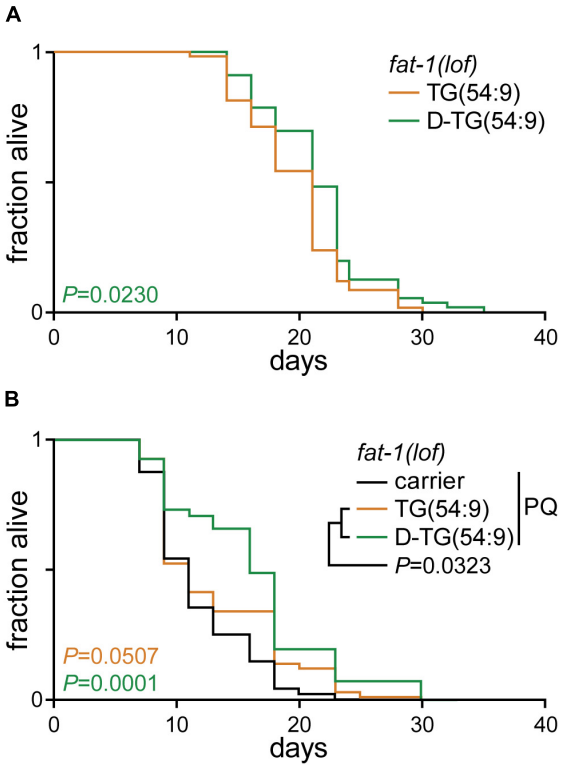

FIGURE 4 | Deuterated trilinolenin reduces lipid peroxidation. **(A)** Lifespan assay of *fat-1*(*lof*) worms fed OP50 supplemented with 0.48 mM trilinolenin [TG(54:9)] or 0.48 mM deuterated trilinolenin [D-TG(54:9)]. Log-rank test to control. **(B)** Lifespan assay of worms fed OP50 supplemented with carrier, trilinolenin [TG(54:9)] or deuterated trilinolenin [D-TG(54:9)] and subjected to 1 mM paraquat (PQ). Log-rank test to control.

Deuterated Trilinolenin Extend Lifespan Under Both Normal and Oxidative Stress Conditions

As D-TG(54:9) reduces oxidative stress, we carried out a lifespan assay of *fat-1*(*lof*) worms fed normal diet supplemented with either TG(54:9) or D-TG(54:9). D-TG(54:9) significantly extended the lifespan of worms compared to the supplementation with TG(54:9) (**Figure 4A** and **Table 1**). This suggests that

D-TG(54:9) might be sufficient to prevent endogenous ROS-induced cellular damages associated with aging. To further assess the role of D-TG(54:9) on the lifespan of *fat-1*(*lof*) worms, we exposed the animals to paraquat from L1 stage. As expected, the lifespan of *fat-1*(*lof*) worms exposed to paraquat was not significantly extended by TG(54:9) (**Figure 4B** and **Table 1**). As *fat-1*(*lof*) worms are unable to synthesize several PUFAs (**Figure 1A**), TG(54:9) might be necessary as a precursor of PUFAs ETA and EPA to extend the lifespan although the animals are under oxidative stress condition. It should be noted that worms were exposed to a fifth of the paraquat concentration used to monitor lipid peroxidation and oxidative stress. The lifespan of *fat-1*(*lof*) worms exposed to paraquat was further extended with D-TG(54:9) compared to paraquat alone and to TG(54:9) in combination with paraquat. This result indicates that D-TG(54:9) is sufficient to promote longevity. Potentially, supplementing a human diet with D-PUFAs might be sufficient to decelerate aging and to prevent the progression of age-associated diseases.

DISCUSSION

Chemically reinforced essential FAs have the potential to target age-related diseases such as Alzheimer's, Friedreich's ataxia and other neurological conditions. Substituting the atoms of hydrogen at the bis-allylic methylene of essential polyunsaturated FAs with isotope deuterium prevents substantial chemical damage. Recently, we developed a novel synthesis approach to reinforced natural FAs (Smarun et al., 2017), which could potentially be scaled up to industrial quantities. These deuterated FAs have the advantage to prevent harmful accumulation of ROS by disfavouring the formation of lipid peroxides while antioxidants are poorly transported within the cell. The results presented in this study show that D-TG(54:9) is sufficient to prevent the accumulation of lipid peroxides in animals and to reduce the accumulation of ROS. We used four different approaches which, together, clearly demonstrate the protective effect of deuterated trilinolenin against paraquat-induced oxidative stress while non-deuterated trilinolenin promotes the propagation of lipid peroxide. Supplementing the diet with D-PUFAs was anticipated to delay aging (Shchepinov, 2007). As predicted, D-TG(54:9) significantly extends the lifespan of worms under both normal and oxidative stress conditions when compared to non-deuterated trilinolenin [TG(54:9)]. It should be noted that D-PUFA must be in low abundance to be beneficial (Kinghorn et al., 2015). Taken together, we have developed a toolkit to monitor the protective role of deuterated FAs against age-related model diseases as well as longevity, allowing future high-throughput discoveries.

During the late nineties, a large boom of research on dietary antioxidants generated hopes as potential agents to slow aging and to prevent the development of ROS-related diseases. However, mixed results emerged from studies conducted in humans (Moller and Loft, 2002). It became clear that human cells generate a certain number of free radicals that play an important role in cellular functions (Halliwell, 2011; Sena and Chandel, 2012; Yan, 2014). A balance of antioxidants and reactive species must be kept *in vivo*, and supplementation of dietary antioxidants might compromise this delicate equilibrium. More importantly, as PUFAs belong to the group of essential nutrients that must be supplied with diet, it was proposed that PUFAs with deuterated bis-allylic methylenes could represent a novel approach to fight against ROS-initiated attacks, leading to lessening the influence of aging and age-associated diseases on human life.

The protective effect of D-PUFAs against ROS has been demonstrated in yeast and in primary co-cultures of neurons and astrocytes (Hill et al., 2011; Cotticelli et al., 2013; Andreyev et al., 2015; Angelova et al., 2015). As unicellular organisms uniformly absorb FAs, it is imperative to assess the protective role of D-PUFA that is absorbed in the intestine and disseminated to different tissues of a multicellular organism. Recently, D-PUFAs was shown to improve cognition and to reduce lipid peroxidation in the brain of several neurodegenerative disease models (Elharram et al., 2017; Hatami et al., 2018; Raefsky et al., 2018). Similarly in *C. elegans*, we have demonstrated that H-PUFA promotes, while D-PUFA reduces, both lipid peroxidation and oxidative stress during paraquat-induced oxidative stress. For the first time, we have demonstrated the beneficial effect of D-PUFAs in extending longevity. In future, *C. elegans* could be used to validate the beneficial role of D-PUFAs in modulating the lifespan of different disease models.

DATA AVAILABILITY

All datasets generated for this study are included in the manuscript and/or the supplementary files.

AUTHOR CONTRIBUTIONS

GT conceived the study, wrote the original draft of the manuscript, and acquired the funding. CB-C and GT performed the methodology. CB-C and LW contributed to formal analysis. CB-C investigated the study. CB-C, AS, MS, and DV performed the resources. MS and GT wrote, reviewed, and edited the manuscript.

FUNDING

This work was supported by funds from the Singapore Ministry of Education Academic Research Fund Tier 2 (MOE2018-T2-1-002) and Nanyang Assistant Professorship program from Nanyang Technological University, Singapore (GT).

ACKNOWLEDGMENTS

We thank members of Thibault lab for critical reading of the manuscript. Some strains were provided by the CGC, which is funded by NIH Office of Research Infrastructure Programs (P40 OD010440).

REFERENCES

Alcantar-Fernandez, J., Navarro, R. E., Salazar-Martinez, A. M., Perez-Andrade, M. E., and Miranda-Rios, J. (2018). Caenorhabditis elegans respond to high-glucose diets through a network of stress-responsive transcription factors. *PLoS One* 13:e0199888. doi: 10.1371/journal.pone.0199888

Aldini, G., Yeum, K. J., Russell, R. M., and Krinsky, N. I. (2001). A method to measure the oxidizability of both the aqueous and lipid compartments of plasma. *Free Radic. Biol. Med.* 31, 1043–1050. doi: 10.1016/s0891-5849(01)00684-0

An, J. H., and Blackwell, T. K. (2003). SKN-1 links C. elegans mesendodermal specification to a conserved oxidative stress response. *Genes Dev.* 17, 1882–1893. doi: 10.1101/gad.1107803

Andreyev, A. Y., Tsui, H. S., Milne, G. L., Shmanai, V. V., Bekish, A. V., Fomich, M. A., et al. (2015). Isotope-reinforced polyunsaturated fatty acids protect mitochondria from oxidative stress. *Free Radic. Biol. Med.* 82, 63–72. doi: 10.1016/j.freeradbiomed.2014.12.023

Angelova, P. R., Horrocks, M. H., Klenerman, D., Gandhi, S., Abramov, A. Y., and Shchepinov, M. S. (2015). Lipid peroxidation is essential for alpha-synuclein-induced cell death. *J. Neurochem.* 133, 582–589. doi: 10.1111/jnc.13024

Apfeld, J., and Kenyon, C. (1999). Regulation of lifespan by sensory perception in *Caenorhabditis elegans*. *Nature* 402, 804–809. doi: 10.1038/45544

Bielski, B. H., Arudi, R. L., and Sutherland, M. W. (1983). A study of the reactivity of HO2/O2- with unsaturated fatty acids. *J. Biol. Chem.* 258, 4759–4761.

Brenna, J. T., and Carlson, S. E. (2014). Docosahexaenoic acid and human brain development: evidence that a dietary supply is needed for optimal development. *J. Hum. Evol.* 77, 99–106. doi: 10.1016/j.jhevol.2014.02.017

Brock, T. J., Browse, J., and Watts, J. L. (2007). Fatty acid desaturation and the regulation of adiposity in *Caenorhabditis elegans*. *Genetics* 176, 865–875. doi: 10.1534/genetics.107.071860

Cotticelli, M. G., Crabbe, A. M., Wilson, R. B., and Shchepinov, M. S. (2013). Insights into the role of oxidative stress in the pathology of friedreich ataxia using peroxidation resistant polyunsaturated fatty acids. *Redox. Biol.* 1, 398–404. doi: 10.1016/j.redox.2013.06.004

Davies, S. S., and Guo, L. (2014). Lipid peroxidation generates biologically active phospholipids including oxidatively N-modified phospholipids. *Chem. Phys. Lipids* 181, 1–33. doi: 10.1016/j.chemphyslip.2014.03.002

De Grey, A. D. (2002). HO2*: the forgotten radical. *DNA Cell Biol.* 21, 251–257. doi: 10.1089/104454902753759672

Deas, E., Cremades, N., Angelova, P. R., Ludtmann, M. H., Yao, Z., Chen, S., et al. (2016). Alpha-synuclein oligomers interact with metal ions to induce oxidative stress and neuronal death in parkinson's disease. *Antioxid. Redox. Signal.* 24, 376–391. doi: 10.1089/ars.2015.6343

Deline, M. L., Vrablik, T. L., and Watts, J. L. (2013). Dietary supplementation of polyunsaturated fatty acids in *Caenorhabditis elegans*. *J. Vis. Exp.* 2013:50879. doi: 10.3791/50879

Dominguez-Rebolledo, A. E., Martinez-Pastor, F., Fernandez-Santos, M. R., del Olmo, E., Bisbal, A., Ros-Santaella, J. L., et al. (2010). Comparison of the TBARS assay and BODIPY C11 probes for assessing lipid peroxidation in red deer spermatozoa. *Reprod. Domest. Anim.* 45, e360–e368. doi: 10.1111/j.1439-0531.2009.01578.x

Elharram, A., Czegledy, N. M., Golod, M., Milne, G. L., Pollock, E., Bennett, B. M., et al. (2017). Deuterium-reinforced polyunsaturated fatty acids improve cognition in a mouse model of sporadic Alzheimer's disease. *FEBS J.* 284, 4083–4095. doi: 10.1111/febs.14291

Gandhi, S., Vaarmann, A., Yao, Z., Duchen, M. R., Wood, N. W., and Abramov, A. Y. (2012). Dopamine induced neurodegeneration in a PINK1 model of Parkinson's disease. *PLoS One* 7:e37564. doi: 10.1371/journal.pone.0037564

Halliwell, B. (2011). Free radicals and antioxidants - quo vadis? *Trends Pharmacol. Sci.* 32, 125–130. doi: 10.1016/j.tips.2010.12.002

Hatami, A., Zhu, C., Relano-Gines, A., Elias, C., Galstyan, A., Jun, M., et al. (2018). Deuterium-reinforced linoleic acid lowers lipid peroxidation and mitigates cognitive impairment in the Q140 knock in mouse model of Huntington's disease. *FEBS J.* doi: 10.1111/febs.14590 [Epub ahead of print].

Hill, S., Hirano, K., Shmanai, V. V., Marbois, B. N., Vidovic, D., Bekish, A. V., et al. (2011). Isotope-reinforced polyunsaturated fatty acids protect yeast cells from oxidative stress. *Free Radic. Biol. Med.* 50, 130–138. doi: 10.1016/j.freeradbiomed.2010.10.690

Huang, X., Atwood, C. S., Hartshorn, M. A., Multhaup, G., Goldstein, L. E., Scarpa, R. C., et al. (1999). The A beta peptide of Alzheimer's disease directly produces hydrogen peroxide through metal ion reduction. *Biochemistry* 38, 7609–7616. doi: 10.1021/bi990438f

Ishii, N., Fujii, M., Hartman, P. S., Tsuda, M., Yasuda, K., Senoo-Matsuda, N., et al. (1998). A mutation in succinate dehydrogenase cytochrome b causes oxidative stress and ageing in nematodes. *Nature* 394, 694–697. doi: 10.1038/29331

Kinghorn, K. J., Castillo-Quan, J. I., Bartolome, F., Angelova, P. R., Li, L., Pope, S., et al. (2015). Loss of PLA2G6 leads to elevated mitochondrial lipid peroxidation and mitochondrial dysfunction. *Brain* 138(Pt 7), 1801–1816. doi: 10.1093/brain/awv132

Koh, J. H., Wang, L., Beaudoin-Chabot, C., and Thibault, G. (2018). Lipid bilayer stress-activated IRE-1 modulates autophagy during endoplasmic reticulum stress. *J. Cell Sci.* 131:jcs217992. doi: 10.1242/jcs.217992

Korneenko, T. V., Pestov, N. B., Hurski, A. L., Fedarkevich, A. M., Shmanai, V. V., Brenna, J. T., et al. (2017). A strong developmental isotope effect in *Caenorhabditis elegans* induced by 5,5-deuterated lysine. *Amino Acids* 49, 887–894. doi: 10.1007/s00726-017-2386-5

Labuschagne, C. F., Stigter, E. C., Hendriks, M. M., Berger, R., Rokach, J., Korswagen, H. C., et al. (2013). Quantification of in vivo oxidative damage in Caenorhabditis elegans during aging by endogenous F3-isoprostane measurement. *Aging Cell* 12, 214–223. doi: 10.1111/acel.12043

Lagman, M., Ly, J., Saing, T., Kaur Singh, M., Vera Tudela, E., Morris, D., et al. (2015). Investigating the causes for decreased levels of glutathione in individuals with type II diabetes. *PLoS One* 10:e0118436. doi: 10.1371/journal.pone.0118436

Lee, J., Kosaras, B., Del Signore, S. J., Cormier, K., McKee, A., Ratan, R. R., et al. (2011). Modulation of lipid peroxidation and mitochondrial function improves neuropathology in Huntington's disease mice. *Acta Neuropathol.* 121, 487–498. doi: 10.1007/s00401-010-0788-5

Link, C. D., and Johnson, C. J. (2002). Reporter transgenes for study of oxidant stress in *Caenorhabditis elegans*. *Methods Enzymol.* 353, 497–505. doi: 10.1016/s0076-6879(02)53072-x

MacLean, C. H., Mojica, W. A., Morton, S. C., Pencharz, J., Hasenfeld Garland, R., Tu, W., et al. (2004). *Effects of Omega-3 Fatty Acids on Lipids and Glycemic Control in Type II Diabetes and the Metabolic Syndrome and on Inflammatory Bowel Disease, Rheumatoid Arthritis, Renal Disease, Systemic Lupus Erythematosus, and Osteoporosis. Evidence Report/Technology Assessment no. 89.* Rockville: Agency for Healthcare Research and Quality (AHRQ).

Malinska, D., Kudin, A. P., Debska-Vielhaber, G., Vielhaber, S., and Kunz, W. S. (2009). Chapter 23 Quantification of superoxide production by mouse brain and skeletal muscle mitochondria. *Methods Enzymol.* 456, 419–437. doi: 10.1016/S0076-6879(08)04423-6

McHugh, D., and Gil, J. (2018). Senescence and aging: causes, consequences, and therapeutic avenues. *J. Cell Biol.* 217, 65–77. doi: 10.1083/jcb.201708092

Moller, P., and Loft, S. (2002). Oxidative DNA damage in human white blood cells in dietary antioxidant intervention studies. *Am. J. Clin. Nutr.* 76, 303–310. doi: 10.1093/ajcn/76.2.303

Naguib, Y. M. (1998). A fluorometric method for measurement of peroxyl radical scavenging activities of lipophilic antioxidants. *Anal. Biochem.* 265, 290–298. doi: 10.1006/abio.1998.2931

Paek, J., Lo, J. Y., Narasimhan, S. D., Nguyen, T. N., Glover-Cutter, K., Robida-Stubbs, S., et al. (2012). Mitochondrial SKN-1/Nrf mediates a conserved starvation response. *Cell Metab.* 16, 526–537. doi: 10.1016/j.cmet.2012.09.007

Paradies, G., Petrosillo, G., Pistolese, M., and Ruggiero, F. M. (2002). Reactive oxygen species affect mitochondrial electron transport complex I activity through oxidative cardiolipin damage. *Gene* 286, 135–141. doi: 10.1016/s0378-1119(01)00814-9

Porter, N. A., Caldwell, S. E., and Mills, K. A. (1995). Mechanisms of free radical oxidation of unsaturated lipids. *Lipids* 30, 277–290. doi: 10.1007/bf02536034

Raefsky, S. M., Furman, R., Milne, G., Pollock, E., Axelsen, P., Mattson, M. P., et al. (2018). Deuterated polyunsaturated fatty acids reduce brain lipid peroxidation and hippocampal amyloid beta-peptide levels, without discernable behavioral effects in an APP/PS1 mutant transgenic mouse model of Alzheimer's disease. *Neurobiol. Aging* 66, 165–176. doi: 10.1016/j.neurobiolaging.2018.02.024

Reed, T. T. (2011). Lipid peroxidation and neurodegenerative disease. *Free Radic. Biol. Med.* 51, 1302–1319. doi: 10.1016/j.freeradbiomed.2011.06.027

Schaar, C. E., Dues, D. J., Spielbauer, K. K., Machiela, E., Cooper, J. F., Senchuk, M., et al. (2015). Mitochondrial and cytoplasmic ROS have opposing effects on lifespan. *PLoS Genet.* 11:e1004972. doi: 10.1371/journal.pgen.1004972

Sena, L. A., and Chandel, N. S. (2012). Physiological roles of mitochondrial reactive oxygen species. *Mol. Cell* 48, 158–167. doi: 10.1016/j.molcel.2012.09.025

Shchepinov, M. S. (2007). Reactive oxygen species, isotope effect, essential nutrients, and enhanced longevity. *Rejuvenation Res.* 10, 47–59. doi: 10.1089/rej.2006.0506

Shchepinov, M. S. (2011). *Alleviating Oxidative Stress Disorders With Pufa Derivatives*. U.S. Patent No 10052299. Los Altos: Retrotope Inc.

Shichiri, M. (2014). The role of lipid peroxidation in neurological disorders. *J. Clin. Biochem. Nutr.* 54, 151–160. doi: 10.3164/jcbn.14-10

Shmookler Reis, R. J., Xu, L., Lee, H., Chae, M., Thaden, J. J., Bharill, P., et al. (2011). Modulation of lipid biosynthesis contributes to stress resistance and longevity of *C. elegans* mutants. *Aging* 3, 125–147. doi: 10.18632/aging.100275

Sies, H., Berndt, C., and Jones, D. P. (2017). Oxidative Stress. *Annu. Rev. Biochem.* 86, 715–748. doi: 10.1146/annurev-biochem-061516-045037

Smarun, A. V., Petkovic, M., Shchepinov, M. S., and Vidovic, D. (2017). Site-specific deuteration of polyunsaturated alkenes. *J. Org. Chem.* 82, 13115–13120. doi: 10.1021/acs.joc.7b02169

Subczynski, W. K., and Hyde, J. S. (1983). Concentration of oxygen in lipid bilayers using a spin-label method. *Biophys. J.* 41, 283–286. doi: 10.1016/S0006-3495(83)84439-7

Ventura, N., Rea, S. L., Schiavi, A., Torgovnick, A., Testi, R., and Johnson, T. E. (2009). p53/CEP-1 increases or decreases lifespan, depending on level of mitochondrial bioenergetic stress. *Aging Cell* 8, 380–393. doi: 10.1111/j.1474-9726.2009.00482.x

Watts, J. L., and Browse, J. (2002). Genetic dissection of polyunsaturated fatty acid synthesis in *Caenorhabditis elegans*. *Proc. Natl. Acad. Sci. U.S.A.* 99, 5854–5859. doi: 10.1073/pnas.092064799

Webster, C. M., Deline, M. L., and Watts, J. L. (2013). Stress response pathways protect germ cells from omega-6 polyunsaturated fatty acid-mediated toxicity in *Caenorhabditis elegans*. *Dev. Biol.* 373, 14–25. doi: 10.1016/j.ydbio.2012.10.002

Wei, Y., and Kenyon, C. (2016). Roles for ROS and hydrogen sulfide in the longevity response to germline loss in *Caenorhabditis elegans*. *Proc. Natl. Acad. Sci. U.S.A.* 113, E2832–E2841. doi: 10.1073/pnas.1524727113

Xu, X., and Kim, S. K. (2012). The GATA transcription factor egl-27 delays aging by promoting stress resistance in Caenorhabditis elegans. *PLoS Genet.* 8:e1003108. doi: 10.1371/journal.pgen.1003108

Yan, L. J. (2014). Positive oxidative stress in aging and aging-related disease tolerance. *Redox. Biol.* 2C, 165–169. doi: 10.1016/j.redox.2014.01.002

Yang, W. S., Kim, K. J., Gaschler, M. M., Patel, M., Shchepinov, M. S., and Stockwell, B. R. (2016). Peroxidation of polyunsaturated fatty acids by lipoxygenases drives ferroptosis. *Proc. Natl. Acad. Sci. U.S.A.* 113, E4966–E4975. doi: 10.1073/pnas.1603244113

Yang, Y., Cheng, J. Z., Singhal, S. S., Saini, M., Pandya, U., Awasthi, S., et al. (2001). Role of glutathione S-transferases in protection against lipid peroxidation. Overexpression of hGSTA2-2 in K562 cells protects against hydrogen peroxide-induced apoptosis and inhibits JNK and caspase 3 activation. *J. Biol. Chem.* 276, 19220–19230. doi: 10.1074/jbc.M100551200

Yin, H., Xu, L., and Porter, N. A. (2011). Free radical lipid peroxidation: mechanisms and analysis. *Chem. Rev.* 111, 5944–5972. doi: 10.1021/cr200084z

Zecca, L., Youdim, M. B., Riederer, P., Connor, J. R., and Crichton, R. R. (2004). Iron, brain ageing and neurodegenerative disorders. *Nat. Rev. Neurosci.* 5, 863–873. doi: 10.1038/nrn1537

Zesiewicz, T., Heerinckx, F., De Jager, R., Omidvar, O., Kilpatrick, M., Shaw, J., et al. (2018). Randomized, clinical trial of RT001: early signals of efficacy in Friedreich's ataxia. *Mov. Disord.* 33, 1000–1005. doi: 10.1002/mds.27353

Conflict of Interest Statement: MS owns stocks in Retrotope.

The remaining authors declare that the research was conducted in the absence of any commercial or financial relationships that could be construed as a potential conflict of interest.

frontiers in Cell and Developmental Biology

MINI REVIEW
published: 31 May 2019
doi: 10.3389/fcell.2019.00092

Lipid Droplet and Peroxisome Biogenesis: Do They Go Hand-in-Hand?

Amit S. Joshi and Sarah Cohen**

Department of Cell Biology and Physiology, The University of North Carolina at Chapel Hill, Chapel Hill, NC, United States

All eukaryotic cells contain membrane bound structures called organelles. Each organelle has specific composition and function. Some of the organelles are generated *de novo* in a cell. The endoplasmic reticulum (ER) is a major contributor of proteins and membranes for most of the organelles. In this mini review, we discuss *de novo* biogenesis of two such organelles, peroxisomes and lipid droplets (LDs), that are formed in the ER membrane. LDs and peroxisomes are highly conserved ubiquitously present membrane-bound organelles. Both these organelles play vital roles in lipid metabolism and human health. Here, we discuss the current understanding of *de novo* biogenesis of LDs and peroxisomes, recent advances on how biogenesis of both the organelles might be linked, physical interaction between LDs and peroxisomes and other organelles, and their physiological importance.

Keywords: lipid droplet, peroxisome, organelle biogenesis, membrane trafficking, lipid metabolism

OPEN ACCESS

Edited by:
Guillaume Thibault,
Nanyang Technological University, Singapore

Reviewed by:
Mlke Henne,
UT Southwestern Medical Center, United States
Joel M. Goodman,
UT Southwestern Medical Center, United States
Michael Schrader,
University of Exeter, United Kingdom

****Correspondence:***
Amit S. Joshi
amtya21@gmail.com
Sarah Cohen
sarahcoh@med.unc.edu

Specialty section:
This article was submitted to Membrane Traffic, a section of the journal Frontiers in Cell and Developmental Biology

Received: *12 March 2019*
Accepted: *14 May 2019*
Published: *31 May 2019*

Citation:
Joshi AS and Cohen S (2019) Lipid Droplet and Peroxisome Biogenesis: Do They Go Hand-in-Hand? Front. Cell Dev. Biol. 7:92. doi: 10.3389/fcell.2019.00092

INTRODUCTION

Peroxisomes and LDs play important roles in cellular lipid metabolism. These organelles are major metabolic hubs in eukaryotic cells. Both organelles play roles in preventing cell toxicity, albeit in dissimilar ways (Kohlwein et al., 2013). Peroxisomes are sites for beta-oxidation of fatty acids in all eukaryotic cells (Mannaerts and Van Veldhoven, 1996). In yeast and plants, the entire pathway occurs on peroxisomes, whereas in animals it occurs in peroxisomes, and mitochondria (Kunau and Hartig, 1992). Other than oxidation of fatty acids, peroxisomes are essential for detoxification of hydrogen peroxide (Walker et al., 2017). In addition, peroxisomes are sites for synthesis of D-amino acids, plasmalogens, and certain precursors of cholesterol. Understandably, defects in peroxisome function lead to several metabolic disorders (Argyriou et al., 2017). These disorders are caused due to mutations in genes encoding peroxisomal biogenesis proteins (PEX) essential for peroxisome function (Gould and Valle, 2000). Taken as a group, peroxisomal disorders occur in 1 in 5000 individuals (Waterham et al., 2016). Some of the commonly known disorders include X-linked adrenoleukodystrophy and peroxisomal biogenesis disorders (PBD) such as Zellweger Syndrome. For detailed discussion on PBD and other peroxisome related metabolic defects we refer other reviews to the readers (Delille et al., 2006; Wanders, 2014). While peroxisomes are sites of lipid degradation, LDs are organelles that prevent cellular toxicity by sequestering and storing free fatty acids in neutral lipids such as triglycerides (TG) and sterol esters (SE) (Cohen, 2018). Recent studies have elucidated new roles of LDs in protein degradation and protection from ER stress and mitochondrial oxidative stress (Olzmann and Carvalho, 2018). Aberrant LD biogenesis is a hallmark of severe disorders including diabetes, atherosclerosis, lipodystrophy, and neurodegeneration (Krahmer et al., 2013; Onal et al., 2017).

PEROXISOME BIOGENESIS

Peroxisomes are organelles enclosed in a single bilayer membrane. Peroxisomes were observed in early electron micrographs as distinct membrane bound organelles highly associated with the ER (Baudhuin et al., 1965; de Duve and Baudhuin, 1966; Tsukada et al., 1968; de Duve, 1969; Novikoff and Novikoff, 1972). It was later demonstrated that, similar to mitochondria and chloroplasts, peroxisomal matrix proteins are directly imported post-translationally from cytosolic ribosomes. Thus, peroxisomes were known as semi-autonomous organelles that follow the growth and division model where a new organelle is formed from the pre-existing one (Lazarow, 1983; Goldman and Blobel, 2006). Under normal physiological conditions, mature peroxisomes receive membrane lipids and proteins from the ER membrane, which contributes to peroxisome growth prior to division (Motley and Hettema, 2007).

In yeast, growth and division is the major pathway of peroxisome biogenesis. However, peroxisomes can also originate by *de novo* biogenesis from the ER (**Figure 1A**; Hoepfner et al., 2005). This pathway was discovered when peroxisome biogenesis mutants (*pex*) devoid of functional peroxisomes were isolated using genetic screens in yeast (Liu et al., 1992; Van der Leij et al., 1992). These mutants exhibited ghost vesicles which were devoid of many matrix proteins. Depletion of some proteins such as Pex3, a peroxisomal membrane protein (PMP) required for localization and stability of other PMPs, Pex19, a chaperone, and receptor for PMPs, and Pex16, a PMP that can recruit Pex3, resulted in cells that were completely devoid of the ghost vesicles. This suggested that these proteins might play a role in the first steps of peroxisome vesicle formation (Hohfeld et al., 1991; Hettema et al., 2000; Tam et al., 2005; Kim et al., 2006; Fujiki et al., 2014; Erdmann et al., 2015). Interestingly, when the missing protein was re-introduced in these cells, mature peroxisomes reappeared, thus challenging the growth, and division model. The resulting *de novo* biogenesis model has two main aspects: formation of new pre-peroxisomal vesicles (PPVs) from a mother organelle followed by targeting of PMPs to these vesicles to form functional mature peroxisomes. The mother organelle is usually ER, as many PMPs are targeted to ER membrane in the absence of functional peroxisomes (Geuze, 2003; van der Zand et al., 2010; Agrawal and Subramani, 2013; Tabak et al., 2013; Kim and Hettema, 2015). However, in the absence of peroxisomes, many PMPs are mistargeted to mitochondria in mammalian cells (Kim and Hettema, 2015). The PMPs possibly leave the ER membrane in the newly formed PPVs (Agrawal et al., 2016; Joshi et al., 2016). Two independent *in vitro* studies reported an essential role for Pex19 in formation of nascent vesicles from the ER membrane. These studies demonstrated that PMPs such as Pex3, Pex15 (a tail-anchored PMP), and Pex11 (required for peroxisome proliferation), are targeted to the ER membrane and traffic to PPVs in a Pex19- and ATP-dependent manner (Agrawal et al., 2011; Lam et al., 2011). The targeting of PMPs to peroxisomes is independent of COPI and COPII proteins (South et al., 2000, 2002; Voorn-Brouwer et al., 2001).

In mammalian cells peroxisomes form through division of preexisting peroxisomes, but can also derive *de novo* under special conditions. Mammalian peroxisome biogenesis differs from yeast in that mitochondrial outer membrane can be a site for PPV formation (**Figure 1A**). Artificial targeting of Pex3 to mitochondrial outer membrane in Pex3-deficient cells resulted in *de novo* peroxisome biogenesis (Rucktäschel et al., 2010). Furthermore, a recent study demonstrated that there are two types of PPVs, one from ER that contains Pex16 and another from mitochondrial outer membrane that contains Pex3 and Pex14. These PPVs fuse to form a functional peroxisome (Sugiura et al., 2017). Existence of more than one type of PPV is controversial in yeast cells. Earlier reports showed that the importomer complex consisting of RING complex (Pex2, Pex10, and Pex12) and docking complex (Pex13, Pex14, and Pex17) sorted in distinct PPVs and fused to form a functional peroxisome (**Figure 1A**; Van Der Zand et al., 2012). The model for existence of two pools of PPVs is consistent with the report that sorting of RING complex proteins, but not the docking complex proteins, in the ER membrane is dependent on Pex3 (Agrawal et al., 2016). Interestingly, the vesicles consisting of docking complex proteins exist in yeast cells lacking Pex3 or Pex19. Therefore, neither Pex3 nor Pex19 is essential for docking complex-containing PPV formation (Knoops et al., 2014; Wróblewska et al., 2017). Thus, there are two pools of PPVs: Pex3- or Pex19-independent PPVs that contain docking complex proteins, and Pex3- and Pex19- dependent PPVs that contain RING complex proteins. The Pex1-Pex6 AAA ATPase proteins are required for fusion of two pools of PPVs (**Figure 1A**; Van Der Zand et al., 2012). In *Y. lipolytica*, the two pools of PPVs were reported to require cytosolic factors, ATP hydrolysis, and functional ATPases (Pex1 and Pex6) for fusion (Titorenko et al., 2000). However, this was challenged by recent findings which suggested that there is only one type of PPV, and that Pex1-Pex6, are mainly involved in import of peroxisomal proteins (Knoops et al., 2015; Motley et al., 2015). Nevertheless, the idea that mature peroxisomes form by fusion of unique pre-peroxisomal structures is appealing, because it provides a mechanism for avoiding the mistargeting of peroxisomal enzymes to parent organelles (mitochondria and/or ER) (Kim, 2017).

Recently, ESCRT-III complex proteins were implicated in scission of PPVs from the ER into the cytosol (**Figure 1A**; Mast et al., 2018). However, ESCRT proteins are known for budding of vesicles away from the cytosol, for example in mutlivesicular body formation, or virus budding. Therefore, the role of ESCRT-III proteins needs further examination. Also, whether these proteins play a role in scission of all PPVs originating from the ER membrane or only a subset is not known.

We clearly do not completely understand PPV biogenesis from the ER membrane. There is no known mutant background that is completely devoid of PPVs, suggesting that there is redundancy among proteins involved in PPV formation. There are many outstanding questions in the field such as: how are PPVs generated? How do PMPs traffic from the ER or mitochondria to PPVs? Where do the RING and docking complex proteins assemble? We are beginning to understand some of these questions. We will discuss the recent advances in the exit sites for PPV biogenesis in Section "Links Between LD and Peroxisomes Biogenesis."

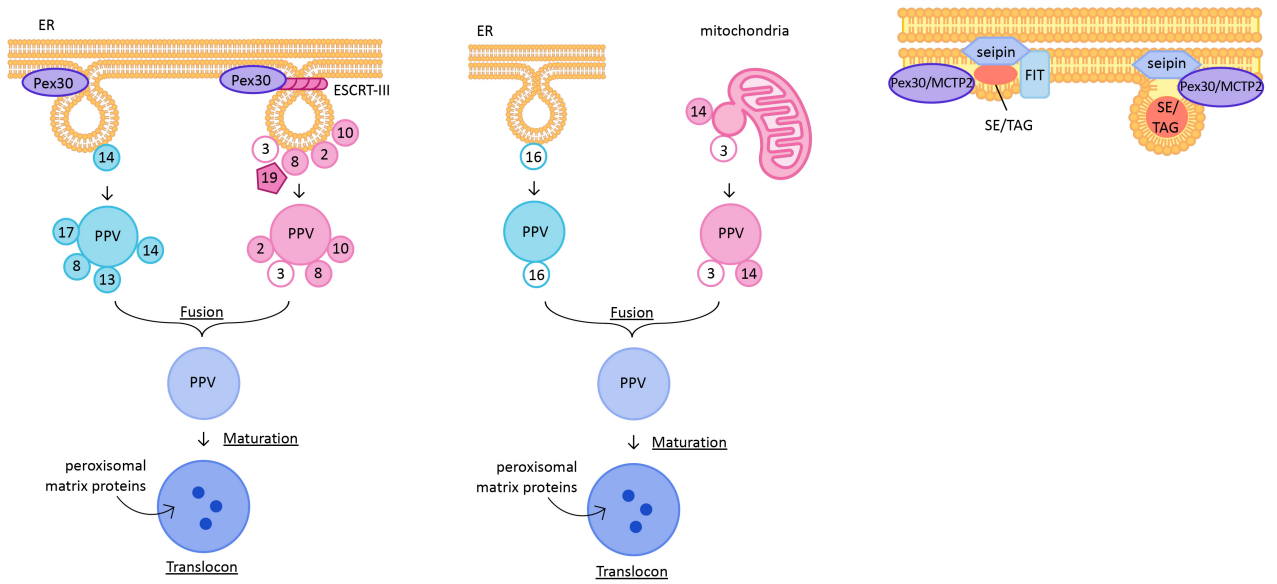

FIGURE 1 | (A) *De novo* peroxisome biogenesis in yeast and mammalian cells. PPVs containing the docking complex proteins are generated independently of Pex3 and Pex19 at ER subdomains containing Pex30. PPVs containing ring complex proteins are generated in a Pex3- and Pex19-dependent manner. ESCRT-III complex is required for scission of PPVs from the ER membrane. The two pools of PPVs fuse to form an import competent mature peroxisome. In mammals, Pex16-containing PPVs from ER and Pex3 and Pex14-containing PPVs from mitochondrial outer membrane fuse to form a functional peroxisome. **(B)** Lipid droplet biogenesis. Neutral lipid synthesizing enzymes generate sterol esters (SE) and triglycerides (TG) to form a lens-like structure in the lipid bilayer. The ER regions are enriched with seipin, FIT proteins, and Pex30/MCTP2. As the lens grows the LD buds into the cytoplasm. In yeast, LDs remain attached to the ER subdomains containing Pex30/MCTP2 and seipin but no FIT proteins.

LD BIOGENESIS

Lipid droplets are ubiquitously present unique organelles that are enclosed in a phospholipid monolayer. Unlike other organelles, the LD core is made of neutral lipids such as TG and SE. Embedded in the phospholipid monolayer are more than 100 proteins, including enzymes that synthesize or degrade lipids for storage or energy, respectively (Ducharme and Bickel, 2008; Khor et al., 2013; Bersuker and Olzmann, 2018; Bersuker et al., 2018). In yeast, LDs remain permanently connected to the ER, whereas in mammalian cells at least some mature LDs are released from the ER (Jacquier et al., 2011; Olzmann and Carvalho, 2018). LD biogenesis begins with synthesis of neutrals lipids between the ER bilayer, by ER-associated neutral lipid synthesis enzymes (Jacquier et al., 2011; Kassan et al., 2013; Choudhary et al., 2015; Kimura et al., 2018). How these enzymes are sequestered at the sites of LD biogenesis is not known. Synthesis of neutral lipids leads to formation of a lens-like structure in the bilayer (**Figure 1B**; Choudhary et al., 2015). After an increase in the concentration of neutral lipids at these sites, they start demixing from the highly charged phospholipid bilayer giving rise to LDs (Choudhary et al., 2018). These LDs are covered with a phospholipid monolayer that eventually acquires several proteins that are required for maturation of LDs (Tan et al., 2014). However, no proteins other than the enzymes involved in synthesizing neutral lipids have been implicated in formation of nascent LDs, suggesting that LD biogenesis is a lipid-driven phenomenon. Indeed, it was demonstrated that the lipid composition of the ER at sites of LD formation regulates the formation of LDs (Zanghellini et al., 2010; Ben M'barek et al., 2017; Deslandes et al., 2017; Choudhary et al., 2018). It was shown that lipids such as lysophospholipids that generate positive intrinsic curvature favor LD budding, whereas lipids such as diacylglycerol (DAG) and phosphatidylethanolamine (PE) that induce negative intrinsic curvature disfavor budding. Lipids and proteins that affect membrane tension also influence the directionality of LD budding (Ben M'barek et al., 2017; Chorlay et al., 2017; Deslandes et al., 2017). There are protein families such as seipin, FIT and Pex30/MCTP2 that play critical roles in LD formation (**Figure 1B**; Fei et al., 2008; Choudhary et al., 2015, 2018; Grippa et al., 2015; Wang et al., 2016; Joshi et al., 2018). These proteins are at the sites of LD biogenesis and are required for efficient generation of LDs. Here, we discuss the current understanding of these proteins in LD biogenesis.

FIT

The fat inducible transmembrane proteins (FITs) are conserved proteins that play a role in LD biogenesis. There are two homologs of FITs, FIT1, which is muscle specific, and FIT2, which is expressed in most tissues in mammals (Kadereit et al., 2007). In yeast, there are two FIT2 proteins, Scs3 and Yft2, whereas only one FIT protein is present in worms (Choudhary et al., 2015). Depletion of FITs leads to decreased LD biogenesis (Miranda et al., 2014). FIT proteins directly bind to TG

(Kadereit et al., 2007). Depletion of FITs in yeast, mammals and worms results in LDs wrapped around with ER membrane suggesting a defect in budding of LDs (Choudhary et al., 2015). Later it was shown that in the absence of FITs, DAG levels in the ER increase, which might affect directionality of LD budding (Choudhary et al., 2018). In the same study, it was demonstrated that supplementation with exogenous lipids such as lyso-phosphatidylcholine and lyso-phosphatidic acid reversed the LD wrapping phenotype observed in the FIT mutants in yeast. Moreover, FIT protein, Yft2, along with DAG, transiently accumulates at sites of LD formation (**Figure 1B**). Thus, FIT proteins probably regulate DAG levels at the sites where LDs are formed. Maintaining the level of DAG in the ER membrane is vital as its accumulation could be toxic. Deletion of worm FIT and mouse FIT2 is lethal, supporting the importance of the cellular function of FIT proteins (Choudhary et al., 2015, 2018).

Seipin

Seipin is a conserved integral ER membrane protein required for efficient LD biogenesis (Liu et al., 2016). The role of seipin in LD biogenesis was first identified in a screen performed in yeast to identify mutants with aberrant LD morphology. In two independent studies it was shown that in the absence of seipin, yeast cells exhibit multiple smaller, or fewer supersized LDs that are clustered together (Li et al., 2007; Fei et al., 2008). It was later shown that seipin is required for efficient incorporation of both proteins and lipids into the LDs (Salo et al., 2016). Seipin forms discrete foci in the ER membrane where nascent LDs are formed. Seipin along with Ldb16 in yeast is localized at ER-LD contact sites (Wang et al., 2014; Grippa et al., 2015). Seipin is highly mobile on the ER membrane until it encounters a nascent LD. Loss of seipin leads to smaller LDs that eventually fuse to form large and fewer LDs (Wang et al., 2016). Recent cryo-EM studies describe oligomeric structures of human (undecamers) and fly (dodecamers) seipin. Each monomer consists of a hydrophobic helix placed toward the ER bilayer and a β-sandwich domain which is structurally similar to lipid-binding proteins. It was shown that this domain binds to anionic phospholipids such as phosphatidic acid (Sui et al., 2018; Yan et al., 2018). Thus, seipin could regulate the local phospholipid levels at the site of LD budding.

NVJ

Lipid droplet biogenesis occurs at specialized nuclear vacuolar junctions (NVJs) during nutrient stress. Mdm1, a molecular tether at the NVJ, and localizes at the site of LD formation. Overexpression of Mdm1 causes accumulation of LDs at the NVJ, supporting its role in LD biogenesis (Hariri et al., 2018). Other players in LD biogenesis at the NVJ include Ldo16 and Ldo45, which are overlapping genes with shared amino acid sequence. These proteins are required for accumulation of LDs at the NVJ during stationary growth phase. These proteins generate new LDs at NVJ under nutrient stress conditions to facilitate lipophagy, the breakdown of LDs through autophagy (Eisenberg-Bord et al., 2018; Teixeira et al., 2018). Whether spatial compartmentalization of LD biogenesis specific to nutrient stress occurs in higher eukaryotes remains to be investigated.

LINKS BETWEEN LD AND PEROXISOMES BIOGENESIS

Several reports have suggested that LDs and peroxisomes are intimately associated (Schrader, 2001; Binns et al., 2006; Valm et al., 2017). Yeast cells grown in the presence of oleic acid exhibit peroxisomes that adhere stably with LDs by forming extended membrane processes called gnarls. These extensions were enriched in fatty acid beta oxidation enzymes, suggesting coupling of lipolysis within the LDs with peroxisomal enzymes (Binns et al., 2006). A recent report suggests that M1 spastin on the LDs physically tethers with ABCD1 on peroxisomal membranes. Moreover, M1 spastin recruits ESCRT III proteins to facilitate fatty acid trafficking from LDs to peroxisomes (Chang et al., 2019). Thus, there is a clear metabolic link between these organelles. In this section we discuss the shared machinery required for the *de novo* biogenesis and function of peroxisomes and LDs. Both organelles originate from the ER membrane (Joshi et al., 2017). Until recently, the sites in the ER membrane for formation of these organelles was not known. Also, it was unclear whether these sites form stochastically or are pre-determined.

Pex30 Subdomains: Sites for Nascent LD and PPV Generation

Recent studies in yeast demonstrated that Pex30 localizes to discrete regions of the ER called ER subdomains. Pex30 is a resident ER protein, however, it localizes to peroxisomes or PPVs when cells are exposed to oleic acid or when Pex30 is overexpressed (Vizeacoumar et al., 2006; Joshi et al., 2016). Pex30 and Pex30-like proteins contain a reticulon homology domain (RHD), a transmembrane domain that is similar to reticulon proteins. Like reticulons, Pex30 proteins tubulate the ER membrane. However, unlike the reticulons, Pex30 and Pex30-like proteins are low abundance proteins localized to discrete regions in the ER. In cells devoid of peroxisomes, it was demonstrated using fluorescence and electron microscopy that newly expressed Pex14 is targeted to ER regions enriched with Pex30. Pex14 eventually leaves the ER membrane in a newly formed PPV (Joshi et al., 2016). This suggests that Pex30 subdomains are novel exit sites of nascent PPV formation (**Figure 1A**). Interestingly, these sites do not overlap with ER exit sites for COPII vesicles (Joshi et al., 2016). Whether other types of PPVs also form at these subdomains remains to be investigated. Deletion of Pex30 and the Pex30-like protein, Pex31, generates small clusters of PPVs closely associated with the ER membrane. The rate of formation of new peroxisomes is also decreased in cells devoid of Pex30 and Pex31 (Joshi et al., 2016). Thus, Pex30 and Pex31 are essential for efficient formation of peroxisomes.

The number of Pex30 subdomains per cell is much greater than the number of PPVs per cell. Thus, Pex30 subdomains could have additional roles. Indeed, it was demonstrated that Pex30 subdomains are also the sites for nascent LD formation (**Figure 1B**; Joshi et al., 2018). Furthermore, in yeast cells PPVs were associated with LDs at Pex30 subdomains, implying that PPV and LD biogenesis might occur at the same sites within the ER (**Figure 2**). It is possible that Pex30 also

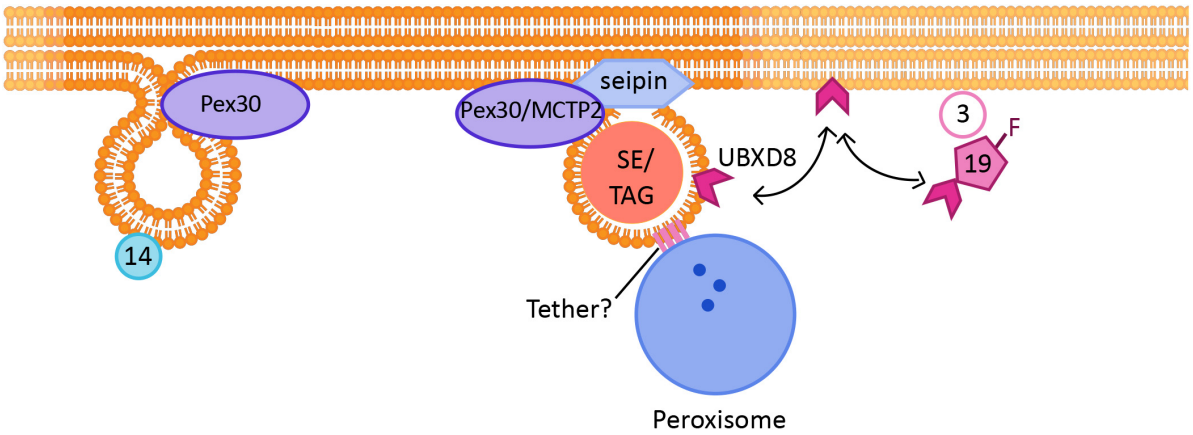

FIGURE 2 | Link between peroxisome and LD biogenesis: The formation of new Pex14-containing PPVs and LDs occur at the same ER subdomains, which are positive for Pex30/MCTP2 proteins. Mature peroxisomes also physically associate with LDs. Tethers identified so far include ABCD1 on peroxisomes, which interacts with Spastin on LDs. Other tethers may also be involved in peroxisome-LD contacts. Pex19 is a cytosolic protein required for peroxisomal protein targeting, which when farnesylated targets a LD protein UBXD8 to LDs.

localizes to the site of new LD formation at the NVJ, as Pex30 is enriched at NVJ especially during stationary growth phase (Joshi et al., 2016). Pex30 subdomains exist even in the absence of LDs, suggesting that the sites at which LDs and PPVs form are stable, pre-determined, and not random. Pex30 has a functional homolog, multiple C2 domain containing transmembrane protein 2 (MCTP2), in higher eukaryotes, which also has an RHD (Joshi et al., 2018). Mammalian cells have two MCTP proteins, MCTP1 and MCTP2, whereas flies and worms have only one MCTP (Shin et al., 2005). Similar to Pex30, MCTP2 is also a low abundance protein that localizes to the sites of LD biogenesis (**Figure 1B**). MCTP2 subdomains also dynamically associate with the peroxisomal vesicles. However, MCTP2 does not localize to peroxisomes (Joshi et al., 2018).

It is possible that in addition to organelle biogenesis, these ER subdomains play roles in lipid trafficking and signaling. In the absence of Pex30, LDs are small and clustered and there is ER membrane proliferation. An independent study showed that loss of Pex31, a paralog of Pex30, also leads to smaller LDs (Lv et al., 2019). The rate of new LD formation was also significantly decreased in cells devoid of Pex30 (Joshi et al., 2018). It is fascinating that loss of Pex30 has similar morphological effects on both PPVs and LDs, suggesting that the mechanism involved in biogenesis of the organelles is shared (Joshi et al., 2016, 2018). Pex30 also colocalizes with several ER membrane proteins, including seipin, that are known markers for the sites of LD biogenesis. Deletion of seipin affected the distribution of Pex30 in the ER, as there was a significant decrease in the number of Pex30 punctae in the seipin mutant. Cells devoid of both Pex30 and seipin exhibited a severe growth defect, and highly clustered small and large LDs (Joshi et al., 2018; Wang et al., 2018). Seipin also affects peroxisome biogenesis, as deletion of seipin alone decreased the rate of formation of new peroxisomes (Wang et al., 2018). Thus, there is a clear link between LD biogenesis and peroxisome biogenesis.

Shared Protein Machinery for Targeting of Peroxisomal and LD Proteins

Pex19, a well-established cytosolic chaperone protein, and Pex3, a PMP, are required for targeting of UBXD8, an LD protein, in the ER membrane of mammalian cells. UBXD8 is delivered to Pex3-enriched ER subdomains by farnesylated Pex19 (**Figure 2**). UBXD8 was mistargeted to the peroxisome if Pex19 was not farnesylated, suggesting that the post-translational modification is vital to gain specificity of protein targeting (Schrul and Kopito, 2016). It is possible that enzymes that are required for LD maturation and growth follow the same route, as cells devoid of Pex3 or Pex19 exhibit smaller LDs (Wang et al., 2013). Another example of a link between peroxisomes and LDs comes from a recent study which demonstrated that in mammalian cells the peroxisomal protein fatty acyl CoA reductase 1 (Far1), is targeted to LDs upon increased triglyceride synthesis. Far1 exhibits two different topologies that differ in orientation of the short hydrophilic C-terminus toward the cytosol or lumen. Out of the two closely spaced hydrophobic domains, one is enough to target the protein to the LDs. Thus, Far1 exhibits dual topologies to peroxisomes and LDs dependent on cellular lipid metabolism (Exner et al., 2019).

CONCLUSION AND FUTURE PERSPECTIVES

There are many open questions about the links between peroxisomes, LDs, and other organelles that originate from the ER. What is the common theme in the biogenesis of peroxisomes and LDs? Structurally, these organelles are very different. It is possible that Pex30 and seipin generate specialized ER subdomains for PPV and LD biogenesis. Seipin specifically binds to anionic phospholipids (Yan et al., 2018), whereas studies using sensor proteins such as the DAG-sensing PKD domain from mammalian cells and Dga1 protein demonstrated that

Pex30 subdomains have enriched DAG and possibly phosphatidic acid, especially upon induction of LDs with oleic acid (Joshi et al., 2018). In addition, the LD defect in cells devoid of seipin and Pex30 was rescued by manipulating ER phospholipid composition (Wang et al., 2018). Thus, the generation of these organelles could be influenced by lipids. Pex30 could induce curvature with its RHD, which might be conducive for the synthesis of certain lipids to facilitate the generation of LDs and PPVs. It is also possible that the biogenesis of these organelles from a common subdomain allows their formation to be coordinated in response to stimuli that require the proliferation of both, such as a lipid challenge. It has been demonstrated that Pex30 subdomains do not overlap with ER exit sites. However, it remains to be determined whether these domains play a role in the biogenesis of other organelles that originate from the ER, such as autophagosomes, which can also be induced in response to excess lipids (Singh et al., 2009). There are hints that LD and autophagosome biogenesis may be related: both autophagosomes and LDs have been observed cradled within "cups" of ER membrane, and LC3 and Atg2, which are involved in autophagosome biogenesis, also localize to LDs (Robenek et al., 2006; Hayashi-Nishino et al., 2009; Shibata et al., 2009, 2010; Velikkakath et al., 2012). These observations suggest that autophagosome and LD biogenesis may share some common machinery, but whether Pex30 ER subdomains are involved in autophagosome biogenesis is currently unknown.

Finally, the ER subdomains involved in organelle biogenesis may also be membrane contact sites through which peroxisomes and LDs communicate with the ER after their biogenesis. In this case they could play roles in organelle remodeling, or in the trafficking of proteins and/or lipids between the ER, peroxisomes, and LDs. Peroxisomes in mammalian cells are tethered to the ER via ACBD5-VAP proteins. This tether is essential for peroxisomes to receive lipids from the ER required for peroxisomal membrane expansion (Costello et al., 2017; Hua et al., 2017). Several tethers have been proposed for ER-LD contact sites. These include interactions between NRZ-SNARE on the ER and Rab18 on LDs in mammalian cells, and between the lipid synthesis enzymes FATP1 on the ER and DGAT2 on LDs in worms (Xu et al., 2012, 2018). Whether Pex30 ER subdomains colocalize with any of these tethers, or whether they form distinct membrane contact sites, is currently unknown. The precise protein composition of these ER-LD-peroxisome membrane contact sites, their physiological function, and regulation all remain to be determined. The recent development of new biochemical and microscopic tools to study membrane microdomains and membrane contact sites is sure to open up many new areas of research in this exciting field.

AUTHOR CONTRIBUTIONS

AJ and SC conceived and wrote the manuscript.

FUNDING

This work was supported by The University of North Carolina at Chapel Hill, by the National Institute on Aging of the National Institutes of Health under award number R00AG052570, and by the Alzheimer's Association under award number 2018-AARG-590347.

ACKNOWLEDGMENTS

We thank Sarah Monroe for help with the figures.

REFERENCES

Agrawal, G., Fassas, S. N., Xia, Z. J., and Subramani, S. (2016). Distinct requirements for intra-ER sorting and budding of peroxisomal membrane proteins from the ER. *J. Cell Biol.* 212, 335–345. doi: 10.1083/jcb.201506141

Agrawal, G., Joshi, S., and Subramani, S. (2011). Cell-free sorting of peroxisomal membrane proteins from the endoplasmic reticulum. *Proc. Natl. Acad. Sci. U.S.A.* 108, 9113–9118. doi: 10.1073/pnas.1018749108

Agrawal, G., and Subramani, S. (2013). Emerging role of the endoplasmic reticulum in peroxisome biogenesis. *Front. Physiol.* 4:286. doi: 10.3389/fphys.2013.00286

Argyriou, C., D'Agostino, M. D., and Braverman, N. (2017). "Peroxisome biogenesis disorders," in *Metabolic Diseases: Foundations of Clinical Management, Genetics, and Pathology*, eds E. Gilbert-Barness, L. A. Barness, and P. M. Farrell (Amsterdam: IOS Press), 847–880. doi: 10.3233/978-1-61499-718-4-847

Baudhuin, P., Beaufay, H., and De Duve, C. (1965). Combined biochemical and morphological study of particulate fractions from rat liver. Analysis of preparations enriched in lysosomes or in particles containing urate oxidase, D-amino acid oxidase, and catalase. *J. Cell Biol.* 26, 219–243. doi: 10.1083/jcb.26.1.219

Ben M'barek, K., Ajjaji, D., Chorlay, A., Vanni, S., Forêt, L., and Thiam, A. R. (2017). ER membrane phospholipids and surface tension control cellular lipid droplet formation. *Dev. Cell* 41, 591–604.e7. doi: 10.1016/j.devcel.2017.05.012

Bersuker, K., and Olzmann, J. A. (2018). In close proximity: the lipid droplet proteome and crosstalk with the endoplasmic reticulum. *Contact* 1, 1–3.

Bersuker, K., Peterson, C. W. H., To, M., Sahl, S. J., Savikhin, V., Grossman, E. A., et al. (2018). A proximity labeling strategy provides insights into the composition and dynamics of lipid droplet proteomes. *Dev. Cell* 44, 97–112.e7. doi: 10.1016/j.devcel.2017.11.020

Binns, D., Januszewski, T., Chen, Y., Hill, J., Markin, V. S., Zhao, Y., et al. (2006). An intimate collaboration between peroxisomes and lipid bodies. *J. Cell Biol.* 173, 719–731. doi: 10.1083/jcb.200511125

Chang, C.-L., Weigel, A. V., Ioannou, M. S., Pasolli, H. A., Xu, C. S., Peale, D. R., et al. (2019). Spastin tethers lipid droplets to peroxisomes and directs fatty acid trafficking through ESCRT-III. *bioRxiv* [Preprint]. doi: 10.1101/544023

Chorlay, A., Forêt, L., Vanni, S., Thiam, A. R., Ajjaji, D., and Ben M'barek, K. (2017). ER membrane phospholipids and surface tension control cellular lipid droplet formation. *Dev. Cell* 41, 591–604.e7. doi: 10.1016/j.devcel.2017.05.012

Choudhary, V., Golani, G., Joshi, A. S., Cottier, S., Schneiter, R., Prinz, W. A., et al. (2018). Architecture of lipid droplets in endoplasmic reticulum is determined by phospholipid intrinsic curvature. *Curr. Biol.* 28, 915–926.e9. doi: 10.1016/j.cub.2018.02.020

Choudhary, V., Ojha, N., Golden, A., and Prinz, W. A. (2015). A conserved family of proteins facilitates nascent lipid droplet budding from the ER. *J. Cell Biol.* 211, 261–271. doi: 10.1083/jcb.201505067

Cohen, S. (2018). Lipid droplets as organelles. *Int. Rev. Cell Mol. Biol.* 337, 83–110. doi: 10.1016/bs.ircmb.2017.12.007

Costello, J. L., Castro, I. G., Hacker, C., Schrader, T. A., Metz, J., Zeuschner, D., et al. (2017). ACBD5 and VAPB mediate membrane associations between peroxisomes and the ER. *J. Cell Biol.* 216, 331–342. doi: 10.1083/jcb.201607055

de Duve, C. (1969). Evolution of the peroxisome. *Ann. N. Y. Acad. Sci.* 168, 369–381. doi: 10.1111/j.1749-6632.1969.tb43124.x

de Duve, C., and Baudhuin, P. (1966). Peroxisomes (microbodies and related particles). *Physiol. Rev.* 46, 323–357. doi: 10.1152/physrev.1966.46.2.323

Delille, H. K., Bonekamp, N. A., and Schrader, M. (2006). Peroxisomes and disease - an overview. *Int. J. Biomed. Sci.* 2, 308–314.

Deslandes, F., Thiam, A. R., and Forêt, L. (2017). Lipid droplets can spontaneously bud off from a symmetric bilayer. *Biophys. J.* 113, 15–18. doi: 10.1016/j.bpj.2017.05.045

Ducharme, N. A., and Bickel, P. E. (2008). Minireview: lipid droplets in lipogenesis and lipolysis. *Endocrinology* 149, 942–949. doi: 10.1210/en.2007-1713

Eisenberg-Bord, M., Mari, M., Weill, U., Rosenfeld-Gur, E., Moldavski, O., Castro, I. G., et al. (2018). Identification of seipin-linked factors that act as determinants of a lipid droplet subpopulation. *J. Cell Biol.* 217, 269–282. doi: 10.1083/jcb.201704122

Erdmann, R., Baumgart, E., Linkert, M., Kunau, W.-H., Götte, K., Girzalsky, W., et al. (2015). Pex19p, a farnesylated protein essential for peroxisome biogenesis. *Mol. Cell. Biol.* 18, 616–628. doi: 10.1128/mcb.18.1.616

Exner, T., Romero-Brey, I., Yifrach, E., Rivera-Monroy, J., Schrul, B., Zouboulis, C. C., et al. (2019). An alternative membrane topology permits lipid droplet localization of peroxisomal fatty acyl-CoA reductase 1. *J. Cell Sci.* 132:223016. doi: 10.1242/jcs.223016

Fei, W., Shui, G., Gaeta, B., Du, X., Kuerschner, L., Li, P., et al. (2008). Fld1p, a functional homologue of human seipin, regulates the size of lipid droplets in yeast. *J. Cell Biol.* 180, 473–482. doi: 10.1083/jcb.200711136

Fujiki, Y., Okumoto, K., Mukai, S., Honsho, M., and Tamura, S. (2014). Peroxisome biogenesis in mammalian cells. *Front. Physiol.* 5:307. doi: 10.3389/fphys.2014.00307

Geuze, H. J. (2003). Involvement of the endoplasmic reticulum in peroxisome formation. *Mol. Biol. Cell* 14, 2900–2907. doi: 10.1091/mbc.e02-11-0734

Goldman, B. M., and Blobel, G. (2006). Biogenesis of peroxisomes: intracellular site of synthesis of catalase and uricase. *Proc. Natl. Acad. Sci. U.S.A.* 75, 5066–5070. doi: 10.1073/pnas.75.10.5066

Gould, S. J., and Valle, D. (2000). Peroxisome biogenesis disorders: genetics and cell biology. *Trends Genet.* 16, 340–345. doi: 10.1016/S0168-9525(00)02056-4

Grippa, A., Buxó, L., Mora, G., Funaya, C., Idrissi, F. Z., Mancuso, F., et al. (2015). The seipin complex Fld1/Ldb16 stabilizes ER-lipid droplet contact sites. *J. Cell Biol.* 211, 829–844. doi: 10.1083/jcb.201502070

Hariri, H., Rogers, S., Ugrankar, R., Liu, Y. L., Feathers, J. R., and Henne, M. (2018). Lipid droplet biogenesis is spatially coordinated at ER–vacuole contacts under nutritional stress. *EMBO Rep.* 19, 57–72. doi: 10.15252/embr

Hayashi-Nishino, M., Fujita, N., Noda, T., Yamaguchi, A., Yoshimori, T., and Yamamoto, A. (2009). A subdomain of the endoplasmic reticulum forms a cradle for autophagosome formation. *Nat. Cell Biol.* 11, 1433–1437. doi: 10.1038/ncb1991

Hettema, E. H., Girzalsky, W., Van Den Berg, M., Erdmann, R., and Distel, B. (2000). *Saccharomyces cerevisiae* Pex3p and Pex19p are required for proper localization and stability of peroxisomal membrane proteins. *EMBO J.* 19, 223–233. doi: 10.1093/emboj/19.2.223

Hoepfner, D., Schildknegt, D., Braakman, I., Philippsen, P., and Tabak, H. F. (2005). Contribution of the endoplasmic reticulum to peroxisome formation. *Cell* 122, 85–95. doi: 10.1016/j.cell.2005.04.025

Hohfeld, J., Veenhuis, M., and Kunau, W. H. (1991). PAS3, a *Saccharomyces cerevisiae* gene encoding a peroxisomal integral membrane protein essential for peroxisome biogenesis. *J. Cell Biol.* 114, 1167–1178. doi: 10.1083/jcb.114.6.1167

Hua, R., Cheng, D., Coyaud, É., Freeman, S., Di Pietro, E., Wang, Y., et al. (2017). VAPs and ACBD5 tether peroxisomes to the ER for peroxisome maintenance and lipid homeostasis. *J. Cell Biol.* 216, 367–377. doi: 10.1083/jcb.201608128

Jacquier, N., Choudhary, V., Mari, M., Toulmay, A., Reggiori, F., and Schneiter, R. (2011). Lipid droplets are functionally connected to the endoplasmic reticulum in *Saccharomyces cerevisiae*. *J. Cell Sci.* 124(Pt 14), 2424–2437. doi: 10.1242/jcs.076836

Joshi, A. S., Huang, X., Choudhary, V., Levine, T. P., Hu, J., and Prinz, W. A. (2016). A family of membrane-shaping proteins at ER subdomains regulates pre-peroxisomal vesicle biogenesis. *J. Cell Biol.* 215, 515–529. doi: 10.1083/jcb.201602064

Joshi, A. S., Nebenfuehr, B., Choudhary, V., Satpute-Krishnan, P., Levine, T. P., Golden, A., et al. (2018). Lipid droplet and peroxisome biogenesis occur at the same ER subdomains. *Nat. Commun.* 9:2940. doi: 10.1038/s41467-018-05277-3

Joshi, A. S., Zhang, H., and Prinz, W. A. (2017). Organelle biogenesis in the endoplasmic reticulum. *Nat. Cell Biol.* 19, 876–882. doi: 10.1038/ncb3579

Kadereit, B., Kumar, P., Torregroza, I., Wang, W.-J., Severina, N., Silver, D. L., et al. (2007). Evolutionarily conserved gene family important for fat storage. *Proc. Natl. Acad. Sci. U.S.A.* 105, 94–99. doi: 10.1073/pnas.0708579105

Kassan, A., Herms, A., Fernández-Vidal, A., Bosch, M., Schieber, N. L., Reddy, B. J. N., et al. (2013). Acyl-CoA synthetase 3 promotes lipid droplet biogenesis in ER microdomains. *J. Cell Biol.* 203, 985–1001. doi: 10.1083/jcb.201305142

Khor, V. K., Shen, W. J., and Kraemer, F. B. (2013). Lipid droplet metabolism. *Curr. Opin. Clin. Nutr. Metab. Care* 16, 632–637. doi: 10.1097/MCO.0b013e3283651106

Kim, P. (2017). Peroxisome biogenesis: a union between two organelles. *Curr. Biol.* 27, R271–R274. doi: 10.1016/j.cub.2017.02.052

Kim, P. K., and Hettema, E. H. (2015). Multiple pathways for protein transport to peroxisomes. *J. Mol. Biol.* 427(6 Pt A), 1176–1190. doi: 10.1016/j.jmb.2015.02.005

Kim, P. K., Mullen, R. T., Schumann, U., and Lippincott-Schwartz, J. (2006). The origin and maintenance of mammalian peroxisomes involves a de novo PEX16-dependent pathway from the ER. *J. Cell Biol.* 173, 521–532. doi: 10.1083/jcb.200601036

Kimura, H., Arasaki, K., Ohsaki, Y., Fujimoto, T., Ohtomo, T., Yamada, J., et al. (2018). Syntaxin 17 promotes lipid droplet formation by regulating the distribution of acyl-CoA synthetase 3. *J. Lipid Res.* 59, 805–819. doi: 10.1194/jlr.M081679

Knoops, K., De Boer, R., Kram, A., and Van Der Klei, I. J. (2015). Yeast pex1 cells contain peroxisomal ghosts that import matrix proteins upon reintroduction of Pex1. *J. Cell Biol.* 211, 955–962. doi: 10.1083/jcb.201506059

Knoops, K., Manivannan, S., Cepińska, M. N., Krikken, A. M., Kram, A. M., Veenhuis, M., et al. (2014). Preperoxisomal vesicles can form in the absence of Pex3. *J. Cell Biol.* 204, 659–668. doi: 10.1083/jcb.201310148

Kohlwein, S. D., Veenhuis, M., and van der Klei, I. J. (2013). Lipid droplets and peroxisomes: key players in cellular lipid homeostasis or a matter of fat-store 'em up or burn 'em down. *Genetics* 193, 1–50. doi: 10.1534/genetics.112.143362

Krahmer, N., Farese, R. V., and Walther, T. C. (2013). Balancing the fat: lipid droplets and human disease. *EMBO Mol. Med.* 5, 973–983. doi: 10.1002/emmm.201100671

Kunau, W. H., and Hartig, A. (1992). Peroxisome biogenesis in *Saccharomyces cerevisiae*. *Antonie Van Leeuwenhoek* 62, 63–78. doi: 10.1007/BF00584463

Lam, S. K., Yoda, N., and Schekman, R. (2011). A vesicle carrier that mediates peroxisome protein traffic from the endoplasmic reticulum. *Proc. Natl. Acad. Sci. U.S.A.* 107, 21523–21528. doi: 10.1073/pnas.1103526108

Lazarow, P. B. (1983). Biogenesis of peroxisomal content proteins: in vivo and in vitro studies. *Methods Enzymol.* 96, 721–728. doi: 10.1016/S0076-6879(83)96061-5

Li, W.-P., Szymanski, K. M., Goodman, J. M., Grishin, N. V., Anderson, R. G. W., Binns, D., et al. (2007). The lipodystrophy protein seipin is found at endoplasmic reticulum lipid droplet junctions and is important for droplet morphology. *Proc. Natl. Acad. Sci. U.S.A.* 104, 20890–20895. doi: 10.1073/pnas.0704154104

Liu, H., Tan, X., Veenhuis, M., McCollum, D., and Cregg, J. M. (1992). An efficient screen for peroxisome-deficient mutants of *Pichia pastoris*. *J. Bacteriol.* 174, 4943–4951. doi: 10.1128/jb.174.15.4943-4951.1992

Liu, X. N., Lin, Q., Walther, T. C., Upadhyayula, S., Farese, R. V., Housden, B. E., et al. (2016). Seipin is required for converting nascent to mature lipid droplets. *eLife* 5:e16582. doi: 10.7554/elife.16582

Lv, X., Liu, J., Qin, Y., Liu, Y., Jin, M., Dai, J., et al. (2019). Identification of gene products that control lipid droplet size in yeast using a high-throughput quantitative image analysis. *Biochim. Biophys. Acta Mol. Cell Biol. Lipids* 1864, 113–127. doi: 10.1016/j.bbalip.2018.11.001

Mannaerts, G. P., and Van Veldhoven, P. P. (1996). Functions and organization of peroxisomal β-oxidation. *Ann. N. Y. Acad. Sci.* 804, 99–115. doi: 10.1111/j.1749-6632.1996.tb18611.x

Mast, F. D., Herricks, T., Strehler, K. M., Miller, L. R., Saleem, R. A., Rachubinski, R. A., et al. (2018). ESC RT-III is required for scissioning new peroxisomes from the endoplasmic reticulum. *J. Cell Biol.* 217, 2087–2102. doi: 10.1083/jcb.201706044

Miranda, D. A., Kim, J. H., Nguyen, L. N., Cheng, W., Tan, B. C., Goh, V. J., et al. (2014). Fat storage-inducing transmembrane protein 2 is required for normal fat storage in adipose tissue. *J. Biol. Chem.* 289, 9560–9572. doi: 10.1074/jbc.M114.547687

Motley, A. M., Galvin, P. C., Ekal, L., Nuttall, J. M., and Hettema, E. H. (2015). Reevaluation of the role of Pex1 and dynamin-related proteins in peroxisome membrane biogenesis. *J. Cell Biol.* 211, 1041–1056. doi: 10.1083/jcb.201412066

Motley, A. M., and Hettema, E. H. (2007). Yeast peroxisomes multiply by growth and division. *J. Cell Biol.* 178, 399–410. doi: 10.1083/jcb.200702167

Novikoff, P. M., and Novikoff, A. B. (1972). Peroxisomes in absorptive cells of mammalian small intestine. *J. Cell Biol.* 53, 532–560. doi: 10.1083/jcb.53.2.532

Olzmann, J. A., and Carvalho, P. (2018). Dynamics and functions of lipid droplets. *Nat. Rev. Mol. Cell Biol.* 20, 137–155. doi: 10.1038/s41580-018-0085-z

Onal, G., Kutlu, O., Gozuacik, D., and Dokmeci Emre, S. (2017). Lipid droplets in health and disease. *Lipids Health Dis.* 16:128. doi: 10.1186/s12944-017-0521-7

Robenek, H., Hofnagel, O., Buers, I., Robenek, M. J., Troyer, D., and Severs, N. J. (2006). Adipophilin-enriched domains in the ER membrane are sites of lipid droplet biogenesis. *J. Cell Sci.* 119(Pt 20), 4215–4224. doi: 10.1242/jcs.03191

Rucktäschel, R., Halbach, A., Girzalsky, W., Rottensteiner, H., and Erdmann, R. (2010). De novo synthesis of peroxisomes upon mitochondrial targeting of Pex3p. *Eur. J. Cell Biol.* 89, 947–954. doi: 10.1016/j.ejcb.2010.06.012

Salo, V. T., Belevich, I., Li, S., Karhinen, L., Vihinen, H., Vigouroux, C., et al. (2016). Seipin regulates ER–lipid droplet contacts and cargo delivery. *EMBO J.* 35, 2699–2716. doi: 10.15252/embj.201695170

Schrader, M. (2001). Tubulo-reticular clusters of peroxisomes in living COS-7 cells: dynamic behavior and association with lipid droplets. *J. Histochem. Cytochem.* 49, 1421–1429. doi: 10.1177/002215540104901110

Schrul, B., and Kopito, R. R. (2016). Peroxin-dependent targeting of a lipid-droplet-destined membrane protein to ER subdomains. *Nat. Cell Biol.* 18, 740–751. doi: 10.1038/ncb3373

Shibata, M., Yoshimura, K., Furuya, N., Koike, M., Ueno, T., Komatsu, M., et al. (2009). The MAP1-LC3 conjugation system is involved in lipid droplet formation. *Biochem. Biophys. Res. Commun.* 382, 419–423. doi: 10.1016/j.bbrc.2009.03.039

Shibata, M., Yoshimura, K., Tamura, H., Ueno, T., Nishimura, T., Inoue, T., et al. (2010). LC3, a microtubule-associated protein1A/B light chain3, is involved in cytoplasmic lipid droplet formation. *Biochem. Biophys. Res. Commun.* 393, 274–279. doi: 10.1016/j.bbrc.2010.01.121

Shin, O. H., Hau, W., Wang, Y., and Südhof, T. C. (2005). Evolutionarily conserved multiple C2 domain proteins with two transmembrane regions (MCTPs) and unusual Ca2+ binding properties. *J. Biol. Chem.* 280, 1641–1651. doi: 10.1074/jbc.M407305200

Singh, R., Kaushik, S., Wang, Y., Xiang, Y., Novak, I., Komatsu, M., et al. (2009). Autophagy regulates lipid metabolism. *Nature* 458, 1131–1135. doi: 10.1038/nature07976

South, S. T., Gould, S. J., Li, X., Sacksteder, K. A., and Liu, Y. (2002). Inhibitors of COPI and COPII do not block *PEX3*-mediated peroxisome synthesis. *J. Cell Biol.* 149, 1345–1360. doi: 10.1083/jcb.149.7.1345

South, S. T., Sacksteder, K. A., Li, X., Liu, Y., and Gould, S. J. (2000). Inhibitors of COPI and COPII do not block PEX3-mediated peroxisome synthesis. *J. Cell Biol.* 149, 1345–1360. doi: 10.1083/jcb.149.7.1345

Sugiura, A., Mattie, S., Prudent, J., and Mcbride, H. M. (2017). Newly born peroxisomes are a hybrid of mitochondrial and ER-derived pre-peroxisomes. *Nature* 542, 251–254. doi: 10.1038/nature21375

Sui, X., Arlt, H., Brock, K. P., Lai, Z. W., DiMaio, F., Marks, D. S., et al. (2018). Cryo–electron microscopy structure of the lipid droplet–formation protein seipin. *J. Cell Biol.* 217, 4080–4091. doi: 10.1083/jcb.201809067

Tabak, H. F., Braakman, I., and van der Zand, A. (2013). Peroxisome formation and maintenance are dependent on the endoplasmic reticulum. *Annu. Rev. Biochem.* 82, 723–744. doi: 10.1146/annurev-biochem-081111-125123

Tam, Y. Y. C., Fagarasanu, A., Fagarasanu, M., and Rachubinski, R. A. (2005). Pex3p initiates the formation of a preperoxisomal compartment from a subdomain of the endoplasmic reticulum in *Saccharomyces cerevisiae*. *J. Biol. Chem.* 280, 34933–34939. doi: 10.1074/jbc.M506208200

Tan, J. S. Y., Seow, C. J. P., Goh, V. J., and Silver, D. L. (2014). Recent advances in understanding proteins involved in lipid droplet formation, growth and fusion. *J. Genet. Genomics* 41, 251–259. doi: 10.1016/j.jgg.2014.03.003

Teixeira, V., Johnsen, L., Martínez-Montañés, F., Grippa, A., Buxó, L., Idrissi, F. Z., et al. (2018). Regulation of lipid droplets by metabolically controlled Ldo isoforms. *J. Cell Biol.* 217:127. doi: 10.1083/jcb.201704115

Titorenko, V. I., Chan, H., and Rachubinski, R. A. (2000). Fusion of small peroxisomal vesicles in vitro reconstructs an early step in the in vivo multistep peroxisome assembly pathway of *Yarrowia lipolytica*. *J. Cell Biol.* 148, 29–44. doi: 10.1083/jcb.148.1.29

Tsukada, H., Mochizuki, Y., and Konishi, T. (1968). Morphogenesis and development of microbodies of hepatocytes of rats during pre- and postnatal growth. *J. Cell Biol.* 37, 231–243. doi: 10.1083/jcb.37.2.231

Valm, A. M., Cohen, S., Legant, W. R., Melunis, J., Hershberg, U., Wait, E., et al. (2017). Applying systems-level spectral imaging and analysis to reveal the organelle interactome. *Nature* 546, 162–167. doi: 10.1038/nature22369

Van der Leij, I., Van den Berg, M., Boot, R., Franse, M., Distel, B., and Tabak, H. F. (1992). Isolation of peroxisome assembly mutants from *Saccharomyces cerevisiae* with different morphologies using a novel positive selection procedure. *J. Cell Biol.* 119, 153–162. doi: 10.1083/jcb.119.1.153

van der Zand, A., Braakman, I., and Tabak, H. F. (2010). Peroxisomal membrane proteins insert into the endoplasmic reticulum. *Mol. Biol. Cell* 21, 2057–2065. doi: 10.1091/mbc.e10-02-0082

Van Der Zand, A., Gent, J., Braakman, I., and Tabak, H. F. (2012). Biochemically distinct vesicles from the endoplasmic reticulum fuse to form peroxisomes. *Cell* 149, 397–409. doi: 10.1016/j.cell.2012.01.054

Velikkakath, A. K. G., Nishimura, T., Oita, E., Ishihara, N., and Mizushima, N. (2012). Mammalian Atg2 proteins are essential for autophagosome formation and important for regulation of size and distribution of lipid droplets. *Mol. Biol. Cell* 23, 896–909. doi: 10.1091/mbc.e11-09-0785

Vizeacoumar, F. J., Vreden, W. N., Aitchison, J. D., and Rachubinski, R. A. (2006). Pex19p binds Pex30p and Pex32p at regions required for their peroxisomal localization but separate from their peroxisomal targeting signals. *J. Biol. Chem.* 281, 14805–14812. doi: 10.1074/jbc.M601808200

Voorn-Brouwer, T., Kragt, A., Tabak, H. F., and Distel, B. (2001). Peroxisomal membrane proteins are properly targeted to peroxisomes in the absence of COPI- and COPII-mediated vesicular transport. *J. Cell Sci.* 114(Pt 11), 2199–2204.

Walker, C. L., Pomatto, L. C. D., Tripathi, D. N., and Davies, K. J. A. (2017). Redox regulation of homeostasis and proteostasis in peroxisomes. *Physiol. Rev.* 98, 89–115. doi: 10.1152/physrev.00033.2016

Wanders, R. J. A. (2014). Metabolic functions of peroxisomes in health and disease. *Biochimie* 98, 36–44. doi: 10.1016/j.biochi.2013.08.022

Wang, C.-W., Miao, Y.-H., and Chang, Y.-S. (2014). Control of lipid droplet size in budding yeast requires the collaboration between Fld1 and Ldb16. *J. Cell Sci.* 127(Pt 6), 1214–1228. doi: 10.1242/jcs.137737

Wang, H., Becuwe, M., Housden, B. E., Chitraju, C., Porras, A. J., Graham, M. M., et al. (2016). Seipin is required for converting nascent to mature lipid droplets. *eLife* 5:e16582. doi: 10.7554/eLife.16582

Wang, S., Horn, P. J., Liou, L. C., Muggeridge, M. I., Zhang, Z., Chapman, K. D., et al. (2013). A peroxisome biogenesis deficiency prevents the binding of alpha-synuclein to lipid droplets in lipid-loaded yeast. *Biochem. Biophys. Res. Commun.* 438, 452–456. doi: 10.1016/j.bbrc.2013.07.100

Wang, S., Idrissi, F. Z., Hermansson, M., Grippa, A., Ejsing, C. S., and Carvalho, P. (2018). Seipin and the membrane-shaping protein Pex30 cooperate in organelle budding from the endoplasmic reticulum. *Nat. Commun.* 9:2939. doi: 10.1038/s41467-018-05278-2

Waterham, H. R., Ferdinandusse, S., and Wanders, R. J. A. (2016). Human disorders of peroxisome metabolism and biogenesis. *Biochim. Biophys. Acta Mol. Cell Res.* 1863, 922–933. doi: 10.1016/j.bbamcr.2015.11.015

Wróblewska, J. P., Cruz-Zaragoza, L. D., Yuan, W., Schummer, A., Chuartzman, S. G., de Boer, R., et al. (2017). *Saccharomyces cerevisiae* cells lacking Pex3

contain membrane vesicles that harbor a subset of peroxisomal membrane proteins. *Biochim. Biophys. Acta Mol. Cell Res.* 1864, 1656–1667. doi: 10.1016/j.bbamcr.2017.05.021

Xu, D., Li, Y., Wu, L., Li, Y., Zhao, D., Yu, J., et al. (2018). Rab18 promotes lipid droplet (LD) growth by tethering the ER to LDs through SNARE and NRZ interactions. *J. Cell Biol.* 217, 975–995. doi: 10.1083/jcb.201704184

Xu, N., Zhang, S. O., Cole, R. A., McKinney, S. A., Guo, F., Haas, J. T., et al. (2012). The FATP1-DGAT2 complex facilitates lipid droplet expansion at the ER-lipid droplet interface. *J. Cell Biol.* 198, 895–911. doi: 10.1083/jcb.201201139

Yan, R., Qian, H., Lukmantara, I., Gao, M., Du, X., Yan, N., et al. (2018). Human SEIPIN binds anionic phospholipids. *Dev. Cell* 47, 248–256.e4. doi: 10.1016/j.devcel.2018.09.010

Zanghellini, J., Wodlei, F., and von Grünberg, H. H. (2010). Phospholipid demixing and the birth of a lipid droplet. *J. Theor. Biol.* 264, 952–961. doi: 10.1016/j.jtbi.2010.02.025

Conflict of Interest Statement: The authors declare that the research was conducted in the absence of any commercial or financial relationships that could be construed as a potential conflict of interest.

frontiers in Cell and Developmental Biology

REVIEW
published: 04 June 2019
doi: 10.3389/fcell.2019.00083

Regulation of Membrane Turnover by Phosphatidic Acid: Cellular Functions and Disease Implications

*Rajan Thakur, Amruta Naik, Aniruddha Panda and Padinjat Raghu**

National Centre for Biological Sciences-TIFR, Bengaluru, India

Phosphatidic acid (PA) is a simple glycerophospholipid with a well-established role as an intermediate in phospholipid biosynthesis. In addition to its role in lipid biosynthesis, PA has been proposed to act as a signaling molecule that modulates several aspects of cell biology including membrane transport. PA can be generated in eukaryotic cells by several enzymes whose activity is regulated in the context of signal transduction and enzymes that can metabolize PA thus terminating its signaling activity have also been described. Further, several studies have identified PA binding proteins and changes in their activity are proposed to be mediators of the signaling activity of this lipid. Together these enzymes and proteins constitute a PA signaling toolkit that mediates the signaling functions of PA in cells. Recently, a number of novel genetic models for the analysis of PA function *in vivo* and analytical methods to quantify PA levels in cells have been developed and promise to enhance our understanding of PA functions. Studies of several elements of the PA signaling toolkit in a single cell type have been performed and are presented to provide a perspective on our understanding of the biochemical and functional organization of pools of PA in a eukaryotic cell. Finally, we also provide a perspective on the potential role of PA in human disease, synthesizing studies from model organisms, human disease genetics and analysis using recently developed PLD inhibitors.

Keywords: lipid signaling, membrane transceptor, endomembrane compartments, model organism, cellular neurobiology, photoreceptores

OPEN ACCESS

Edited by:
Sarita Hebbar,
Max-Planck-Institut für Molekulare Zellbiologie und Genetik, Germany

Reviewed by:
Nicolas Vitale,
Centre National de la Recherche Scientifique (CNRS), France
Nicholas Ktistakis,
Babraham Institute (BBSRC), United Kingdom

***Correspondence:**
Padinjat Raghu
praghu@ncbs.res.in

Specialty section:
This article was submitted to Membrane Traffic, a section of the journal Frontiers in Cell and Developmental Biology

Received: *04 March 2019*
Accepted: *03 May 2019*
Published: *04 June 2019*

Citation:
Thakur R, Naik A, Panda A and Raghu P (2019) Regulation of Membrane Turnover by Phosphatidic Acid: Cellular Functions and Disease Implications. Front. Cell Dev. Biol. 7:83. doi: 10.3389/fcell.2019.00083

INTRODUCTION AND HISTORICAL PERSPECTIVE

Phosphatidic acid (PA) is the simplest glycerophospholipid whose oldest known function is to serve as the backbone for the synthesis of a number of classes of glycerophospholipids. It consists of two fatty acyl chains esterified at positions *sn-1* and *sn-2* of glycerol and a free phosphate group at *sn-3* (**Figure 1**) reviewed in Athenstaedt and Daum (1999). Subsequently, it has become apparent that PA is also produced by biochemical reactions that are well understood as part of signal transduction pathways that mediate information transfer in eukaryotic cells. Through these pathways PA can mediate a diverse range of effects on eukaryotic cells that have been studied both in terms of basic cellular and molecular mechanisms and their potential involvement in disease processes. In this review we focus specifically on those functions of PA that relate to its ability to regulate membrane transport events in eukaryotic cells.

Compartmentalization into membrane bound organelles is a fundamental feature of eukaryotic cells (Rout and Field, 2017). Although the core principles of how membrane bound vesicles exchange material between the organelles of a cell have been known for some time (Pfeffer, 2013), there remains much interest in the mechanism by which this process is regulated. In this setting, the interest in the function of PA as a regulator of membrane transport rose from two strands of work. First, the study of secretion control in yeast had identified SEC14 as a PI/PC transfer protein required to support secretion and transport from the Golgi (Bankaitis et al., 1990). A genetic screen to identify suppressers and enhancers of *sec14* mutants had identified so called "bypass" mutants which encoded proteins involved in phosphatidylinositol (PI) and phosphatidylcholine (PC) biosynthesis (Cleves et al., 1991). Work in the Bankaitis lab uncovered the finding that for the bypass mutants to supress SEC14 function, yeast strains must have an intact SPO14 gene. SPO14 encodes phospholipase D (PLD), and enzyme that converts PC to PA (Sreenivas et al., 1998; Xie et al., 1998). Although SPO14 is a non-essential gene during vegetative growth, it is required for both prospore formation and PA production during starvation induced sporulation (Rudge et al., 1998, 2001); loss of spo14p leads to the accumulation of undocked membrane bound vesicles at the spindle pole body (Nakanishi et al., 2006). Subsequent elegant studies from the Neiman lab have shown that PA binds to spo20p, a v-SNARE required for fusion of vesicles to the prospore membrane (De Los Santos and Neiman, 2004; Liu et al., 2007). To date, these studies represent the most detailed analysis of a role for PA in regulating events in intracellular membrane transport in eukaryotic cells.

Secondly, in the context of metazoan biology, a role for PA in regulating intracellular membrane transport arose from two types of analyses (i) *in vitro* biochemical analysis which showed that small GTPases of the Arf family, known regulators of membrane transport can stimulate PLD activity (Brown et al., 1993; Cockcroft et al., 1994). (ii) Overexpression of PLD in multiple metazoan cells was able to modulate exocytosis (Vitale et al., 2001; Choi et al., 2002; Cockcroft et al., 2002; Huang et al., 2005), promote the generation of β-amyloid precursor protein containing vesicles at the TGN (Cai et al., 2006a). It was also shown that elevation of PA levels by multiple methods in *Drosophila* photoreceptors results in altered protein trafficking to the apical domain of these cells, collapse of the apical plasma membrane and the accumulation of endomembranes within the cell body (Raghu et al., 2009a). However, in contrast to the yeast system, until recently there had been limited evidence to support a role for PA in regulating intracellular transport in metazoan cells. A recent study has presented evidence supporting a role for endogenous PLD in regulating intracellular transport in *Drosophila* photoreceptors (Thakur et al., 2016).

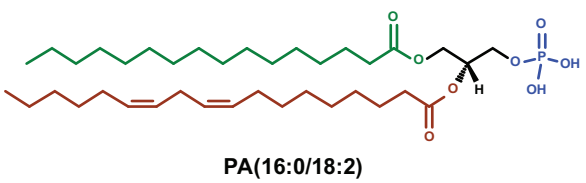

FIGURE 1 | The chemical structure of phosphatidic acid. The glycerol backbone (black) of PA has esterified fatty acids at *sn-1* (green) and *sn-2* (red) position with carbon chain length of 16:0 and 18:2, respectively. The phosphate head group esterified at *sn-3* is shown in blue.

PA SYNTHESIS AND TURNOVER

Cellular levels of PA are controlled in a spatiotemporal manner through the activity of multiple enzymes (**Figure 2**). These enzymes are located at distinct sub-cellular locations and use specific sources of substrate to maintain PA homeostasis and dynamics within cells.

The *de novo* synthesis of PA occurs by two acylation reactions wherein the first reaction leads to formation of monoacylated PA[also called lysophosphatidic acid (LPA)]. LPA formation can occur via one of two pathways; the first, seen in all organisms from bacteria to mammals utilizes glycerol-3-phosphate by the action of glycerol-3-P acyltransferase whereas the second occurs via the dihydroxyacetone phosphate pathway starting with the substrate dihydroxyacetone phosphate (DHAP). The LPA formed undergoes a second acylation catalyzed by lysophosphatidic acid acyl transferase (LPAAT). PA thus formed can be converted to diacylglycerol (DAG) by phosphatidic acid phosphatase (Carman and Han, 2009). DAG further serves as an intermediate in the biosynthesis of triacylglycerols and phospholipids like PC, phosphatidylethanolamine (PE) and phosphatidylserine (PS)that are important structural lipids. CDP-DAG synthase can also act on PA to form cytidine diphosphate diacylglycerol (CDP-DAG) that is also an intermediate in synthesis of various phospholipids like PI, phosphatidylglycerol (PG) and cardiolipin (CL) (Heacock and Agranoff, 1997).

The enzymes that generate pools of signaling PA are mainly PLD, diacylglycerol kinase (DGK) and LPAAT. PC-specific PLD hydrolyses PC to form membrane bound PA and free choline. PA thus formed performs various downstream signaling functions. Although PLD like genes are found in both prokaryotes and eukaryotes, in eukaryotes, in addition to the catalytic HKD motifs, a number of additional domains such as the PX, PH, myristoylation sequence and phosphatidylinositol 4,5-bisphosphate (PIP_2) binding site are found that may serve to target the enzyme to specific membrane compartments reviewed in Selvy et al. (2011). While simpler eukaryote genomes contain a single gene encoding PLD activity, large and complex genomes such as those of mammals contain two genes PLD1 and PLD2 that biochemically show PLD activity [reviewed in Selvy et al. (2011)]. A recent study has suggested that the single PLD gene in *Drosophila melanogaster* encodes a protein that is functionally more similar to hPLD1 than hPLD2 (Panda et al., 2018). Though PLD1 and PLD2 are the most extensively studied, there are 4 other reported members of the mammalian PLD family, defined by the presence of a HKD motif. PLD3 and PLD4 are type II transmembrane proteins located at the ER and lysosomal compartments (Otani et al., 2011; Gonzalez et al., 2018). Although they belong to the PLD family, no canonical PLD

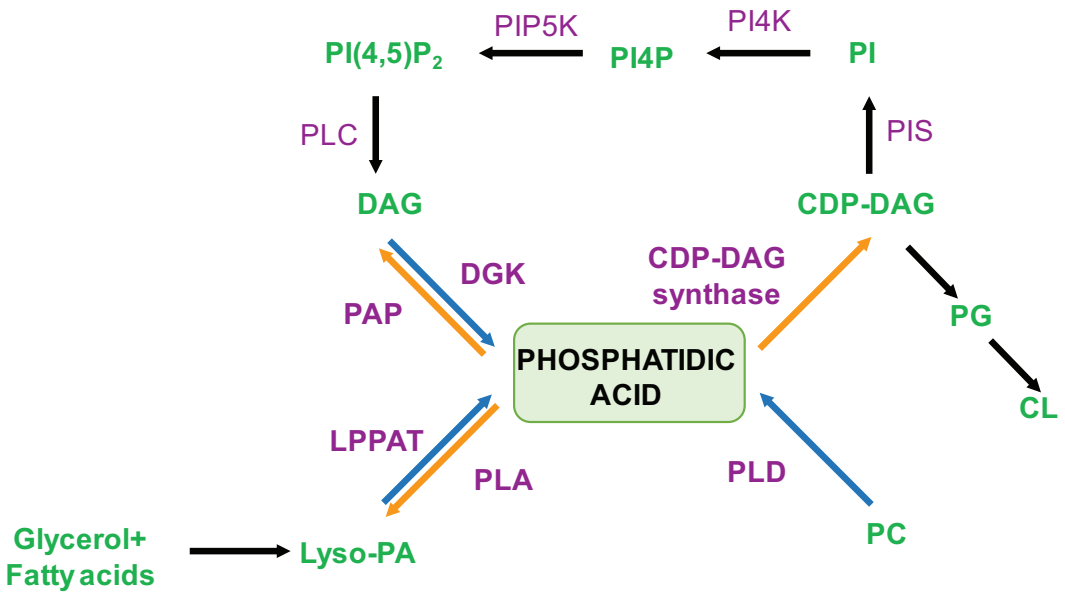

FIGURE 2 | Schematic representation for biochemical pathways for the synthesis and metabolism of PA. Blue arrows indicate PA synthesis while orange arrows indicate turnover. Enzymes involved are marked in purple and the ones directly affecting PA levels are indicated in bold. Lipids species are marked in green. DAG, Diacylglycerol; CDP-DAG, Cytidine Diphosphate Diacylglycerol; PI, Phosphatidylinositol; PI4P, Phosphatidylinositol-4-phosphate; PI(4,5)P_2, Phosphatidlyinositol-4,5-bis-phosphate; Lyso-PA, Lyso-phosphatidic acid; PC, Phosphatidylcholine; PG, Phosphatidylglycerol; CL, Cardiolipin; DGK, Diacylglycerol kinase; PAP, PA Phosphatase; LPAAT, Lyso-PA Acyl Transferase; PLA, Phospholipase A; PLD, Phospholipase D; PI4K, Phosphatidylinositol-4-kinase; PIP5K, Phosphatidylinositol-4-phosphate-5-kinase; PLC, Phospholipase C.

enzyme activity has been reported. PLD5 is similar to PLD3 and PLD4 in that biochemical activity has not been demonstrated; a mouse knockout of PLD 5 has not shown any significant abnormalities (Karp et al., 2010). PLD6 or Mito PLD can hydrolyse cardiolipin on the outer membrane of mitochondria to generate PA (Choi et al., 2006). Along with this it has also functions as an endonuclease (phosphodiesterase) in piRNAs biogenesis (Watanabe et al., 2011).

It has been known since the 1980s that PLD is a signal activated enzyme in mammalian cells. Many agonists including hormones and neurotransmitters activate PLD [reviewed in Liscovitch (1991)]; interestingly many of these agonists also activate phospholipase C (PLC) resulting in PIP_2 hydrolysis, a concomitant increase in intracellular calcium $[Ca^{2+}]_i$ and the production of DAG, an activator of protein kinase C (PKC). Interestingly, both Ca^{2+} and PKC have been studied as stimulators of PLD activity (Exton, 2002). In addition, small G-proteins of the Arf family appear to be required for full activation of PLD during GPCR signaling. A recent study has presented evidence that in *Drosophila* photoreceptors, where photons activate the GPCR rhodopsin leading to PLC activation, PLD dependent PA production also occurs but this does not requires Gq activity (Thakur et al., 2016). However, the biochemical steps leading to PLD activation during agonist mediated activation of G-protein coupled receptors (GPCR) remains unresolved.

Diacylglycerol kinases (DGK) are a family of lipid kinases that phosphorylate DAG to produce PA. DGKs are present in organisms from prokaryotes to mammals. In mammals, ten isoforms of DGK are reported that are grouped into 5 classes, each of which contains the DGK catalytic domain along with a range of additional domains that presumably lend both localization and regulatory properties [reviewed in Topham and Epand (2009)]. DGK activity is required to metabolize the DAG generated during receptor activated PLC signaling; loss of DGK results in enhanced PLC signaling based outputs in studies of multiple model systems (Rodriguez de Turco et al., 2001; Hardie et al., 2002; Zhong et al., 2003; Olenchock et al., 2006). Although direct evidence of a role for PA in phenotypes resulting from DGK deficiency have not been presented, it has been proposed that reduction of PA levels in *rdgA* mutants (diacylglycerol kinase in *Drosophila*) may result in transport defects to the apical membrane of photoreceptors (Suzuki et al., 1990). However, *laza* mutants (Type II PA phosphatase in *Drosophila*) that show elevated PA levels are able to suppress the retinal degeneration of *rdgA* mutants (Garcia-Murillas et al., 2006) suggesting that PA levels may be important for the phenotypes of DGK deficiency.

QUANTIFICATION OF PHOSPHATIDIC ACID

Phosphatidic acid is a low abundance phospholipid in cells, being about two log orders less abundant compared to lipid classes such as PC; in biological samples PA is estimated to be 0.1–0.3 mole % of the total membrane lipids (Guan et al., 2013). Levels of PA can be estimated using multiple approaches such as

thin layer chromatography (Holland et al., 2003), radionuclide (Munnik et al., 2000) or fluorescent labeling (Zhang et al., 2004). However, each of these methods has limitations ranging from low sensitivity to the inability to label total lipids in tissues. This poses a challenge in determining the levels of PA from tissue or cell samples without the benefit of radioactive labeling. Mass spectrometry has also been used to measure PA levels in tissues. The majority of published literature for PA analysis relies on triple quadrupole mass spectrometry coupled to reverse phase high performance liquid chromatography (HPLC) (Aaltonen et al., 2010; Bathena et al., 2011; Buré et al., 2013), although quantification of PA has also been reported using normal phase (Raghu et al., 2009a) and hydrophilic interaction liquid chromatography (HILIC) (Buré et al., 2013; Triebl et al., 2014). PA levels have previously been quantified from lipid extracts using the high resolution (100,000) and high mass accuracy ($\leq$3 ppm) provided by Orbitrap technology (Yadav et al., 2015; Thakur et al., 2016). This method identifies lipids based on class specific chemical formulae generated from their monoisotopic mass; hence the exact composition of the fatty acyl chains cannot be determined. Recent work has established a new mass spectrometry-based method which can establish the fatty acyl chain composition of individual PA species and also quantify them. This method uses differential fragmentation patterns obtained from multiple reaction monitoring (MRM)-triggered information dependent (IDA) "on the fly" MS/MS' (recorded as EPI) experiments, to establish *sn-1* and *sn-2* positional isomers present in PA from biological samples. This method should facilitate the analysis of PA in the context of cell signaling (Panda et al., 2018).

In addition to PA mass estimation, it is also informative to determine the spatial distribution of PA in cells. The spatial distribution of PA can be studied using PA binding domains (PABD) of proteins fused to fluorescent reporters. Such PABD are described below; some of the mostly commonly used PA probes are the PABD of SPO20 (Nakanishi, 2004), Opi1p (Loewen et al., 2004), PDE41A (Baillie et al., 2002), and Raf1 (Cells et al., 1996). In cells the PABD of SPO20 is localized to compartments like plasma membrane and nucleus (Nakanishi, 2004; Zeniou-Meyer et al., 2007) whereas the PABD of Opi1p is localized to the endoplasmic reticulum (ER) and nucleus (Loewen et al., 2004) and the PABD of PDE41A is found at the Golgi apparatus (Baillie et al., 2002). The differential localization of PABDs might be due to recognition of distinct pools of PA in a specific environment (Kassas et al., 2017) or additional regulators of their localization. However, these methods cannot give quantitative information about PA.

PHOSPHATIDIC ACID BINDING MODULE

Phosphatidic acid is a negatively charged lipid that regulates diverse cellular processes ranging from membrane trafficking to growth control (Jones et al., 1999; Foster, 2009). Some of these functions have been proposed to depend on its ability, as a cone shaped molecule, to alter lipid packing in a leaflet of the bilayer and thus membrane curvature. Many actions of PA are attributed to its ability to interact with PA binding proteins. Thus, in order to understand the *in vivo* regulatory functions of PA, it is important to study PA binding proteins. There have been various biochemical analyses primarily utilizing lipid affinity purification and LC–MS/MS mass spectrometry to identify novel PA binding proteins from tissue extracts (Manifava et al., 2001; Park et al., 2015). Such studies have revealed a broad range of PA binding proteins [reviewed in Raghu et al. (2009b), Stace and Ktistakis (2006)], however, in contrast to other lipid classes such as phosphoinositides that bind to specific domains (e.g., PX domain), to date no PA binding protein domain has been identified. Rather, it is thought that positively charged amino acids (e.g., lysine, arginine, and histidine) in PA-binding proteins interact with the negatively charged head group of PA (Stace and Ktistakis, 2006; Lemmon, 2008). PA-protein interactions can also be mediated by presence of the positively charged amino acids in well-defined domains of proteins like the PH domain of Sos (Zhao et al., 2007) or it can be in unstructured regions harboring several basic amino acids such as in the proteins Raf-1, mTOR,PIP5K, and DOCK2 (Fang et al., 2001; Stace and Ktistakis, 2006; Nishikimi et al., 2009; Roach et al., 2012). A recent review has highlighted factors that are likely to influence that ability of PA to bind to proteins given its unique physicochemical properties (Tanguy et al., 2018). Although a primary role for positively charged amino acids in mediating PA binding to proteins is central, the protonated state of PA, the presence of other zwitterionic lipids such as PE and the concentration of Ca^{2+} ions can also influence PA binding properties. The physicochemical properties of PA binding to proteins in the context of membranes is summarized in an excellent, recent review by Vitale et al. (2001), Tanguy et al. (2018).

PHOSPHATIDIC ACID FUNCTIONS

Phosphatidic acid is a cone shaped, low abundance membrane phospholipid (van Meer et al., 2008). By virtue of its shape, it can impart negative curvature to membranes and hence in principle influence membrane budding and fusion during vesicular trafficking. PA can also modulate membrane trafficking by binding to proteins that regulate various aspect of vesicular trafficking (Jones et al., 1999; Roth et al., 1999). Some of the important functions of PA in the context of membrane trafficking are described below:

Receptor Transport

The ability of a cell to respond optimally to environmental changes is determined by the numbers and types of plasma membrane receptors. Upon ligand binding plasma membrane receptors like receptor tyrosine kinases (RTKs) and G protein coupled receptors (GPCRs) are activated and mediate the downstream signaling (Gether, 2000). Post-activation, these receptors are internalized either via clathrin mediated endocytosis (CME) (Wolfe and Trejo, 2007) or clathrin-independent endocytic mechanisms (Mayor and Pagano, 2007) or via fast-endophilin-mediated endocytosis (FEME) (Boucrot et al., 2015). Removal of cell surface receptors serves as a

mechanism to regulate the levels of activated receptors on the surface and modulate the downstream signaling to a given ligand. The internalized receptors are subsequently degraded via lysosomes or recycled back to the plasma membrane (Irannejad and Von Zastrow, 2014).

Phosphatidic acid has been reported to play a regulatory role in CME (Antonescu et al., 2010). PLD activity itself has been implicated in trafficking and signaling from various membrane receptors (Exton, 2002; Selvy et al., 2011). Ligand induced endocytosis of EGFR requires PA generated by PLD1 (Lee C.S. et al., 2009). In presence of EGF, activated EGFR is internalized via CME with the help of the adaptor protein AP2 that recognizes EGFR via its μ2 subunit. In this context, it was seen that the PLD1 protein itself is an effector of PA and the auto-regulatory interaction between the PX domain of PLD1 and PA promotes the binding of PH domain of PLD1 with μ2 subunit and thereby facilitates EGFR endocytosis (Lee J.S. et al., 2009). PA also regulates the cell surface vs. intracellular distribution of inactive EGFR independent of the ligand. Inhibition of PA phosphatase activity causes acute increases in PA levels, inducing internalization of inactive EGFR in absence of ligand. It was seen that the internalization of inactive EGFR is through a PA effector-rolipram-sensitive type 4 phosphodiesterase (PDE4) that mediated down-regulation of PKA activity. The internalized EGFR accumulates in recycling endosomes and can either stay there without degradation for several hours or return to the cell surface when PA levels are reduced (Andres and Alfonso, 2010).

Micro-opioid receptors (MOPr) are a class of opioid receptors belonging to superfamily of seven transmembrane helix receptors. Activation of opioid receptors causes neuronal inhibition via multiple downstream effectors (Koch and Höllt, 2008). It has been shown that the agonist D-Ala2, Me Phe4, Glyol5-enkephalin (DAMGO) induced activation of MOPr also causes activation of PLD2 in an ARF dependent manner (Haberstock-Debic et al., 2003; Koch et al., 2003; Rankovic et al., 2009). MOPr and PLD2 physically interact with each other via the PX domain of PLD2 and regulate agonist-induced MOPr endocytosis (Koch et al., 2003). PLD2 activity has also been shown to be important for MOPr re-sensitization, as inhibition of PLD2 results in a decrease of agonist induced MOPr desensitization (Koch et al., 2004).

In neurons, class 1 metabotropic glutamate receptors (mGluR1 and mGluR5) are constitutively internalized via β-arrestin dependent and independent mechanisms (Sallese et al., 2000; Dale et al., 2001; Fourgeaud et al., 2003; Pula et al., 2004). PLD2 activity regulates the constitutive internalization of mGluR. It has been noted that PLD2 forms a complex with Ral and its guanine nucleotide exchange factor Ral-GDS. This novel complex constitutively interact with mGluRs by forming an adaptor and this agonist independent internalization does not appear to require β-arrestin (Bhattacharya et al., 2004).

In *Drosophila* photoreceptors, illumination activates the phototransduction cascade. Following light absorption, the GPCR Rhodopsin 1 (Rh1) undergoes photoisomerization to meta-rhodopsin (M). M is phosphorylated at its C-terminus, binds β-arrestin and this complex is removed from the microvillar plasma membrane via clathrin-dependent endocytosis to be either recycled back to the microvillar plasma membrane (Wang et al., 2014) or trafficked to the lysosome for degradation (Chinchore et al., 2009) [reviewed in Xiong and Bellen (2013)]. Tight regulation of this process is critical for rhabdomere integrity during illumination as mutants defective in any of the several steps of the rhodopsin cycle undergo light-dependent collapse of the rhabdomere [reviewed in Raghu et al. (2012) and see below]. During illumination, PA produced by dPLD regulates the recycling of Rh1 from late endosomal compartment in a ARF1 and retromer complex dependent manner back to the plasma membrane (Thakur et al., 2016). Hence during illumination, dPLD activity couples endocytosis of Rh1 loaded vesicles with their recycling to the plasma membrane thus maintaining plasma membrane composition and size. In summary, PA regulates the transport and signaling activity of several GPCRs by controlling their levels on the plasma membrane.

Exocytosis

Phosphatidic acid produced by PLD activity plays an important role in regulating exocytosis. Early evidence implicating PLD in exocytosis emerged from studies of mast cells and neutrophils (Bader and Vitale, 2009). Ethanol, known to inhibit PA production by PLD, also inhibited exocytosis in mast cells stimulated via their high affinity FcεR1 receptor (Gruchalla et al., 1990) and degranulation in neutrophils (Korchak et al., 1988; Tou and Gill, 2005). Subsequently several studies have reported similar observations with regard to PLD activity and exocytosis in differentiated HL60 cells (Stutchfield and Cockcroft, 1993), sperm acrosome (Roldan and Dawes, 1993), adherent human polymorph nuclear leukocytes (Nakamura et al., 1994), pancreatic β-cells (Hughes et al., 2004) and neuroendocrine chromaffin cells (Bader and Vitale, 2009). PA generated via diacylglycerol kinase (DGK) has also been to shown to regulate release of azurophilic granules in anti-neutrophil cytoplasmic antibodies induced neutrophil exocytosis (Holden et al., 2011). Although these studies implicate PA in regulating exocytosis, mechanistic insights as to which specific step of the exocytic process might be regulated remains to be discovered.

Phagocytosis

Phagocytosis is an essential process which enables immune cells like macrophages to internalize large particles (like extracellular particles, invasive pathogens, necrotic cells) into membrane-bound structure called the phagosomes (Niedergang and Chavrier, 2004). Such processes involve the ongoing extension of actin-rich protrusions and the consequent formation of phagosomes and macropinosomes (Flannagan et al., 2012). Lipids in general play a critical role in organizing various events of phagocytosis and PA also regulates multiple aspects of phagocytosis. In murine macrophages, PLD1 and PLD2 activity are necessary for efficient phagocytosis and PA is found to be transiently produced at the sites of phagosomes formation. In cells undergoing phagocytosis, PLD1 is recruited to nascent and internalized phagosomes, whereas PLD2 is only observed on nascent phagosomes. Thus both PLD isoforms are required for phagosome formation, but only PLD1 is implicated in later

stages of phagocytosis occurring after phagosomal internalization (Corrotte et al., 2006). It was also seen that during phagocytosis, PLD2 forms a heterotrimeric protein complex with growth factor receptor-bound protein 2 (Grb2) and Wiskott-Aldrich syndrome protein (WASp). It is by virtue of this interaction that PLD2 can regulate the localization and activity of WASp. PLD2 anchors WASp to the cell membrane via Grb2 by protein-protein interactions and the PA produced by PLD2 leads to synthesis of PIP_2 through PIP5K activity which in turn regulates the activity of WASp. This heterotrimeric interaction enables actin nucleation at the phagocytic cup and phagocytosis (Di Fulvio et al., 2007; Kantonen et al., 2011). In macrophages and dendrites, the basal PA required for constitutive membrane ruffling during micropinocytosis is primarily contributed by DGK and not by PLD activity (Bohdanowicz et al., 2013). PA is also known to regulate NADPH oxidase activity which plays important role in phagocytosis (Erickson et al., 1999; Palicz et al., 2001). Structural analysis of PX domain of the NADPH oxidase p47phox subunit by X-ray crystallography has identified two distinct pockets for phosphoinositide and PA binding (Karathanassis et al., 2002).

Neuronal Function

Phosphatidic acid is proposed to play an important role in neurotransmission (Humeau et al., 2001; Bader and Vitale, 2009). PA is generated at the presynaptic ribbon terminals where it can regulate various steps of synaptic vesicle trafficking (Schwarz et al., 2011). PA produced by PLD has been shown to bind and modulate the activity of several proteins involved in synaptic vesicle endo and exocytosis such as NSF, PI4P5K, and syntaxin-1A (Manifava et al., 2001; Lam et al., 2007; Mima and Wickner, 2009; Roach et al., 2012). The interaction between PA and syntaxin 1A is believed to be necessary for regulating the energetics of membrane fusion (Lam et al., 2007). PA can bind and activate PIP5K (Moritz et al., 1992; Jenkins et al., 1994) to synthesize PIP_2, an lipid important for neurotransmission and coupling of vesicular endocytosis to exocytosis at the synapse (Koch and Holt, 2012; Martin, 2015). Although there are number of studies linking PA produced by DGK to have a neuronal function *in vivo*, however, there is no direct evidence for the specific role of PA in the synaptic vesicle cycle (Tu-Sekine et al., 2015; Lee et al., 2016; Raben and Barber, 2017). In addition to multiple roles in the synaptic vesicle cycle, several studies have implicated PA produced by PLD1 and PLD2 in the intracellular trafficking of β-amyloid precursor protein (APP) and presenilin with important implications for amyloidogenesis (Cai et al., 2006a,b; Oliveira and Di Paolo, 2010; Oliveira et al., 2010b; Bravo et al., 2018). PLD1 is also reported to regulate autophagy mediated clearance of protein aggregates like p62 and Tau (Dall'Armi et al., 2010).

FUNCTIONAL ORGANIZATION OF SIGNALING POOLS OF PA

Although numerous roles have been described for PA in regulating various aspects of cell biology, there are limited examples where the generation and functions of PA pools derived from multiple sources have been studied in a single cell type. One such cell type is the budding yeast *Saccharomyces cerevisiae* where metabolic labeling experiments and mutant analysis have tracked the generation and interconversion of PA pools [reviewed in Ganesan et al. (2016)]. These studies have primarily provided insights into the pools of PA involved in lipid biosynthesis.

By contrast, in *Drosophila* photoreceptors, the dynamics and functions of signaling PA generated by multiple enzymes has been studied in a single cell type allowing a synthesis of the control of cellular processes by multiple pools of PA (**Figure 3**). *Drosophila* photoreceptors are polarized cells whose cell biology is specialized for signal transduction during photon detection. During phototransduction, photon absorption by Rh1 triggers G-protein coupled phospholipase C (PLC) activity leading to a sequence of biochemical reactions during which PA is formed as a key intermediate. Mutants have been isolated and studied for several enzymes involved in PA metabolism in the context of signaling offering a setting in which the regulation and cellular functions of PA in a single cell type can be studied (Raghu et al., 2012).

Detailed genetic and biochemical analysis in *Drosophila* photoreceptors has shown that adult photoreceptors contain two main pools of PA generated by DGK (encoded by *rdgA*) and PLD (encoded by *dPLD*), respectively. Loss of either enzyme results in a reduction in levels of PA in adult photoreceptors (Inoue et al., 1989; Garcia-Murillas et al., 2006; Thakur et al., 2016). *Drosophila* photoreceptors also contain two enzymes that can metabolize PA; a single gene encodes CDP-DAG synthase activity (*cds*) (Wu et al., 1995); in cds^1, a hypomorphic allele of *cds*, photoreceptors show elevated levels of PA during illumination confirming the requirement of this enzyme in metabolizing PA generated by DGK activity through conversion to CDP-DAG (Raghu et al., 2009a). In addition, photoreceptors also contain a Type II PA phosphatase activity (encoded by *laza*) that appears to be required for control of PA levels during illumination (Garcia-Murillas et al., 2006) and overexpression of *laza* further reduces the levels of PA in $rdgA^3$ photoreceptors (Garcia-Murillas et al., 2006). Together, these biochemical findings imply that DGK and Type II PA phosphatase can likely control the same biochemical pool of PA in photoreceptors.

Drosophila photoreceptors also contain a light stimulated PLD activity; loss of this PLD activity results in a reduction in PA levels (Thakur et al., 2016). Thus PLD activity contributes to PA levels in photoreceptors and since PLD knockout photoreceptors still express DGK, this observation implies that biochemically, these two enzymes contribute non-redundant pools of PA to photoreceptors. The PA levels in a *rdgA;dPLD* double mutant have not been described and it is presently unclear if at the biochemical level, there is any redundancy in the pools of PA generated by these two enzymes. These reduced PA levels can be rescued by either overexpression of RDGA or by loss of function of *laza* implying that PA arising from DGK activity can substitute for the loss of PA normally generated by PLD.

Since PA is a lipid, it is not freely diffusible across the cytoplasm and therefore restricted to the membrane at

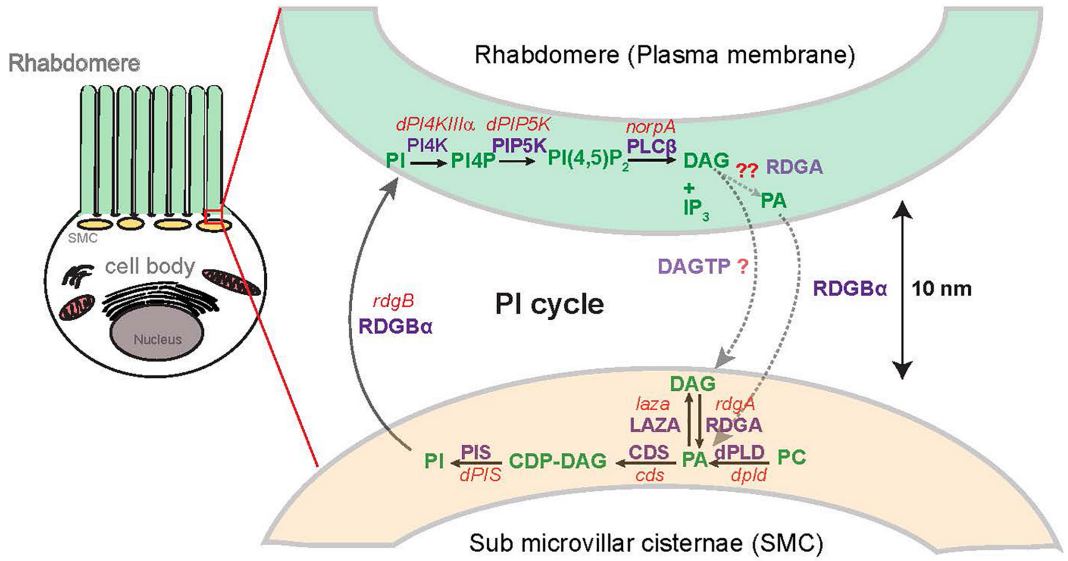

FIGURE 3 | Spatial organization of the known pools of phosphatidic acid turnover in photoreceptors: Representation of *Drosophila* photoreceptor showing the spatial organization of lipid intermediate in the rhabdomere microvilli with respect to the sub-microvillar cisternae (SMC) and the cell body [Adapted from Yadav et al. (2018)]. Enzymes involved are mentioned in purple, gene names are mentioned in red and lipids involved are marked in green. The reactions marked in light green and light purple are proposed and experimental evidence remains to be established. PA, phosphatidic acid; DAG, diacylglycerol; CDP-DAG, cytidine diphosphate diacylglycerol; PI, phosphatidylinositol; PC, phosphatidylcholine; PIP, phosphatidylinositol 4 phosphate; $PI(4,5)P_2$, phosphatidylinositol 4,5 bisphosphate; RDGA, diacylglycerol kinase encoded by the *rdgA* gene; LAZA-Type II PA phosphatase encoded by the *laza* gene; CDS-CDP-DAG, synthase encoded by the *cds* gene; dPLD, *Drosophila* PLD; PIS, phosphatidylinositol synthase.

which it is produced. While the biosynthetic pool of PA is presumably generated at the ER membrane, signaling pools of PA are generated at membranes where the enzymes that generate them are localized; this would determine the spatial distribution of signaling PA. In *Drosophila* photoreceptors, phospholipase C is localized at the apical plasma membrane of photoreceptors and thus DAG is produced at this membrane. RDGA that phosphorylates DAG to generate PA is localized on the sub-microvillar cisternae (SMC). The SMC are a specialized ER derived membrane compartment that is located at the base of the microvillar membrane where it forms a membrane contact site (MCS) with the microvillar plasma membrane (Yadav et al., 2016). The importance of precisely localizing RDGA is underscored by the phenotype of $rdgA^1$, the most severe allele of *rdgA*; $rdgA^1$ photoreceptors express normal levels of RDGA protein but an elegant immune electron microscopy study has demonstrated that the RDGA protein expressed in $rdgA^1$ photoreceptors is no longer localized to the SMC but distributed throughout the general ER in photoreceptors (Masai et al., 1997). Interestingly, PLD the other major source of signaling PA in photoreceptors is also localized to the region of the MCS between the plasma membrane and the SMC using immunofluorescence studies (Lalonde et al., 2005; Raghu et al., 2009a) although it is presently unclear at which of the two membranes the protein is localized; immunoelectron microscopy studies will be required to establish this point. The localization of endogenous LAZA in photoreceptors remains unknown; CDP-DAG synthase has been reported to be broadly distributed across the cellular ER in photoreceptors (Wu et al., 1995).

Functional analysis has also suggests that photoreceptors contain two major functional pools of PA. PA generated by RDGA, which is critical for normal electrical responses to light is generated in the context of G-protein coupled PIP_2 turnover (Raghu et al., 2000; Hardie et al., 2002). Loss of RDGA function leads to deregulated lipid turnover during PLC mediated PIP_2 turnover, excessive activation of TRP channels and retinal degeneration (Raghu et al., 2000; Hardie et al., 2004; Georgiev et al., 2005). From a cell biological perspective, retinal degeneration involves the collapse of the apical plasma membrane although the mechanism by which loss of RDGA and reduced PA levels leads to apical domain collapse remains unclear; Ca^{2+} influx through TRP channels is clearly an intermediate since retinal degeneration in *rdgA* mutants can be suppressed by loss of function mutants in *trp* (Raghu et al., 2000).

Loss of dPLD by contrast does not result in any detectable defects in phototransduction (Thakur et al., 2016) suggesting that this pool of PA does not contribute directly to PLC induced PIP_2 turnover and TRP channel activation. Further, overexpression of dPLD in *rdgA* mutants does not suppress retinal degeneration suggesting that PA derived from PLD cannot support those sub-cellular processes normally underpinned by RDGA. The major function of PA derived from PLD activity is to support membrane transport processes associated with rhodopsin trafficking in photoreceptors. Recent work shows that in dPLD mutants Rh1 containing vesicles accumulate in

the cell body following illumination. PA generated by dPLD seems to be required for the recycling of these rhodopsin containing vesicles back to the plasma membrane through the activity of the retromer complex [(Thakur et al., 2016) and see previous section]. Although the direct targets of PA that mediate control of vesicle recycling have yet to be identified, a role for Arf1, a known PA binding protein in this process has been proposed. In summary, the two major sources of PA in photoreceptors, DGK and PLD support distinct sub-cellular processes in photoreceptors.

Enzymes that metabolize PA have also been analyzed in the context of photoreceptor function. Hypomorphic alleles of *cds*, that encodes CDP-DAG synthase affect the electrical response to light (Wu et al., 1995) and also the re-synthesis of PIP_2 during PLC signaling (Hardie et al., 2001). Independent studies using transmission electron microscopy have also demonstrated endomembrane defects in the photoreceptor cell body of *cds* mutants (Raghu et al., 2009a) and these defects appear to occur in the context of ongoing Arf1 activity under scoring the importance of CDP-DAG in controlling PA pools that regulate membrane transport. Thus CDP-DAG synthase is able to impact functions dependent on PA generated by both DGK and non-DGK sources.

LAZA, the Type II PA phosphatase is required to metabolize PA in photoreceptors generating DAG. *Laza* mutants show an altered electrical response to light (Kwon and Montell, 2006), are able to suppress the retinal degeneration of *rdgA* (Garcia-Murillas et al., 2006) and overexpression of *laza* enhances this phenotype (Garcia-Murillas et al., 2006). Therefore, LAZA is able to metabolize a pool of PA generated by DGK activity. *laza* mutants are also able to restore the levels of PA in *dPLD* loss-of-function mutants and also suppress the retinal degeneration seen in *dPLD* mutants (Thakur et al., 2016). Thus, a pool of PA controlled by LAZA is also able to regulate functions mediated by PA generated via dPLD activity.

In summary, while DGK and PLD generate biochemically and functionally distinct pools of PA, the enzymes that metabolize PA, namely CDP-DAG synthase and LAZA seem able to access both pools of this lipid in photoreceptors (**Figure 4**). The cell biological basis of how these pools of PA are segregated and support unique functions remains unknown and will be an interesting topic to analyze in the future.

PA AND HUMAN DISEASE

Infectious Diseases

Several studies have implicated cellular PLD activity in influencing the ability of viruses to enter and replicate in mammalian cells. Infection of respiratory epithelial cells with influenza virus is reported to stimulate PLD activity and chemical inhibitors of PLD2, RNAi depletion of PLD2 and pre-treatment with primary alcohols have all been reported to decrease the number of cells infected with viral particles and also the viral titer produced post-infection (O'Reilly et al., 2014; Oguin et al., 2014). Since PLD enzymes can form PtOH that is enriched in endosomal membranes and can influence membrane curvature, there has been interest in the idea that PLD activity can influence the ability of viral particles to enter cells and traffic through the endosomal system. PLD inhibitors have demonstrated anti-viral activity against HIV and also impact survival of intracellular parasites but the proposed mechanism of action does not appear to involve modulation of host trafficking systems.

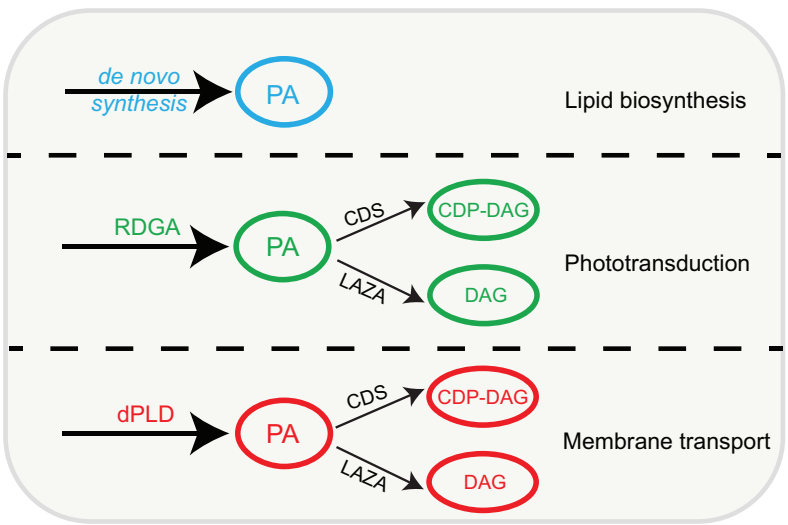

FIGURE 4 | Model conceptualizing the major pools of PA in Drosophila photoreceptors. Individual, distinct pools are marked in specific colors, enzymes that can generate and metabolize these pools based on available experimental evidence are shown. PA, phosphatidic acid; DAG, diacylglycerol; CDP-DAG, cytidine diphosphate diacylglycerol; RDGA, diacylglycerol kinase encoded by the *rdgA* gene; LAZA, Type II PA, phosphatase encoded by the *laza* gene; CDS-CDP-DAG, synthase encoded by the *cds* gene; dPLD, *Drosophila* PLD.

Central Nervous System

A number of studies in animal models have implicated PLD activity in the pathogenesis of stroke, injury, inflammation and neurodegenerative diseases of the central nervous system. Multiple mechanisms for these functions have been proposed [reviewed in Oliveira and Di Paolo (2010)]. In the context of the CNS, it is reported that PA produced by PLD activity can regulate the trafficking of amyloidogenic peptides (Cai et al., 2006a,b) and PLD2 ablation is reported to ameliorate synaptic dysfunction and cognitive defects in a mouse model of Alzheimer's disease (Oliveira et al., 2010a). It has also been reported that rare variants in PLD3 confer risk for the development of Alzheimer's disease (Cruchaga et al., 2014) and may do so via altering the levels of amyloidogenic peptides. However, a recent report using a mouse model of PLD3 has suggested that this may not be the mechanism of action although interestingly, this study also reported defects in the endo-lysosomal system in PLD3 mutants (Fazzari et al., 2017). Coffin-Lowry syndrome is a very rare form of X-linked mental retardation associated with growth and skeletal abnormalities[1]. A mutation in the protein Ribosomal S6 kinase 2 (RSK2) has been implicated as a cause of disease in some individuals with Coffin Lowry syndrome. Interestingly and pertinent to the topic of this review, phospholipase D has been reported to be phosphorylated by RSK2 and analysis in neural cell lines has suggested that this phosphorylation by RSK2 controls PLD1 activity and NGF induced neurite outgrowth; this study has proposed that PA may regulate vesicular transport in the growing neurite (Ammar et al., 2013, 2015). It has also been reported that the mRNA encoding diacylglycerol kinase kappa (DGKk) is one of the major RNA's associated with the Fragile-X mental retardation protein (FMRP) in mouse cortical neurons (Tabet et al., 2016). Fragile X is the commonest form of inherited intellectual disability in children. Since the FMRP protein is thought to function by binding mRNA molecules and regulating their translation, FMRP is expected to control the levels of DGKk thereby tuning the switch of neurons between DAG and PA signaling states; molecular evidence for this was presented by Tabet et al. (2016) along with phenotypic similarities between the *Fmr1*$^{-/y}$ mice and DGKk$^{-/-}$ mice. It has been proposed that the switch between DAG and PA signaling may work via alteration in vesicular transport within dendritic spines (Moine and Vitale, 2019).

Cancer

A number of studies have reported that PLD expression and activity are upregulated in a range of cancer types [(Bruntz et al., 2014; Kang et al., 2014) and references therein]. In genetically engineered mouse models, PLD1 can modulate tumor progression (Chen et al., 2012; Kang et al., 2015) and similar effects have been reported for PLD2 (Henkels et al., 2013; Wang et al., 2017). Since PA is the key product of PLD activity, it is possible that dysregulated PA signaling might contribute to one or more steps of cancer initiation or progression. A number of mechanisms are possible and some have been experimentally tested: (i) Since altered receptor tyrosine kinase signaling is a conserved feature of many cancers, it is possible that PA generated by PLD might contribute to tumor progression by propagating such signals (Henkels et al., 2013). In support of this idea one study has mapped the production of PA by PLD2 in relation to RTK signal transduction and shown its requirement for maintaining such signaling (Zhang et al., 2014). (ii) PA might contribute to the trafficking and secretion of factors that promote tumor progression; a potential role for PA generated by PLD2 in secretion of Type 1 Matrix metalloproteases, enzymes that are implicated in metastasis, has recently been presented (Wang et al., 2017). (iii) a third mechanism by which PA might play a role in cancer biology is through its ability to bind to and influence the mammalian target of rapamycin (mTOR) (Fang et al., 2001; Toschi et al., 2009), a key regulator of cell proliferation and growth. The source of PA that is sensed by mTOR has been debated; it has been suggested that PA generated by lipid synthesis rather than PLD/DGK signaling may be a nutritional signal in cells for mTOR (Foster, 2013) and experimental evidence to support this model has recently been presented (Menon et al., 2017). *De novo* synthesized PA is likely to contribute to membrane biogenesis and hence there are multiple mechanisms by which PA may contribute to cancer via altered membrane turnover.

Human Genetic Disorders

With the development of modern methods of Next Generation Sequencing based genotyping, it has become possible to rapidly sequence and identify potential pathogenic DNA sequence variants in human genes of interest. In some cases, such variants show clear genetic transmissibility and the inheritance of such a variant can be clearly correlated with disease phenotype, strengthening the evidence implicating such variants in disease phenotypes. In the context of PA metabolizing enzymes, two such mutations have been reported. In the case of the PLD1 gene, studies have implicated mutations in the PLD1 gene in two families with congenital cardiac valvular defects (Ta-Shma et al., 2017). These mutations segregate with disease phenotypes and were assessed to have a functional impact through studies in model organism systems. In addition, a pathogenic variant in PLD3 that reduces PLD3 activity has been reported in a family with spinocerebellar ataxia (van Dijk et al., 1995; Nibbeling et al., 2017). Finally, mutations in DGKe have been reported to result in hemolytic uremic syndrome (Nephrotic syndrome Type 7) (Lemaire et al., 2013; Ozaltin et al., 2013). The cell biological and molecular mechanism by which these mutations in PLD and DGK lead to the phenotypes described in these human patients remains to be elucidated.

In addition to the aforementioned studies on individual human families with defined clinical features, variants in PLD1, PLD2 and most DGK isoform genes have been linked in Genome Wide Association Studies (GWAS) with a range of human phenotypes including several diseases of the brain, autoimmune diseases, physical traits such as body mass Index and metabolic disorders. A catalog of these variations and the studies in which they were analyzed can be found at https://www.ebi.ac.uk/gwas/. Detailed analysis using experimental models will be required to understand the specific roles of PA metabolizing enzymes in these contexts.

[1] https://www.omim.org/entry/303600

SUMMARY AND FUTURE DIRECTIONS

Although numerous studies have implicated PA in the regulation of membrane transport and sub-cellular organization of compartments in eukaryotes, until recently, there has been limited progress in establishing the function of PA using model systems *in vivo*. With the recent availability of new genetic knockout models in multiple organisms including worms, flies, zebrafish and mice, is should now be possible to perform insightful studies into the function of PA in endogenous cell types. Further, novel ways of measuring PA in cells using fluorescent probes and mass spectrometry with the need for radiolabeling should facilitate such analysis *in vivo* using these genetic models. A number of key questions remain with respect to the signaling functions of PA:(i) As a signaling lipid how is the production and metabolism of PA coupled to ongoing cellular changes by controlling the activity of enzymes that tune its levels in cells? (ii) How does PA exert its effects on cells. Although a number of PA binding proteins have been described, the mechanisms by which it controls membrane transport remain poorly understood. PA can also be metabolized to lyso-PA and DAG both of whom may exert cellular effects by themselves and it has also been proposed that due to its cone shape, PA may also work independent of protein targets by altering local membrane curvature. Biophysical and biochemical studies using *in vitro* reconstitution will likely play a key role in answering these questions. These open questions represent interesting areas of analysis for the future. Finally, with the availability of high-throughput methods of NGS sequencing it should be possible to catalog variations in human PLD genes and link them to interesting phenotypic outcomes in health and disease.

AUTHOR CONTRIBUTIONS

All authors listed have made a substantial, direct and intellectual contribution to the work, and approved it for publication.

FUNDING

Work in the authors' laboratory is supported by the National Centre for Biological Sciences-TIFR and by a Wellcome Trust DBT India Alliance Senior Fellowship (IA/S/14/2/501540) to PR.

REFERENCES

Aaltonen, N., Laitinen, J. T., and Lehtonen, M. (2010). Quantification of lysophosphatidic acids in rat brain tissue by liquid chromatography-electrospray tandem mass spectrometry. *J. Chromatogr. B* 878, 1145–1152. doi: 10.1016/j.jchromb.2010.03.030

Ammar, M.-R., Humeau, Y., Hanauer, A., Nieswandt, B., Bader, M.-F., and Vitale, N. (2013). The coffin-lowry syndrome-associated protein RSK2 regulates neurite outgrowth through phosphorylation of phospholipase D1 (PLD1) and synthesis of phosphatidic acid. *J. Neurosci.* 33, 19470–19479. doi: 10.1523/JNEUROSCI.2283-13.2013

Ammar, M. R., Thahouly, T., Hanauer, A., Stegner, D., Nieswandt, B., and Vitale, N. (2015). PLD1 participates in BDNF-induced signalling in cortical neurons. *Sci. Rep.* 5:14778. doi: 10.1038/srep14778

Andres, N., and Alfonso, G. (2010). Phosphatidic acid induces ligand-independent EGFR endocytic traffic through PDE4 activation. *Mol. Biol. Cell* 21, 2916–2929. doi: 10.1091/mbc.E10-02-0167

Antonescu, C. N., Danuser, G., and Schmid, S. L. (2010). Phosphatidic acid plays a regulatory role in clathrin-mediated endocytosis. *Mol. Biol. Cell* 21, 2944–2952. doi: 10.1091/mbc.E10-05-0421

Athenstaedt, K., and Daum, G. (1999). Phosphatidic acid, a key intermediate in lipid metabolism. *Eur. J. Biochem.* 266, 1–16. doi: 10.1046/j.1432-1327.1999.00822.x

Bader, M. F., and Vitale, N. (2009). Phospholipase D in calcium-regulated exocytosis: lessons from chromaffin cells. *Biochim. Biophys. Acta* 1791, 936–941. doi: 10.1016/j.bbalip.2009.02.016

Baillie, G. S., Huston, E., Scotland, G., Hodgkin, M., Gall, I., Peden, A. H., et al. (2002). TAPAS-1, a novel microdomain within the unique N-terminal region of the PDE4A1 cAMP-specific phosphodiesterase that allows rapid, Ca2+-triggered membrane association with selectivity for interaction with phosphatidic acid. *J. Biol. Chem.* 277, 28298–28309. doi: 10.1074/jbc.M108353200

Bankaitis, V. A., Aitken, J. R., Cleves, A. E., and Dowhan, W. (1990). An essential role for a phospholipid transfer protein in yeast Golgi function. *Nature* 347, 561–562. doi: 10.1038/347561a0

Bathena, S. P., Huang, J., Nunn, M. E., Miyamoto, T., Parrish, L. C., Lang, M. S., et al. (2011). Quantitative determination of lysophosphatidic acids (LPAs) in human saliva and gingival crevicular fluid (GCF) by LC-MS/MS. *J. Pharm. Biomed. Anal.* 56, 402–407. doi: 10.1016/j.jpba.2011.05.041

Bhattacharya, M., Babwah, A. V., Godin, C., Anborgh, P. H., Dale, L. B., Poulter, M. O., et al. (2004). Ral and phospholipase D2-dependent pathway for constitutive metabotropic glutamate receptor endocytosis. *J. Neurosci.* 24, 8752–8761. doi: 10.1523/JNEUROSCI.3155-04.2004

Bohdanowicz, M., Schlam, D., Hermansson, M., Rizzuti, D., Fairn, G. D., Ueyama, T., et al. (2013). Phosphatidic acid is required for the constitutive ruffling and macropinocytosis of phagocytes. *Mol. Biol. Cell* 24, 1700–1712. doi: 10.1091/mbc.E12-11-0789

Boucrot, E., Ferreira, A. P. A., Almeida-Souza, L., Debard, S., Vallis, Y., Howard, G., et al. (2015). Endophilin marks and controls a clathrin-independent endocytic pathway. *Nature* 517, 460–465. doi: 10.1038/nature14067

Bravo, F. V., Da Silva, J., Chan, R. B., Di Paolo, G., Teixeira-Castro, A., and Oliveira, T. G. (2018). Phospholipase D functional ablation has a protective effect in an Alzheimer's disease *Caenorhabditis elegans* model. *Sci. Rep.* 8:3540.

Brown, H. A., Gutowski, S., Moomaw, C. R., Slaughter, C., and Sternweis, P. C. (1993). ADP-ribosylation factor, a small GTP-dependent regulatory protein, stimulates phospholipase D activity. *Cell* 75, 1137–1144. doi: 10.1016/0092-8674(93)90323-i

Bruntz, R. C., Lindsley, C. W., and Brown, H. A. (2014). Phospholipase D signaling pathways and phosphatidic acid as therapeutic targets in cancer. *Pharmacol. Rev.* 66, 1033–1079. doi: 10.1124/pr.114.009217

Buré, C., Ayciriex, S., Testet, E., and Schmitter, J. M. (2013). A single run LC-MS/MS method for phospholipidomics. *Anal. Bioanal. Chem.* 405, 203–213. doi: 10.1007/s00216-012-6466-9

Cai, D., Netzer, W. J., Zhong, M., Lin, Y., Du, G., Frohman, M., et al. (2006a). Presenilin-1 uses phospholipase D1 as a negative regulator of beta-amyloid formation. *Proc. Natl. Acad. Sci. U.S.A.* 103, 1941–1946. doi: 10.1073/pnas.0510708103

Cai, D., Zhong, M., Wang, R., Netzer, W. J., Shields, D., Zheng, H., et al. (2006b). Phospholipase D1 corrects impaired betaAPP trafficking and neurite outgrowth in familial Alzheimer's disease-linked presenilin-1 mutant neurons. *Proc. Natl. Acad. Sci. U.S.A.* 103, 1936–1940. doi: 10.1073/pnas.0510710103

Carman, G. M., and Han, G.-S. (2009). Phosphatidic acid phosphatase, a key enzyme in the regulation of lipid synthesis. *J. Biol. Chem.* 284, 2593–2597. doi: 10.1074/jbc.R800059200

Cells, M. C. K., Ghosh, S., Strum, J. C., Sciorra, V. A., Daniel, L., Bell, R. M., et al. (1996). Raf-1 kinase possesses distinct binding domains for phosphatidylserine and phosphatidic acid. *Biochemistry* 271, 8472–8480. doi: 10.1074/jbc.271.14.8472

Chen, Q., Hongu, T., Sato, T., Zhang, Y., Ali, W., Cavallo, J.-A., et al. (2012). Key roles for the lipid signaling enzyme phospholipase D1 in the tumor microenvironment during tumor angiogenesis and metastasis. *Sci. Signal.* 5:ra79. doi: 10.1126/scisignal.2003257

Chinchore, Y., Mitra, A., and Dolph, P. J. (2009). Accumulation of rhodopsin in late endosomes triggers photoreceptor cell degeneration. *PLoS Genet.* 5:e1000377. doi: 10.1371/journal.pgen.1000377

Choi, S.-Y., Huang, P., Jenkins, G. M., Chan, D. C., Schiller, J., and Frohman, M. A. (2006). A common lipid links Mfn-mediated mitochondrial fusion and SNARE-regulated exocytosis. *Nat. Cell Biol.* 8, 1255–1262. doi: 10.1038/ncb1487

Choi, W. S., Kim, Y. M., Combs, C., Frohman, M. A., and Beaven, M. A. (2002). Phospholipases D1 and D2 regulate different phases of exocytosis in mast cells. *J. Immunol.* 168, 5682–5689. doi: 10.4049/jimmunol.168.11.5682

Cleves, A. E., McGee, T. P., Whitters, E. A., Champion, K. M., Aitken, J. R., Dowhan, W., et al. (1991). Mutations in the CDP-choline pathway for phospholipid biosynthesis bypass the requirement for an essential phospholipid transfer protein. *Cell* 64, 789–800. doi: 10.1016/0092-8674(91)90508-v

Cockcroft, S., Thomas, G. M., Fensome, A., Geny, B., Cunningham, E., Gout, I., et al. (1994). Phospholipase D: a downstream effector of ARF in granulocytes. *Science* 263, 523–526. doi: 10.1126/science.8290961

Cockcroft, S., Way, G., O'Luanaigh, N., Pardo, R., Sarri, E., and Fensome, A. (2002). Signalling role for ARF and phospholipase D in mast cell exocytosis stimulated by crosslinking of the high affinity FcepsilonR1 receptor. *Mol. Immunol.* 38, 1277–1282. doi: 10.1016/s0161-5890(02)00075-5

Corrotte, M., Chasserot-Golaz, S., Huang, P., Du, G., Ktistakis, N. T., Frohman, M. A., et al. (2006). Dynamics and function of phospholipase D and phosphatidic acid during phagocytosis. *Traffic* 7, 365–377. doi: 10.1111/j.1600-0854.2006.00389.x

Cruchaga, C., Karch, C. M., Jin, S. C., Benitez, B. A., Cai, Y., Guerreiro, R., et al. (2014). Rare coding variants in the phospholipase D3 gene confer risk for Alzheimer's disease. *Nature* 505, 550–554. doi: 10.1038/nature12825

Dale, L. B., Bhattacharya, M., Seachrist, J. L., Anborgh, P. H., and Ferguson, S. S. G. (2001). Agonist-stimulated and tonic internalization of metabotropic glutamate receptor 1a in human embryonic kidney 293 cells: agonist-stimulated endocytosis is beta-arrestin1 isoform-specific. *Mol. Pharmacol.* 60, 1243–1253. doi: 10.1124/mol.60.6.1243

Dall'Armi, C., Hurtado-Lorenzo, A., Tian, H., Morel, E., Nezu, A., Chan, R. B., et al. (2010). The phospholipase D1 pathway modulates macroautophagy. *Nat. Commun.* 1:142. doi: 10.1038/ncomms1144

De Los Santos, P., and Neiman, A. (2004). Positive and negative regulation of a SNARE protein by control of intracellular localization. *Mol. Biol. Cell* 15, 1802–1815. doi: 10.1091/mbc.e03-11-0798

Di Fulvio, M., Frondorf, K., Henkels, K. M., Lehman, N., and Gomez-Cambronero, J. (2007). The Grb2/PLD2 interaction is essential for lipase activity, intracellular localization and signaling in response to EGF. *J. Mol. Biol.* 367, 814–824. doi: 10.1016/j.jmb.2007.01.021

Erickson, R. W., Langel-Peveri, P., Traynor-Kaplan, A. E., Heyworth, P. G., and Curnutte, J. T. (1999). Activation of human neutrophil NADPH oxidase by phosphatidic acid or diacylglycerol in a cell-free system. Activity of diacylglycerol is dependent on its conversion to phosphatidic acid. *J. Biol. Chem.* 274, 22243–22250. doi: 10.1074/jbc.274.32.22243

Exton, J. H. (2002). Regulation of phospholipase D. *FEBS Lett.* 531, 58–61.

Fang, Y., Bachmann, R., Flanigan, A., and Chen, J. (2001). Phosphatidic acid – mediated mitogenic activation of mTOR signaling. *Science* 294, 1942–1946. doi: 10.1126/science.1066015

Fazzari, P., Horre, K., Arranz, A. M., Frigerio, C. S., Saito, T., Saido, T. C., et al. (2017). PLD3 gene and processing of APP. *Nature* 541, E1–E2. doi: 10.1038/nature21030

Flannagan, R. S., Jaumouillé, V., and Grinstein, S. (2012). The cell biology of phagocytosis. *Annu. Rev. Pathol.* 7, 61–98.

Foster, D. A. (2009). Phosphatidic acid signaling to mTOR: signals for the survival of human cancer cells. *Biochim. Biophys. Acta* 1791, 949–955. doi: 10.1016/j.bbalip.2009.02.009

Foster, D. A. (2013). Phosphatidic acid and lipid-sensing by mTOR. *Trends Endocrinol. Metab.* 24, 272–278. doi: 10.1016/j.tem.2013.02.003

Fourgeaud, L., Bessis, A. S., Rossignol, F., Pin, J. P., Olivo-Marin, J. C., and Hémar, A. (2003). The metabotropic glutamate receptor mGluR5 is endocytosed by a clathrin-independent pathway. *J. Biol. Chem.* 278, 12222–12230. doi: 10.1074/jbc.M205663200

Ganesan, S., Shabits, B. N., and Zaremberg, V. (2016). Tracking diacylglycerol and phosphatidic acid pools in budding yeast. *Lipid Insights* 8, 75–85. doi: 10.4137/LPI.S31781

Garcia-Murillas, I., Pettitt, T., Macdonald, E., Okkenhaug, H., Georgiev, P., Trivedi, D., et al. (2006). lazaro encodes a lipid phosphate phosphohydrolase that regulates phosphatidylinositol turnover during Drosophila phototransduction. *Neuron* 49, 533–546. doi: 10.1016/j.neuron.2006.02.001

Georgiev, P., Garcia-Murillas, I., Ulahannan, D., Hardie, R. C., and Raghu, P. (2005). Functional INAD complexes are required to mediate degeneration in photoreceptors of the *Drosophila rdgA* mutant. *J. Cell Sci.* 118(Pt 7), 1373–1384. doi: 10.1242/jcs.01712

Gether, U. (2000). Uncovering molecular mechanisms involved in activation of G protein-coupled receptors. *Endocr. Rev.* 21, 90–113. doi: 10.1210/edrv.21.1.0390

Gonzalez, A. C., Schweizer, M., Jagdmann, S., Bernreuther, C., Reinheckel, T., Saftig, P., et al. (2018). Unconventional trafficking of mammalian phospholipase D3 to lysosomes. *Cell Rep.* 22, 1040–1053. doi: 10.1016/j.celrep.2017.12.100

Gruchalla, R. S., Dinh, T. T., and Kennerly, D. A. (1990). An indirect pathway of receptor-mediated 1,2-diacylglycerol formation in mast cells. I. IgE receptor-mediated activation of phospholipase D. *J. Immunol.* 144, 2334–2342.

Guan, X. L., Cestra, G., Shui, G., Kuhrs, A., Schittenhelm, R. B., Hafen, E., et al. (2013). Biochemical membrane lipidomics during *Drosophila* development. *Dev. Cell* 24, 98–111. doi: 10.1016/j.devcel.2012.11.012

Haberstock-Debic, H., Wein, M., Barrot, M., Colago, E. E., Rahman, Z., Neve, R. L., et al. (2003). Morphine acutely regulates opioid receptor trafficking selectively in dendrites of nucleus accumbens neurons. *J. Neurosci.* 23, 4324–4332. doi: 10.1523/jneurosci.23-10-04324.2003

Hardie, R. C., Gu, Y., Martin, F., Sweeney, S. T., and Raghu, P. (2004). *In vivo* light-induced and basal phospholipase C activity in *Drosophila* photoreceptors measured with genetically targeted phosphatidylinositol 4,5-bisphosphate-sensitive ion channels (Kir2.1). *J. Biol. Chem.* 279, 47773–47782. doi: 10.1074/jbc.M407525200

Hardie, R. C., Raghu, P., Moore, S., Juusola, M., Baines, R. A., and Sweeney, S. T. (2001). Calcium influx via TRP channels is required to maintain PIP2 levels in *Drosophila* photoreceptors. *Neuron* 30, 149–159. doi: 10.1016/s0896-6273(01)00269-0

Hardie, R. C. C., Martin, F., Cochrane, G. W. W., Juusola, M., Georgiev, P., and Raghu, P. (2002). Molecular basis of amplification in *Drosophila* phototransduction: roles for G protein, phospholipase C, and diacylglycerol kinase. *Neuron* 36, 689–701. doi: 10.1016/s0896-6273(02)01048-6

Heacock, A. M., and Agranoff, B. W. (1997). CDP-diacylglycerol synthase from mammalian tissues. *Biochim. Biophys. Acta* 1348, 166–172. doi: 10.1016/s0005-2760(97)00096-9

Henkels, K. M., Boivin, G. P., Dudley, E. S., Berberich, S. J., and Gomez-Cambronero, J. (2013). Phospholipase D (PLD) drives cell invasion, tumor growth and metastasis in a human breast cancer xenograph model. *Oncogene* 32, 5551–5562. doi: 10.1038/onc.2013.207

Holden, N. J., Savage, C. O. S., Young, S. P., Wakelam, M. J., Harper, L., and Williams, J. M. (2011). A dual role for diacylglycerol kinase generated phosphatidic acid in autoantibody-induced neutrophil exocytosis. *Mol. Med.* 17, 1242–1252. doi: 10.2119/molmed.2011.00028

Holland, W. L., Stauter, E. C., and Stith, B. J. (2003). Quantification of phosphatidic acid and lysophosphatidic acid by HPLC with evaporative light-scattering detection. *J. Lipid Res.* 44, 854–858. doi: 10.1194/jlr.D200040-JLR200

Huang, P., Altshuller, Y. M., Hou, J. C., Pessin, J. E., and Frohman, M. A. (2005). Insulin-stimulated plasma membrane fusion of Glut4 glucose transporter-containing vesicles is regulated by phospholipase D1. *Mol. Biol. Cell* 16, 2614–2623. doi: 10.1091/mbc.e04-12-1124

Hughes, W. E., Elgundi, Z., Huang, P., Frohman, M. A., and Biden, T. J. (2004). Phospholipase D1 regulates secretagogue-stimulated insulin release in pancreatic β-cells. *J. Biol. Chem.* 279, 27534–27541. doi: 10.1074/jbc.M403012200

Humeau, Y., Vitale, N., Chasserot-Golaz, S., Dupont, J.-L., Du, G., Frohman, M. A., et al. (2001). A role for phospholipase D1 in neurotransmitter release. *Proc. Natl. Acad. Sci. U.S.A.* 98, 15300–15305. doi: 10.1073/pnas.261358698

Inoue, H., Yoshioka, T., and Hotta, Y. (1989). Diacylglycerol kinase defect in a *Drosophila* retinal degeneration mutant *rdgA*. *J. Biol. Chem.* 264, 5996–6000.

Irannejad, R., and Von Zastrow, M. (2014). GPCR signaling along the endocytic pathway. *Curr. Opin. Cell Biol.* 27, 109–116. doi: 10.1016/j.ceb.2013.10.003

Jenkins, G. H., Fisette, P. L., and Anderson, R. A. (1994). Type I phosphatidylinositol 4-phosphate 5-kinase isoforms are specifically stimulated by phosphatidic acid. *J. Biol. Chem.* 269, 11547–11554.

Jones, D., Morgan, C., and Cockcroft, S. (1999). Phospholipase D and membrane traffic. Potential roles in regulated exocytosis, membrane delivery and vesicle budding. *Biochim. Biophys. Acta* 1439, 229–244.

Kang, D. W., Choi, C. Y., Cho, Y.-H., Tian, H., Di Paolo, G., Choi, K.-Y., et al. (2015). Targeting phospholipase D1 attenuates intestinal tumorigenesis by controlling β-catenin signaling in cancer-initiating cells. *J. Exp. Med.* 212, 1219–1237. doi: 10.1084/jem.20141254

Kang, D. W., Choi, K.-Y., and Min, D. S. (2014). Functional regulation of phospholipase D expression in cancer and inflammation. *J. Biol. Chem.* 289, 22575–22582. doi: 10.1074/JBC.R114.569822

Kantonen, S., Hatton, N., Mahankali, M., Henkels, K. M., Park, H., Cox, D., et al. (2011). A novel phospholipase D2-Grb2-WASp heterotrimer regulates leukocyte phagocytosis in a two-step mechanism. *Mol. Cell. Biol.* 31, 4524–4537. doi: 10.1128/MCB.05684-11

Karathanassis, D., Stahelin, R. V., Bravo, J., Perisic, O., Pacold, C. M., Cho, W., et al. (2002). Binding of the PX domain of $p47^{phox}$ to phosphatidylinositol 3, 4-bisphosphate and phosphatidic acid is masked by an intramolecular interaction. *EMBO J.* 21, 5057–5068. doi: 10.1093/emboj/cdf519

Karp, N. A., Baker, L. A., Gerdin, A.-K. B., Adams, N. C., Ramírez-Solis, R., and White, J. K. (2010). Optimising experimental design for high-throughput phenotyping in mice: a case study. *Mamm. Genome* 21, 467–476. doi: 10.1007/s00335-010-9279-1

Kassas, N., Tanguy, E., Thahouly, T., Fouillen, L., Heintz, D., Chasserot-Golaz, S., et al. (2017). Comparative characterization of phosphatidic acid sensors and their localization during frustrated phagocytosis. *J. Biol. Chem.* 292, 4266–4279. doi: 10.1074/jbc.M116.742346

Koch, M., and Holt, M. (2012). Coupling exo-and endocytosis: an essential role for PIP 2 at the synapse. *Biochim. Biophys. Acta* 1821, 1114–1132. doi: 10.1016/j.bbalip.2012.02.008

Koch, T., Brandenburg, L. O., Liang, Y., Schulz, S., Beyer, A., Schröder, H., et al. (2004). Phospholipase D2 modulates agonist-induced μ-opioid receptor desensitization and resensitization. *J. Neurochem.* 88, 680–688. doi: 10.1046/j.1471-4159.2003.02189.x

Koch, T., Brandenburg, L. O., Schulz, S., Liang, Y., Klein, J., and Hollt, V. (2003). ADP-ribosylation factor-dependent phospholipase D2 activation is required for agonist-induced mu-opioid receptor endocytosis. *J. Biol. Chem.* 278, 9979–9985. doi: 10.1074/jbc.M206709200

Koch, T., and Höllt, V. (2008). Role of receptor internalization in opioid tolerance and dependence. *Pharmacol. Ther.* 117, 199–206. doi: 10.1016/j.pharmthera.2007.10.003

Korchak, H. M., Vosshall, L. B., Haines, K. A., Wilkenfeld, C., Lundquist, K. F., and Weissmann, G. (1988). Activation of the human neutrophil by calcium-mobilizing ligands. II. Correlation of calcium, diacyl glycerol, and phosphatidic acid generation with superoxide anion generation. *J. Biol. Chem.* 263, 11098–11105.

Kwon, Y., and Montell, C. (2006). Dependence on the Lazaro phosphatidic acid phosphatase for the maximum light response. *Curr. Biol.* 16, 723–729. doi: 10.1016/j.cub.2006.02.057

Lalonde, M. M., Janssens, H., Rosenbaum, E., Choi, S. Y., Gergen, J. P., Colley, N. J., et al. (2005). Regulation of phototransduction responsiveness and retinal degeneration by a phospholipase D-generated signaling lipid. *J. Cell Biol.* 169, 471–479. doi: 10.1083/jcb.200502122

Lam, A. D., Tryoen-Toth, P., Tsai, B., Vitale, N., and Stuenkel, E. L. (2007). SNARE-catalyzed fusion events are regulated by syntaxin1A-lipid interactions. *Mol. Biol. Cell* 19, 485–497. doi: 10.1091/mbc.e07-02-0148

Lee, C. S., Kim, K. L., Jang, J. H., Choi, Y. S., Suh, P. G., and Ryu, S. H. (2009). The roles of phospholipase D in EGFR signaling. *Biochim. Biophys. Acta* 1791, 862–868. doi: 10.1016/j.bbalip.2009.04.007

Lee, J. S., Kim, I. S., Kim, J. H., Cho, W., Suh, P. G., and Ryu, S. H. (2009). Determination of EGFR endocytosis kinetic by auto-regulatory association of PLD1 with μ2. *PLoS One* 4:e7090. doi: 10.1371/journal.pone.0007090

Lee, D., Kim, E., and Tanaka-Yamamoto, K. (2016). Diacylglycerol kinases in the coordination of synaptic plasticity. *Front. Cell. Dev. Biol.* 4:92. doi: 10.3389/fcell.2016.00092

Lemaire, M., Frémeaux-Bacchi, V., Schaefer, F., Choi, M., Tang, W. H., Le Quintrec, M., et al. (2013). Recessive mutations in DGKE cause atypical hemolytic-uremic syndrome. *Nat. Genet.* 45, 531–536. doi: 10.1038/ng.2590

Lemmon, M. A. (2008). Membrane recognition by phospholipid-binding domains. *Nat. Rev. Mol. Cell Biol.* 9, 99–111. doi: 10.1038/nrm2328

Liscovitch, M. (1991). Signal-dependent activation of phosphatidylcholine hydrolysis: role of phospholipase D. *Biochem. Soc. Trans.* 19, 402–407. doi: 10.1042/bst0190402

Liu, S., Wilson, K., Rice-Stitt, T., and Neiman, A. (2007). In vitro fusion catalyzed by the sporulation-specific t-SNARE light-Chain Spo20p is stimulated by phosphatidic acid. *Traffic* 8, 1630–1643. doi: 10.1111/j.1600-0854.2007.00628.x

Loewen, C. J. R., Gazpar, M. L., Jesch, S. A., Delon, C., Ktistakis, N. T., Henry, S. A., et al. (2004). Phospholipid metabolism regulated by a transcription factor sensing phosphatidic acid. *Science* 304, 1644–1647. doi: 10.1126/science.1096083

Manifava, M., Thuring, J. W., Lim, Z. Y., Packman, L., Holmes, A. B., and Ktistakis, N. T. (2001). Differential binding of traffic-related proteins to phosphatidic acid- or phosphatidylinositol (4,5)- bisphosphate-coupled affinity reagents. *J. Biol. Chem.* 276, 8987–8994. doi: 10.1074/jbc.m010308200

Martin, T. F. J. (2015). PI(4,5)P2-binding effector proteins for vesicle exocytosis. *Biochim. Biophys. Acta* 1851, 785–793. doi: 10.1016/j.bbalip.2014.09.017

Masai, I., Suzuki, E., Yoon, C. S., Kohyama, A., and Hotta, Y. (1997). Immunolocalization of *Drosophila* eye-specific diacylgylcerol kinase, *rdgA*, which is essential for the maintenance of the photoreceptor. *J. Neurobiol.* 32, 695–706. doi: 10.1002/(sici)1097-4695(19970620)32:7<695::aid-neu5>3.0.co;2-#

Mayor, S., and Pagano, R. E. (2007). Pathways of clathrin-independent endocytosis. *Nat. Rev. Mol. Cell Biol.* 8, 603–612. doi: 10.1038/nrm2216

Menon, D., Salloum, D., Bernfeld, E., Gorodetsky, E., Akselrod, A., Frias, M. A., et al. (2017). Lipid sensing by mTOR complexes via *de novo* synthesis of phosphatidic acid. *J. Biol. Chem.* 292, 6303–6311. doi: 10.1074/jbc.M116.772988

Mima, J., and Wickner, W. (2009). Complex lipid requirements for SNARE- and SNARE chaperone-dependent membrane fusion. *J. Biol. Chem.* 284, 27114–27122. doi: 10.1074/jbc.M109.010223

Moine, H., and Vitale, N. (2019). Of local translation control and lipid signaling in neurons. *Adv. Biol. Regul.* 71, 194–205. doi: 10.1016/j.jbior.2018.09.005

Moritz, A., De Graan, P. N., Gispen, W. H., and Wirtz, K. W. (1992). Phosphatidic acid is a specific activator of phosphatidylinositol-4-phosphate kinase. *J. Biol. Chem.* 267, 7207–7210.

Munnik, T., Meijer, H. J. G., Ter Riet, B., Hirt, H., Frank, W., Bartels, D., et al. (2000). Hyperosmotic stress stimulates phospholipase D activity and elevates the levels of phosphatidic acid and diacylglycerol pyrophosphate. *Plant J.* 22, 147–154. doi: 10.1046/j.1365-313X.2000.00725.x

Nakamura, T., Suchard, S. J., Abe, A., Shayman, J. A., and Boxer, L. A. (1994). Role of diradylglycerol formation in H2O2 and lactoferrin release in adherent human polymorphonuclear leukocytes. *J. Leukoc. Biol.* 56, 105–109. doi: 10.1002/jlb.56.2.105

Nakanishi, H. (2004). Positive and negative regulation of a SNARE protein by control of intracellular localization. *Mol. Biol. Cell* 15, 1802–1815. doi: 10.1091/mbc.e03-11-0798

Nakanishi, H., Morishita, M., Schwartz, C. L., Coluccio, A., Engebrecht, J., and Neiman, A. M. (2006). Phospholipase D and the SNARE Sso1p are necessary for vesicle fusion during sporulation in yeast. *J. Cell Sci.* 119(Pt 7), 1406–1415. doi: 10.1242/jcs.02841

Nibbeling, E. A. R., Duarri, A., Verschuuren-Bemelmans, C. C., Fokkens, M. R., Karjalainen, J. M., Smeets, C. J. L. M., et al. (2017). Exome sequencing and network analysis identifies shared mechanisms underlying spinocerebellar ataxia. *Brain* 140, 2860–2878. doi: 10.1093/brain/awx251

Niedergang, F., and Chavrier, P. (2004). Signaling and membrane dynamics during phagocytosis: many roads lead to the phagos(R)ome. *Curr. Opin. Cell Biol.* 16, 422–428. doi: 10.1016/j.ceb.2004.06.006

Nishikimi, A., Fukuhara, H., Su, W., Hongu, T., Takasuga, S., Mihara, H., et al. (2009). Sequential regulation of DOCK2 dynamics by two phospholipids during neutrophil chemotaxis. *Science* 324, 384–387. doi: 10.1126/science.1170179

Oguin, T. H., Sharma, S., Stuart, A. D., Duan, S., Scott, S. A., Jones, C. K., et al. (2014). Phospholipase D facilitates efficient entry of influenza virus, allowing escape from innate immune inhibition. *J. Biol. Chem.* 289, 25405–25417. doi: 10.1074/jbc.M114.558817

Olenchock, B. A., Guo, R., Carpenter, J. H., Jordan, M., Topham, M. K., Koretzky, G. A., et al. (2006). Disruption of diacylglycerol metabolism impairs the induction of T cell anergy. *Nat. Immunol.* 7, 1174–1181. doi: 10.1038/ni1400

Oliveira, T. G., Chan, R. B., Tian, H., Laredo, M., Shui, G., Staniszewski, A., et al. (2010a). Phospholipase d2 ablation ameliorates Alzheimer's disease-linked synaptic dysfunction and cognitive deficits. *J. Neurosci.* 30, 16419–16428. doi: 10.1523/JNEUROSCI.3317-10.2010

Oliveira, T. G., Chan, R. B., Tian, H., Laredo, M., Shui, G., Staniszewski, A., et al. (2010b). Phospholipase D2 ablation ameliorates Alzheimer's diseaselinked synaptic dysfunction and cognitive deficits. *J. Neurosci.* 199, 1442–1448. doi: 10.1086/597422.Tumor

Oliveira, T. G., and Di Paolo, G. (2010). Phospholipase D in brain function and Alzheimer's disease. *Biochim. Biophys. Acta* 1801, 799–805. doi: 10.1016/j.bbalip.2010.04.004

O'Reilly, M. C., Oguin, T. H., Scott, S. A., Thomas, P. G., Locuson, C. W., Morrison, R. D., et al. (2014). Discovery of a highly selective PLD2 inhibitor (ML395): a new probe with improved physiochemical properties and broad-spectrum antiviral activity against influenza strains. *ChemMedChem* 9, 2633–2637. doi: 10.1002/cmdc.201402333

Otani, Y., Yamaguchi, Y., Sato, Y., Furuichi, T., Ikenaka, K., Kitani, H., et al. (2011). PLD$ is involved in phagocytosis of microglia: expression and localization changes of PLD4 are correlated with activation state of microglia. *PLoS One* 6:e27544. doi: 10.1371/journal.pone.0027544

Ozaltin, F., Li, B., Rauhauser, A., An, S.-W., Soylemezoglu, O., Gonul, I. I., et al. (2013). DGKE variants cause a glomerular microangiopathy that mimics membranoproliferative GN. *J. Am. Soc. Nephrol.* 24, 377–384. doi: 10.1681/ASN.2012090903

Palicz, A., Foubert, T. R., Jesaitis, A. J., Marodi, L., and McPhail, L. C. (2001). Phosphatidic acid and diacylglycerol directly activate NADPH oxidase by interacting with enzyme components. *J. Biol. Chem.* 276, 3090–3097. doi: 10.1074/jbc.M007759200

Panda, A., Thakur, R., Krishnan, H., Naik, A., Shinde, D., and Raghu, P. (2018). Functional analysis of mammalian phospholipase D enzymes. *Biosci. Rep.* 38:BSR20181690. doi: 10.1042/BSR20181690

Park, C., Kang, D.-S., Shin, G.-H., Seo, J., Kim, H., Suh, P.-G., et al. (2015). Identification of novel phosphatidic acid-binding proteins in the rat brain. *Neurosci. Lett.* 595, 108–113. doi: 10.1016/j.neulet.2015.04.012

Pfeffer, S. R. (2013). A prize for membrane magic. *Cell* 155, 1203–1206. doi: 10.1016/j.cell.2013.11.014

Pula, G., Mundell, S. J., Roberts, P. J., and Kelly, E. (2004). Agonist-independent internalization of metabotropic glutamate receptor 1a is arrestin- and clathrin-dependent and is suppressed by receptor inverse agonists. *J. Neurochem.* 89, 1009–1020. doi: 10.1111/j.1471-4159.2004.02387.x

Raben, D. M., and Barber, C. N. (2017). Phosphatidic acid and neurotransmission. *Adv. Biol. Regul.* 63, 15–21. doi: 10.1016/j.jbior.2016.09.004

Raghu, P., Coessens, E., Manifava, M., Georgiev, P., Pettitt, T., Wood, E., et al. (2009a). Rhabdomere biogenesis in *Drosophila* photoreceptors is acutely sensitive to phosphatidic acid levels. *J. Cell Biol.* 185, 129–145. doi: 10.1083/jcb.200807027

Raghu, P., Manifava, M., Coadwell, J., and Ktistakis, N. T. (2009b). Emerging findings from studies of phospholipase D in model organisms (and a short update on phosphatidic acid effectors). *Biochim. Biophys. Acta* 1791, 889–897. doi: 10.1016/j.bbalip.2009.03.013

Raghu, P., Usher, K., Jonas, S., Chyb, S., Polyanovsky, A., and Hardie, R. C. (2000). Constitutive activity of the light-sensitive channels TRP and TRPL in the *Drosophila* diacylglycerol kinase mutant, *rdgA*. *Neuron* 26, 169–179. doi: 10.1016/s0896-6273(00)81147-2

Raghu, P., Yadav, S., and Mallampati, N. B. N. (2012). Lipid signaling in *Drosophila* photoreceptors. *Biochim. Biophys. Acta* 1821, 1154–1165. doi: 10.1016/j.bbalip.2012.03.008

Rankovic, M., Jacob, L., Rankovic, V., Brandenburg, L. O., Schröder, H., Höllt, V., et al. (2009). ADP-ribosylation factor 6 regulates mu-opioid receptor trafficking and signaling via activation of phospholipase D2. *Cell. Signal.* 21, 1784–1793. doi: 10.1016/j.cellsig.2009.07.014

Roach, A. N., Wang, Z., Wu, P., Zhang, F., Chan, R. B., Yonekubo, Y., et al. (2012). Phosphatidic acid regulation of PIPKI is critical for actin cytoskeletal reorganization. *J. Lipid Res.* 53, 2598–2609. doi: 10.1194/jlr.M028597

Rodriguez de Turco, E. B., Tang, W., Topham, M. K., Sakane, F., Marcheselli, V. L., Chen, C., et al. (2001). Diacylglycerol kinase epsilon regulates seizure susceptibility and long-term potentiation through arachidonoyl- inositol lipid signaling. *Proc. Natl. Acad. Sci. U.S.A.* 98, 4740–4745. doi: 10.1073/pnas.081536298

Roldan, E. R. S., and Dawes, E. N. (1993). Phospholipase D and exocytosis of the ram sperm acrosome. *Biochim. Biophys. Acta* 1210, 48–54. doi: 10.1016/0005-2760(93)90048-E

Roth, M. G., Bi, K., Ktistakis, N. T., and Yu, S. (1999). Phospholipase D as an effector for ADP-ribosylation factor in the regulation of vesicular traffic. *Chem. Phys. Lipids* 98, 141–152. doi: 10.1016/s0009-3084(99)00026-2

Rout, M. P., and Field, M. C. (2017). The evolution of organellar coat complexes and organization of the eukaryotic cell. *Annu. Rev. Biochem.* 86, 637–657. doi: 10.1146/annurev-biochem-061516-044643

Rudge, S. A., Morris, A. J., and Engebrecht, J. (1998). Relocalization of phospholipase D activity mediates membrane formation during meiosis. *J. Cell Biol.* 140, 81–90. doi: 10.1083/jcb.140.1.81

Rudge, S. A., Pettitt, T. R., Zhou, C., Wakelam, M. J., and Engebrecht, J. A. (2001). SPO14 separation-of-function mutations define unique roles for phospholipase D in secretion and cellular differentiation in *Saccharomyces cerevisiae*. *Genetics* 158, 1431–1444.

Sallese, M., Salvatore, L., D'Urbano, E., Sala, G., Storto, M., Launey, T., et al. (2000). The G-protein-coupled receptor kinase GRK4 mediates homologous desensitization of metabotropic glutamate receptor 1. *FASEB J.* 14, 2569–2580. doi: 10.1096/fj.00-0072com

Schwarz, K., Natarajan, S., Kassas, N., Vitale, N., and Schmitz, F. (2011). The synaptic ribbon is a site of phosphatidic acid generation in ribbon synapses. *J. Neurosci.* 31, 15996–16011. doi: 10.1523/JNEUROSCI.2965-11.2011

Selvy, P. E., Lavieri, R. R., Lindsley, C. W., and Brown, H. A. (2011). Phospholipase D: enzymology, functionality, and chemical modulation. *Chem. Rev.* 111, 6064–6119. doi: 10.1021/cr200296t

Sreenivas, A., Patton-Vogt, J. L., Bruno, V., Griac, P., and Henry, S. A. (1998). A role for phospholipase D (Pld1p) in growth, secretion, and regulation of membrane lipid synthesis in yeast. *J. Biol. Chem.* 273, 16635–16638. doi: 10.1074/jbc.273.27.16635

Stace, C. L., and Ktistakis, N. T. (2006). Phosphatidic acid- and phosphatidylserine-binding proteins. *Biochim. Biophys. Acta* 1761, 913–926. doi: 10.1016/j.bbalip.2006.03.006

Stutchfield, J., and Cockcroft, S. (1993). Correlation between secretion and phospholipase D activation in differentiated HL60 cells. *Biochem. J.* 293(Pt 3), 649–655. doi: 10.1042/bj2930649

Suzuki, E., Hirosawa, K., and Hotta, Y. (1990). Analysis of photoreceptor membrane turnover in a *Drosophila* visual mutant, *rdgA*, by electron-microscope autoradiography. *J. Electron Microsc.* 39, 50–53.

Tabet, R., Moutin, E., Becker, J. A. J., Heintz, D., Fouillen, L., Flatter, E., et al. (2016). Fragile X mental retardation protein (FMRP) controls diacylglycerol kinase activity in neurons. *Proc. Natl. Acad. Sci. U.S.A.* 113, E3619–E3628. doi: 10.1073/pnas.1522631113

Tanguy, E., Kassas, N., and Vitale, N. (2018). Protein–phospholipid interaction motifs: a focus on phosphatidic acid. *Biomolecules* 8:E20. doi: 10.3390/biom8020020

Ta-Shma, A., Zhang, K., Salimova, E., Zernecke, A., Sieiro-Mosti, D., Stegner, D., et al. (2017). Congenital valvular defects associated with deleterious mutations in the *PLD1* gene. *J. Med. Genet.* 54, 278–286. doi: 10.1136/jmedgenet-2016-104259

Thakur, R., Panda, A., Coessens, E., Raj, N., Yadav, S., Balakrishnan, S., et al. (2016). Phospholipase D activity couples plasma membrane endocytosis with retromer dependent recycling. *eLife* 5:e18515. doi: 10.7554/eLife.18515

Topham, M. K., and Epand, R. M. (2009). Mammalian diacylglycerol kinases: molecular interactions and biological functions of selected isoforms. *Biochim. Biophys. Acta* 1790, 416–424. doi: 10.1016/j.bbagen.2009.01.010

Toschi, A., Lee, E., Xu, L., Garcia, A., Gadir, N., and Foster, D. A. (2009). Regulation of mTORC1 and mTORC2 complex assembly by phosphatidic acid: competition with rapamycin. *Mol. Cell. Biol.* 29, 1411–1420. doi: 10.1128/MCB.00782-08

Tou, J. S., and Gill, J. S. (2005). Lysophosphatidic acid increases phosphatidic acid formation, phospholipase D activity and degranulation by human neutrophils. *Cell. Signal.* 17, 77–82. doi: 10.1016/j.cellsig.2004.06.003

Triebl, A., Trötzmüller, M., Eberl, A., Hanel, P., Hartler, J., and Köfeler, H. C. (2014). Quantitation of phosphatidic acid and lysophosphatidic acid molecular species using hydrophilic interaction liquid chromatography coupled to electrospray ionization high resolution mass spectrometry. *J. Chromatogr. A* 1347, 104–110. doi: 10.1016/j.chroma.2014.04.070

Tu-Sekine, B., Goldschmidt, H., and Raben, D. M. (2015). Diacylglycerol, phosphatidic acid, and their metabolic enzymes in synaptic vesicle recycling. *Adv. Biol. Regul.* 57, 147–152. doi: 10.1016/j.jbior.2014.09.010

van Dijk, G. W., Wokke, J. H., Oey, P. L., Franssen, H., Ippel, P. F., and Veldman, H. (1995). A new variant of sensory ataxic neuropathy with autosomal dominant inheritance. *Brain* 118(Pt 6), 1557–1563. doi: 10.1093/brain/118.6.1557

van Meer, G., Voelker, D. R., and Feigenson, G. W. (2008). Membrane lipids: where they are and how they behave. *Nat. Rev. Mol. Cell Biol.* 9, 112–124. doi: 10.1038/nrm2330

Vitale, N., Caumont, A. S., Chasserot-Golaz, S., Du, G., Wu, S., Sciorra, V. A., et al. (2001). Phospholipase D1: a key factor for the exocytotic machinery in neuroendocrine cells. *EMBO J.* 20, 2424–2434. doi: 10.1093/emboj/20.10.2424

Wang, S., Tan, K. L., Agosto, M. A., Xiong, B., Yamamoto, S., Sandoval, H., et al. (2014). The retromer complex is required for rhodopsin recycling and its loss leads to photoreceptor degeneration. *PLoS Biol.* 12:e1001847. doi: 10.1371/journal.pbio.1001847

Wang, Z., Zhang, F., He, J., Wu, P., Tay, L. W. R., Cai, M., et al. (2017). Binding of PLD2-generated phosphatidic acid to KIF5B promotes MT1-MMP surface trafficking and lung metastasis of mouse breast cancer cells. *Dev. Cell* 43, 186–197.e7. doi: 10.1016/j.devcel.2017.09.012

Watanabe, T., Chuma, S., Yamamoto, Y., Kuramochi-Miyagawa, S., Totoki, Y., Toyoda, A., et al. (2011). MITOPLD is a mitochondrial protein essential for nuage formation and piRNA biogenesis in the mouse germline. *Dev. Cell* 20, 364–375. doi: 10.1016/j.devcel.2011.01.005

Wolfe, B. L., and Trejo, J. A. (2007). Clathrin-dependent mechanisms of G protein-coupled receptor endocytosis. *Traffic* 8, 462–470. doi: 10.1111/j.1600-0854.2007.00551.x

Wu, L., Niemeyer, B., Colley, N., Socolich, M., and Zuker, C. S. (1995). Regulation of PLC mediated signalling in vivo by CDp-diacylglycerol synthase. *Nature* 373, 216–222. doi: 10.1038/373216a0

Xie, Z., Fang, M., Rivas, M. P., Faulkner, A. J., Sternweis, P. C., Engebrecht, J. A., et al. (1998). Phospholipase D activity is required for suppression of yeast phosphatidylinositol transfer protein defects. *Proc. Natl. Acad. Sci. U.S.A.* 95, 12346–12351. doi: 10.1073/pnas.95.21.12346

Xiong, B., and Bellen, H. J. (2013). Rhodopsin homeostasis and retinal degeneration: lessons from the fly. *Trends Neurosci.* 36, 652–660. doi: 10.1016/j.tins.2013.08.003

Yadav, S., Cockcroft, S., and Raghu, P. (2016). The *Drosophila* photoreceptor as a model system for studying signalling at membrane contact sites. *Biochem. Soc. Trans.* 44, 447–451. doi: 10.1042/BST20150256

Yadav, S., Garner, K., Georgiev, P., Li, M., and Gomez-espinosa, E. (2015). RDGB, a PI-PA transfer protein regulates G-protein coupled PtdIns (4, 5)*P2* signalling during *Drosophila* phototransduction. *J. Cell Sci.* 123, 3330–3344. doi: 10.1242/jcs.173476

Yadav, S., Thakur, R., Georgiev, P., Deivasigamani, S., Krishnan, H., Ratnaparkhi, G., et al. (2018). RDGBα localization and function at a membrane contact site is regulated by FFAT/VAP interactions. *J. Cell Sci.* 131:jcs207985. doi: 10.1242/jcs.207985

Zeniou-Meyer, M., Zabari, N., Ashery, U., Chasserot-Golaz, S., Haeberle, A. M., Demais, V., et al. (2007). Phospholipase D1 production of phosphatidic acid at the plasma membrane promotes exocytosis of large dense-core granules at a late stage. *J. Biol. Chem.* 282, 21746–21757. doi: 10.1074/jbc.M702968200

Zhang, F., Wang, Z., Lu, M., Yonekubo, Y., Liang, X., Zhang, Y., et al. (2014). Temporal production of the signaling lipid phosphatidic acid by phospholipase D2 determines the output of extracellular signal-regulated kinase signaling in cancer cells. *Mol. Cell. Biol.* 34, 84–95. doi: 10.1128/MCB.00987-13

Zhang, W., Qin, C., Zhao, J., and Wang, X. (2004). Phospholipase D 1-derived phosphatidic acid interacts with ABI1 phosphatase 2C and regulates abscisic acid signaling. *Proc. Natl. Acad. Sci. U.S.A.* 101, 9508–9513. doi: 10.1073/pnas.0402112101

Zhao, C., Du, G., Skowronek, K., Frohman, M. A., and Bar-Sagi, D. (2007). Phospholipase D2-generated phosphatidic acid couples EGFR stimulation to Ras activation by Sos. *Nat. Cell Biol.* 9, 707–712. doi: 10.1038/ncb1594

Zhong, X.-P., Hainey, E. A., Olenchock, B. A., Jordan, M. S., Maltzman, J. S., Nichols, K. E., et al. (2003). Enhanced T cell responses due to diacylglycerol kinase ζ deficiency. *Nat. Immunol.* 4, 882–890. doi: 10.1038/ni958

Conflict of Interest Statement: The authors declare that the research was conducted in the absence of any commercial or financial relationships that could be construed as a potential conflict of interest.

frontiers in Cell and Developmental Biology

REVIEW
published: 25 June 2019
doi: 10.3389/fcell.2019.00097

Integration Through Separation – The Role of Lateral Membrane Segregation in Nutrient Uptake

Jon V. Busto[1,2] *and Roland Wedlich-Söldner*[1]*

[1] *Institute of Cell Dynamics and Imaging, University of Münster, Münster, Germany,* [2] *Biofisika Institute (CSIC, UPV/EHU) and Department of Biochemistry, University of the Basque Country, Leioa, Spain*

Nutrient transporters are prominent and ubiquitous components of the plasma membrane in all cell types. Their expression and regulation are tightly linked to the cells' needs. Environmental factors such as nutrient starvation or osmotic stress prompt an acute remodeling of transporters and the plasma membrane to efficiently maintain homeostasis in cell metabolism. Lateral confinement of nutrient transporters through dynamic segregation within the plasma membrane has recently emerged as an important phenomenon that facilitates spatiotemporal control of nutrient uptake and metabolic regulation. Here, we review recent studies highlighting the mechanisms connecting the function of amino acid permeases with their endocytic turnover and lateral segregation within the plasma membrane. These findings indicate that actively controlled lateral compartmentalization of plasma membrane components constitutes an important level of regulation during acute cellular adaptations.

Keywords: plasma membrane, membrane domains, yeast, nutrient transporter, endocytosis

OPEN ACCESS

Edited by:
Rachel Susan Kraut, Max Planck Institute of Molecular Cell Biology and Genetics (MPI-CBG), Germany

Reviewed by:
Erdinc Sezgin, University of Oxford, United Kingdom
Alessandra Cambi, Radboud University Nijmegen, Netherlands

***Correspondence:**
Roland Wedlich-Söldner
wedlich@uni-muenster.de

Specialty section:
This article was submitted to Membrane Physiology and Membrane Biophysics, a section of the journal Frontiers in Cell and Developmental Biology

Received: *01 February 2019*
Accepted: *21 May 2019*
Published: *25 June 2019*

Citation:
Busto JV and Wedlich-Söldner R (2019) Integration Through Separation – The Role of Lateral Membrane Segregation in Nutrient Uptake. Front. Cell Dev. Biol. 7:97. doi: 10.3389/fcell.2019.00097

INTRODUCTION

Cells are constantly exposed to environmental fluctuations and thus require rapid adaptations to sustain proper growth and survival. The plasma membrane (PM) constitutes the primary cell boundary and therefore acts as initial site for stress recognition and signaling. The PM is a highly dynamic structure that is compartmentalized in a complex manner. Various models support the lateral segregation of PM lipids and proteins into distinct domains. The budding yeast *Saccharomyces cerevisiae* represents a promising model system for the study of such segregation. Both lipids and proteins of the yeast PM exhibit unusually slow lateral diffusion, and they form large domains that can be studied by conventional light microscopy (Spira et al., 2012a). This allowed the systematic study of a large set of integral PM proteins that revealed an intricate organization of many overlapping domains into a PM patchwork (Spira et al., 2012b).

A critical environmental stress that cells constantly face is nutrient limitation. Starvation is regulated at the PM through a tight remodeling of nutrient transporters, highly abundant and conserved components of the PM in all cells. Transporter turnover in response to substrate availability is modulated *via* two major mechanisms. On the one hand, increased transcription and PM delivery of transporters occur when nutrients are scarce. TORC1 (target of rapamycin complex 1) acts as a central coordinator between protein synthesis, transporter delivery, and metabolic state (Gonzalez and Hall, 2017). On the other hand, transcriptional repression and ubiquitin-dependent internalization prevent excessive substrate uptake when nutrients are abundant. In yeast, selective ubiquitination and downregulation of PM transporters are driven by the concerted action of the E3 ubiquitin ligase Rsp5 and cargo-selective adaptors of the α-arrestin family (Nikko and Pelham, 2009).

Nutrient transporters at the yeast PM have been shown to segregate into different compartments. Prominent examples are the members of the major facilitator (MFS) and amino acid-polyamine-organocation (APC) superfamilies of secondary carriers (Reddy et al., 2012; Vastermark et al., 2014). Various MFS transporters, including hexose and polyamine transporters, distribute into dense, network-like patterns (Spira et al., 2012b). On the other hand, several amino acid and nucleobase transporters of the APC superfamily cluster into defined patches (Malinska et al., 2003, 2004; Grossmann et al., 2007; Bianchi et al., 2018; Busto et al., 2018). Interestingly, all clustered transporters exhibit proton symport activity during substrate uptake. This is particularly striking considering the spatial segregation of the H^+-symporters from the H^+-ATPase Pma1 (Malinska et al., 2003). This essential protein drives proton efflux to maintain intracellular pH homeostasis and to generate an electrochemical gradient that provides the basis for metabolite uptake into cells. The segregation of proton-based activities has led to the suggestion that membrane potential regulates lateral distribution of proteins and lipids within the yeast PM (Grossmann et al., 2007; Herman et al., 2015; Malinsky et al., 2016).

Understanding the biological implications behind distinct PM distributions of nutrient transporters and the connection between their function, turnover, and PM compartmentalization has become of broad interest. In this review, we address recent studies on yeast amino acid permeases that reveal their dynamic segregation across different domains in response to substrate availability. These studies show that lateral segregation of transporters can provide protection from endocytic turnover. They also reveal that PM distribution and turnover are regulated *via* a combination of specific protein–lipid interactions and changes in protein conformation that occur during substrate transport. The emerging picture is that lateral PM segregation provides an important and efficient regulatory level to ensure coordination of biological function and turnover for a multitude of nutrient transporters.

NUTRIENT TRANSPORTER DISTRIBUTION AT THE PLASMA MEMBRANE

Membrane transporters are ubiquitous components of cell membranes and pivotal in supporting proper cell growth, differentiation, and survival. Transporters can be classified into three main classes: ion channels, primary transporters that mostly use energy in the form of ATP (e.g., ABC transporters, ATPases), and secondary transporters that use an electrochemical gradient to transport a large variety of ions, nutrients (e.g., sugars, amino acids, vitamins, nucleobases, peptides), or small molecules (Saier et al., 2016). The majority of nutrient transporters are expressed at the PM, and their expression levels are tightly regulated by substrate availability. The mechanisms behind expression, PM delivery, and endocytic turnover of nutrient transporters have extensively been studied in budding yeast (Lin et al., 2008; Nikko and Pelham, 2009; Loewith and Hall, 2011; Gonzalez and Hall, 2017). However, detailed knowledge on their dynamic lateral segregation within the PM has only recently emerged.

In a systematic study, Spira et al. (2012b) described the complex distribution of yeast PM proteins into numerous overlapping but distinct patterns that ranged from branched or network-like distributions to patches or clusters. The patterns formed by 46 different proteins were resolved using a combination of TIRF microscopy and 2D deconvolution. The protein set included various nutrient transporters such as the hexose uniporters Hxt1, 2, 3, 6, and the polyamine H^+-antiporter Tpo1 that all distributed into network-like patterns. These MFS transporters contain 12 transmembrane domains (TMDs) and are structurally organized as two repeat units of six TMDs (Reddy et al., 2012).

The yeast arginine permease Can1 was the first permease shown to cluster within a specific compartment at the PM (Malinska et al., 2003), the correspondingly named "membrane compartment occupied by Can1" or MCC. The uracil permease Fur4 (Malinska et al., 2004), the tryptophan and tyrosine permease Tat2 (Grossmann et al., 2007), the lysine permease Lyp1 (Bianchi et al., 2018), and the methionine permease Mup1 (Busto et al., 2018) have been shown to also cluster within the MCC compartment. All five transporters are proton symporters, belong to the APC superfamily, contain at least 12 TMDs, and follow a 5 + 5-fold structural organization with two inverted repeats of five TMDs (Vastermark et al., 2014). Aside from nutrient transporters, the MCC contains various tetraspan proteins and surrounds membrane invaginations called eisosomes that are stabilized by the cytosolic proteins Lsp1 and Pil1. The MCC/eisosome domain has been shown to play a role in sphingolipid (SL) homeostasis, cell wall morphogenesis, and, most relevant for the present discussion, PM organization. Recent studies using super-resolution microscopy confirmed the partition of Can1 and Lyp1 into the outer edge of the MCC/eisosome (Bianchi et al., 2018). A similar observation was made for the methionine permease Mup1 (**Figure 1**) (Busto et al., 2018).

But what drives particular nutrient transporters to cluster within a specific PM compartment? Previous and recent data converge in showing that clustering is driven by a combination of two main factors: substrate-dependent changes in the conformation of transporters and weak interactions with various proteins and lipids within the established PM domain.

DYNAMIC LATERAL RELOCATION THROUGH A CONFORMATIONAL SWITCH

Endocytic events at the yeast PM have been shown to be excluded from the MCC/eisosome compartment (Grossmann et al., 2008; Brach et al., 2011). As many transporters that cluster in the MCC undergo substrate-dependent endocytosis (Nikko and Pelham, 2009), this would suggest prior relocation out of the MCC. Two independent studies on different nutrient transporters have recently demonstrated this behavior and shed light on the mechanisms underlying such controlled lateral relocation

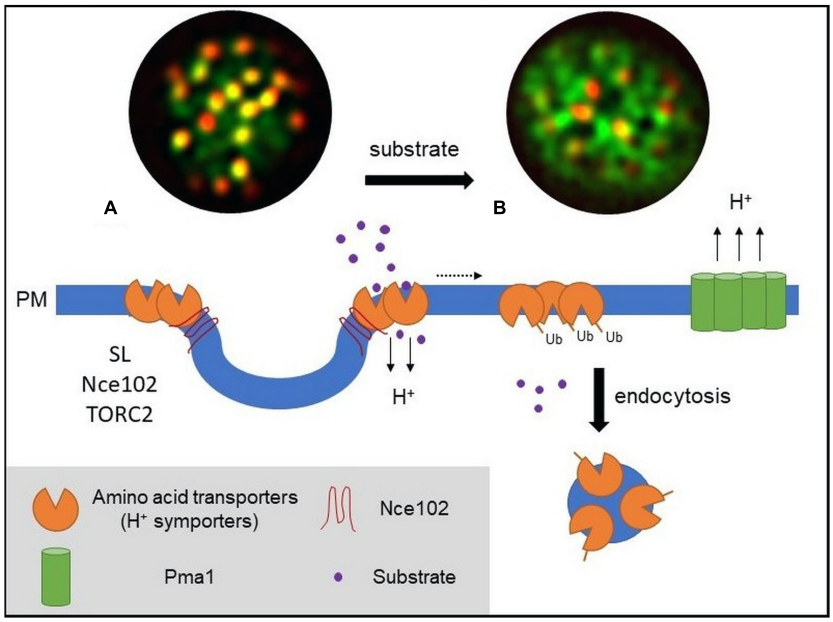

FIGURE 1 | Model of PM amino acid transporter regulation in yeast. **(A)** Amino acid transporters, generally proton symporters, accumulate at the membrane compartment occupied by Can1 (MCC) during substrate starvation. The MCC represents the edge area of PM furrows (also termed eisosome). Clustering of permeases depends on sphingolipids (SL), the tetraspan protein Nce102, and TORC2 signaling. Clustered transporters adopt an open (outward facing) conformation. **(B)** Substrate transport triggers a conformational switch to a closed (inward facing) conformation. This switch is linked to lateral relocation of the transporters out of the MCC (dotted arrow) into a unique PM area that is distinct from that occupied by the H^+-ATPase Pma1 (MCP). The conformational switch and lateral relocation precede transporter ubiquitination. Ubiquitinated transporters then act as a molecular beacon for the recruitment of the endocytic machinery. Fluorescent images (TIRF) have been adapted from Busto et al. (2018) and represent composites of a ubiquitination-deficient mutant of the methionine permease Mup1 (Mup1-2KR, green) and the eisosomal core component Pil1 (red). Mup1-2KR clusters within the MCC in the absence of methionine (left, colocalization with Pil1 in yellow patches) and relocates out of MCC clusters upon substrate addition.

(Busto et al., 2018; Gournas et al., 2018). Busto et al. (2018) showed that, upon substrate uptake, the methionine permease Mup1 undergoes rapid lateral relocation from the MCC into a unique network-like domain at the PM. Lateral relocation occurred rapidly after methionine transport and was independent of ubiquitination and reversible upon substrate washout (Busto et al., 2018). In a remarkable parallel, Gournas et al. (2018) described a nearly identical mechanism for Can1 upon control of the arginine supply. Both studies conclude that a change in the conformational state of the transporters directly controls their lateral segregation within the PM. In the absence of substrate, the transporters are stabilized in an open or outward-facing (OF) conformation that favors MCC association. During substrate transport the permeases shift to a closed or inward-facing (IF) conformation, which drives their lateral relocation out of the clusters (see **Figure 1**).

More specifically, Gournas et al. (2018) showed that the Can1 S176N mutant, which binds arginine but is locked in the OF conformation (Ghaddar et al., 2014), remains clustered upon substrate addition. In contrast, the inactive Can1 E184Q mutant that is stabilized in the IF conformation is no longer able to cluster in the MCC, even in substrate-free media (Gournas et al., 2018). The case of Mup1 is of particular interest as it is the only yeast amino acid permease that belongs to the L-type amino acid transporters (LAT), a subgroup within the APC superfamily of transporters that has a large number of mammalian members, including the tumor-associated LAT1 (Zhao et al., 2015). One notable feature is a loop in the cytosolic carboxy-terminus of Mup1. Its predicted structure resembles that of a "plug" in the bacterial glutamate-GABA antiporter GadC. Surprisingly, this plug has been shown to insert into the core of GadC and to facilitate a conformational transition during substrate transport (Ma et al., 2012). Consistently, truncation of the C-terminal plug in Mup1 led to Mup1 stabilization within MCC clusters regardless of substrate presence. In contrast, mutation of a conserved motif within the tip of the plug abolished any detectable clustering. Thus, the data clearly support a link between lateral PM segregation of Mup1 and its conformational state, with a key role for the C-terminal plug during the proposed structural switch.

Interestingly, the structural transition to an IF conformation has been proposed to also mediate release of the cytosolic amino-termini, which is crucial for transporter ubiquitination. Recent studies have shown that displacement of the N-terminus in Can1 (Gournas et al., 2017) and Mup1 (Guiney et al., 2016) unmasks PM proximal sequences that are recognized by the α-arrestin Art1 in a first step of transporter ubiquitination and subsequent internalization. However, proper Art1 binding to Mup1 has been shown to require additional recognition sites (Guiney et al., 2016). The C-terminal plug may constitute that additional site. This would then suggest an active role of both cytosolic termini in the conformational switch and in lateral

relocation of Mup1. Similar structural rearrangements of the C-terminus upon substrate uptake have been proposed for the abovementioned GadC (Ma et al., 2012) and for the bacterial proton-coupled xylose permease XylE (Wisedchaisri et al., 2014). In addition, C-terminal motifs have been documented to influence transporter activity and structure in Hup1, a heterologously expressed hexose/H^+-symporter from the green alga *Chlorella kessleri* (Grassl et al., 2000). These findings suggest that common mechanisms and principles might apply to the regulation of transporters in various cells and organisms.

A distinct aspect connecting protein conformation and lateral transporter segregation has recently been put forward (Moharir et al., 2018). Most nutrient transporters that concentrate within MCC clusters are not fully restricted to this domain but can also be observed to various degrees in dispersed networks (Busto et al., 2018; Gournas et al., 2018; Moharir et al., 2018). This suggests a dynamic equilibrium between clustered and non-clustered transporter pools (Brach et al., 2011; Busto et al., 2018; Gournas et al., 2018; Moharir et al., 2018). For the uracil transporter Fur4, it was proposed that the clustered pool within the MCC is kept inactive due to restricted movement in the dense MCC environment. When substrate becomes available, only the non-clustered Fur4 pool would be able to undergo the conformational changes required for substrate uptake. The conformational switch then, in turn, would prevent the transporter from entering the MCC, shifting the equilibrium to the non-clustered PM area. This hypothesis partially contradicts the results with Can1 and Mup1 (Busto et al., 2018; Gournas et al., 2018), which show fully functional uptake of methionine and arginine by transporters that were forced to localize to the MCC domain. Nonetheless, the three studies jointly highlight an active role of conformational states for transporter clustering.

CELLULAR REGULATION OF NUTRIENT TRANSPORTER CLUSTERING

Lateral segregation of nutrient transporters not only depends on conformational changes during the transport process but also is tightly linked to the local PM composition. One prominent factor regulating MCC integrity is the lipid composition of the PM, in particular SLs. SL homeostasis has been proposed to affect MCC composition (Frohlich et al., 2009). Complete inhibition of SL synthesis and selective depletion of complex SLs abolishes Mup1 and Can1 clustering. Both permeases dissociate from the MCC during SL stress. This reorganization is independent of substrate binding and restored by recovery of SL levels (Busto et al., 2018; Gournas et al., 2018). In addition, interfering with yeast sterol biosynthesis also led to reduced clustering of the plant hexose/H^+-symporter Hup1 within the MCC (Grossmann et al., 2006). In a separate study, the same authors showed that MCC integrity was regulated by the PM-resident tetraspan protein Nce102 (Grossmann et al., 2008), with deletion of NCE102 leading to reduced Can1 and Fur4 clustering. Nce102 was later found to act as a general sensor for SL stress and to regulate Pil1 phosphorylation and stability *via* modulation of Pkh kinase activity (Frohlich et al., 2009). Importantly, a more direct role for Nce102 in clustering of Mup1 and Can1 has been recently advanced. In conditions where Pil1 phosphorylation and, therefore, MCC/eisosome disassembly were prevented, deletion of NCE102 still led to a reduction in permease clustering (Busto et al., 2018; Gournas et al., 2018). This effect was much more prominent for Mup1, which also exhibits much stronger enrichment in MCC clusters to begin with (Busto et al., 2018). Importantly, both studies showed that dispersion of transporters upon SL inhibition occurred even in cells where Nce102 was anchored to MCC clusters either artificially (Gournas et al., 2018) or because it was unaffected by SL stress in methionine-free medium (Busto et al., 2018). The results therefore indicate that lateral segregation of permeases requires a combination of Nce102 and correct lipid composition in the MCC domain.

Signaling through the target of rapamycin complex 2 (TORC2) has been clearly linked to PM organization (Eltschinger and Loewith, 2016). TORC2 localizes to the PM as defined static patches that are segregated from other described PM domains (Berchtold and Walther, 2009). It coordinates actin organization and endocytosis (Rispal et al., 2015) and is a central regulator of SL homeostasis (Berchtold et al., 2012). The recent description of a rapamycin-sensitive TORC2 mutant (Gaubitz et al., 2015) provides an important tool to specifically study its role in PM organization. Noticeably, clustering of Mup1 was regulated by TORC2, as acute TORC2 inhibition by rapamycin led to a strong and rapid reduction in Mup1 clustering (Busto et al., 2018). Concomitantly, an almost complete Nce102 dispersion from the MCC was observed. TORC2 might therefore constitute a central regulator for permease segregation in the PM by simultaneously regulating distribution of tetraspan proteins such as Nce102 and maintaining proper SL homeostasis.

A LINK BETWEEN PLASMA MEMBRANE SEGREGATION AND THE MEMBRANE POTENTIAL

Under low substrate availability, various proton symporters concentrate on static MCC clusters at the yeast PM. These clusters are spatially segregated from the H^+-ATPase Pma1, which couples ATP hydrolysis to proton efflux. Using a variety of approaches to perturb membrane potential and the PM proton gradient, Grossmann et al. (2007) demonstrated that the proton symporters, but not the structural MCC resident Sur7, reversibly relocate out of the MCC in response to membrane depolarization. This was shown for Can1, Fur4, Tat2, and, most interestingly, the heterologously expressed Hup1. The authors then proposed that clustering of proton symporters could directly be linked to the activity of Pma1 and highlighted a role of the membrane potential in the lateral compartmentalization of PM domains. Hup1 belongs to the MFS superfamily, while yeast permeases are APC transporters. The common denominator for MCC clustering and membrane potential-mediated relocalization seems to therefore not reside within the intrinsic transporter structure but rather in their proton symport activity.

Remarkably, forced relocation of Mup1 and Can1 from MCC clusters to the Pma1-enriched compartment strongly inhibited the respective substrate uptake (Spira et al., 2012b; Busto et al., 2018). In contrast, MCC disassembly upon depletion of Pil1 with subsequent loss of permease clustering did not affect the transport activity (Busto et al., 2018; Gournas et al., 2018). This suggests that the Pma1 domain has an inhibitory effect on symporter activity, rather than the MCC environment having a stimulatory function. Together, the data suggest that the Pma1 domain constitutes a physicochemical environment that is harmful for proton symporters and that lateral segregation may be an efficient way to separate the generation and utilization of the electrochemical gradient across the PM (**Figure 1**). Future analysis in different cellular systems will have to show whether this is a fundamental feature that also holds true for proton gradients in plants or Na^+–K^+ gradients in animal cells.

INTERPLAY BETWEEN LATERAL SEGREGATION OF NUTRIENT TRANSPORTERS AND ENDOCYTIC TURNOVER

Lateral confinement of nutrient transporters and specifically of proton symporters in yeast not only impacts nutrient uptake but also is intimately linked to endocytic recycling and degradation of the transporters. A physiological role of the MCC as protective area from endocytosis was proposed earlier (Grossmann et al., 2008). However, while the absence of endocytosis within the MCC was later confirmed (Brach et al., 2011), the remaining pool of MCC-associated Can1 after substrate addition questioned an active role of the MCC in endocytic regulation (Brach et al., 2011). The recent studies add further details to the consequences of transporter clustering on endocytic recycling. For both Mup1 and Can1, clustering and substrate-induced lateral relocation are ubiquitination-independent processes (Busto et al., 2018; Gournas et al., 2018). Importantly, forced retention of the transporters within the MCC patches does not prevent substrate uptake – i.e., the required conformational shifts – but completely precludes transporter endocytosis. In addition, ubiquitination of Can1 was already blocked when the transporter was physically tethered to the MCC *via* an artificial anchor (Gournas et al., 2018). MCC disassembly restored Mup1 and Can1 endocytosis, including that of a constitutively clustered Mup1-ubiquitin fusion. The results therefore indicate that clustering of transporters in the MCC compartment provides protection from both ubiquitination and endocytosis.

Why would a cell need areas on the PM where proteins cannot be internalized? Possible physiological scenarios where this becomes highly relevant are systematic cell stress (temperature, salt) or acute starvation. In these conditions, cells will actively remove proteins and lipids from the PM to gain metabolic building blocks and reduce energy consumption (particularly by the H^+ pump). Such a global downregulation can occur by autophagy (Boya et al., 2013) or widespread ubiquitin-mediated endocytosis (Muller et al., 2015; Huber and Teis, 2016). Importantly, cells still need to be able to sense nutrients even in an adapted or depleted state. Therefore, a small population of nutrient transporters retained in the PM would pose a significant advantage. Exactly such a role for the MCC in providing a safe haven under acute starvation conditions has been proposed for Can1 (Gournas et al., 2018). The authors showed that upon general amino acid starvation and in stationary phase, the number and surface area of MCC clusters were increased, providing a protected reservoir for transporters during a global TORC-mediated removal of PM proteins.

While clustering of transporters is an efficient way to regulate global turnover, it is not sufficient to explain the metabolic fine-tuning that cells can perform in response to availability fluctuations of individual substrates. Clustering is a dynamic process and there will always be a large portion of PM proteins outside of the MCC domain. An important question for specific regulation of transporter abundance is therefore how internalization can be focused on one particular cargo. The recent finding of substrate-induced assembly of endocytic structures (Busto et al., 2018) could provide the required link. It was shown that ubiquitinated Mup1, once relocated outside of the MCC, acts as a molecular beacon for recruitment of the endocytic machinery and subsequent internalization. These endocytic sites are clearly segregated from the area containing Pma1 and likely also do not include unrelated transporters that are partially present in the internalized PM region (**Figure 1**). The combination of conformation-mediated lateral relocation and cargo-dependent assembly of endocytic coats could provide a good pathway for specific adjustment of PM composition and cellular metabolic activity.

The recent studies on turnover of yeast nutrient transporters provide general insights into a role of lateral PM segregation for compartmentalization of biological functions. However, the molecular details of the PM regulation of nutrient transporters are far from being fully understood. Future experiments attempting to directly visualize PM lipid distribution during transporter activation and lateral relocation could help to better assess the nature of the molecular interactions behind transporter segregation. Such experiments will help to untangle the respective roles of protein–lipid vs. protein–protein interactions for dynamic cluster formation. Furthermore, isolation and quantitative analysis of endocytic vesicles during substrate-induced transporter turnover will provide a more comprehensive picture of the molecular composition of endocytic PM areas.

AUTHOR CONTRIBUTIONS

RW-S and JVB wrote the manuscript and coordinated the project.

FUNDING

This work was supported by the German Research Foundation (SFB944, SFB1348, and WE2750/4-1 to RW-S) and the Cells-in-Motion Cluster of Excellence (EXC1003-CiM, University of Münster to RW-S). JVB was supported by a postdoctoral fellowship from the Basque Government.

REFERENCES

Berchtold, D., Piccolis, M., Chiaruttini, N., Riezman, I., Riezman, H., Roux, A., et al. (2012). Plasma membrane stress induces relocalization of Slm proteins and activation of TORC2 to promote sphingolipid synthesis. *Nat. Cell Biol.* 14, 542–547. doi: 10.1038/ncb2480

Berchtold, D., and Walther, T. C. (2009). TORC2 plasma membrane localization is essential for cell viability and restricted to a distinct domain. *Mol. Biol. Cell* 20, 1565–1575. doi: 10.1091/mbc.E08-10-1001

Bianchi, F., Syga, L., Moiset, G., Spakman, D., Schavemaker, P. E., Punter, C. M., et al. (2018). Steric exclusion and protein conformation determine the localization of plasma membrane transporters. *Nat. Commun.* 9:501. doi: 10.1038/s41467-018-02864-2

Boya, P., Reggiori, F., and Codogno, P. (2013). Emerging regulation and functions of autophagy. *Nat. Cell Biol.* 15, 713–720. doi: 10.1038/ncb2788

Brach, T., Specht, T., and Kaksonen, M. (2011). Reassessment of the role of plasma membrane domains in the regulation of vesicular traffic in yeast. *J. Cell Sci.* 124, 328–337. doi: 10.1242/jcs.078519

Busto, J. V., Elting, A., Haase, D., Spira, F., Kuhlman, J., Schafer-Herte, M., et al. (2018). Lateral plasma membrane compartmentalization links protein function and turnover. *EMBO J.* 37:e99473. doi: 10.15252/embj.201899473

Eltschinger, S., and Loewith, R. (2016). TOR complexes and the maintenance of cellular homeostasis. *Trends Cell Biol.* 26, 148–159. doi: 10.1016/j.tcb.2015.10.003

Frohlich, F., Moreira, K., Aguilar, P. S., Hubner, N. C., Mann, M., Walter, P., et al. (2009). A genome-wide screen for genes affecting eisosomes reveals Nce102 function in sphingolipid signaling. *J. Cell Biol.* 185, 1227–1242. doi: 10.1083/jcb.200811081

Gaubitz, C., Oliveira, T. M., Prouteau, M., Leitner, A., Karuppasamy, M., Konstantinidou, G., et al. (2015). Molecular basis of the rapamycin insensitivity of target of rapamycin complex 2. *Mol. Cell* 58, 977–988. doi: 10.1016/j.molcel.2015.04.031

Ghaddar, K., Krammer, E. M., Mihajlovic, N., Brohee, S., Andre, B., and Prevost, M. (2014). Converting the yeast arginine can1 permease to a lysine permease. *J. Biol. Chem.* 289, 7232–7246. doi: 10.1074/jbc.M113.525915

Gonzalez, A., and Hall, M. N. (2017). Nutrient sensing and TOR signaling in yeast and mammals. *EMBO J.* 36, 397–408. doi: 10.15252/embj.201696010

Gournas, C., Gkionis, S., Carquin, M., Twyffels, L., Tyteca, D., and Andre, B. (2018). Conformation-dependent partitioning of yeast nutrient transporters into starvation-protective membrane domains. *Proc. Natl. Acad. Sci. U.S.A.* 115, E3145–E3154. doi: 10.1073/pnas.1719462115

Gournas, C., Saliba, E., Krammer, E. M., Barthelemy, C., Prevost, M., and Andre, B. (2017). Transition of yeast can1 transporter to the inward-facing state unveils an alpha-arrestin target sequence promoting its ubiquitylation and endocytosis. *Mol. Biol. Cell* 28, 2819–2832. doi: 10.1091/mbc.E17-02-0104

Grassl, R., Robl, I., Opekarova, M., and Tanner, W. (2000). The C-terminal tetrapeptide HWFW of the chlorella HUP1 hexose/H(+)-symporter is essential for full activity and an alpha-helical structure of the C-terminus. *FEBS Lett.* 468, 225–230. doi: 10.1016/s0014-5793(00)01230-8

Grossmann, G., Malinsky, J., Stahlschmidt, W., Loibl, M., Weig-Meckl, I., Frommer, W. B., et al. (2008). Plasma membrane microdomains regulate turnover of transport proteins in yeast. *J. Cell Biol.* 183, 1075–1088. doi: 10.1083/jcb.200806035

Grossmann, G., Opekarova, M., Malinsky, J., Weig-Meckl, I., and Tanner, W. (2007). Membrane potential governs lateral segregation of plasma membrane proteins and lipids in yeast. *EMBO J.* 26, 1–8. doi: 10.1038/sj.emboj.7601466

Grossmann, G., Opekarova, M., Novakova, L., Stolz, J., and Tanner, W. (2006). Lipid raft-based membrane compartmentation of a plant transport protein expressed in Saccharomyces cerevisiae. *Eukaryotic Cell* 5, 945–953. doi: 10.1128/ec.00206-05

Guiney, E. L., Klecker, T., and Emr, S. D. (2016). Identification of the endocytic sorting signal recognized by the Art1–Rsp5 ubiquitin ligase complex. *Mol. Biol. Cell* 27, 4043–4054. doi: 10.1091/mbc.e16-08-0570

Herman, P., Vecer, J., Opekarova, M., Vesela, P., Jancikova, I., Zahumensky, J., et al. (2015). Depolarization affects the lateral microdomain structure of yeast plasma membrane. *FEBS J.* 282, 419–434. doi: 10.1111/febs.13156

Huber, L. A., and Teis, D. (2016). Lysosomal signaling in control of degradation pathways. *Curr. Opin. Cell Biol.* 39, 8–14. doi: 10.1016/j.ceb.2016.01.006

Lin, C. H., MacGurn, J. A., Chu, T., Stefan, C. J., and Emr, S. D. (2008). Arrestin-related ubiquitin-ligase adaptors regulate endocytosis and protein turnover at the cell surface. *Cell* 135, 714–725. doi: 10.1016/j.cell.2008.09.025

Loewith, R., and Hall, M. N. (2011). Target of rapamycin (TOR) in nutrient signaling and growth control. *Genetics* 189, 1177–1201. doi: 10.1534/genetics.111.133363

Ma, D., Lu, P., Yan, C., Fan, C., Yin, P., Wang, J., et al. (2012). Structure and mechanism of a glutamate–GABA antiporter. *Nature* 483, 632–636. doi: 10.1038/nature10917

Malinska, K., Malinsky, J., Opekarova, M., and Tanner, W. (2003). Visualization of protein compartmentation within the plasma membrane of living yeast cells. *Mol. Biol. Cell* 14, 4427–4436. doi: 10.1091/mbc.e03-04-0221

Malinska, K., Malinsky, J., Opekarova, M., and Tanner, W. (2004). Distribution of Can1p into stable domains reflects lateral protein segregation within the plasma membrane of living S. cerevisiae cells. *J. Cell Sci.* 117, 6031–6041. doi: 10.1242/jcs.01493

Malinsky, J., Tanner, W., and Opekarova, M. (2016). Transmembrane voltage: potential to induce lateral microdomains. *Biochim. Biophys. Acta* 1861, 806–811. doi: 10.1016/j.bbalip.2016.02.012

Moharir, A., Gay, L., Appadurai, D., Keener, J., and Babst, M. (2018). Eisosomes are metabolically regulated storage compartments for APC-type nutrient transporters. *Mol. Biol. Cell* 29, 2113–2127. doi: 10.1091/mbc.E17-11-0691

Muller, M., Schmidt, O., Angelova, M., Faserl, K., Weys, S., Kremser, L., et al. (2015). The coordinated action of the MVB pathway and autophagy ensures cell survival during starvation. *eLife* 4, e07736. doi: 10.7554/eLife.07736

Nikko, E., and Pelham, H. R. (2009). Arrestin-mediated endocytosis of yeast plasma membrane transporters. *Traffic* 10, 1856–1867. doi: 10.1111/j.1600-0854.2009.00990.x

Reddy, V. S., Shlykov, M. A., Castillo, R., Sun, E. I., and Saier, M. H. Jr. (2012). The major facilitator superfamily (MFS) revisited. *FEBS J.* 279, 2022–2035. doi: 10.1111/j.1742-4658.2012.08588.x

Rispal, D., Eltschinger, S., Stahl, M., Vaga, S., Bodenmiller, B., Abraham, Y., et al. (2015). Target of rapamycin complex 2 regulates actin polarization and endocytosis via multiple pathways. *J. Biol. Chem.* 290, 14963–14978. doi: 10.1074/jbc.M114.627794

Saier, M. H., Reddy, V. S., Tsu, B. V., Ahmed, M. S., Li, C., and Moreno-Hagelsieb, G. (2016). The transporter classification database (TCDB): recent advances. *Nucleic Acids Res.* 44, D372–D379. doi: 10.1093/nar/gkv1103

Spira, F., Dominguez-Escobar, J., Muller, N., and Wedlich-Soldner, R. (2012a). Visualization of cortex organization and dynamics in microorganisms, using total internal reflection fluorescence microscopy. *J. Vis. Exp.* 63, e3982. doi: 10.3791/3982

Spira, F., Mueller, N. S., Beck, G., von Olshausen, P., Beig, J., and Wedlich-Soldner, R. (2012b). Patchwork organization of the yeast plasma membrane into numerous coexisting domains. *Nat. Cell Biol.* 14, 640–648. doi: 10.1038/ncb2487

Vastermark, A., Wollwage, S., Houle, M. E., Rio, R., and Saier, M. H. (2014). Expansion of the APC superfamily of secondary carriers. *Proteins* 82, 2797–2811. doi: 10.1002/prot.24643

Wisedchaisri, G., Park, M. S., Iadanza, M. G., Zheng, H., and Gonen, T. (2014). Proton-coupled sugar transport in the prototypical major facilitator superfamily protein XylE. *Nat. Commun.* 5:4521. doi: 10.1038/ncomms5521

Zhao, Y., Wang, L., and Pan, J. (2015). The role of L-type amino acid transporter 1 in human tumors. *Intractable Rare Dis. Res.* 4, 165–169. doi: 10.5582/irdr.2015.01024

Conflict of Interest Statement: The authors declare that the research was conducted in the absence of any commercial or financial relationships that could be construed as a potential conflict of interest.

frontiers in Cell and Developmental Biology

ORIGINAL RESEARCH
published: 25 July 2019
doi: 10.3389/fcell.2019.00142

Impact of Autophagy and Aging on Iron Load and Ferritin in *Drosophila* Brain

Anne-Claire Jacomin[1†], Kalotina Geraki[2], Jake Brooks[3], Vindy Tjendana-Tjhin[3], Joanna F. Collingwood[3†] and Ioannis P. Nezis[1†]*

[1] School of Life Sciences, University of Warwick, Coventry, United Kingdom, [2] Diamond Light Source, Harwell Science and Innovation Campus, Didcot, United Kingdom, [3] School of Engineering, University of Warwick, Coventry, United Kingdom

Biometals such as iron, copper, potassium, and zinc are essential regulatory elements of several biological processes. The homeostasis of biometals is often affected in age-related pathologies. Notably, impaired iron metabolism has been linked to several neurodegenerative disorders. Autophagy, an intracellular degradative process dependent on the lysosomes, is involved in the regulation of ferritin and iron levels. Impaired autophagy has been associated with normal pathological aging, and neurodegeneration. Non-mammalian model organisms such as *Drosophila* have proven to be appropriate for the investigation of age-related pathologies. Here, we show that ferritin is expressed in adult *Drosophila* brain and that iron and holoferritin accumulate with aging. At whole-brain level we found no direct relationship between the accumulation of holoferritin and a deficit in autophagy in aged *Drosophila* brain. However, synchrotron X-ray spectromicroscopy revealed an additional spectral feature in the iron-richest region of autophagy-deficient fly brains, consistent with iron–sulfur. This potentially arises from iron–sulfur clusters associated with altered mitochondrial iron homeostasis.

Keywords: aging, autophagy, brain, *Drosophila*, ferritin, iron, synchrotron X-ray fluorescence microscopy

OPEN ACCESS

Edited by:
Rachel Susan Kraut, Max Planck Institute of Molecular Cell Biology and Genetics (MPI-CBG), Germany

Reviewed by:
Fanis Missirlis, Center for Research and Advanced Studies (CINVESTAV), Mexico
Qing-Ming Qin, Jilin University, China

***Correspondence:**
Ioannis P. Nezis
I.Nezis@warwick.ac.uk

† These authors have contributed equally to this work as senior authors

Specialty section:
This article was submitted to Membrane Traffic, a section of the journal Frontiers in Cell and Developmental Biology

Received: *07 February 2019*
Accepted: *10 July 2019*
Published: *25 July 2019*

Citation:
Jacomin A-C, Geraki K, Brooks J, Tjendana-Tjhin V, Collingwood JF and Nezis IP (2019) Impact of Autophagy and Aging on Iron Load and Ferritin in Drosophila Brain. Front. Cell Dev. Biol. 7:142. doi: 10.3389/fcell.2019.00142

INTRODUCTION

Iron is an essential biometal, widely used as a cofactor by a variety of proteins. Imbalance in iron metabolism, where either a deficiency or excess of iron may have harmful effects, and impaired iron metabolism may be modulators of neurodegeneration in several genetic or sporadic neurodegenerative disorders, such as Alzheimer's disease, Parkinson's disease, Huntington's disease, amyotrophic lateral sclerosis, and multiple sclerosis (Ward et al., 2014; Angelova and Brown, 2015; Biasiotto et al., 2016).

Ferritin is a universal iron storage protein. Two types of subunits, the heavy (H) and light (L) chains, assemble in different ratios into 24-subunit heteropolymers, in which iron can be stored in a mineralized form. Expression of both H and L ferritin chains are closely related to iron bioavailability (Gray and Hentze, 1994). Like in mammals, *Drosophila* genome encodes two types of subunits, known as heavy-chain homolog (Fer1HCH) and light-chain homolog (Fer2LCH) (Georgieva et al., 2002; Nichol et al., 2002; Hamburger et al., 2005). A mitochondrial ferritin subunit was lately identified in both mammals and insects (Levi et al., 2001; Missirlis et al., 2006). On the contrary to other ferritins, mitochondrial ferritin assembles as homopolymers (Levi et al., 2001).

When cells exhibit an iron deficiency, iron can be released from the ferritin. However, an excess of free iron may cause substantial damage to lipids, DNA, and proteins through the generation of highly reactive hydroxyl radicals (Zecca et al., 2004b; Angelova and Brown, 2015). Therefore, strict regulation of iron storage is essential to maintain cellular homeostasis and integrity. *Drosophila* has been successfully used as a model to evaluate the impact of iron storage deregulation on cell physiology and animal behavior. Notably, iron metabolism has been linked to circadian rhythms (Freeman et al., 2013; Rudisill et al., 2019), the autosomal recessive disease Friedreich's ataxia (Navarro et al., 2015; Soriano et al., 2016), neurodegenerative diseases and age-associated defects (Xun et al., 2008; Rival et al., 2009; Kosmidis et al., 2011, 2014; Tang and Zhou, 2013).

Cells use two main cytosolic degradative processes: the ubiquitin-proteasome pathway (UPS) and the autophagy-lysosomal pathway. While the UPS is specialized in the degradation of monomeric, short-lived proteins; autophagy has the potency to degrade large protein complexes and organelles (Korolchuk et al., 2010; Nam et al., 2017). Autophagy is divided into three different processes that differ by the way substrates are being delivered to the lysosome for degradation. Chaperone-mediated autophagy and microautophagy are defined by their ability to transfer proteins directly to the lysosomes through pores or membrane invagination respectively (Tekirdag and Cuervo, 2017). However, macroautophagy (referred to as autophagy) requires the isolation of cytoplasmic content into double-membraned autophagosomes that eventually fuse with the lysosomes (Yin et al., 2016). The molecular components involved in autophagy progression are highly conserved among Eukaryotes and most of these proteins have orthologs in *Drosophila* (Mulakkal et al., 2014; Bhattacharjee et al., 2019). The complexes of Atg (Autophagy) proteins regulating the formation of autophagosomes are well-conserved and characterized. One essential component of this machinery is the protein Atg8a (LC3 in mammals), which is cleaved and lipidated before anchoring into the autophagosomal membrane (Nagy et al., 2015). Atg8a is essential to the recruitment of other components of the autophagic machinery, as well as for the selection of receptors and their cargoes for selective degradation (Alemu et al., 2012; Wild et al., 2014; Schaaf et al., 2016). The best known selective cargo receptor in *Drosophila* is Ref(2)P (homologous to mammalian p62/SQSTM1) (Nezis et al., 2008; De Castro et al., 2013; Bartlett et al., 2014; Nagy et al., 2014). Selective autophagy can also contribute to the regulation of ferritin turnover (Hou et al., 2016; Gatica et al., 2018). The selective degradation of ferritin by autophagy is referred to as ferritinophagy and requires the cargo receptor NCOA4 in mammals (Mancias et al., 2014, 2015); no homologous receptor has been yet identified in *Drosophila*.

It has been extensively shown that autophagy declines during aging. Indeed, essential autophagy genes are transcriptionally down-regulated during healthy aging (Lipinski et al., 2010; Schultz et al., 2013; Omata et al., 2014). Accumulation of damaged proteins and organelles also constitutes a hallmark of numerous age-associated neurodegenerative disorders (Nixon, 2017; Colacurcio et al., 2018). Alteration of autophagy has been identified as an early onset feature in Alzheimer's disease-affected neurons (Zare-Shahabadi et al., 2015). However, the interplay between autophagy, iron and neurodegeneration is poorly understood.

In the present study, we used the model organism *Drosophila melanogaster* to investigate the effect of aging and autophagy disruption on the load of iron in the brain. We show that iron and holoferritin (where ferritin – Fer1HCH and Fer2LCH heteropolymer – protein surrounds an iron oxide core) accumulate in the brain from old flies regardless of their autophagy status, suggesting that autophagy is not essential to regulate total iron levels in the *Drosophila* brain. The spectrum of iron phases present is unchanged within the limits of detection for wild-type as a function of aging, but there is evidence of a distinct iron fraction in the autophagy-deficient fly brain, consistent with a proportional elevation in an iron–sulfur phase. This may, in turn, indicate disrupted mitochondrial iron homeostasis (Rouault and Tong, 2005).

MATERIALS AND METHODS

Drosophila Stocks and Maintenance

Flies were maintained on standard yeast-cornmeal medium at 25°C, 70% humidity with a 12 h light-dark cycle. The following fly strains were used: wild-type w^{1118} (BDRC #3605), Atg8a-deficient $Atg8a^{KG07569}$ (gift from Dr. Gabor Juhasz), Atg7-deficient $Atg7^{\Delta 77}$ and $Atg7^{\Delta 14}/CyO$ (Juhasz et al., 2007) (gift from Dr. Gabor Juhasz), $Fer1HCH^{G188}/TM3$ (DGRC #110-620; this line encodes a GFP-tagged version of the Fer1HCH subunit) (Missirlis et al., 2007), *hml*(delta)-*GAL4 UAS-eGFP* (BDRC # 30140) and *hml*(delta)-*GAL4 UAS-eGFP UAS-hid/CyO* (gift from Dr. François Leulier). For the generation of Atg7-deficient flies, virgin females $Atg7^{\Delta 14}/CyO$ were crossed with males $Atg7^{\Delta 77}$ and the progeny lacking balancer chromosome was collected after hatching. Stocks were backcrossed to w^{1118} to isogenise the genetic background.

Aging and Lifespan Measurement

For all experiments, age-matched adult male flies were used. Flies were collected within 24 h of hatching and aged in cohorts of 20 individuals. Flies were transferred every 2–3 days on fresh medium until collection after 1 week, 1 or 2 months. Because of their shorter lifespan, old autophagy-deficient flies were collected at 1 month.

Generation of Hemizygous GFP-Fer1HCH Expressing Flies

Homozygous virgin females wild-type (w^{1118}) or autophagy-deficient ($Atg8a^{KG07569}$) were crossed with males $Fer1HCH^{G188}/TM3$. From the progeny, only hemizygous males w^{1118}/Y; $Fer1HCH^{G188}/+$ and $Atg8a^{KG07569}/Y$; $Fer1HCH^{G188}/+$ were collected, and aged or fed as mentioned where appropriate in the figure legends.

Feeding With Iron or Bortezomib-Supplemented Diets

Adult males were selected within 24 h from hatching and placed onto Nutri-Fly Instant *Drosophila* Medium (Genesee Scientific, 66–117) prepared in water supplemented with 1 mM FAC (ferric ammonium citrate) or 20 mM bortezomib in DMSO (#2204 Cell Signaling Technology). Flies were flipped onto freshly made food every day for 5 days. The same diet without FAC or with 0.002% DMSO were used as respective control for regular diets.

Protein Extraction From Adult *Drosophila* Heads and Bodies

Age-matched adult males were flash frozen in liquid nitrogen. Flies were decapitated by short burst vortexing in 15 mL tubes. Heads, bodies, and appendices were separated using sieves (no. 25 and no. 40) chilled with liquid nitrogen beforehand. Heads were collected in microcentrifuge tubes and homogenized in ice-cold lysis buffer (20 mM Tris pH 7.5, 137 mM NaCl, 1% Triton X-100, 1% glycerol) supplemented with complete protease inhibitor cocktail (cOmplete^{TM}, Mini, EDTA-free Protease Inhibitor Cocktail; Sigma-Aldrich, 04693159001 Roche) and 50 mM *N*-ethylmaleimide (Sigma-Aldrich, E3876). Protein concentrations were determined using Bradford assay.

Hemocyte Ablation

The cell-specific ablation of mature hemocytes was performed by crossing virgin females *Fer1HCH*^{G188}*/TM3* with males *hml*(delta)-*GAL4 UAS-eGFP UAS-hid/CyO*. As a control, virgin females *Fer1HCH*^{G188}*/TM3* were crossed with males *hml*(delta)-*GAL4 UAS-eGFP/CyO*. From the progeny, adult flies lacking the balancer chromosomes were selected and aged for 5 days onto regular diet before collection of their hemolymph.

Hemolymph Collection

Immediately before hemolymph collection, anesthetized flies were surface sterilized by dipping them briefly in 70% ethanol. Excess ethanol was blotted off on filter paper. Flies were punctured with a tungsten needle in their thorax and immediately placed in a collection tube on ice. Collection tubes were made by piercing through the bottom of a 0.5 mL centrifuge tube with a 25G needle and placing it into a 1.5 mL centrifuge tube. A total of 40 punctured flies per genotype were pooled per collection tube. Hemolymph was isolated by centrifugation at 5000 rpm for 5 min at 4°C. Collected hemolymph samples were then diluted in Laemmli loading buffer and heated for 5 min at 95°C.

In gel Iron Staining

Protein extracts were prepared in 2x concentrated non-denaturing/non-reducing loading buffer (62.5 mM Tris-HCl pH 6.8, 25% glycerol, 1% bromophenol blue). Protein concentrations were determined using Bradford assay; 20 μg of total protein for each sample was separated on 6% native-PAGE gel in ice-cold running buffer (25 mM Tris, 192 mM glycine) after pre-run of the gel for 30 min at 100 V. Following protein separation, the gel was stained for 48 h with Prussian blue staining solution (10% $K_4Fe(CN)_6$, 350 mM HCl) at room temperature with gentle agitation. After washes in ultrapure water, holoferritin was visible as blue bands. All the glassware and tanks were acid-rinsed (1% HCl in ultrapure water) and left to air dry before use.

Western Blotting and Antibodies

Protein extracts were prepared in Laemmli loading buffer containing 2.5% beta-mercaptoethanol (except for experiment in non-reducing condition where no beta-mercaptoethanol was added) and heated for 5 min at 95°C before separation of 20 μg total proteins on 8 or 12% SDS-PAGE gels. Separated proteins were transferred onto nitrocellulose or PVDF membranes. The membranes were blocked in TBS (Tris-buffered saline; 50 mM Tris-Cl, pH 7.6, 150 mM NaCl), 0.1% Tween-20, 5% non-fat milk. The following antibodies were used: anti-GFP (Santa Cruz sc-9996, 1:1,000), anti-GABARAP/Atg8a (Cell Signaling Technology No. 13733, 1:2,000), anti-Ref(2)P (Abcam ab178440, 1:1,000), anti-β actin (Abcam ab8227, 1:2,000), anti-α tubulin (Sigma-Aldrich T5168, 1:40,000), HRP-coupled secondary antibodies anti-rabbit and anti-mouse (Thermo Scientific No. 31460 and 31450, 1:10,000). Signals were developed using the ECL detection reagents (Amersham, RPN2209).

Immunocytochemistry

Dissected brains from adult males *Fer1HCH*^{G188} were fixed for 30 min in 4% paraformaldehyde in 1x PBS (phosphate buffered saline; 137 mM NaCl, 10 mM Phosphate, 2.7 mM KCl, pH 7.4). The brains were permeabilized for 1 h in permeabilization buffer (0.1% Triton X-100, 0.3% BSA in PBS) before incubation overnight at 4°C with anti-Brp (DSHB, nc82 supernatant; 1:10 in permeabilization buffer) (Wagh et al., 2006) or anti-Elav (DSHB, Elav-9F8A9 supernatant; 1:100 in permeabilization buffer) (O'neill et al., 1994). Subsequent incubation with an Alexa568-coupled secondary antibody (Sigma No. SAB4600082, 1:500) was conducted in permeabilization buffer for 2 h at room temperature. Nuclei were stained with Hoechst 33342 (1 μg/mL in PBS). All washes were performed with 0.1% Triton X-100 in PBS. Images were captured with a Zeiss LSM880 confocal microscope.

X-Ray Fluorescence Imaging and Spectroscopy on Isolated Brains

Whole dissected brain from flies at the desired age were dissected using tungsten-coated titanium tweezers in ultrapure deionized water. Dissected brains were mounted onto ultralene film and allow to air dry for a minimum of 2 h (nine brains per slide: three brains per genotype/age).

Specimens were analyzed at the I18 Microfocus Spectroscopy beamline at the Diamond Light Source in Oxford, United Kingdom, using a pair of opposing Si detectors to maximize recovery of the fluorescence emitted from the ultralene-mounted samples. The focused beam was tuned to 10.5 keV, with a beam spot diameter of 60 μm for initial surveys with microfocus X-ray Fluorescence (μXRF), and 20 μm for mapping over the area of each intact brain. The method used here is not as precise in determining absolute concentration

as mass spectrometry imaging, but it is non-destructive and highly sensitive to relative differences in concentration between samples (Collingwood and Adams, 2017). Three to nine intact brains were imaged at room temperature for each group of flies. Detector position and acquisition times were kept consistent throughout the experiment to facilitate the subsequent comparative analysis. Subsequently, site-specific X-ray Absorption Near Edge Spectroscopy with a microfocused beam (μXANES) analysis was performed at the iron K-edge, using the 20 μm diameter beam to acquire a spectrum from the iron-richest region in the central brain from each fly, where the region of interest (ROI) was confirmed using the μXRF intensity image for iron. The absorption edge position in energy was calibrated with reference to an iron foil spectrum obtained during the same experiment, with alignment and removal of background being performed using the established workflow in the IFEFFIT Athena software package for XAFS analysis (Ravel and Newville, 2005).

Genomic DNA Extraction and PCR

Genomic DNA (gDNA) from 15 flies per genotype was extracted using DNeasy Blood and Tissues Kit (Qiagen 69504). PCR amplifications were conducted on 100 ng of gDNA with DreamTaq Green PCR Master Mix (Thermo Scientific K1081) in a Bio-Rad T100 thermal cycler. Samples were loaded on 1% (w/v) agarose gel in 1x TAE (40 mM Tris-base, 20 mM acetic acid, 1 mM EDTA pH 8.0). GelRed (VWR 41003) was used to stain nuclei acids. Primer sequences are listed in **Table 1**.

RNA Extraction and Real Time (RT)-qPCR

Total RNA extraction was performed on adult males using the PureLinkTM RNA Mini kit (Life Technologies Ambion) according to the manufacturer protocol. For all subsequent steps, 1 μg of RNA was used for each condition. Genomic DNA were digested out using DNase I (Thermo Scientific K1622). Synthesis of cDNA was done using the RevertAid Kit (Thermo Scientific K1622). Relative quantitation of gene expression was performed in an Agilent MxPro4005P qPCR system using the GoTaq qPCR Master Mix (Promega A6002). Primer sequences are listed in **Table 1**.

RESULTS

Ferritin Is Expressed in Adult *Drosophila* Brain

It has been previously shown that ferritin is expressed in various tissues in *Drosophila*. The protein expression of a GFP-knock-in mutant for *fer1hch* has been used to show the localization of Fer1HCH protein in different tissues and organs, including the larval brain where it accumulates primarily in the optic lobes and notochord (Georgieva et al., 2002; Mehta et al., 2009). However, no information is readily available concerning the localization of the GFP-Fer1HCH in adult fly brain. To evaluate the expression of GFP-Fer1HCH in the head of adult flies, we performed western blot on lysates from isolated heads and bodies from a fly strain expressing GFP-tagged Fer1HCH due to the genomic insertion of GFP between the first and second exons of the gene (*Fer1HCH*^{G188} flies) (Missirlis et al., 2007). Wild-type flies were used as a negative control. As expected from previous studies, GFP-Fer1HCH was detected in samples from both heads and bodies (**Figure 1A**).

Drosophila ferritin is known to be secreted in the hemolymph, which is analogous to vertebrates' blood, and remains in direct contact with tissues. In order to evaluate whether the GFP-Fer1HCH protein we detected in *Drosophila* heads corresponds to secreted or cytosolic ferritin, we extracted the hemolymph from adult *Fer1HCH*^{G188} flies. As expected, GFP-Fer1HCH strongly accumulates in the hemolymph, but also remains present in the bodies after draining their hemolymph (**Figure 1B**). It was shown that GFP-Fer1HCH accumulates in hemocytes (Gonzalez-Morales et al., 2015). To make the distinction between ferritin which is secreted in the hemolymph and expressed in the hemocytes, we compare the level of GFP-Fer1HCH protein in the hemolymph from flies lacking mature hemocytes (phagocytes) and flies with a normal hemocytes pool (**Figures 1C,D**). Tubulin was used as a marker for the successful ablation of

TABLE 1 | Primer sequences used in this study.

PCR primers		
HmlΔ forward	CCAACAATTTCCGATTAGCCTAAC	
GAL4 reverse	CGATACAGTCAACTGTCTTTGACC	
pUAST3′	AACCAAGTAAATCAACTGC	
Hid reverse	GAATGGTGTGGCATCATGTGC	
EGFP reverse	CTTGTAGTTGCCGTCGTCCTTGAA	
RT-qPCR	**Forward primer sequences**	**Reverse primer sequences**
fer1hch	TCTGATCAATGTGCCGACTG	TGGTAGTGGTTGTAGGGCTTG
fer2lch	GCCAGAACACTGTAATCACCG	GGCTCAATATGGTCAATGCCA
Atg8a	GGTCAGTTCTACTTCCTCATTCG	GATGTTCCTGGTACAGGGAGC
Atg7	TCGTGGGCTGGGAGCTAAATA	GGTTTACAGAGTTCTCAGCGAG
rp49	AAGAAGTTCCTGGTGCACAACGTG	AATCTCCTTGCGCTTCTTGGAGGA

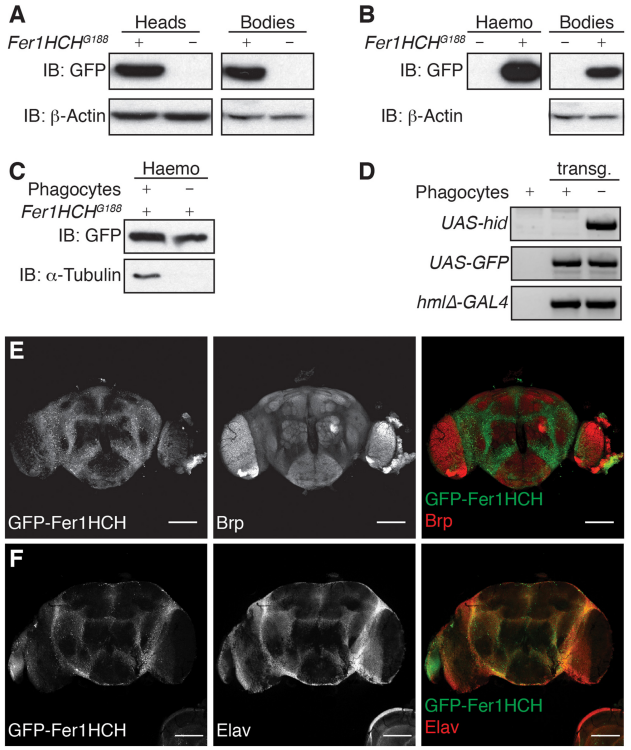

FIGURE 1 | Ferritin heavy chain is expressed in adult *Drosophila* brain. **(A–C)** Western blot analysis of GFP-Fer1HCH in reduced/denaturated protein samples extracted from **(A)** fly heads or bodies; **(B)** hemolymph (Haemo) or bodies drained from their hemolymph (Bodies); **(C)** hemolymph from flies depleted (–) or not (+) of their phagocytes. **(D)** Gel electrophoresis on PCR products from gDNA extracted from transgenic (transg.) flies used in **(C)**, gDNA from w^{1118} wild-type flies was used as negative control. **(E,F)** Confocal imaging of an adult *Drosophila* brain expressing GFP-Fer1HCH (left panel, green in merged panel) and stained for either **(E)** Bruchpilot (Brp) or **(F)** Elav (middle panel, red in merged channel). For all the experiments, 1-week-old adult males were used.

the phagocytes (**Figure 1C**) and the presence of the relevant transgenes was validated by PCR on gDNA (**Figure 1D**). We observed a moderate reduction of GFP-Fer1HCH in the hemolymph from the flies lacking phagocytes, meaning that most of the ferritin in the hemolymph corresponds to secreted ferritin (**Figure 1C**).

To confirm that ferritin detected in the adult *Drosophila* head comes mainly from the tissues rather than the surrounding hemolymph, we used fluorescence microscopy to establish the distribution of ferritin in *Drosophila* adult brain. We observed that GFP-Fer1HCH is expressed in the cell bodies surrounding the neuropil, marked using an antibody against the presynaptic protein Bruchpilot (Brp) (Wagh et al., 2006) (**Figure 1E**). The localization of GFP-Fer1HCH also matches the expression of Elav, a neuron-specific protein (**Figure 1F**).

Taken together, the above results show that ferritin heavy chain is expressed in the brain of adult *Drosophila* fly and accumulates in the neuronal cell bodies.

Decline of Autophagy Induces Accumulation of High Molecular Weight Ferritin Heavy Chain

Various studies have demonstrated that autophagy, which declines with age, is implicated in the degradation of ferritin and iron turnover (Asano et al., 2011; Mancias et al., 2014; Ott et al., 2016). To evaluate whether autophagy and aging affect the level of ferritin in adult *Drosophila* heads, we made use of the GFP-Fer1HCH expressing flies. First, extracts from adult heads of wild-type or Atg8a mutant males heterozygous for the *Fer1HCH*^{G188} allele were analyzed. Atg8a mutant fly heads were used as a negative control for GFP-Fer1HCH expression. Western blots probed with anti-GFP antibody revealed the presence of a band at the expected size of 50 kDa consistent with the fusion of the 27 kDa GFP protein to the 23 kDa Fer1HCH chain (**Figure 2A**). No noticeable difference was observed between wild-type and autophagy mutant. However, 1-week old Atg8a mutant fly head samples, but not young age-matched wild-type, exhibited the accumulation of a higher molecular weight band around 120 kDa (**Figure 2A**). Similarly, we noted the presence of higher molecular weight bands in old (2-months old) *Fer1HCH*^{G188} male fly heads that were not detected in young (1-week old) wild-type flies (**Figure 2B**).

To test whether this high molecular weight ferritin in Atg8a mutant and aged wild-type fly heads corresponds to aggregates, we performed a differential detergent protein extraction (Nezis et al., 2008; Simonsen et al., 2008; Jacomin and Nezis, 2019). Soluble proteins from fly heads were first extracted in a 0.1% Triton X-100 lysis buffer. The pellets, containing aggregated proteins, were then broken down by sonication in a 2% SDS lysis buffer. Samples were reduced and denaturated before separation by SDS-PAGE. We observed that 50 kDa GFP-Fer1HCH is predominantly located in the soluble fraction (Triton). High molecular weight ferritin heavy chains were solely detected in the soluble fraction and were excluded entirely from the insoluble fraction (SDS) (**Figure 2C**). Some proteins can form oligomers that can be identified using reduced and non-reduced lysis condition. We compared the effect of reducing agent on the formation of higher molecular weight GFP-Fer1HCH. Lysis of wild-type and Atg8a mutant fly heads was performed in lysis buffer supplemented with 50 mM *N*-ethylmaleimide to prevent the formation of new disulfide bond during the lysis procedures. Loading samples were then prepared by boiling in SDS-loading buffer in the presence (reduced) or absence (non-reduced) of 2.5% β-mercaptoethanol (**Figure 2D**). The preparation of the samples from in non-reduced condition had no effect on the accumulation of the high molecular weight GFP-Fer1HCH which was consistently observed in 1-week old autophagy mutant (but not age-matched wild-type) fly heads samples. To evaluate the implication of the proteasome in the clearance of ferritin, we have fed flies expressing GFP-Fer1HCH with bortezomib – an inhibitor of the proteasome – and looked at the accumulation of GFP-Fer1HCH high molecular weight band; no significant effect was observed (**Figure 2E**). The efficiency of bortezomib to block the proteasome was checked by probing the membrane with an antibody against

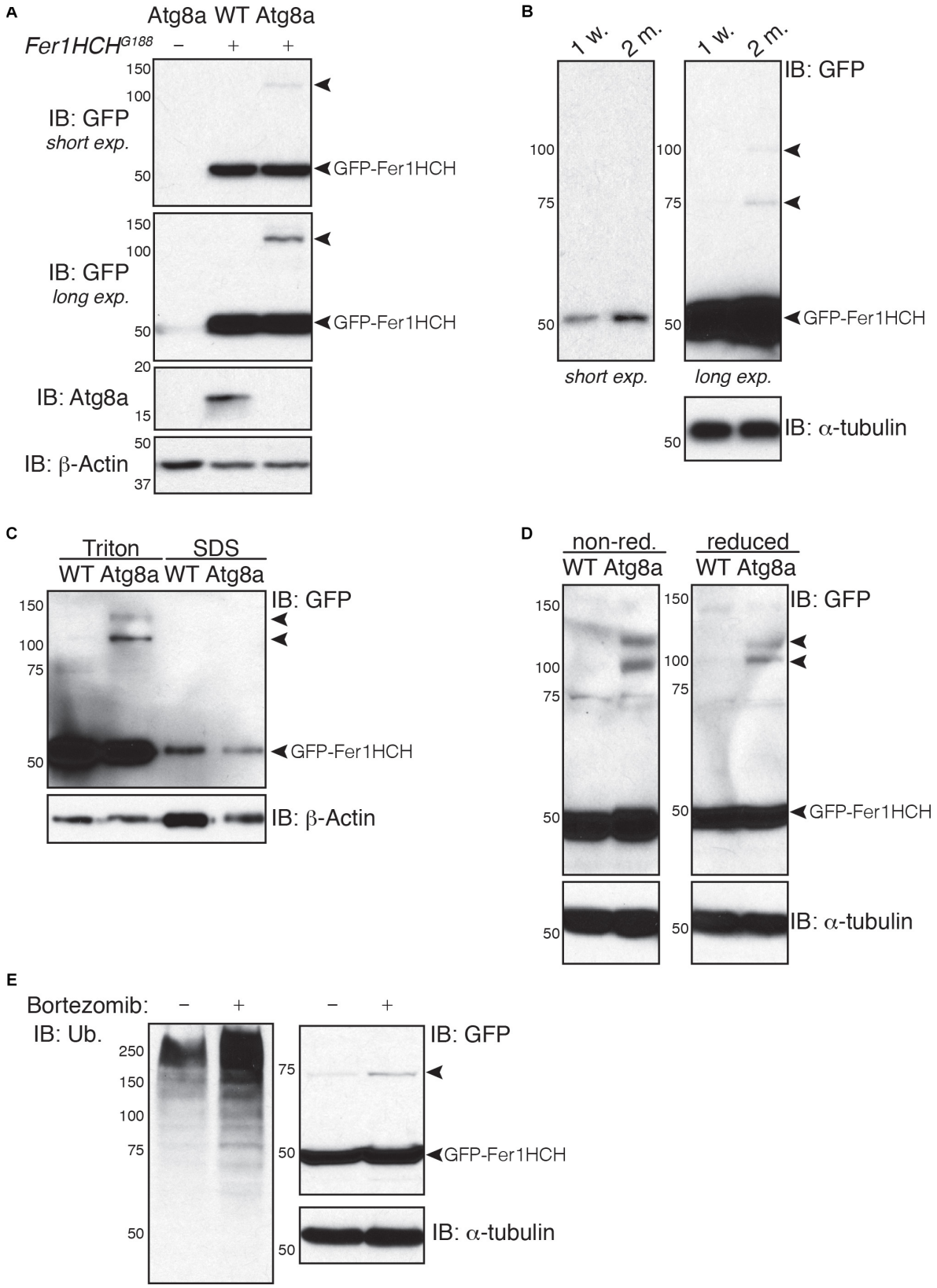

FIGURE 2 | Continued

FIGURE 2 | Soluble high molecular weight heavy-chain ferritin accumulates in autophagy-deficient fly heads. **(A,B)** Western blot analysis of GFP-Fer1HCH after samples reduction/denaturation in total protein lysates from **(A)** 1-week old wild-type (WT) and Atg8a mutant flies or **(B)** 1-week or 2-months old wild-type flies. **(C)** Western blot analysis of GFP-Fer1HCH in soluble (Triton) and insoluble/aggregated (SDS) proteins fraction from 1-week old wild-type (WT) and Atg8a mutant fly heads. **(D)** Western blot analysis of GFP-Fer1HCH in total protein lysates from 1-week old wild-type (WT) and Atg8a mutant fly heads prepared in either reduced or non-reduced conditions before SDS-PAGE and western blotting. **(E)** Western blot analysis of GFP-Fer1HCH in total protein lysates from Fer1HCHG188 fly heads after feeding for 6 days on 10 μM bortezomib or vehicles. Membranes were probed for GFP, Atg8a **(A)**, ubiquitinated proteins **(E)**; β-actin **(A,C)** or α-tubulin **(B,D,E)** were used as loading control. Arrowheads show high molecular weight bands of GFP-Fer1HCH. The terms 'short exp.' and 'long exp.' refer to the duration of film exposure on the membrane before developing. A longer exposure (long exp.) was necessary for the observation of the high molecular weight GFP-Fer1HCH which are less abundant than 50 kDa GFP-Fer1HCH.

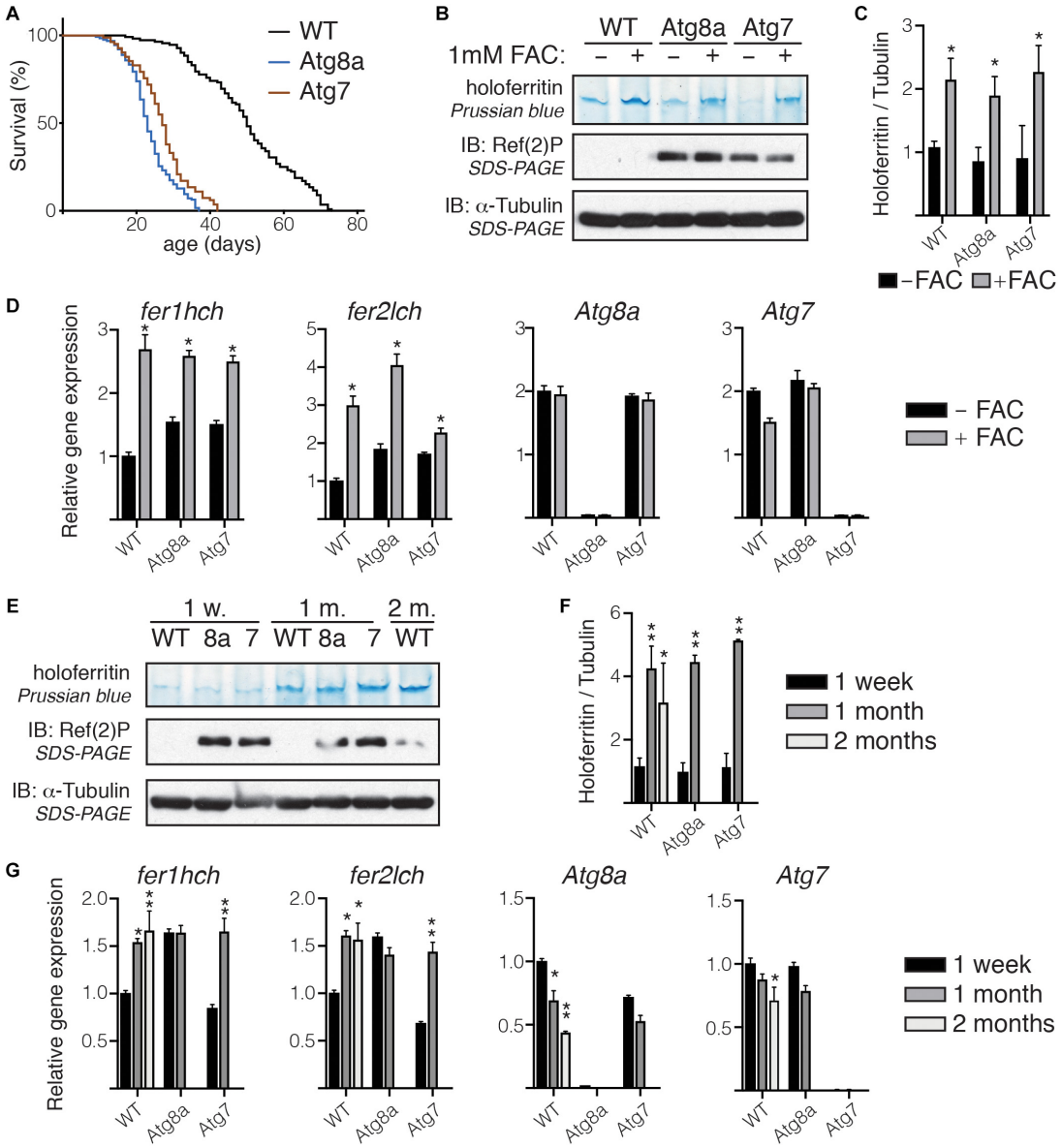

FIGURE 3 | Holoferritin accumulation in fly head. **(A)** Lifespan of a 100 wild-type and Atg8a and Atg7 mutant flies reared in standard conditions. **(B)** *In gel* staining for holoferritin in protein lysates from wild-type and Atg8a and Atg7 mutant flies fed on either normal diet or diet supplemented with 1 mM FAC. **(C)** Relative quantity of holoferritin normalized to loading control. **(D)** Analysis by RT-qPCR of mRNA level for *fer1hch*, *fer2lch*, *Atg8a,* and *Atg7* in flies fed on either normal or FAC-supplemented diet. **(E)** *In gel* staining for holoferritin on protein lysates from wild-type (WT) Atg8a (8a) and Atg7 (7) mutant fly heads at 1-week, 1-month and 2-month old. **(F)** Relative quantity of holoferritin normalized to loading control. **(G)** Analysis by RT-qPCR of mRNA level for *fer1hch*, *fer2lch*, *Atg8a,* and *Atg7* in aged flies. The bar charts show mean ± SD. Statistical significance was determined using one-way ANOVA, $^{*}P < 0.05$, $^{**}P < 0.01$. Western blots on denaturated samples were probed for Ref(2)P as an autophagy-deficiency control and α-tubulin as a loading control.

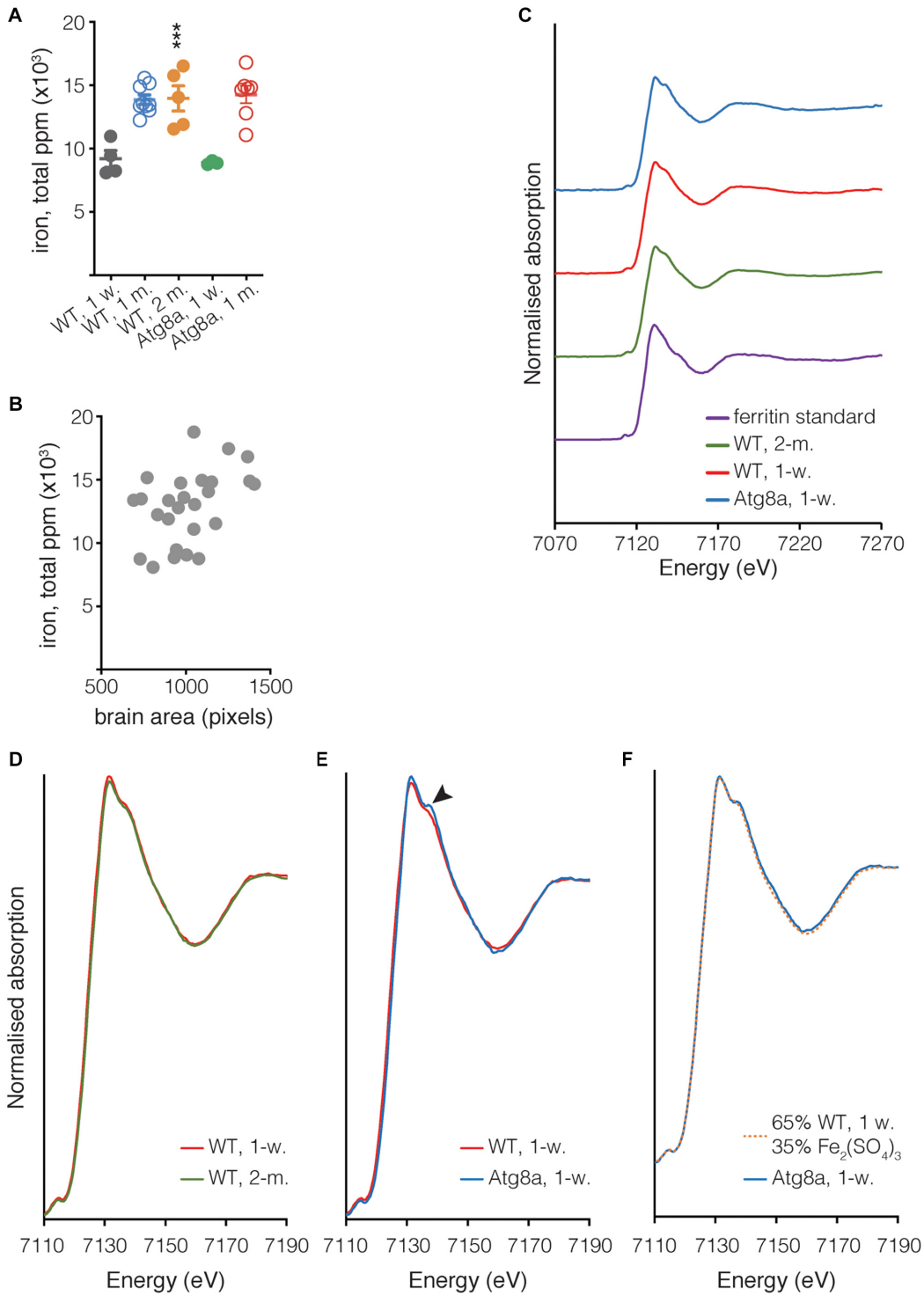

FIGURE 4 | Quantification of iron in isolated *Drosophila* brain. **(A)** The total quantity of iron per whole fly brain was measured from complete brain images obtained using μXRF at 20 μm resolution. Individual biological samples are shown as circles. Open circle data were acquired during a different experiment than close circle data. Bar represents mean ± SD. Statistical significance was determined using one-way ANOVA; significant values are indicated above the bars, $^{***}P < 0.001$. **(B)** Correlation between the area of the brain in pixels (px) and the quantity of iron. Spearman's rank correlation coefficient $\rho = 0.3311$. **(C)** Fe K-edge XANES from *Drosophila* and ferritin standard, with spectra vertically offset for clarity. **(D,E)** Overlay of spectra shown in **(C)**, focussing on the region where the spectra from Atg8a and wild-type differ (arrowhead). **(F)** Linear combination fitting of Atg8a spectrum. The Atg8 spectrum was shown to be consistent with that of the wild-type model + Fe(III) sulfate ($Fe_2(SO_4)_3$), with a χ^2 value of 0.01 obtained for the fit. All XANES spectra were subjected to an edge-step normalization and flattened using Athena fitting software prior to fitting.

ubiquitinated proteins, which accumulate when the proteasome is blocked (**Figure 2E**).

Taken together, these results show that ferritin does not form aggregates in *Drosophila* head when autophagy is impaired.

Holoferritin Is Not Affected in Autophagy Mutant Fly Heads

It has been well-documented that iron bioavailability and ferritin levels are correlated. We have verified that we can detect changes in holoferritin in wild-type and autophagy-deficient *Drosophila* by feeding adult flies on either normal diet or on a diet supplemented in iron in the form of FAC. Flies lacking either Atg8a or Atg7, two major regulators of autophagy, were used as autophagy-deficient *Drosophila*. We performed Prussian blue staining for holoferritin in protein samples from whole adult flies separated on native-PAGE. As expected, holoferritin accumulated in flies fed on iron-supplemented diet (**Figures 3B,C**) and correlated with an increase in the mRNA expression level of *fer1hch* and *fer2lch*, while Atg8a and Atg7 remained unchanged (**Figure 3D**).

We then performed *in gel* Prussian blue staining on protein lysates prepared from wild-type or autophagy-deficient fly heads collected from age-matched flies at 1-week, 1-month, or 2-months old. Because of their significantly shorter lifespan, samples from old Atg8a and Atg7 mutant flies were collected at 1-month old only, solely wild-type samples were collected at 2-month old (**Figure 3A**). We observed that holoferritin accumulated in protein samples from heads isolated from old flies, regardless of their autophagy-deficiency status. No difference was observed in heads from young autophagy-deficient flies when compared to age-matched wild-type (**Figures 3E,F**). The quantity of holoferritin was normalized against α-tubulin, used as a loading control, from the same samples separated by SDS-PAGE after denaturation and reduction of the samples in Laemmli loading buffer and boiling at 95°C. Gene expression of *fer1hch* and *fer2lch*, as well as *Atg8a* and *Atg7*, was accessed by RT-qPCR. Wild-type and Atg7 mutant flies showed an increased level in *fer1hch* and *fer2lch* as a result of their respective aging, which correlated with the accumulation of holoferritin, while no significant change was observed in Atg8a mutants (**Figure 3G**). As expected, Atg8a expressing is reduced in old wild-type flies (Simonsen et al., 2008; Omata et al., 2014).

Altogether, these results suggest that the accumulation of holoferritin during the course of aging in *Drosophila* head is independent of autophagy.

Ferric Iron Accumulates in the Brain of Aged Flies

X-ray fluorescence microscopy was previously demonstrated to be a robust way to image and quantify biometals in the non-mammalian model organisms, *Drosophila* and *Caenorhabditis elegans* (Lye et al., 2011; Jones et al., 2015; Ganio et al., 2016). Therefore, we used synchrotron μXRF imaging to measure the concentration of iron in the brain of *Drosophila*. Elemental maps were collected from whole brains dissected from young and old wild-type flies and young autophagy-deficient flies (*Atg8a* mutant). Three to nine entire brains per fly group were imaged at 20 μm resolution, providing an excellent signal to noise for the elements of interest. The data collected were used to quantify and compare iron concentrations (ppm) between each group. The quantification was done by first defining the ROI encompassing each brain based on the iron distribution map, and calculating the mass fraction for elements of interest after subtraction of the background signal (accounting for any background scatter reaching the detector, including any signal from the ultralene). As the present study focuses on iron, the other elements simultaneously acquired in the XRF imaging merit further investigation and will be the subject of future work. We observed that iron accumulated as a function of aging in the wild-type and autophagy-deficient brains (**Figure 4A**). Checking the relationship between the area mapped and the total metal ion signal confirmed that there was no correlation between the size of the brain and the amount of iron as shown by the Spearman's rank correlation coefficient $\rho = 0.3311$ (**Figure 4B**).

In addition to determining the elemental distribution of iron by μXRF, we performed site-specific microfocus X-ray Absorption Near Edge Structure (μXANES) spectroscopy analysis to obtain information about the dominant iron phase(s) present in the central brain region where iron deposition was the highest for each of the three groups. The μXANES spectra from wild-type and autophagy deficient flies incorporate the sum of contributions from the iron phases present at the iron-richest region in the central brain, including signal from the mineralized iron in holoferritin, typically a ferrihydrite-like hydrated iron oxide (Collingwood and Telling, 2016); the spectrum from the iron in purified horse spleen ferritin is included for comparison (**Figure 4C**). The μXANES spectra from these iron-rich sites in the 1-week and 2-months old wild-type flies are indistinguishable in this experiment (**Figure 4D**), whereas comparison of 1-week old wild-type and Atg8a-deficient reveals an additional feature in the autophagy-deficient fly at 7138 eV (**Figure 4E**). Linear combination fitting was undertaken for the 1-week old Atg8a-deficient fly spectrum using the 1-week wild-type spectrum and a range of reference standards (including those measured recently at the same beamline: iron metal reference foil, ferric sulfate, ferric and ferrous chloride, ferric citrate, horse spleen ferritin, previously-acquired iron nitride, and iron oxide standards including ferrihydrite, magnetite, and wustite). The best fitting result indicated that the feature can be well-accounted for by including a ferric sulfate reference standard (**Figure 4F**), suggesting that approximately 1/3 of the signal might be attributed to iron–sulfur complexes, and 2/3 attributed to the spectrum of iron phases found in the central brain of the wild-type fly.

DISCUSSION

During the course of aging, the load of iron in the brain increases significantly, possibly due to decreased efficiency of the iron

homeostasis system. Neurodegenerative pathologies associated with aging, such as Parkinson's or Alzheimer's diseases, have previously been associated with changes in iron homeostasis (Zecca et al., 2004a; Ward et al., 2014).

Our data corroborate previous studies of iron accumulation in the brain during aging in *Drosophila* (Massie et al., 1985, 1993). However, it was surprising to observe that neither iron nor ferritin heavy-chain levels are affected in autophagy-deficient flies. Indeed, an increase in iron in those flies was anticipated because of the recent studies pinpointing at the impact of autophagy on iron mobilization and recycling (Kurz et al., 2011; Mancias et al., 2014; Ott et al., 2016). The lack of accumulation of iron and holoferritin in autophagy-deficient flies at any age, matched to the age of wild-type individuals, suggests that autophagy is either not required or plays a minor role in the turnover of ferritin and iron during the course of aging in *Drosophila* brain. A recent study showed that lysosomal trafficking of ferritin could be independent of macroautophagy (Goodwin et al., 2017). Nonetheless, we noticed the presence of supernumerary GFP-Fer1HCH bands in the heads of young Atg8a-deficient flies while the main GFP-Fer1HCH band remained unchanged in age-match wild-type fly heads. This high molecular weight GFP-Fer1HCH probably corresponds to a non-functional form of ferritin heavy-chain as there is no accumulation of holoferritin in these flies as demonstrated by Prussian Blue *in gel* staining and μXRF. Autophagy has been extensively described for its role in the degradation of protein aggregates, and ferritin has been shown to be degraded by autophagy (Hyttinen et al., 2014; Mancias et al., 2014). However, using a differential-detergent protein fractionation protocol, we have observed that high molecular weight GFP-Fer1HCH bands do not correspond to insoluble aggregates. A shift in protein molecular weight could be associated with post-translational modifications. A study has shown that both ferritin subunits are ubiquitinated in muscles from a rat model of Amyotrophic Lateral Sclerosis (Halon et al., 2010). Ferritin has also been detected as being pupylated (prokaryotic homolog of ubiquitination) in the bacterium *Corynebacterium glutamicum* (Kuberl et al., 2016). Ferritin is also known to be glycosylated in mammals and insects; notably, secreted ferritin L has been shown to be N-glycosylated in culture hepatocytes (Cragg et al., 1981; Ketola-Pirie, 1990; Ghosh et al., 2004; Cohen et al., 2010). Therefore, it is possible that high molecular weight Fer1HCH corresponds to a modified, soluble form of the protein.

It was previously shown that iron storage increases significantly with age in both mammals and insects (Massie et al., 1985; Zecca et al., 2001). The control of ferritin subunit synthesis frequently occurs at the translational level. Ferritin mRNAs contain an iron-responsive element (IRE) in 5′ UTR that can be recognized by iron regulatory proteins (IRPs). Depending on iron availability, the translation of ferritin subunits is modulated by the binding or releasing of the IRPs to the mRNA (Gray and Hentze, 1994; Lind et al., 1998; Missirlis et al., 2007). Interestingly, no noticeable increase in the quantity of GFP-Fer1HCH with age was observed in the fly brain while the iron levels and holoferritin levels were significantly increased. Most of the studies aiming at elucidating the IRE/IRP-dependent regulation of ferritin are based on supplementation of animal food with iron or chelators. It is possible that such changes in the diet have more drastic effects on the iron uptake by the cells than that which would occur under physiological conditions. It is also possible that intestinal ferritin is more prone to transcriptional regulation as the gut is the first organ to be affected by dietary iron.

The evidence for an additional minor peak at 7138 eV in the iron absorption spectrum for autophagy deficient flies, but not in wild-type, is consistent with signal contribution from an iron–sulfur-rich material. The good fit achieved with the inclusion of ferric sulfate does not exclude other possibilities; we note that iron-phosphorus-containing material can also exhibit a peak in this energy region. However, examination of the XRF signal at the sites where the XANES spectra were acquired indicate that sulfur was significantly more abundant than phosphorus, and that while iron and sulfur levels at sites of XANES acquisition were equivalent for wild-type and autophagy mutant, the phosphorus level at the XANES site in the autophagy deficient fly was lower (approximately $1/5^{th}$) of that measured in wild-type. Therefore, it is more likely that the additional feature in the autophagy mutant is associated with iron–sulfur than with iron–phosphorus. Iron–sulfur clusters might account for this signal, a ubiquitous class of metalloproteins involved in many regulatory processes, including mitochondrial iron homeostasis (Rouault and Tong, 2005).

In summary, we have shown that holoferritin accumulates in the brain from old flies but not young Atg8a-deficient flies, suggesting that macroautophagy is not a dominant process in ferritin and iron turnover in the *Drosophila* adult head. The origin of increased iron in the brain during the course of aging in *Drosophila* brain remains unclear but appears not to be related to, or sufficient to induce the synthesis of, ferritin heavy-chain. In addition, our work provides evidence of the feasibility to accurately detect variation in biometal levels and distributions in intact isolated adult *Drosophila* brain, thus opening new fields of investigation for normal and pathological aging. Most neurodegenerative diseases are linked to altered metabolism of biometals, including iron, in the brain. *Drosophila* has been successfully used as model for a broad range of neuropathologies. Further studies combining those readily-available model strains with synchrotron spectromicroscopy methods should contribute to uncovering the relationships between disrupted metabolism of biometals and neurodegeneration.

AUTHOR CONTRIBUTIONS

A-CJ, KG, JB, VT-T, and JC performed the experiments and analyzed the data. KG, JB, VT-T, and JC provided material, expertise, and technical help in synchrotron X-ray fluorescence microscopy data acquisition and analysis. A-CJ, IN, and JC designed the study. A-CJ wrote the manuscript and analyzed the data. All authors read and contributed to the manuscript.

FUNDING

This work was supported by the BBSRC grants BB/L006324/1 and BB/P007856/1 to IN. We thank the Diamond Light Source for access to beamline I18 (proposals SP12879 to JC and SP24642 to A-CJ).

ACKNOWLEDGMENTS

We thank Drs. G. Juhasz and F. Leulier and the *Drosophila* Genomics Resource Center (supported by the NIH grant 2P40OD010949) for providing the fly stocks, and M. Ward for the fly food preparation.

REFERENCES

Alemu, E. A., Lamark, T., Torgersen, K. M., Birgisdottir, A. B., Larsen, K. B., Jain, A., et al. (2012). ATG8 family proteins act as scaffolds for assembly of the ULK complex: sequence requirements for LC3-interacting region (LIR) motifs. *J. Biol. Chem.* 287, 39275–39290. doi: 10.1074/jbc.M112.378109

Angelova, D., and Brown, D. (2015). Iron. *Aging Neurodegeneration. Metals* 5, 2070–2092.

Asano, T., Komatsu, M., Yamaguchi-Iwai, Y., Ishikawa, F., Mizushima, N., and Iwai, K. (2011). Distinct mechanisms of ferritin delivery to lysosomes in iron-depleted and iron-replete cells. *Mol. Cell Biol.* 31, 2040–2052. doi: 10.1128/MCB.01437-10

Bartlett, B. J., Isakson, P., Lewerenz, J., Sanchez, H., Kotzebue, R. W., Cumming, R. C., et al. (2014). p62, Ref(2)P and ubiquitinated proteins are conserved markers of neuronal aging, aggregate formation and progressive autophagic defects. *Autophagy* 7, 572–583. doi: 10.4161/auto.7.6.14943

Bhattacharjee, A., Szabo, A., Csizmadia, T., Laczko-Dobos, H., and Juhasz, G. (2019). Understanding the importance of autophagy in human diseases using drosophila. *J. Genet. Genomics.* 46, 157–169. doi: 10.1016/j.jgg.2019.03.007

Biasiotto, G., Di Lorenzo, D., Archetti, S., and Zanella, I. (2016). Iron and neurodegeneration: is ferritinophagy the link? *Mol. Neurobiol.* 53, 5542–5574. doi: 10.1007/s12035-015-9473-y

Cohen, L. A., Gutierrez, L., Weiss, A., Leichtmann-Bardoogo, Y., Zhang, D. L., Crooks, D. R., et al. (2010). Serum ferritin is derived primarily from macrophages through a nonclassical secretory pathway. *Blood* 116, 1574–1584. doi: 10.1182/blood-2009-11-253815

Colacurcio, D. J., Pensalfini, A., Jiang, Y., and Nixon, R. A. (2018). Dysfunction of autophagy and endosomal-lysosomal pathways: roles in pathogenesis of down syndrome and Alzheimer's Disease. *Free Radi.c Biol. Med.* 114, 40–51. doi: 10.1016/j.freeradbiomed.2017.10.001

Collingwood, J. F., and Adams, F. (2017). Chemical imaging analysis of the brain with X-ray methods. *Spectrochimica Acta Part BAt. Spectrosc.* 130, 101–118. doi: 10.1016/j.sab.2017.02.013

Collingwood, J. F., and Telling, N. D. (2016). *Iron Oxides in the Human Brain*. Hoboken, NJ: Wiley.

Cragg, S. J., Wagstaff, M., and Worwood, M. (1981). Detection of a glycosylated subunit in human serum ferritin. *Biochem. J.* 199, 565–571. doi: 10.1042/bj1990565

De Castro, I. P., Costa, A. C., Celardo, I., Tufi, R., Dinsdale, D., Loh, S. H., et al. (2013). Drosophila ref(2)P is required for the parkin-mediated suppression of mitochondrial dysfunction in pink1 mutants. *Cell. Death Dis.* 4:e873. doi: 10.1038/cddis.2013.394

Freeman, A. A., Mandilaras, K., Missirlis, F., and Sanyal, S. (2013). An emerging role for Cullin-3 mediated ubiquitination in sleep and circadian rhythm: insights from drosophila. *Fly* 7, 39–43. doi: 10.4161/fly.23506

Ganio, K., James, S. A., Hare, D. J., Roberts, B. R., and Mccoll, G. (2016). Accurate biometal quantification per individual caenorhabditis elegans. *Analyst* 141, 1434–1439. doi: 10.1039/c5an02544c

Gatica, D., Lahiri, V., and Klionsky, D. J. (2018). Cargo recognition and degradation by selective autophagy. *Nat. Cell. Biol.* 20, 233–242. doi: 10.1038/s41556-018-0037-z

Georgieva, T., Dunkov, B. C., Dimov, S., Ralchev, K., and Law, J. H. (2002). Drosophila melanogaster ferritin: CDNA encoding a light chain homologue, temporal and tissue specific expression of both subunit types. *Insect Biochem. Mol. Biol.* 32, 295–302. doi: 10.1016/s0965-1748(01)00090-x

Ghosh, S., Hevi, S., and Chuck, S. L. (2004). Regulated secretion of glycosylated human ferritin from hepatocytes. *Blood* 103, 2369–2376. doi: 10.1182/blood-2003-09-3050

Gonzalez-Morales, N., Mendoza-Ortiz, M. A., Blowes, L. M., Missirlis, F., and Riesgo-Escovar, J. R. (2015). Ferritin is required in multiple tissues during drosophila melanogaster development. *PLoS One* 10:e0133499. doi: 10.1371/journal.pone.0133499

Goodwin, J. M., Dowdle, W. E., Dejesus, R., Wang, Z., Bergman, P., Kobylarz, M., et al. (2017). Autophagy-independent lysosomal targeting regulated by ULK1/2-FIP200 and ATG9. *Cell Rep.* 20, 2341–2356. doi: 10.1016/j.celrep.2017.08.034

Gray, N. K., and Hentze, M. W. (1994). Iron regulatory protein prevents binding of the 43S translation pre-initiation complex to ferritin and eALAS mRNAs. *EMBO J* 13, 3882–3891. doi: 10.1002/j.1460-2075.1994.tb06699.x

Halon, M., Sielicka-Dudzin, A., Wozniak, M., Ziolkowski, W., Nyka, W., Herbik, M., et al. (2010). Up-regulation of ferritin ubiquitination in skeletal muscle of transgenic rats bearing the G93A hmSOD1 gene mutation. *Neuromuscul Disord* 20, 29–33. doi: 10.1016/j.nmd.2009.08.014

Hamburger, A. E., West, A. P. Jr., Hamburger, Z. A., Hamburger, P., and Bjorkman, P. J. (2005). Crystal structure of a secreted insect ferritin reveals a symmetrical arrangement of heavy and light chains. *J. Mol. Biol.* 349, 558–569. doi: 10.1016/j.jmb.2005.03.074

Hou, W., Xie, Y., Song, X., Sun, X., Lotze, M. T., Zeh, H. J., et al. (2016). Autophagy promotes ferroptosis by degradation of ferritin. *Autophagy* 12, 1425–1428. doi: 10.1080/15548627.2016.1187366

Hyttinen, J. M., Amadio, M., Viiri, J., Pascale, A., Salminen, A., and Kaarniranta, K. (2014). Clearance of misfolded and aggregated proteins by aggrephagy and implications for aggregation diseases. *Ageing Res. Rev.* 18, 16–28. doi: 10.1016/j.arr.2014.07.002

Jacomin, A. C., and Nezis, I. P. (2019). Assays to monitor aggrephagy in drosophila brain. *Methods Mol. Biol.* 1854, 147–157. doi: 10.1007/7651_2018_157

Jones, M. W., De Jonge, M. D., James, S. A., and Burke, R. (2015). Elemental mapping of the entire intact Drosophila gastrointestinal tract. *J. Biol. Inorg. Chem.* 20, 979–987. doi: 10.1007/s00775-015-1281-3

Juhasz, G., Erdi, B., Sass, M., and Neufeld, T. P. (2007). Atg7-dependent autophagy promotes neuronal health, stress tolerance, and longevity but is dispensable for metamorphosis in drosophila. *Genes Dev.* 21, 3061–3066. doi: 10.1101/gad.1600707

Ketola-Pirie, C. A. (1990). Characterization of an insect ferritin subunit synthesized in a cell-free system. *Biochem. Cell Biol.* 68, 1005–1011. doi: 10.1139/o90-148

Korolchuk, V. I., Menzies, F. M., and Rubinsztein, D. C. (2010). Mechanisms of cross-talk between the ubiquitin-proteasome and autophagy-lysosome systems. *FEBS Lett.* 584, 1393–1398. doi: 10.1016/j.febslet.2009.12.047

Kosmidis, S., Botella, J. A., Mandilaras, K., Schneuwly, S., Skoulakis, E. M., Rouault, T. A., et al. (2011). Ferritin overexpression in drosophila glia leads to iron deposition in the optic lobes and late-onset behavioral defects. *Neurobiol. Dis.* 43, 213–219. doi: 10.1016/j.nbd.2011.03.013

Kosmidis, S., Missirlis, F., Botella, J. A., Schneuwly, S., Rouault, T. A., and Skoulakis, E. M. (2014). Behavioral decline and premature lethality upon pan-neuronal ferritin overexpression in drosophila infected with a virulent form of Wolbachia. *Front. Pharmacol.* 5:66. doi: 10.3389/fphar.2014.00066

Kuberl, A., Polen, T., and Bott, M. (2016). The pupylation machinery is involved in iron homeostasis by targeting the iron storage protein ferritin. *Proc. Natl. Acad. Sci. U. S. A.* 113, 4806–4811. doi: 10.1073/pnas.1514529113

Kurz, T., Eaton, J. W., and Brunk, U. T. (2011). The role of lysosomes in iron metabolism and recycling. *Int. J. Biochem. Cell. Biol.* 43, 1686–1697. doi: 10.1016/j.biocel.2011.08.016

Levi, S., Corsi, B., Bosisio, M., Invernizzi, R., Volz, A., Sanford, D., et al. (2001). A human mitochondrial ferritin encoded by an intronless gene. *J. Biol. Chem.* 276, 24437–24440. doi: 10.1074/jbc.c100141200

Lind, M. I., Ekengren, S., Melefors, O., and Soderhall, K. (1998). Drosophila ferritin mRNA: alternative RNA splicing regulates the presence of the iron-responsive element. *FEBS Lett.* 436, 476–482. doi: 10.1016/s0014-5793(98)01186-7

Lipinski, M. M., Zheng, B., Lu, T., Yan, Z., Py, B. F., Ng, A., et al. (2010). Genome-wide analysis reveals mechanisms modulating autophagy in normal brain aging and in Alzheimer's disease. *Proc. Natl. Acad. Sci. U. S. A.* 107, 14164–14169. doi: 10.1073/pnas.1009485107

Lye, J. C., Hwang, J. E., Paterson, D., De Jonge, M. D., Howard, D. L., and Burke, R. (2011). Detection of genetically altered copper levels in Drosophila tissues by synchrotron x-ray fluorescence microscopy. *PLoS One* 6:e26867. doi: 10.1371/journal.pone.0026867

Mancias, J. D., Pontano Vaites, L., Nissim, S., Biancur, D. E., Kim, A. J., Wang, X., et al. (2015). Ferritinophagy via NCOA4 is required for erythropoiesis and is regulated by iron dependent HERC2-mediated proteolysis. *eLife* 4:e10308. doi: 10.7554/eLife.10308

Mancias, J. D., Wang, X., Gygi, S. P., Harper, J. W., and Kimmelman, A. C. (2014). Quantitative proteomics identifies NCOA4 as the cargo receptor mediating ferritinophagy. *Nature* 509, 105–109. doi: 10.1038/nature13148

Massie, H. R., Aiello, V. R., and Williams, T. R. (1985). Iron accumulation during development and ageing of drosophila. *Mech. Ageing Dev.* 29, 215–220. doi: 10.1016/0047-6374(85)90020-x

Massie, H. R., Aiello, V. R., and Williams, T. R. (1993). Inhibition of iron absorption prolongs the life span of drosophila. *Mech. Ageing Dev.* 67, 227–237. doi: 10.1016/0047-6374(93)90001-8

Mehta, A., Deshpande, A., Bettedi, L., and Missirlis, F. (2009). Ferritin accumulation under iron scarcity in Drosophila iron cells. *Biochimie* 91, 1331–1334. doi: 10.1016/j.biochi.2009.05.003

Missirlis, F., Holmberg, S., Georgieva, T., Dunkov, B. C., Rouault, T. A., and Law, J. H. (2006). Characterization of mitochondrial ferritin in Drosophila. *Proc. Natl. Acad. Sci. U. S. A.* 103, 5893–5898. doi: 10.1073/pnas.0601471103

Missirlis, F., Kosmidis, S., Brody, T., Mavrakis, M., Holmberg, S., Odenwald, W. F., et al. (2007). Homeostatic mechanisms for iron storage revealed by genetic manipulations and live imaging of drosophila ferritin. *Genetics* 177, 89–100. doi: 10.1534/genetics.107.075150

Mulakkal, N. C., Nagy, P., Takats, S., Tusco, R., Juhasz, G., and Nezis, I. P. (2014). Autophagy in Drosophila: from historical studies to current knowledge. *Biomed. Res. Int.* 2014:273473. doi: 10.1155/2014/273473

Nagy, P., Karpati, M., Varga, A., Pircs, K., Venkei, Z., Takats, S., et al. (2014). Atg17/FIP200 localizes to perilysosomal Ref(2)P aggregates and promotes autophagy by activation of atg1 in drosophila. *Autophagy* 10, 453–467. doi: 10.4161/auto.27442

Nagy, P., Varga, A., Kovacs, A. L., Takats, S., and Juhasz, G. (2015). How and why to study autophagy in drosophila: it's more than just a garbage chute. *Methods* 75, 151–161. doi: 10.1016/j.ymeth.2014.11.016

Nam, T., Han, J. H., Devkota, S., and Lee, H. W. (2017). Emerging paradigm of crosstalk between autophagy and the ubiquitin-proteasome system. *Mol. Cells* 40, 897–905. doi: 10.14348/molcells.2017.0226

Navarro, J. A., Botella, J. A., Metzendorf, C., Lind, M. I., and Schneuwly, S. (2015). Mitoferrin modulates iron toxicity in a drosophila model of friedreich's ataxia. *Free Radic Biol. Med.* 85, 71–82. doi: 10.1016/j.freeradbiomed.2015.03.014

Nezis, I. P., Simonsen, A., Sagona, A. P., Finley, K., Gaumer, S., Contamine, D., et al. (2008). Ref(2)P, the drosophila melanogaster homologue of mammalian p62, is required for the formation of protein aggregates in adult brain. *J. Cell Biol.* 180, 1065–1071. doi: 10.1083/jcb.200711108

Nichol, H., Law, J. H., and Winzerling, J. J. (2002). Iron metabolism in insects. *Annu. Rev. Entomol.* 47, 535–559.

Nixon, R. A. (2017). Amyloid precursor protein and endosomal-lysosomal dysfunction in Alzheimer's disease: inseparable partners in a multifactorial disease. *FASEB J.* 31, 2729–2743. doi: 10.1096/fj.201700359

Omata, Y., Lim, Y. M., Akao, Y., and Tsuda, L. (2014). Age-induced reduction of autophagy-related gene expression is associated with onset of Alzheimer's disease. *Am. J. Neurodegener. Dis.* 3, 134–142.

O'neill, E. M., Rebay, I., Tjian, R., and Rubin, G. M. (1994). The activities of two Ets-related transcription factors required for Drosophila eye development are modulated by the Ras/MAPK pathway. *Cell* 78, 137–147. doi: 10.1016/0092-8674(94)90580-0

Ott, C., Konig, J., Hohn, A., Jung, T., and Grune, T. (2016). Reduced autophagy leads to an impaired ferritin turnover in senescent fibroblasts. *Free Radic Biol. Med.* 101, 325–333. doi: 10.1016/j.freeradbiomed.2016.10.492

Ravel, B., and Newville, M. (2005). Athena. Artemis, Hephaestus: data analysis for X-ray absorption spectroscopy using IFEFFIT. *J. Synchrotron. Radiat.* 12, 537–541. doi: 10.1107/s0909049505012719

Rival, T., Page, R. M., Chandraratna, D. S., Sendall, T. J., Ryder, E., Liu, B., et al. (2009). Fenton chemistry and oxidative stress mediate the toxicity of the beta-amyloid peptide in a Drosophila model of Alzheimer's disease. *Eur. J. Neurosci.* 29, 1335–1347. doi: 10.1111/j.1460-9568.2009.06701.x

Rouault, T. A., and Tong, W. H. (2005). Iron-sulphur cluster biogenesis and mitochondrial iron homeostasis. *Nat. Rev. Mol. Cell Biol.* 6, 345–351. doi: 10.1038/nrm1620

Rudisill, S. S., Martin, B. R., Mankowski, K. M., and Tessier, C. R. (2019). Iron deficiency reduces synapse formation in the drosophila clock circuit. *Biol. Trace. Elem. Res.* 189, 241–250. doi: 10.1007/s12011-018-1442-7

Schaaf, M. B., Keulers, T. G., Vooijs, M. A., and Rouschop, K. M. (2016). LC3/GABARAP family proteins: autophagy-(un)related functions. *FASEB J.* 30, 3961–3978. doi: 10.1096/fj.201600698r

Schultz, S. W., Brech, A., and Nezis, I. P. (2013). "Time Flies: autophagy during ageing in drosophila," in *Autophagy - A Double-Edged Sword - Cell Survival or Death?*, ed. Y. Bailly (Croatia: In-Tech), 487–511.

Simonsen, A., Cumming, R. C., Brech, A., Isakson, P., Schubert, D. R., and Finley, K. D. (2008). Promoting basal levels of autophagy in the nervous system enhances longevity and oxidant resistance in adult Drosophila. *Autophagy* 4, 176–184. doi: 10.4161/auto.5269

Soriano, S., Calap-Quintana, P., Llorens, J. V., Al-Ramahi, I., Gutierrez, L., Martinez-Sebastian, M. J., et al. (2016). Metal homeostasis regulators suppress frda phenotypes in a drosophila model of the disease. *PLoS One* 11:e0159209. doi: 10.1371/journal.pone.0159209

Tang, X., and Zhou, B. (2013). Ferritin is the key to dietary iron absorption and tissue iron detoxification in drosophila melanogaster. *FASEB J.* 27, 288–298. doi: 10.1096/fj.12-213595

Tekirdag, K. A., and Cuervo, A. M. (2017). Chaperone-mediated autophagy and endosomal microautophagy: joint by a chaperone. *J. Biol. Chem.* 293, 5414–5424. doi: 10.1074/jbc.R117.818237

Wagh, D. A., Rasse, T. M., Asan, E., Hofbauer, A., Schwenkert, I., Durrbeck, H., et al. (2006). Bruchpilot, a protein with homology to ELKS/CAST, is required for structural integrity and function of synaptic active zones in Drosophila. *Neuron* 49, 833–844. doi: 10.1016/j.neuron.2006.02.008

Ward, R. J., Zucca, F. A., Duyn, J. H., Crichton, R. R., and Zecca, L. (2014). The role of iron in brain ageing and neurodegenerative disorders. *Lancet Neurol.* 13, 1045–1060. doi: 10.1016/S1474-4422(14)70117-6

Wild, P., Mcewan, D. G., and Dikic, I. (2014). The LC3 interactome at a glance. *J. Cell Sci.* 127, 3–9. doi: 10.1242/jcs.140426

Xun, Z., Kaufman, T. C., and Clemmer, D. E. (2008). Proteome response to the panneural expression of human wild-type alpha-synuclein: a drosophila model of Parkinson's disease. *J. Proteome Res.* 7, 3911–3921. doi: 10.1021/pr800207h

Yin, Z., Pascual, C., and Klionsky, D. J. (2016). Autophagy: machinery and regulation. *Microb. Cell* 3, 588–596. doi: 10.15698/mic2016.12.546

Zare-Shahabadi, A., Masliah, E., Johnson, G. V., and Rezaei, N. (2015). Autophagy in Alzheimer's disease. *Rev. Neurosci.* 26, 385–395. doi: 10.1515/revneuro-2014-0076

Zecca, L., Gallorini, M., Schunemann, V., Trautwein, A. X., Gerlach, M., Riederer, P., et al. (2001). Iron, neuromelanin and ferritin content in the substantia nigra of normal subjects at different ages: consequences for iron storage and neurodegenerative processes. *J. Neurochem.* 76, 1766–1773. doi: 10.1046/j.1471-4159.2001.00186.x

Zecca, L., Stroppolo, A., Gatti, A., Tampellini, D., Toscani, M., Gallorini, M., et al. (2004a). The role of iron and copper molecules in the neuronal vulnerability of locus coeruleus and substantia nigra during aging. *Proc. Nat. Acad. Sci.* 101, 9843–9848. doi: 10.1073/pnas.0403495101

Zecca, L., Youdim, M. B., Riederer, P., Connor, J. R., and Crichton, R. R. (2004b). Iron, brain ageing and neurodegenerative disorders. *Nat. Rev. Neurosci.* 5, 863–873. doi: 10.1038/nrn1537

Conflict of Interest Statement: The authors declare that the research was conducted in the absence of any commercial or financial relationships that could be construed as a potential conflict of interest.

frontiers in Cell and Developmental Biology

BRIEF RESEARCH REPORT
published: 02 August 2019
doi: 10.3389/fcell.2019.00145

Monensin Sensitive 1 Regulates Dendritic Arborization in *Drosophila* by Modulating Endocytic Flux

Rohit Krishnan Harish[1†‡], Shweta Tendulkar[1‡], Senthilkumar Deivasigamani[1†], Anuradha Ratnaparkhi[2*] and Girish S. Ratnaparkhi[1*]*

[1] Indian Institutes of Science Education and Research, Pune, India, [2] Agharkar Research Institute, Pune, India

OPEN ACCESS

Edited by:
Sarita Hebbar,
Max Planck Institute of Molecular Cell Biology and Genetics (MPI-CBG), Germany

Reviewed by:
Carsten Duch,
Johannes Gutenberg University Mainz, Germany
Daniel N. Cox,
Georgia State University, United States

***Correspondence:**
Senthilkumar Deivasigamani
senthilkumar.deivasigamani@embl.it
Anuradha Ratnaparkhi
anu.aripune@gmail.com
Girish S. Ratnaparkhi
girish@iiserpune.ac.in;
girish.iiserpune@gmail.com

†Present address:
Rohit Krishnan Harish,
Technische Universität Dresden, Center for Regenerative Therapies, Dresden, Germany
Senthilkumar Deivasigamani,
Neurobiology and Epigenetics Unit, European Molecular Biology Laboratory, Monterotondo, Italy

‡These authors have contributed equally to this work

Specialty section:
This article was submitted to Membrane Traffic, a section of the journal Frontiers in Cell and Developmental Biology

Received: 11 March 2019
Accepted: 16 July 2019
Published: 02 August 2019

Citation:
Harish RK, Tendulkar S, Deivasigamani S, Ratnaparkhi A and Ratnaparkhi GS (2019) Monensin Sensitive 1 Regulates Dendritic Arborization in Drosophila by Modulating Endocytic Flux. Front. Cell Dev. Biol. 7:145. doi: 10.3389/fcell.2019.00145

Monensin Sensitive 1 (Mon1) is a component of the Mon1:Ccz1 complex that mediates Rab5 to Rab7 conversion in eukaryotic cells by serving as a guanine nucleotide exchange factor for Rab7 during vesicular trafficking. We find that Mon1 activity modulates the complexity of Class IV dendritic arborization (da) neurons during larval development. Loss of Mon1 function leads to an increase in arborization and complexity, while increased expression, leads to reduced arborization. The ability of Mon1 to influence dendritic development is possibly a function of its interactions with Rab family GTPases that are central players in vesicular trafficking. Earlier, these GTPases, specifically Rab1, Rab5, Rab10, and Rab11 have been shown to regulate dendritic arborization. We have conducted genetic epistasis experiments, by modulating the activity of Rab5, Rab7, and Rab11 in da neurons, in *Mon1* mutants, and demonstrate that the ability of Mon1 to regulate arborization is possibly due to its effect on the recycling pathway. Dendritic branching is critical for proper connectivity and physiological function of the neuron. An understanding of regulatory elements, such as Mon1, as demonstrated in our study, is essential to understand neuronal function.

Keywords: flux, endocytic recycling, Rab conversion, epistasis, Class IV neuron

INTRODUCTION

Dendritic arbors are complex neuronal structures with distinct morphological features (Cajal, 1999; Garcia-Lopez et al., 2010; Berry and Nedivi, 2017). During neuronal development, morphogenetic processes that are not yet completely understood, lead to formation of arbors with defined size, geometry, innervation, and tiling patterns. The dendritic tree structure is unique to a given neuronal cell type and plays a fundamental role in establishing specific neuronal connectivity. An intrinsic genetic program patterns the arbors using molecular processes that are distinct from those that make axons. These are found to be dependent on both, internal as well as external cues (Parrish et al., 2007; Jan and Jan, 2010). The growth and development of dendritic arbors are also concurrent in time and space with synapse formation with proteins of the post-synaptic density playing an integral role in morphogenesis (Cantallops et al., 2000; Cline, 2001; Peng et al., 2009).

The embryonic and larval peripheral nervous system (PNS) in *Drosophila melanogaster* has served as an excellent model system for studying mechanisms that govern dendritic arbor complexity and tiling. The PNS consists of 45 sensory neurons per hemisegment which are classified into type I and type II neurons (Grueber et al., 2003; Orgogozo and Grueber, 2005). The type II neurons are multidendritic whose dendrites innervate the epidermis. Dendritic arborization (da) neurons are a type of multidendritic neurons which are further classified into class I to IV on the

basis of their dendrite field complexity with class IV da neurons having the most complexity in terms of the number of dendrites and their branching (Grueber et al., 2002). The arbor complexity in da neurons is determined through a combinatorial expression of transcription factors indicating the process is hard-wired and intrinsic to the neuronal class (Jinushi-Nakao et al., 2007).

As in other organisms (Dong et al., 2015; Prigge and Kay, 2018) the process of morphogenesis is regulated by signaling mediated by external cues such as Slit and Semaphorins (Jan and Jan, 2010; Meltzer et al., 2016), kinases such as Tricornered (Emoto et al., 2004) and a range of cellular processes that include intracellular trafficking, translational control and cytoskeletal dynamics (Ye et al., 2004; Satoh et al., 2008; Delandre et al., 2016).

Rab proteins are key regulators of intracellular trafficking. Both endocytic and exocytic pathways are believed to contribute to dendrite growth and branching (Jan and Jan, 2010; Dong et al., 2015; Valnegri et al., 2015). Constituents implicated include Rab5 (Satoh et al., 2008; Mochizuki et al., 2011; Copf, 2014; Zhang et al., 2014; Kanamori et al., 2015; Wang et al., 2017), Rab10 (Zou et al., 2016), Shrub (Sweeney et al., 2006), and Rop (Peng et al., 2015).

In this study we demonstrate that *Drosophila* Monensin Sensitivity 1 (DMon1; Yousefian et al., 2013; Deivasigamani et al., 2015; Dhiman et al., 2019), a core component of the Mon1:CCZ1 complex (Wang et al., 2002; Nordmann et al., 2010; Poteryaev et al., 2010), and central to conversion of early endosomes to late endosomes, regulates morphogenesis of Class IV da (CIVda) neurons. We uncover a role for Mon1 by demonstrating that CIVda patterning can be regulated by increasing or decreasing Mon1 function during embryonic/larval development: loss of Mon1 leads to increased branching while overexpression suppresses it. Consistent with its position in the endocytic pathway, we find that Mon1 functions genetically downstream of Rab5. Surprisingly however, the regulation by Mon1 does not seem to be dependent on the late endosomal-lysosomal pathway. Rather, the modulation appears to be via the Rab11 mediated recycling pathway. We propose that in the context of the da neurons, Mon1 serves to balance the endocytic flux flowing through the endo-lysosmal and recycling pathways to regulate dendrite morphogenesis.

RESULTS

Mon 1 Modulates Dendritic Branching in Class IV da Neurons

CIVda neurons express *pickpocket* (*ppk*), a gene involved in nociception in *Drosophila* (Adams et al., 1998; Crozatier and Vincent, 2008). We recombined *ppk-Gal4* (BL32079; Grueber et al., 2007; Kanamori et al., 2013) with a membrane localized GFP expressed under a *ppk* regulatory element (*ppk-GFP* (BL35843) (Kanamori et al., 2013), and generated a reporter line ('R,' see section "Materials and Methods") that allows visualization of CIVda neuron morphology in response to genetic manipulation either through gene knock-down and overexpression in the third instar larva of *Drosophila* (**Figure 1A**). This reporter ('R') line was used to observe the arborization of CIVda in the $Dmon1^{\Delta 181}$ (Δ181) line, a loss of function allele of *Mon1* (Deivasigamani et al., 2015). When compared to a wild-type control, CIVda in *Dmon1* mutant showed enhanced dendritic branching with a ramification index (R.I), of approximately 80 as compared to 60 in wild-type larvae. On normalization, with the reporter line set to 100, *Dmon1* mutant shows 45% increase in R.I (**Figures 1B,G**). This increase in R.I was however not observed in a heterozygous condition (**Figures 1C,G**), suggesting that a single copy of *Dmon1* is sufficient to regulate dendritic arborization in the CIVda neurons. In order to confirm the result, we quantified R.I in $Dmon1^{\Delta 181}/Df(9062)$, an allelic combination, where Df(9062) is a deficiency that uncovers the *Mon1* locus (Deivasigamani et al., 2015). An increase in RI by 47% (**Figure 1G**) similar to that in $Dmon1^{\Delta 181}$ homozygote confirmed that it is the loss of *Dmon1* that leads increased R.I of CIVda neurons. Other parameters (see section "Materials and Methods"), such as dendritic area (D.A; μM^2), dendritic length (D.L; μM) and number of dendritic branch points (D.BP) were also measured for the same set of images. Loss of *Dmon1* also led to an increase in average values, as compared to controls for D.A (51843 vs. 65787 μM^2), D.L (14549 vs. 17811 μM) and D.BP (492 vs. 829). Normalized values, with the control R/+ set to 100 are displayed in the figures (**Figures 1H–J**).

Further confirmation for the role for Mon1 in regulating CIVda branching was demonstrated by rescue of the dendritic phenotypes in homozygous $Dmon1^{\Delta 181}$ (**Figure 1E**) and $Dmon1^{\Delta 181}$/ Df(9062) animals through expression of DMon1 in the *ppk* domain (**Figure 1G**). In both examples, the R.I, D.A, D.L, and D.BP were restored to wild-type or near wild-type levels (**Figure 1**).

In addition, overexpression of Mon1 in wild-type animals using *ppk-GAL4* led to reduction of all four parameters measured (**Figure 1**). R.I, D.L, and D.BP were reduced significantly, while the reduction of D.A had lower statistical significance ('*'; **Figure 1H**). Together, these results demonstrate that arborization of the CIVda neurons during development is sensitive to the dose of Mon1 with decrease in Mon1 function leading to increased branching, dendritic length and area while enhancement of Mon1 function leads to a decrease in the measured parameters.

Rabs Modulate Dendritic Arborization

Mon1/SAND1 regulates Rab conversion in yeast, *C. elegans* and mammalian cells (Nordmann et al., 2010; Poteryaev et al., 2010; Yousefian et al., 2013). Mon1 in complex with Ccz1 functions as a guanine nucleotide exchange factor for Ypt7, the yeast ortholog of Rab7 (Nordmann et al., 2010). As in other model systems, in *Drosophila*, the recruitment of Rab7 on late endosomes is mediated by the Mon1-Ccz1 complex (Yousefian et al., 2013). In the study by Yousefian et al. (2013), Mon1 loss of function leads to enlargement/enrichment of Rab5 positive early endosomes and concomitant loss of association of mature endosomes with Rab7, a feature that is replicated in CIVda neurons (**Supplementary Figure S1**). Rab4 and Rab5 co-localized on early endosomes while Rab11 distributions between mutant and wild-type cells were

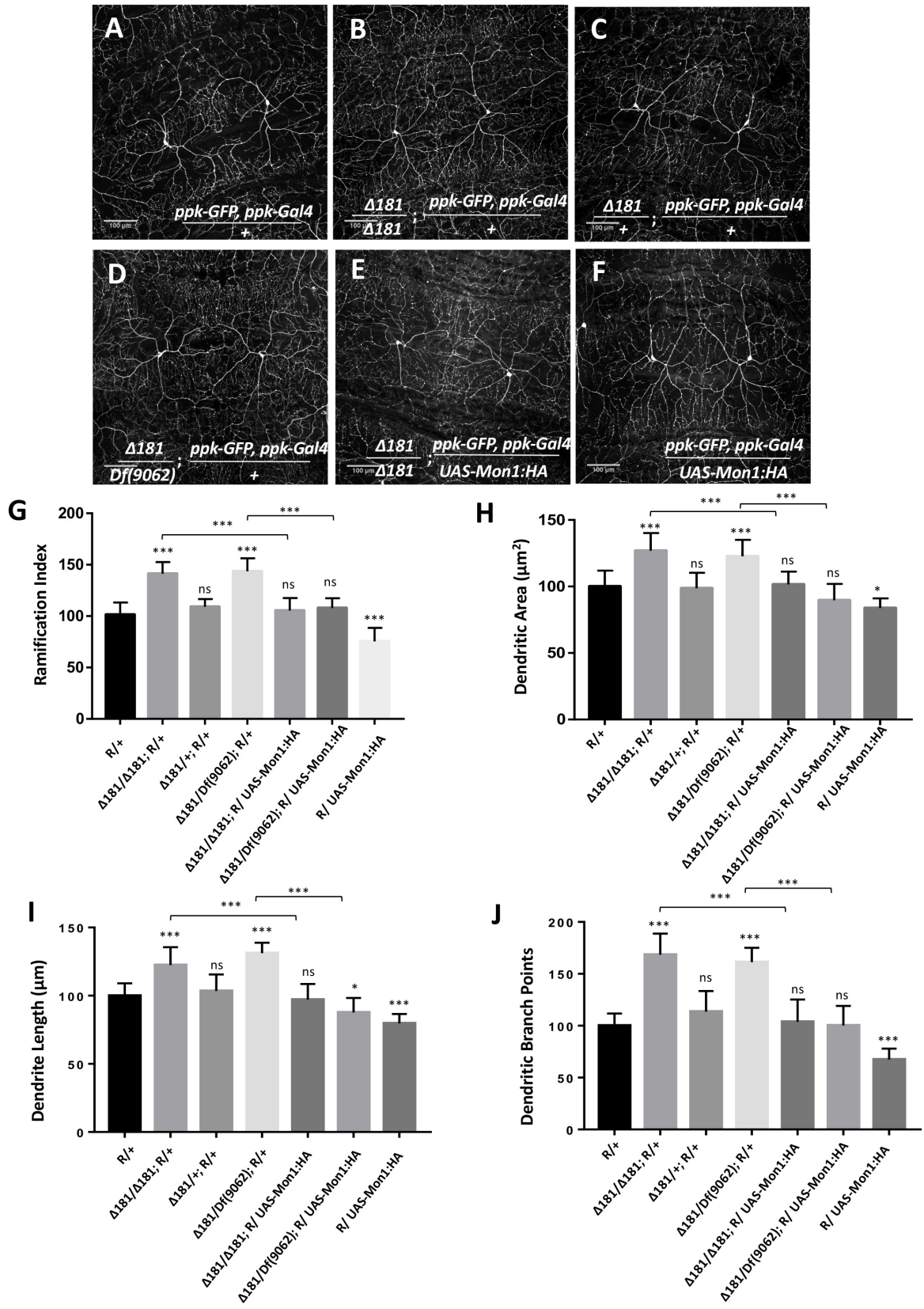

FIGURE 1 | Continued

FIGURE 1 | *Dmon1* modulates dendritic arborization in Class IV da -neurons. **(A)** A reporter (*ppk-Gal4; ppk-GFP*, diminutive 'R') line is used to visualize arborization in CIVda neurons at the third instar larval stage in *Drosophila melanogaster*. Sholl analysis (Image J) is used to calculate Ramification Index (R.I), which is then normalized, setting the 'R/+' at 100. The IMARIS software is used for neuron tracing and calculation of Dentritic area (D.A), Dendrite length (D.L) and Dendritic branch points (D.BP), with each parameter for the R/+ set at 100. n = 15 (neurons), N = 4 animals. Representative images are shown for this and other images **(B–F)**. **(B)** $Dmon1^{\Delta 181}/Dmon1^{\Delta 181}$ larvae show enhanced arborization for Class IV arbors. n = 15, N = 4. **(C)** A Single copy of *Dmon1* ($Dmon1^{\Delta 181}$/+) does not show any significant increase in arborization. n = 14 neurons, N = 4. **(D)** $Dmon1^{\Delta 181}/Df(9062)$ increases arborization to the same extent as $Dmon1^{\Delta 181}/Dmon1^{\Delta 181}$. n = 15, N = 4. **(E)** *UAS-Mon1:HA* driven by *ppk-Gal4* in $Dmon1^{\Delta 181}$ larvae, rescues the arborization defect in $Dmon1^{\Delta 181}/Dmon1^{\Delta 181}$ and $Dmon1^{\Delta 181}/Df(9062)$ (Image not displayed) to near normal levels. n = 18, N = 5 and n = 9, N = 4 respectively. **(F)** Overexpression of *Dmon1* in a wild-type background, reduces the branching (D.BP), R.I and D.L significantly. The reduction in D.A is less significant. n = 35, N = 8. **(G–J)** Quantitation of the extent of arborization in CIVDa using four parameters, R.I, D.A, D.L, and D.BP. Statistical analysis using Dunnet's multiple comparison test using GraphPad Prism 7 with exact p-values listed in **Supplementary Table S1**. ns, not significant. *$p < 0.05$ and ***$p < 0.001$. Error bars represent standard error.

indistinguishable (Yousefian et al., 2013), a feature seen here in CIVda neurons (**Supplementary Figure S1**).

Given the role of Mon1 in endocytic trafficking, we sought to explore the role of Rab proteins in Mon1 mediated CIVda morphogenesis (**Figure 2** and **Supplementary Figures S2A,B**). An earlier study in *Drosophila* has implicated Rab5 and the distribution of Rab5 endosomes in the patterning of da neurons (Satoh et al., 2008), while Rab11 mediated recycling has been shown to be important in dendritic branching in rat hippocampal neurons (Satoh et al., 2008; Lazo et al., 2013). In *Drosophila*, the roles of Rab11 mediated recycling pathway or the Rab7 mediated degradative pathway in dendrite morphology has not been tested. We therefore sought to test this in the context of Mon1 mutants through genetic epistasis, by using loss-of-function and gain-of-function transgenic lines against *Drosophila* Rab5, Rab7, and Rab11 genes. In agreement with earlier studies (Satoh et al., 2008), expression of Rab5 dominant negative (Rab5DN; Rab5 in a GDP-bound form) or knockdown using RNA interference, using *ppk-Gal4*, show a drastic reduction in the extent of arborization and branching (**Figures 2B,D,J,K** and **Supplementary Figures S2A,B**), with hypomorphic RNAi alleles demonstrating weaker effects. Our analysis indicated a 60–70% decrease in R.I, D.A, D.L, and D.BP for the Rab5DN allele. In contrast, the constitutively active (CA) form of Rab5 (RAB5CA, GTP-bound form) did not show any significant differences in R.I, D.A, and D.L (**Figures 2C,J,K** and **Supplementary Figure S2B**), while the D.BP were decreased by 20% (**Supplementary Figure S2A**) in CIVda as compared to the control (**Figures 2A,J,K** and **Supplementary Figures S2A,B**).

Cargo present in Rab5 positive early endosome cycle can be channeled down the degradation pathway involving Rab7 or the recycling pathway, marked by Rab11. We tested the involvement of these pathways by modulating the activity of Rab7 and Rab11. We found that increasing Rab7 activity through expression of a CA form, or decreasing Rab7 function by using a dominant negative (DN) form of Rab7 or through expression of Rab7 RNAi the *ppk* domain (**Figures 2E,F,G,J,K** and **Supplementary Figures S2A,B**) does not affect the arborization, branching, length or area of CIVda neurons. In contrast, expression of both, Rab11CA and Rab11DN altered arborization patterns in an opposing manner: increase in Rab11 activity increased R.I, D.A, D.L and D.BP, while a decrease in Rab11 activity reduced these parameters (**Figures 2H–K** and **Supplementary Figures S2A,B**). Interestingly, the increase in parameters (15–40%) seen upon expression of Rab11CA (**Figures 2H–K**) were correlated to and comparable with increase seen in Mon1 mutants, with the exception of D.BP, where Rab11CA has a weaker effect, suggesting that the Rab11 mediated recycling pathway plays a central role in CIVda patterning.

Mon1 Interacts With Rabs to Modulate da

Since the activity of Rab5 and Rab11 strongly modulates arborization of CIVda neurons, we explored the nature of the interaction between these Rabs 5, 7, and 11 and Mon1 to uncover features of vesicular recycling that are important for CIVda morphogenesis (**Figure 3** and **Supplementary Figures S2C–H**). We tested this by modulating activity of Rab5, Rab7, and Rab11 in the *Dmon1* loss-of-function line ($Dmon1^{\Delta 181}$ or $\Delta 181$), in combination with the reporter line (R) generated earlier (**Figure 1A** and see section "Materials and Methods"). Expression of Rab5CA in the $Dmon1^{\Delta 181}$ larvae showed a partial rescue (**Figures 3C,G,J** and **Supplementary Figures S2C,F**) of the increase in R.I, D.A, D.L and D.BP, seen in the mutants, while expression of Rab5DN in the $Dmon1^{\Delta 181}$ larvae led to a quantitative parameters (D.A., D.L, and D.BP) that were comparable to that of Rab5DN alone (**Figures 3D,G,J** and **Supplementary Figures S2C,F**).

Although Rab7 on its own does not seem to participate in the regulation of da (**Figures 2F,G,J,K**), we found that expression of Rab7CA leads to a significant reduction of R.I, D.A., D.L and D.BP, as compared to control $Dmon1^{\Delta 181}$ larvae (**Figures 3H–K** and **Supplementary Figures S2D,G**; Images not displayed) suggesting that activation of the downstream endo-lysosomal pathway can suppress excess arborization in the mutant. This may be an outcome of a flux change due to modulation of the lysosomal branch. Interestingly, Rab7 RNAi also suppresses Mon1 loss of function phenotype (**Figures 3H,K** and **Supplementary Figures S2D,G**; Images not displayed), again suggesting change in flux of recycling vesicular trafficking in response to modulation of the lysosomal pathway. Expression of Rab11CA in $Dmon1^{\Delta 181}$ larvae (weakly) rescues all measured parameters (R.I, D.A, D.L) except D.BP. Expression of Rab11DN, with or without $Dmon1^{\Delta 181}$ in the background leads to lower values (decrease of 60–70%) of R.I, D.A., D.L, and D.BP. This lends support to the view that the Rab11 mediated re-cycling pathway functions downstream of Mon1 and may play an important role in manifestation of the arborization defect in $Dmon1^{\Delta 181}$ mutants.

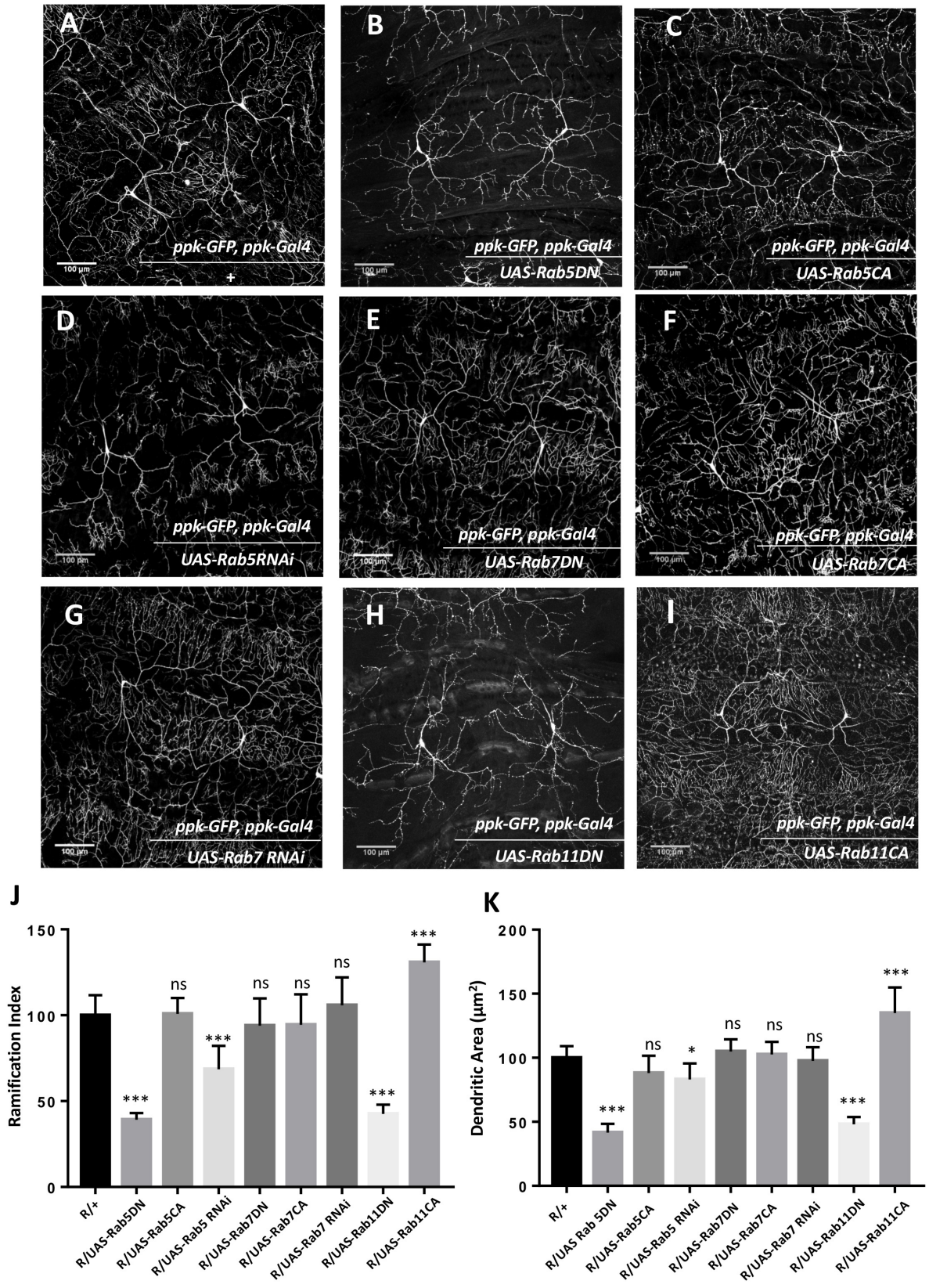

FIGURE 2 | Continued

FIGURE 2 | Rabs modulate dendritic arborization. **(A)** CIVda larvae imaged with the 'wild-type' reporter line (R/+: *ppk-GFP, ppk-Gal4*). Representative images are shown **(B–I)** for all experiments. **(B–D)** Rab5DN mutant expression or Rab5 knockdown using RNAi, reduces arborization (for Rab5 DN: $n = 23$, $N = 4$; for Rab5 RNAi: $n = 40$, $N = 7$) in Class IV neurons but Rab5CA mutant expression does not show any change ($n = 18$, $N = 4$), when compared to control R/+($n = 55$, $N = 5$). **(E–G)** Rab7DN mutant expression, Rab7 knockdown using RNAi and Rab7CA mutant expression using *ppk-Gal4*, do not show any difference in arborization as compared to wild-type control (for Rab7DN: $n = 35$, $N = 6$; for Rab7 RNAi: $n = 43$, $N = 7$; for Rab7CA: $n = 16$, $N = 4$). **(H,I)** Rab11DN reduces arborization ($n = 18$, $N = 4$) when expressed in Class IV da neurons whereas Rab11CA mutant expression increases dendritic arbor complexity ($n = 8$, $N = 3$). **(J,K)** Quantitation of the extent of arborization in CIVDa using R.I and D.A. Values for D.L and D.BP are displayed in **Supplementary Figure S2**. ns, not significant. $^{*}p < 0.05$ and $^{***}p < 0.001$. Error bars represent standard error. Statistical analysis using Dunnet's multiple comparison test using GraphPad Prism 7 with exact *p*-values listed in **Supplementary Table S1**.

DISCUSSION

Mon1 is a conserved eukaryotic protein with a 'longin' domain. The domain has an alpha-beta-alpha sandwich architecture and is a feature of endocytic trafficking proteins (De Franceschi et al., 2014). Protein containing 'longin' domains include SANDs, SNAREs, targetins, adaptins, and sedlins (De Franceschi et al., 2014). The dimeric Mon1:CCZ complex is involved in Rab conversion and is a GEF for Rab7 (**Figure 4A**). Additionally, there is evidence that Mon1 can be secreted by neurons, either in membrane bound or unbound form (Deivasigamani et al., 2015). Mon1 may thus regulate anterograde signaling in synapses, both neuron:neuron or neuron:muscle. Recent research from our laboratory (Dhiman et al., 2019) also suggests that Mon1 in Octopaminergic neurons regulates systemic insulin signaling by regulating insulin producing cells.

CIVda neurons are sensitive to the dose of DMon1 in the cell (**Figure 4B**). Decrease in *Dmon1* leads to increased complexity of arborization, which includes increase in branching, length and area covered by the axons. Increase in *Dmon1* decreases complexity of arborization and reduces the values of the parameters measured. Since Mon1 is primarily known for its role as a Rab converter in eukaryotic cells, we explored functions of Rab proteins Rab5, Rab7, and Rab11 in regulating da by themselves and also in the context of *Dmon1* loss of function. Amongst the Rabs tested, Rab7 activity did not appear to affect dendritic morphology, suggesting that perturbation of late endosomal trafficking does not affect morphogenesis of CIVda neurons in larvae. This premise however can be strengthened by using Mosaic analysis with a repressible cell marker, studies. In contrast, Rab11 activity altered arbor complexity with decrease in Rab11 activity leading to a dramatic decrease in arborization and expression of Rab11CA having an opposite effect (**Figure 3**). This suggests that recycling endosomes play critical roles in determining arbor complexity which is in agreement with the role of Rab11 in dendrite morphogenesis in vertebrate systems (Villarroel-Campos et al., 2014; Peng et al., 2015; Gu et al., 2016). Since reduction of Rab5 activity also decreases arbor complexity, and Rab5 'sorting' endosomes are upstream (**Figure 4A**) of both recycling endosomes (RE) and late endosomes (LE), we propose that vesicular flux through the RE but not the LE is a central determinant of CIVda morphogenesis (**Figure 4C**). Loss of Rab5 leads to a decrease in the rate of RE formation, while loss of DMon1 changes the endocytic flux, shunting excess early endosomes (EE's) toward the RE pathway. In our model (**Figure 4C**), increase in activity of Mon1 enhances Rab5 to Rab7 conversion, reducing RE traffic leading to decreased arborization.

How does increase in RE flux lead to increase in dendritic complexity? Since endosomes marked with Rab11 can be exocytosed, we suggest that enhanced vesicular flux in the RE pathway leads to enhanced exocytosis, which in turn is correlated to increase dendritic arborization. This is in agreement with earlier studies where trafficking of cargo in Rab11 vesicles regulated dendritic complexity. For example, Lazo et al. (2013) demonstrate that Rab11 regulates trafficking of brain derived neurotrophic factor along with its receptor TrkB while Peng et al. (2015) have shown that the Rop-exocyst complex is important for dendritic branching in CIVda neurons. In contrast, data from the Klein lab (Yousefian et al., 2013), with experiments performed in the wing imaginal disk, suggest that Rab11 is not affected in the $Dmon1^{mut4}$ lines, and instead find changes in the Rab4 associated fast recycling pathway. In addition to protein and RNA based cargo, exocytosis also provides neuronal membrane that is critical for growth of the arbor, underscoring the importance of RE flux and exocytosis.

The balance of endocytosis and exocytosis is crucial for the growth and maintenance of CIVda arbors. Mon1 activity in the early 'sorting' endosomes may be important for modulating the flux through either the LE or RE pathways which in turn could lead to modulation of neuronal architecture. Our results thus underscore the role of endocytic flux in dendrite morphogenesis. The genetic interactions described here suggest a cell-autonomous role for Mon1. Given the ability of Mon1 to be secreted, it would be interesting, in future studies, to test for possible non-autonomous roles in dendrite development.

MATERIALS AND METHODS

Fly Husbandry

Fly lines were maintained at 25°C on standard cornmeal agar medium. UAS-GAL4 system (Brand and Perrimon, 1993) was used for over-expression of transgenes.

Transgenic Lines

$Dmon1^{\Delta 181}$ was generated earlier through excision of *pUAST-Rab21:: YFP* insertion (Deivasigamani et al., 2015). Lines procured through the Bloomington *Drosophila* Stock Centre include Df(2L)9062, 35843 (*ppk-GFP*), 32079 (*ppk-Gal4*), 9772 (*UAS-Rab5-DN*), 9773 (*Rab5CA*), 34832 (*Rab5 RNAi*), 9779 (*UAS-YFP:Rab7CA*), 9778 (*UAS-Rab7DN*), 27051 (*UAS-Rab7 RNAi*), 9792 (*UAS-Rab11DN*), 9791 (*UAS-Rab11CA*). *UAS-Mon1:HA/TM6Tb* is a kind gift from Prof. Thomas Klein.

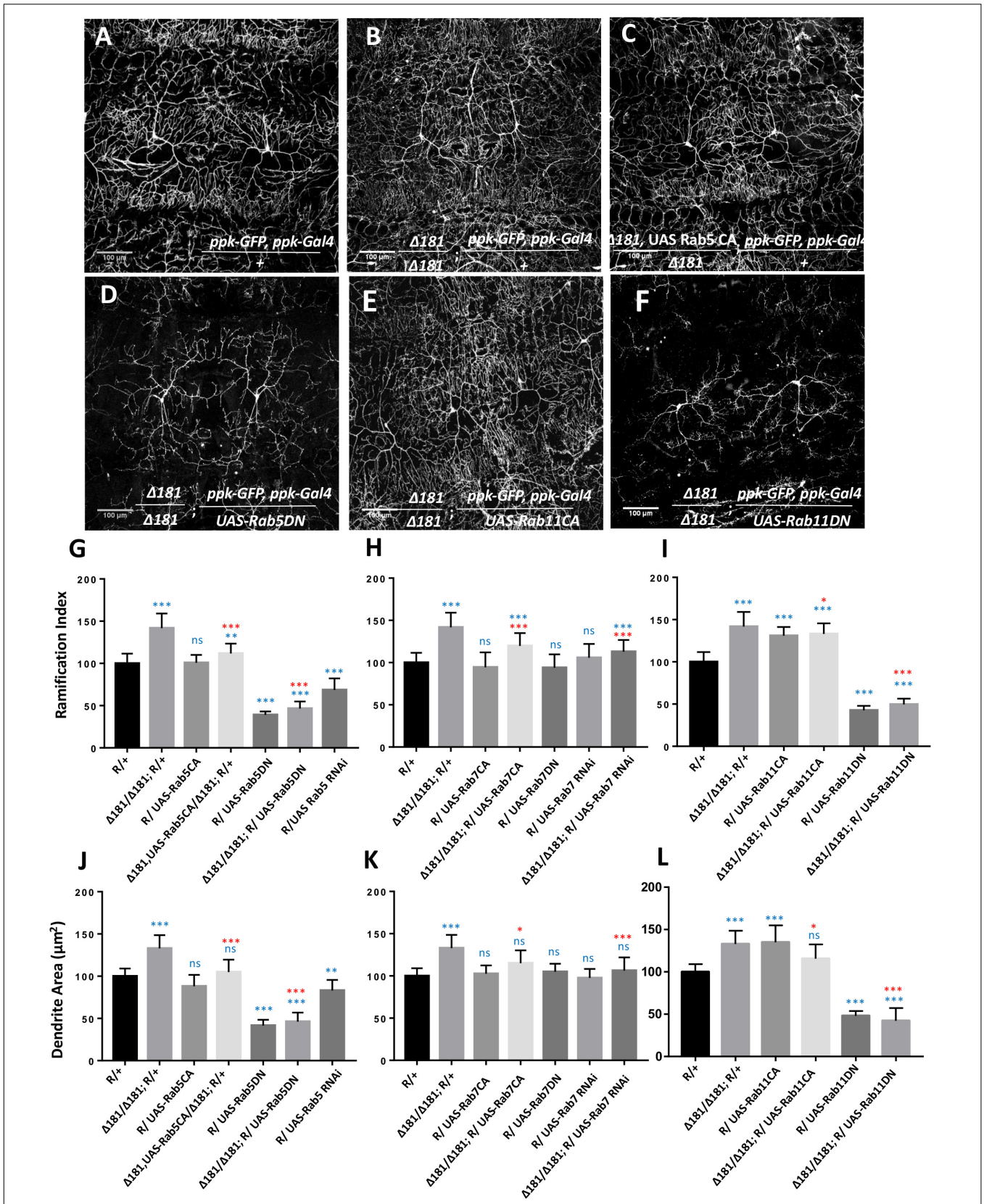

FIGURE 3 | Continued

FIGURE 3 | Mon1 interacts with Rabs to modulate dendritic arborization. **(A,B)** ClVda larvae imaged with the reporter line R/+ (n = 55, N = 7) and the $Dmon1^{\Delta 181}/Dmon1^{\Delta 181}$; R/+ ($n$ = 38, N = 7). Representative images are shown **(B–F)** for all experiments. For **(G–L)**, blue asterisk/n.s represents statistical comparison with wild-type (R/+) while red asterisk/n.s is a comparison with $Dmon1^{\Delta 181}$. **(C,D)** Rab5CA expression in $Dmon1^{\Delta 181}$ larvae shows significant reduction in parameters measured (R.I, D.A, D.L, D.BP) as compared to $Dmon1^{\Delta 181}$ (n = 30, N = 7). Rab5DN in $Dmon1^{\Delta 181}$ larvae shows reduction in arborization as compared to both $Dmon1^{\Delta 181}$ (n = 26, N = 5) and wild-type larvae (n = 26, N = 5). Rab7CA expression in $Dmon1^{\Delta 181}$ larvae shows reduction in arborization as compared to $Dmon1^{\Delta 181}$ (n = 20, N = 4) and increase with respect to the wild-type (n = 20, N = 4). Rab7 RNAi in $Dmon1^{\Delta 181}$ larave shows reduction in arborization as compared to $Dmon1^{\Delta 181}$ (n = 43, N = 7) and increase with respect to the wild-type (n = 43, N = 7). Images for these experiments are not shown but data is quantified in **(H,K)**. **(E,F)** Rab11CA in $Dmon1^{\Delta 181}$ background shows reduction in arborization as compared to $Dmon1^{\Delta 181}$ larvae (n = 36, N = 6) and increase with respect to the wild-type larvae (n = 36, N = 6). Rab11 DN in $Dmon1^{\Delta 181}$ larvae shows reduction in arborization as compared to $Dmon1^{\Delta 181}$ (n = 19, N = 4) and decrease with respect to the control larvae (n = 19, N = 4). **(G,L)** Quantitation of the extent of arborization in ClVDa using R.I and D.A. Values for D.L and D.BP are displayed in **Supplementary Figure S2**. ns, not significant. *$p < 0.05$, **$p < 0.01$, and ***$p < 0.001$. Error bars represent standard error. Statistical analysis using Dunnet's multiple comparison test using GraphPad Prism 7 with exact p-values listed in **Supplementary Table S1**.

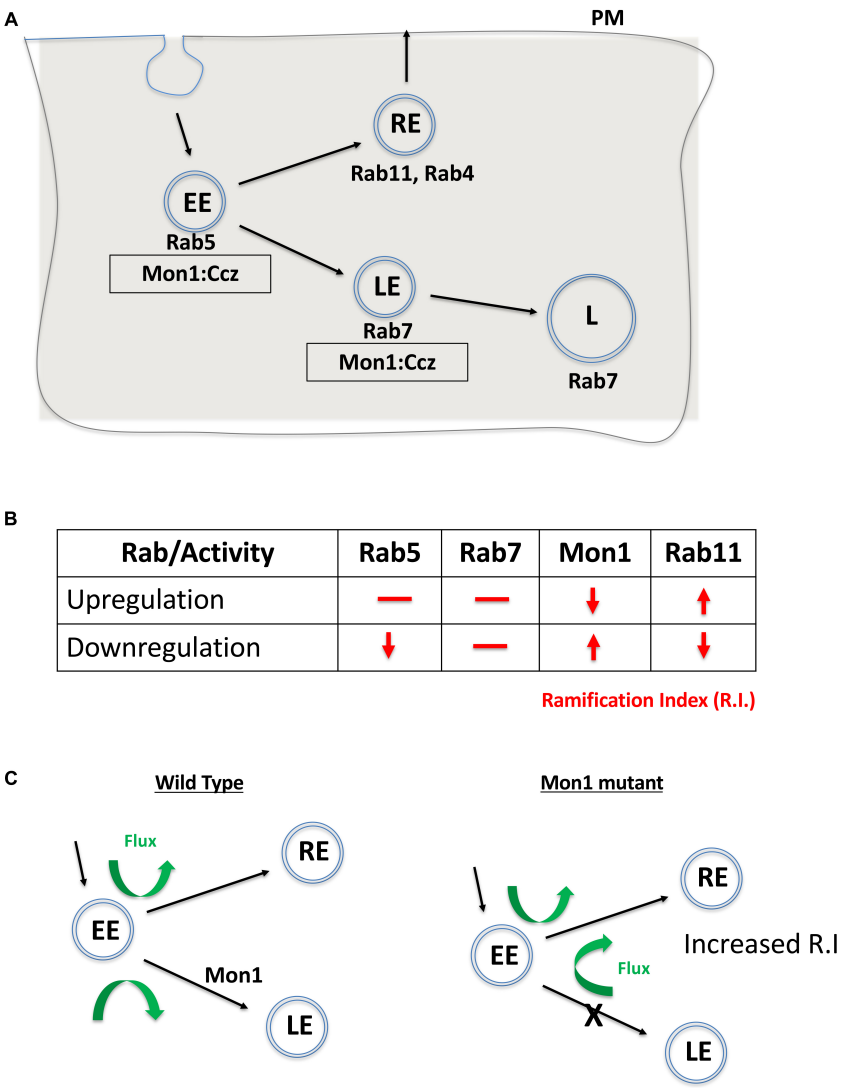

FIGURE 4 | Mon1 levels may regulate vesicular flux through the recycling pathway. **(A)** Schematic shows the endocytic pathway branching at the early endosome, with vesicles entering either the degradative or recycling pathways. Rab5 marks early endosomes (EE), Rab7 marks late endosomes (LE) while Rab11 marks the recycling endosome (RE). The Mon1:Ccz complex acts as a GEF for conversion of EE to LE. **(B)** Effect of upregulation or downregulation of Rab or Mon1 activity on complexity of dendritic arborisation, as measured by change in R.I (red lines/arrows). R.I decreases with decrease in Rab5 and Rab11 activity as also with increase of Mon1 function. In contrast, R.I increases with decrease in Mon1 function and increase in Rab11 activity. Similar trends are seen in D.A, D.L, and D.BP. **(C)** A hypothetical model, that agrees with our data, is the requirement of endocytic recycling for increase in dendritic arborization. Thus, increase in RE endosomal flux may influence branching. This can be done directly by increasing RE by overexpressing Rab11, or indirectly by increasing the endocytic flux to the RE pathway, either by decreasing Mon1 function or by decreasing Rab5 activity. The proposed model relies on a minimal role for Rab7 in regulating R.I. Green arrows depict the increase in flux of vesicular trafficking in the RE pathway when Mon1 function is reduced.

Immunohistochemistry and Imaging

Wandering third instar larvae were collected, fileted in 1X PBS, dissected and fixed in Bouins solution (HT10132, Sigma) for 7 min. The tissues were then blocked in 1X PBS +0.3%Triton (194854, MP Biomedicals) and 2% BSA stained overnight in anti-GFP (Chk, A10262, Invitrogen, 1:500 and Rb, A6455, 1:1000) incubated in 4°C overnight. This was followed by washes with 1X PBS +0.3%Triton and 2% Triton-X and incubated in secondary antibody at room temperature for 1.5 h. The final step involved washes and mounting of tissues in 70% glycerol with n-propyl gallate. Confocal imaging was carried out using a Zeiss LSM 710 microscope at 20X magnification. For Rab staining, dilutions used were as follows. Anti Rab5 (1:500), Rab7(1:500), Rab11(1:500) (Tanaka and Nakamura, 2008). Fixative used for staining with Rab antibodies was 4% PFA. Secondaries used were, Rab5 (1:1000 Guinea Pig Alexa fluor 568, Invitrogen A11075), Rab7 and Rab11 (1:1000 Rabbit Alexa Fluor 647, Invitrogen A21244), Chicken Alexa Fluor 488 from Invitrogen (A11039) and Rabbit Alexa Fluor 488 from Invitrogen (A11034). Rab antibodies were a kind gift by Prof. Akira Nakamura (RIKEN Center for Developmental Biology, Kobe, Japan). For Rabs, confocal imaging was carried out using a Zeiss LSM 710 microscope at 63X magnification.

Sholl Analysis

Sholl analysis, to measure the ramification index (R.I), was performed using the NIH ImageJ Sholl Analysis Plugin (v1.0)[1], as distributed by Fiji. Briefly, the maximum intensity projection for z stacks of each neuron was converted to a segmented grayscale image using ImageJ. Background dendrites extending into the image view from neighboring neurons were manually deleted. Sholl analysis was performed by drawing a straight line from the cell body to the distal tip of the neuron. The area for the analysis was hence defined by this straight line which is considered as the radii for each image. The origin of the concentric radii was set at the midpoint of the longest axis of the soma. Analysis was performed in automated way using the following parameters: starting radius, 1 μm; radius step size, 2 μm; span, 1 μm; span type, median. The number of dendrite intersections for each circle is measured and the highest value is divided by the number of primary dendrites (intersections at the starting radius) to obtain the Schoen ramification index (R.I). This parameter is dependent on maximum number of intersections and the number of primary dendrites. Statistics were performed using the Prism statistical package (GraphPad, San Diego, CA, United States).

Neuromorphometric Analysis of da Neurons

The Filament dendrite tracer plug-in of the IMARIS 7 software was used to trace the dendrites in 3D and generate quantitative data for each genotype. The analysis was performed on dendritic arbor's arising from a single neuron and the branches from neighboring neurons were deleted manually. The cell body was defined as the origin by adjusting the threshold for the largest diameter. The 'Dendritic Area (D.A)' measured in μm^2 refers to the total area occupied by the traced filament. The 'Dendritic length (D.L)' measured in μm refers to the sum of all filaments traced within an arbor. The total number of 'Dendritic Branch points (D.BP)' in each arbor have also been measured for each genotype. The numbers for D.BP are the sum of all branch points in the image (primary, secondary, and tertiary).

[1] https://imagej.net/Sholl_Analysis

DATA AVAILABILITY

All datasets generated for this study are included in the manuscript and/or the **Supplementary Files**.

ETHICS STATEMENT

This study was carried out in accordance with the recommendations of the IISER Institutional Biosafety Committee (IBSC). The IBSC is a statutory committee established by the Department of Biotechnology, Government of India and has approved the protocols used in our study.

AUTHOR CONTRIBUTIONS

SD, RKH, AR, and GR conceived the project and designed the experiments. RKH, ST, and SD performed all the experiments. RKH, SD, AR, ST, and GR analyzed the data and wrote the manuscript.

FUNDING

This work was funded by a research grant from the Department of Biotechnology, Government of India (BT/PR23318/BRB/10/1597/2017) and intramural grants to AR and GR from ARI and IISER Pune respectively. ST and SD were graduate students supported by senior research fellowships from IISER Pune and CSIR, Govt. of India respectively.

ACKNOWLEDGMENTS

We thank Bloomington *Drosophila* Stock Center (BDSC), Indiana, supported by NIH grant P40OD018537, for fly stocks. We thank IISER Microscopy/Confocal Facility for access and training. We thank Prof. Akira Nakamura, Laboratory for Germline Development, RIKEN Center for Developmental Biology, Japan for his generous gift of anti Rab antibodies.

SUPPLEMENTARY MATERIAL

The Supplementary Material for this article can be found online at: https://www.frontiersin.org/articles/10.3389/fcell.2019.00145/full#supplementary-material

FIGURE S1 | Antibody staining of cell body of ClVDa neurons with antibodies against GFP, Rab5, Rab7, and Rab11. **(A)** Control larvae with the reporter (R: ppk-GFP, ppk-Gal4) show localization of Rab5 and Rab7 as distinct punctate. **(B)** $Dmon1^{\Delta 181}/Dmon1^{\Delta 181}$ displays enhanced accumulation of Rab5 as compared to the control, while the Rab7 does not show localization in endosomes. **(C)** Control larvae with the reporter (R: ppk-GFP, ppk-Gal4) show localization of Rab5 and Rab 11 as distinct punctate. **(D)** $Dmon1^{\Delta 181}/Dmon1^{\Delta 181}$ mutant shows enhanced accumulation of Rab5, as compared to control, with increase in punctae. Rab11 punctae do not appear to change significantly.

FIGURE S2 | Quantitative parameters (D.BP, D.L, and D.A) for experiments displayed in main **Figures 1–3**. For all panels, blue asterisk/ns represents statistical comparison with wild-type (R/+) while red asterisk/ns is a comparison with $Dmon1^{\Delta 181}$. **(A)** Graph represents normalized values that appear to follow similar trend as that of the R.I (**Figure 2**). Statistical values for the genotypes when expressed in the ppk-Gal4 domain in wild-type animals: Rab5CA expression ($N = 4$, $p = 0.0073$), Rab5DN expression ($N = 4$, $p = 0.0001$), Rab5 knockdown using RNAi ($N = 4$, $p = 0.0002$), Rab7CA expression ($N = 4$, $p = 0.9999$), Rab7DN expression ($N = 4$, $p = 0.9997$), Rab7 knockdown using RNAi ($N = 4$, $p = 0.9999$), Rab11CA expression ($N = 4$, $p = 0.0329$), Rab11DN expression ($N = 4$, $p = 0.0001$). n(number of neurons) analyzed for each genotype is 10. **(B)** Quantitation of (total) dendritic length (D.L). Statistical Values for the genotypes when expressed using ppk-Gal4 in wild-type background are as follows: Rab5CA expression ($N = 4$, $p = 0.3142$), Rab5DN expression ($N = 4$, $p = 0.0001$), Rab5 knockdown using RNAi ($N = 4$, $p = 0.0164$), Rab7CA expression ($N = 4$, $p = 0.9991$), Rab7DN expression ($N = 4$, $p = 0.9754$), Rab7 knockdown using RNAi ($N = 4$, $p = 0.9996$), Rab11 expression ($N = 4$, $p = 0.0329$), Rab11DN expression ($N = 4$, $p = 0.0001$). **(C–E)** Quantification of number of Dendrite Branch points (D.BP) for the interaction of Mon1 with different Rabs. Statistical values (blue *'s or ns), for the genotypes when expressed using ppk-Gal4 in $Dmon1^{\Delta 181}$ background as compared to control alone are as follows: Rab5CA expression ($N = 4$, $p = 0.9990$), Rab5DN expression ($N = 4$, $p = 0.0001$), Rab7CA expression ($N = 4$, $p = 0.0019$), Rab7 knockdown using RNAi ($N = 4$, $p = 0.0992$), Rab11CA expression ($N = 4$, $p = 0.0001$), Rab11DN expression ($N = 4$, $p = 0.0001$). Statistical values (red *'s or ns) for the genotypes when expressed with ppk-Gal4 in $Dmon1^{\Delta 181}$ background as compared to $Dmon1^{\Delta 181}$ are as follows: Rab5CA expression ($N = 4$, $p = 0.0002$), Rab5DN expression ($N = 4$, $p = 0.0001$), Rab7CA expression ($N = 4$, $p = 0.8603$), Rab7 knockdown using RNAi ($N = 4$, $p = 0.1021$), Rab11CA expression ($N = 4$, $p = 0.9999$), Rab11DN expression ($N = 4$, $p = 0.0001$). **(F–H)** Quantification of Dendrite Length (D.L) for the interaction of Mon1 with different Rabs. The graph represents normalized values which follow similar trend as that of the R.I (**Figure 3**). Statistical values (blue *'s or ns) for each of the genotypes when expressed in the ppk-Gal4 domain in $Dmon1^{\Delta 181}$ background as compared to control alone are as follows: Rab5CA expression ($N = 4$, $p = 0.9997$), Rab5DN expression ($N = 4$, $p = 0.0001$), Rab7CA expression ($N = 4$, $p = 0.0125$), Rab7 knockdown using RNAi ($N = 4$, $p = 0.7656$), Rab11CA expression ($N = 4$, $p = 0.7089$), Rab11DN expression ($N = 4$, $p = 0.0001$). Statistical values (red *'s or ns) for the genotypes when expressed using ppk-Gal4 in $Dmon1^{\Delta 181}$ background as compared to $Dmon1^{\Delta 181}$ are as follows: Rab5CA mutant overexpression ($N = 4$, $p = 0.0001$), Rab5DN expression ($N = 4$, $p = 0.0001$), Rab7CA expression ($N = 4$, $p = 0.1130$), Rab7 knockdown using RNAi ($N = 4$, $p = 0.0002$), Rab11CA expression ($N = 4$, $p = 0.0003$), Rab11DN expression ($N = 4$, $p = 0.0001$). Number of neurons analyzed for all genotypes = 10, ns, not significant. $^*p < 0.05$, $^{**}p < 0.01$, $^{***}p < 0.001$. Error bars represent standard error. p-Values generated using Dunnet's multiple comparison test using GraphPad Prism 7.

TABLE S1 | p-values for analysis of experiments conducted for this study.

REFERENCES

Adams, C. M., Anderson, M. G., Motto, D. G., Price, M. P., Johnson, W. A., and Welsh, M. J. (1998). Ripped pocket and pickpocket, novel *Drosophila* DEG/ENaC subunits expressed in early development and in mechanosensory neurons. *J. Cell Biol.* 140, 143–152. doi: 10.1083/jcb.140.1.143

Berry, K. P., and Nedivi, E. (2017). Spine dynamics: are they all the same? *Neuron* 96, 43–55. doi: 10.1016/j.neuron.2017.08.008

Brand, A. H., and Perrimon, N. (1993). Targeted gene expression as a means of altering cell fates and generating dominant phenotypes. *Development* 118, 401–415.

Cajal, S. R. (1999). *Texture of the Nervous System of Man and the Vertebrates*. Berlin: Springer.

Cantallops, I., Haas, K., and Cline, H. T. (2000). Postsynaptic CPG15 promotes synaptic maturation and presynaptic axon arbor elaboration in vivo. *Nat. Neurosci.* 3, 1004–1011. doi: 10.1038/79823

Cline, H. T. (2001). Dendrite arbor development and synaptogenesis. *Curr. Opin. Neurobiol.* 11, 118–126. doi: 10.1016/s0959-4388(00)00182-3

Copf, T. (2014). Developmental shaping of dendritic arbors in *Drosophila* relies on tightly regulated intra-neuronal activity of protein kinase A (PKA). *Dev. Biol.* 393, 282–297. doi: 10.1016/j.ydbio.2014.07.002

Crozatier, M., and Vincent, A. (2008). Control of multidendritic neuron differentiation in *Drosophila*: the role of Collier. *Dev. Biol.* 315, 232–242. doi: 10.1016/j.ydbio.2007.12.030

De Franceschi, N., Wild, K., Schlacht, A., Dacks, J. B., Sinning, I., and Filippini, F. (2014). Longin and GAF domains: structural evolution and adaptation to the subcellular trafficking machinery. *Traffic* 15, 104–121. doi: 10.1111/tra.12124

Deivasigamani, S., Basargekar, A., Shweta, K., Sonavane, P., Ratnaparkhi, G. S., and Ratnaparkhi, A. (2015). A presynaptic regulatory system acts transsynaptically via Mon1 to regulate glutamate receptor levels in *Drosophila*. *Genetics* 201, 651–654. doi: 10.1534/genetics.115.177402

Delandre, C., Amikura, R., and Moore, A. W. (2016). Microtubule nucleation and organization in dendrites. *Cell Cycle* 15, 1685–1692. doi: 10.1080/15384101.2016.1172158

Dhiman, N., Shweta, K., Tendulkar, S., Deshpande, G., Ratnaparkhi, G. S., and Ratnaparkhi, A. (2019). *Drosophila* Mon1 constitutes a novel node in the brain-gonad axis that is essential for female germline maturation. *Development* 146:dev166504. doi: 10.1242/dev.166504

Dong, X. T., Shen, K., and Bulow, H. E. (2015). Intrinsic and extrinsic mechanisms of dendritic morphogenesis. *Annu. Rev. Physiol.* 77, 271–300. doi: 10.1146/annurev-physiol-021014-071746

Emoto, K., He, Y., Ye, B., Grueber, W. B., Adler, P. N., Jan, L. Y., et al. (2004). Control of dendritic branching and tiling by the tricornered-kinase/furry signaling pathway in *Drosophila* sensory neurons. *Cell* 119, 245–256. doi: 10.1016/j.cell.2004.09.036

Garcia-Lopez, P., Garcia-Marin, V., Martinez-Murillo, R., and Freire, M. (2010). Cajal's achievements in the field of the development of dendritic arbors. *Int. J. Dev. Biol.* 54, 1405–1417. doi: 10.1387/ijdb.093001pg

Grueber, W. B., Jan, L. Y., and Jan, Y. N. (2002). Tiling of the *Drosophila* epidermis by multidendritic sensory neurons. *Development* 129, 2867–2878.

Grueber, W. B., Ye, B., Moore, A. W., Jan, L. Y., and Jan, Y. N. (2003). Dendrites of distinct classes of *Drosophila* sensory neurons show different capacities for homotypic repulsion. *Curr. Biol.* 13, 618–626. doi: 10.1016/s0960-9822(03)00207-0

Grueber, W. B., Ye, B., Yang, C. H., Younger, S., Borden, K., Jan, L. Y., et al. (2007). Projections of *Drosophila* multidendritic neurons in the central nervous system: links with peripheral dendrite morphology. *Development* 134, 55–64. doi: 10.1242/dev.02666

Gu, Y., Chiu, S. L., Liu, B., Wu, P. H., Delannoy, M., Lin, D. T., et al. (2016). Differential vesicular sorting of AMPA and GABA(A) receptors. *Proc. Natl. Acad. Sci. U.S.A.* 113, E922–E931. doi: 10.1073/pnas.1525726113

Jan, Y. N., and Jan, L. Y. (2010). Branching out: mechanisms of dendritic arborization. *Nat. Rev. Neurosci.* 11, 316–328. doi: 10.1038/nrn2836

Jinushi-Nakao, S., Arvind, R., Amikura, R., Kinameri, E., Liu, A. W., and Moore, A. W. (2007). Knot/Collier and cut control different aspects of dendrite cytoskeleton and synergize to define final arbor shape. *Neuron* 56, 963–978. doi: 10.1016/j.neuron.2007.10.031

Kanamori, T., Kanai, M. I., Dairyo, Y., Yasunaga, K., Morikawa, R. K., and Emoto, K. (2013). Compartmentalized calcium transients trigger dendrite pruning in drosophila sensory neurons. *Science* 340, 1475–1478. doi: 10.1126/science.1234879

Kanamori, T., Yoshino, J., Yasunaga, K., Dairyo, Y., and Emoto, K. (2015). Local endocytosis triggers dendritic thinning and pruning in *Drosophila* sensory neurons. *Nat. Commun.* 6:6515. doi: 10.1038/ncomms7515

Lazo, O. M., Gonzalez, A., Ascano, M., Kuruvilla, R., Couve, A., and Bronfman, F. C. (2013). BDNF regulates Rab11-mediated recycling endosome dynamics to induce dendritic branching. *J. Neurosci.* 33, 6112–6122. doi: 10.1523/JNEUROSCI.4630-12.2013

Meltzer, S., Yadav, S., Lee, J., Soba, P., Younger, S. H., Jin, P., et al. (2016). Epidermis-derived semaphorin promotes dendrite self-avoidance by regulating dendrite-substrate adhesion in *Drosophila* sensory neurons. *Neuron* 89, 741–755. doi: 10.1016/j.neuron.2016.01.020

Mochizuki, H., Toda, H., Ando, M., Kurusu, M., Tomoda, T., and Furukubo-Tokunaga, K. (2011). Unc-51/ATG1 controls axonal and dendritic development via kinesin-mediated vesicle transport in the *Drosophila* brain. *PLoS One* 6:e19632. doi: 10.1371/journal.pone.0019632

Nordmann, M., Cabrera, M., Perz, A., Brocker, C., Ostrowicz, C., Engelbrecht-Vandre, S., et al. (2010). The Mon1-Ccz1 complex is the GEF of the late endosomal Rab7 homolog Ypt7. *Curr. Biol.* 20, 1654–1659. doi: 10.1016/j.cub.2010.08.002

Orgogozo, V., and Grueber, W. B. (2005). FlyPNS, a database of the *Drosophila* embryonic and larval peripheral nervous system. *BMC Dev. Biol.* 5:4. doi: 10.1186/1471-213X-5-4

Parrish, J. Z., Emoto, K., Kim, M. D., and Jan, Y. N. (2007). Mechanisms that regulate establishment, maintenance, and remodeling of dendritic fields. *Annu. Rev. Neurosci.* 30, 399–423. doi: 10.1146/annurev.neuro.29.051605.112907

Peng, Y., Lee, J., Rowland, K., Wen, Y. H., Hua, H., Carlson, N., et al. (2015). Regulation of dendrite growth and maintenance by exocytosis. *J. Cell Sci.* 128, 4279–4292. doi: 10.1242/jcs.174771

Peng, Y. R., He, S., Marie, H., Zeng, S. Y., Ma, J., Tan, Z. J., et al. (2009). Coordinated changes in dendritic arborization and synaptic strength during neural circuit development. *Neuron* 61, 71–84. doi: 10.1016/j.neuron.2008.11.015

Poteryaev, D., Datta, S., Ackema, K., Zerial, M., and Spang, A. (2010). Identification of the switch in early-to-late endosome transition. *Cell* 141, 497–508. doi: 10.1016/j.cell.2010.03.011

Prigge, C. L., and Kay, J. N. (2018). Dendrite morphogenesis from birth to adulthood. *Curr. Opin. Neurobiol.* 53, 139–145. doi: 10.1016/j.conb.2018.07.007

Satoh, D., Sato, D., Tsuyama, T., Saito, M., Ohkura, H., Rolls, M. M., et al. (2008). Spatial control of branching within dendritic arbors by dynein-dependent transport of Rab5-endosomes. *Nat. Cell Biol.* 10, 1164–1171. doi: 10.1038/ncb1776

Sweeney, N. T., Brenman, J. E., Jan, Y. N., and Gao, F. B. (2006). The coiled-coil protein shrub controls neuronal morphogenesis in *Drosophila*. *Curr. Biol.* 16, 1006–1011. doi: 10.1016/j.cub.2006.03.067

Tanaka, T., and Nakamura, A. (2008). The endocytic pathway acts downstream of Oskar in *Drosophila* germ plasm assembly. *Development* 135, 1107–1117. doi: 10.1242/dev.017293

Valnegri, P., Puram, S. V., and Bonni, A. (2015). Regulation of dendrite morphogenesis by extrinsic cues. *Trends Neurosci.* 38, 439–447. doi: 10.1016/j.tins.2015.05.003

Villarroel-Campos, D., Gastaldi, L., Conde, C., Caceres, A., and Gonzalez-Billault, C. (2014). Rab-mediated trafficking role in neurite formation. *J. Neurochem.* 129, 240–248. doi: 10.1111/jnc.12676

Wang, C. W., Stromhaug, P. E., Shima, J., and Klionsky, D. J. (2002). The Ccz1-Mon1 protein complex is required for the late step of multiple vacuole delivery pathways. *J. Biol. Chem.* 277, 47917–47927. doi: 10.1074/jbc.m208191200

Wang, Y., Zhang, H., Shi, M., Liou, Y. C., Lu, L., and Yu, F. W. (2017). Sec71 functions as a GEF for the small GTPase Arf1 to govern dendrite pruning of *Drosophila* sensory neurons. *Development* 144, 1851–1862. doi: 10.1242/dev.146175

Ye, B., Petritsch, C., Clark, I. E., Gavis, E. R., Jan, L. Y., and Jan, Y. N. (2004). Nanos and pumilio are essential for dendrite morphogenesis in *Drosophila* peripheral neurons. *Curr. Biol.* 14, 314–321. doi: 10.1016/s0960-9822(04)00046-6

Yousefian, J., Troost, T., Grawe, F., Sasamura, T., Fortini, M., and Klein, T. (2013). Dmon1 controls recruitment of Rab7 to maturing endosomes in *Drosophila*. *J. Cell Sci.* 126, 1583–1594. doi: 10.1242/jcs.114934

Zhang, H., Wang, Y., Wong, J. J. L., Lim, K. L., Liou, Y. C., Wang, H. Y., et al. (2014). Endocytic pathways downregulate the L1-type cell adhesion molecule neuroglian to promote dendrite pruning in *Drosophila*. *Dev. Cell* 30, 463–478. doi: 10.1016/j.devcel.2014.06.014

Zou, W., Shen, A., Dong, X. T., Tugizova, M., Xiang, Y. K., and Shen, K. (2016). A multi-protein receptor-ligand complex underlies combinatorial dendrite guidance choices in *C. elegans*. *eLife* 5:e18345. doi: 10.7554/eLife.18345

Conflict of Interest Statement: The authors declare that the research was conducted in the absence of any commercial or financial relationships that could be construed as a potential conflict of interest.

frontiers in Cell and Developmental Biology

ORIGINAL RESEARCH
published: 02 August 2019
doi: 10.3389/fcell.2019.00129

The BEACH Domain Is Critical for Blue Cheese Function in a Spatial and Epistatic Autophagy Hierarchy

*Joan Sim[1], Kathleen A. Osborne[1], Irene Argudo García[1,2], Artur S. Matysik[1,3] and Rachel Kraut[1,4]**

[1] School of Biological Sciences, Nanyang Technological University, Singapore, Singapore, [2] Champalimaud Centre for the Unknown, Lisbon, Portugal, [3] Singapore Centre on Environmental Life Sciences Engineering, Nanyang Technological University, Singapore, Singapore, [4] Max Planck Institute of Molecular Cell Biology and Genetics, Dresden, Germany

OPEN ACCESS

Edited by:
Yanzhuang Wang,
University of Michigan, United States

Reviewed by:
Kartik Venkatachalam,
The University of Texas Health Science Center at Houston, United States
Aron Szabo,
Biological Research Centre (MTA), Hungarian Academy of Sciences, Hungary
Anne Simonsen,
University of Oslo, Norway

***Correspondence:**
Rachel Kraut
rkraut@mpi-cbg.de

Specialty section:
This article was submitted to Membrane Traffic, a section of the journal Frontiers in Cell and Developmental Biology

Received: 31 October 2018
Accepted: 02 July 2019
Published: 02 August 2019

Citation:
Sim J, Osborne KA, Argudo García I, Matysik AS and Kraut R (2019) The BEACH Domain Is Critical for Blue Cheese Function in a Spatial and Epistatic Autophagy Hierarchy. Front. Cell Dev. Biol. 7:129. doi: 10.3389/fcell.2019.00129

Drosophila blue cheese (*bchs*) encodes a BEACH domain adaptor protein that, like its human homolog ALFY, promotes clearance of aggregated proteins through its interaction with Atg5 and p62. *bchs* mutations lead to age-dependent accumulation of ubiquitinated inclusions and progressive neurodegeneration in the fly brain, but neither the influence of autophagy on *bchs*-related degeneration, nor *bchs'* placement in the autophagic hierarchy have been shown. We present epistatic evidence in a well-defined larval motor neuron paradigm that in *bchs* mutants, synaptic accumulation of ubiquitinated aggregates and neuronal death can be rescued by pharmacologically amplifying autophagic initiation. Further, pharmacological rescue requires at least one intact BEACH-containing isoform of the two identified in this study. Genetically augmenting a late step in autophagy, however, rescues even a strong mutation which retains only a third, non-BEACH containing isoform. Using living primary larval brain neurons, we elucidate the primary defect in *bchs* to be an excess of early autophagic compartments and a deficit in mature compartments. Conversely, rescuing the mutants by full-length Bchs over-expression induces mature compartment proliferation and rescues neuronal death. Surprisingly, only the longest Bchs isoform colocalizes well with autophagosomes, and shuttles between different vesicular locations depending on the type of autophagic impetus applied. Our results are consistent with Bchs promoting autophagic maturation, and the BEACH domain being required for this function.

HIGHLIGHTS

The autophagic adaptor *blue cheese* is placed in an epistatic hierarchy, using pharmacological and genetic modulation of *bchs*- motor neuron degeneration. An intact BEACH isoform can promote autophagic proliferation, and in primary larval brain neurons Bchs shuttles to different components of the autophagy machinery, dependent on the stimulus.

Keywords: blue cheese, *Drosophila*, autophagy, BEACH domain, motor neuron, neurodegeneration

INTRODUCTION

A common pathological hallmark in many neurodegenerative disorders is the accumulation of intracellular toxic aggregates. Degradation of misfolded proteins and protein aggregates is mediated by two main intracellular systems, the ubiquitin-proteasome system (UPS) and autophagy (Glickman and Ciechanover, 2002; Levine and Klionsky, 2004). Both pathways are responsible for the recycling of different types of substrates depending on their solubility, half-life and composition, e.g., organelles versus misfolded proteins, type of substrate modification or the presence of specific degradation motifs (Nedelsky et al., 2008). Autophagy appears to function in part as a compensatory degradative pathway, because its activity increases when UPS is impaired (Iwata et al., 2005; Pandey et al., 2007). On the other hand, autophagic efficacy declines with ageing (Cuervo, 2008), acting as a possible mechanistic link to sporadic late-onset neurodegeneration.

During macroautophagy, elongation of the isolation membrane requires the E1-like activating enzyme Atg7 and E2-like conjugating enzyme Atg10 to bring Atg12 to Atg5 (an E3-like ligase) which then binds Atg16 to form the Atg12-Atg5-Atg16 multimeric complex (Ohsumi, 2001; Kuma et al., 2002). This E3-like ligase complex aids in the lipidation of Atg8 protein and dissociates from the membrane upon formation of the autophagosome (Kabeya et al., 2000; Hanada et al., 2007). Although the process of induction by signaling kinases to autophagosome formation and subsequent fusion with lysosomes has been extensively studied (Mizushima et al., 2002; Ganley, 2013), the receptors and adaptors that play a role in selective recognition of cargoes in specific cellular locations have been relatively unknown until recently (Lynch-Day and Klionsky, 2010). In mammals one of these adaptors, ALFY (autophagy-linked FYVE protein), scaffolds the machinery associated with isolation membrane elongation around sequestered protein aggregates by binding to the autophagy receptor, p62, through its PH-BEACH (Beige and Chediak–Higashi) domain, Atg5 through its WD40 repeats, and phosphatidylinositol 3-phosphate (PI3P)-containing autophagic membrane via its FYVE domain (Clausen et al., 2010; Filimonenko et al., 2010).

Loss of function mutations in *Drosophila blue cheese* (Bchs), the ortholog of ALFY, lead to age-dependent accumulation of ubiquitinated inclusions in adult brains, progressive degeneration throughout the nervous system and reduced adult longevity (Finley et al., 2003). A targeted genetic modifier screen in which lysosomal and autophagy candidate genes were able to modify a rough-eye phenotype induced by Bchs over-expression suggested that Bchs function may be involved in an autolysosomal trafficking pathway (Simonsen et al., 2007). A defect in size and anterograde transport of lysosomal compartments along motor neuron axons in *bchs* mutants supported this premise (Lim and Kraut, 2009). In both these studies, *bchs* mutants exhibited morphological features characteristic of atrophying neurons, such as axonal varicosities, ubiquitinated inclusions in the brain and disorganized microtubule bundles. Notably, the degeneration caused by loss of function for *bchs* was never tested for genetic modification by interference with autophagy.

A previous study has reported that ALFY, while not required for autophagy to occur, is associated with autophagic membranes and clears ubiquitinated aggregates from HeLa and neuronal cells (Simonsen et al., 2004; Filimonenko et al., 2010). However, no studies have examined in detail any changes in the autophagic machinery that may occur in *bchs*, or Bchs dynamic behavior with respect to autophagic components. Therefore, we set out to investigate the spatial localization of Bchs in relation to different steps along the autophagy-lysosomal pathway under various stresses and how these respond to *bchs* mutation.

We first present epistatic arguments, combining loss of function *bchs* alleles with genetic and pharmacological manipulations of autophagy, to show that Bchs occupies a specific position in an autophagy hierarchy that can be bypassed by late-acting Atg7, but not by early autophagic initiation. Further, we demonstrate that rescue of the degeneration by increasing autophagy requires at least one BEACH domain containing member of three newly identified isoforms, and that the full length protein strongly induces mature autophagic compartment formation, in keeping with earlier reported functions of BEACH domain proteins in vesiculation events.

RESULTS

The *bchs* Locus Produces Three Isoforms That Are Differentially Localized With Autophagic Markers and Produce Different Phenotypes

The existence of a single long isoform of Bchs has been reported, with smaller bands in Westerns being attributed to non-specific cross-reaction of the antibody (Khodosh et al., 2006; Simonsen et al., 2007). In our hands, Western blot analysis with a polyclonal antibody raised against the C-terminal 1008 amino acids of Bchs (Lim and Kraut, 2009) recognized three Bchs isoforms, all with apparent weights above 300 kDa, both in third instar larval brains and adult heads of *yw* control animals (**Figures 1A,A′**). A pan-neuronal Gal4 driver (elav-Gal4) driving expression via the gene insertion EP*bchs*2299 resulted in the over-expression of all three of these Bchs isoforms (**Figure 1A**; visible as separate bands in **Figure 1A′**, arrowheads), whereas driving *bchs* RNAi (**Figure 1A**) or mutation of *bchs* (**Figure 1A′**) resulted in loss of all three. The EMS alleles *beach17* and *beach58* [referred to here as *bchs58(O)*] were isolated by Khodosh et al. (2006) in the EP*bchs*2299 background. From these lines, we generated *bchs17(M)* and *bchs58(M)* by precise excision of the EP insertion. *bchs17(M)* introduces a stop codon at Trp2640, and is expected to disrupt isoforms 1 and 2 (**Figure 1B**). *bchsLL03462* is a strong allele resulting from an insertion into *bchs* of a splice acceptor site followed by stop codons into the 7th coding exon at aa 1229 preceding the BEACH domain (Flybase allele report FBti0124589). Our sequence analysis of *bchs58(O)*, which was characterized as a strong loss of function mutation, detects an insertion of 3 bases and a deletion of 17 bases, resulting in a frame shift and subsequent stop codon. Thus, the *bchs58* lesion is expected to remove only the longest Bchs isoform 1, but

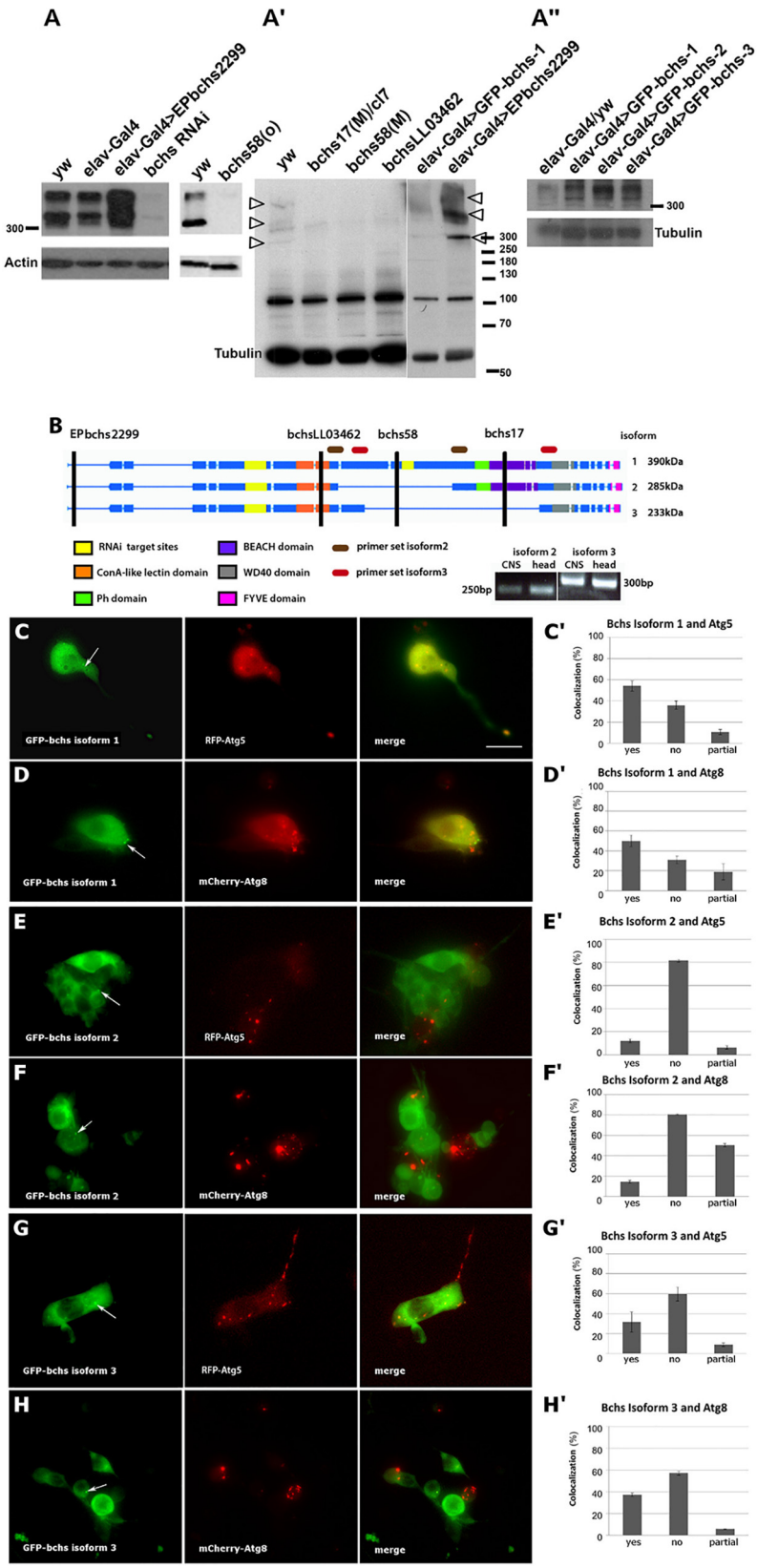

FIGURE 1 | Continued

FIGURE 1 | Blue cheese (Bchs) is alternatively spliced, and the isoforms colocalize to different extents with autophagosomes. **(A)** Left blot: Western of third instar larval brains from control wild type (*yw*) and elav-Gal4 alone, elav-Gal4-driven over-expression of *bchs* (elav-Gal4>EP*bchs*2299), and *bchs*RNAi. Right blot: adult heads, *yw* vs. *bchs58(O)*. **(A′)** Adult heads of *yw* vs. *bchs17(M)/Df(2L)cl7, bchs58(M)*, and *bchsLL03462* show loss of three bands >300 kDa (arrowheads). Right-most two lanes: shorter exposure of the identical blot, with elav-Gal4>GFP-bchs1 and elav-Gal4>EP*bchs*2299 showing increased expression of the same three separate bands >300 kDa (arrowheads) also present in *yw*, relative to non-specific band at ∼100 kDa. **(A″)** Adult heads of elav-Gal4 over *yw* control (left lane) vs. elav-Gal4 driven *bchs* isoforms 1, 2, and 3. Note that *bchs* isoform 2 is smaller than *bchs* isoform 1. Actin and tubulin were used as loading controls. **(B)** Schematic illustrating domains excluded from splice isoforms identified by RT-PCR from larval CNS and adult head. The positions of *EPbchs2299* insertion, *bchsLL03462, bchs58*, *bchs17* mutations are indicated by vertical black lines. Splice isoforms 1, 2, and 3 have expected sizes of 390, 285, and 233 kDa, respectively. However, note that the three products in part **A** (arrowheads) all appear to run >300 kDa; isoform 3 (right-most lane, **A″**) lacks the PH-BEACH domain and therefore may not be as well detected by the antibody, which was raised against the C-terminal third of Bchs, including the PH-BEACH domain (green, purple bands). Using the primer sets shown to detect splice isoform 2 (brown ovals) and splice isoform 3 (red ovals), 250 and 300 bp bands were detected, from which we deduced that splice isoform 1 is 2.8 kb larger than isoform 2 and 4.1 kb larger than isoform 3. **(C–H)** Live images and colocalization tally of elav-Gal4-driven **(C,C′)** GFP-bchs-1, the longest isoform, with RFP-Atg5 in primary larval neurons; **(D,D′)** GFP-bchs-1 with mCherry-Atg8a; **(E,E′)** GFP-bchs-2, which retains a BEACH domain, with RFP-Atg5; **(F,F′)** GFP-bchs-2 with mCherry-Atg8a; **(G,G′)** GFP-bchs-3, the non-BEACH isoform, with RFP-Atg5; **(H,H′)** GFP-bchs-3 with mCherry-Atg8a. Arrows point to vesicularly localized GFP-bchs isoforms. Contrast in GFP panels was enhanced to bring out visibility of the vesicles. Scalebar = 10 μm.

may produce a chimaeric protein that is not recognized by our antibody. However, the strong loss of all three bands in *bchs58(O)* and *bchs58(M)* (**Figure 1A**′), as well as the appearance of additional bands after overexpression of all three isoforms (**Figures 1A**′,**A**″), suggests that positive autoregulation by Bchs may be involved.

The three isoforms of Bchs (depicted in **Figure 1B**) were cloned as N-terminal GFP fusions and expressed in the nervous system via elav-Gal4 (**Figure 1A**″). Larval brains expressing each of the isoforms were dissociated into primary neuronal cultures (**Figures 1C–H**). Live imaging of these primary neurons in the background of transgenic RFP-Atg5 and mCherry-Atg8a expression to label early and late autophagic compartments showed that, in cases where GFP-Bchs can be detected in vesicles, only BEACH-containing isoform 1 (GFP-bchs-1) was predominantly coincident with autophagosomes (**Figures 1C,D**), whereas isoforms 2 and 3 had much less association with either Atg5 or Atg8 (**Figures 1E–H**), and indeed were often mutually exclusive in cells (this can be seen particularly well in **Figures 1F,H**). Autophagosomal association does not appear to depend on the BEACH domain, since BEACH domain-containing isoform 2 is less autophagosomal than isoform 3, which lacks the BEACH domain.

Autophagic Modulation of Neurodegeneration in Loss of Function *bchs* Mutants Depends on the BEACH Domain

A specific function of Bchs in aggrephagy was demonstrated by the observation that Bchs and its homolog ALFY interact physically with the autophagy machinery, and that both are able to reduce aggregates induced in human and *Drosophila* cells (Filimonenko et al., 2010). However, the loss of function neurodegenerative phenotype in the fly was not tested for interactions with either pharmacological or genetic modulators of autophagy, which should occur if *Drosophila* Bchs functions as an autophagic adaptor. Here, as in our earlier study (Lim and Kraut, 2009), the loss of larval aCC and RP2 motor neurons was used as a means of quantifying neurodegeneration in *bchs*. Using this method, we compared the extent of neurodegeneration in *bchs* alleles that differentially affect the three isoforms, and assessed the effects of autophagy-modulating drugs in these genetic backgrounds. aCC and RP2 motor neurons, which were shown to have a high frequency of TUNEL-labeling in the previous study, are specifically labeled in our assay by driving membrane-localized CD8-GFP with an *even-skipped* driver (this driver-reporter combination, used in **Figure 2** and thereafter is referred to as eve>GFP). In combination with a genetic deficiency *Df(2L)cl7* (referred to as *cl7*), *bchs58(O)*, which retains the EP element of EPbchs2299, had lower motor neuron survival (∼32%) than either *bchs58(M)* (∼85%) or *bchs17(M)* (∼70%), the two alleles where the EP element was excised (**Figure 2A**). The phenotypic strength of the three alleles in the order *bchs58(O)* > *bchs17(M)* > *bchs58(M)* was thus established by this assay.

We next tested the effects of feeding the autophagy-modulating drugs rapamycin, 3-methyladenine, and Wortmannin on motor neuron death in larvae of the above allelic combinations. Larvae that were fed rapamycin, a well-established autophagy inducer (Rubinsztein and Nixon, 2010), grew more slowly (7–8 days vs. 3 days), and high concentrations (50 or 100 μM) resulted in widespread larval mortality before third instar. All treatments showed a change in the pattern of the mTOR effector phosphorylated S6 kinase (p-S6K) relative to controls in Westerns of larval brain (**Supplementary Figure S1A**). A comparison of mCherry-Atg8a in muscles of drug-fed larvae also showed increases or decreases in numbers of punctae (**Supplementary Figure S1B**), and rapamycin increased autophagosome formation (more Atg8 spots/cell) and flux (fewer p62 spots/cell) when applied to larval neurons in culture (**Supplementary Figure S1D**).

Feeding larvae rapamycin at 1 uM resulted in a significant amelioration of motor neuron death in all alleles over deficiency *cl7*, with *bchs58M* being rescued to nearly 100% survival (**Figure 2A**). Notably, however, the allele that putatively removes both BEACH domain isoforms, *bchs17(M),* was rescued only marginally (from 70 to 78%). This suggests that the presumptive autophagic deficit in *bchs* mutants can be more effectively compensated by amplification of autophagy if a BEACH- isoform is present, as is the case in *bchs58*. Because rapamycin acts through inhibition of TORC1 and subsequent activation of the Atg1 complex (Ravikumar et al., 2004; Sarkar et al., 2008; Bové et al., 2011), an epistatic interpretation of this result would

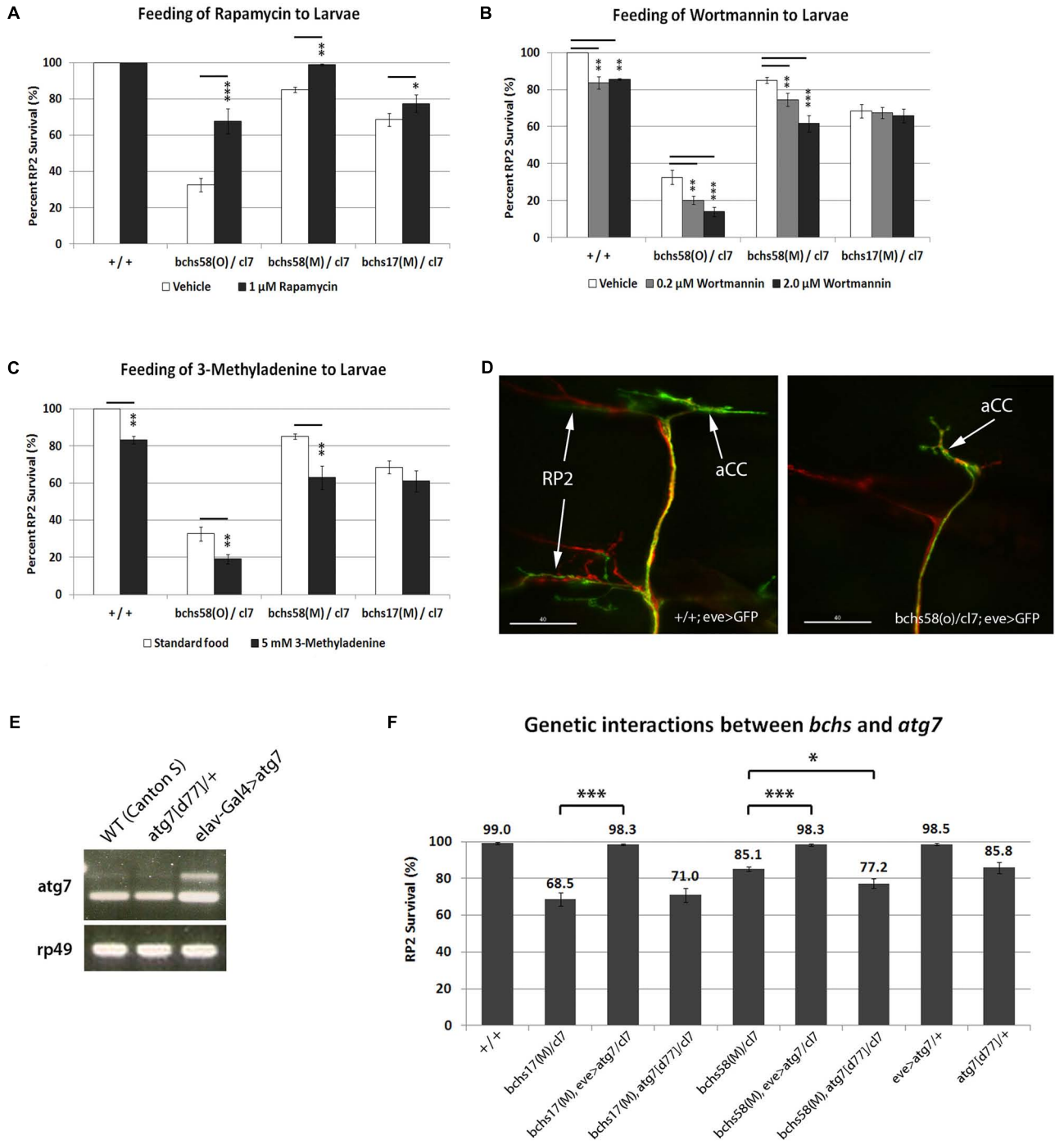

FIGURE 2 | *bchs'* neurodegenerative phenotype is sensitive to autophagy-modulating drugs and genetic enhancement of autophagy. **(A–D)** Larvae of the indicated genotypes were fed on standard food containing either **(A)** rapamycin, **(B)** Wortmannin, or **(C)** 3-methyladenine. All third instar larval motor neurons were labeled as shown in the example in **(D)** with anti-Futsch (22C10; red), and co-labeled with anti-GFP to detect eve>GFP in aCC and RP2 motor neurons (green; arrows). RP2 is absent in the bchs mutant (right panel). Scalebar = 40 µM. Percent survival of RP2 motor neurons over ∼100 hemisegments was calculated for each treatment, and experiments were performed in triplicate. Chi-square test was used to determine statistical significance; $*p < 0.05$, $**p < 0.01$, $***p < 0.001$. **(E)** Over-expression of *atg7* shown by RT-PCR on total RNA from adult heads of wild type (WT, CantonS), atg7[d77]/+ heterozygotes, and elav-Gal4>atg7, using primers specific for *atg7* mRNA and *rp49* rRNA as loading control. **(F)** Over-expression of *atg7* increases RP2 motor neuron survival in *bchs17(M)* and *bchs58(M)* (lanes 3 vs. 2 and 6 vs. 5). A single allelic deletion of *atg7* by itself (lane 9) gives a similar rate of RP2 death as *bchs58(M)* and mildly exacerbates it (lanes 5 vs. 7) but does not significantly change *bchs17(M)* (lanes 2 vs. 4). Experiments were performed in triplicate, and $N > 100$ (hemisegments) for each genotype. All genotypes include the driver/reporter combination eve>GFP in homozygosity. Error bars represent standard deviation, and Chi-square test was used to calculate statistical significance. $*p < 0.05$, $**p < 0.01$, $***p < 0.001$.

be that complete rescue requires Bchs with an intact BEACH domain, downstream of Atg1 in the autophagy hierarchy. It also identifies BEACH-containing isoforms of Bchs as the primary participants in autophagy.

Wortmannin and 3-methyladenine (3-MA) are widely used broad-spectrum phosphatidylinositol 3-kinase (PI3K) inhibitors that act mainly via the suppression of class III PI3K activity to inhibit the nucleation of phagophores through PI3P production (Seglen and Gordon, 1982; Powis et al., 1994). 0.2 or 2 μM Wortmannin significantly reduced motor neuron survival in wild-type control, *bchs58(O)/cl7* and *bchs58(M)/cl7*, but did not exacerbate *bchs17(M)/cl7* (**Figure 2B**), the genetic background that lacks the two BEACH-containing isoforms. Similarly, suppression of autophagy by 3-MA caused motor neuron death in wild-type (phenocopying *bchs* motor neuron loss, a typical example of which is shown in **Figure 2D**) and exacerbated *bchs58(O)/cl7* and *bchs58(M)/cl7*, but did not significantly exacerbate *bchs17(M)/cl7* (**Figure 2C**). These data again point to the BEACH domain isoforms being responsible for the residual autophagic capacity that appears to be present in the rescuable *bchs58* alleles.

Activation of a Late-Stage Autophagy Step by *atg7* Rescues the *bchs* Degenerative Phenotype

There is evidence that ALFY interacts physically with the autophagy machinery, but a *bona fide* genetic interaction between a loss of function *bchs* phenotype and autophagy has not been tested. Therefore, we examined whether manipulation of autophagy genes could modify *bchs* motor neuron death. Atg7, an E1-like ubiquitin activating enzyme that is involved in the conjugation of phosphatidylethanolamine (PE) to Atg8, and formation of the Atg5-Atg12 conjugate, has been shown to suppress the accumulation of ubiquitinated aggregates, thereby contributing to *Drosophila* adult longevity (Juhasz et al., 2007; Geng and Klionsky, 2008). Adult heads of *Atg7[EY10058],* which has upstream activating sequences (UAS) inserted before the *atg7* transcriptional start site, driven with elav-Gal4 (elav-Gal4>atg7 in **Figure 2E**), showed an increase in *atg7* transcripts by reverse-transcription (RT)-PCR (**Figure 2E**, lane 3), and an increase in p-S6K compared to control (**Supplementary Figure S1C**). Therefore, we used this line to over-express Atg7 in the presence or absence of Bchs.

Strikingly, over-expression of Atg7 via eve-Gal4 (eve>atg7 in **Figure 2F**) rescued motor neuron survival to almost 100% in both the strong allele *bchs17(M)/cl7* and the hypomorph *bchs58(M)/cl7* (**Figure 2F**, lanes 3 and 6). Notably, this genetic augmentation of a later-occurring autophagy step via Atg7 was more effective than rapamycin feeding at rescuing *bchs17(M)*, which only mildly improved *bchs17(M)/cl7* degeneration (**Figure 2A**). *bchs58(M)/cl7* showed a similar percentage of neuronal death as the loss of function allele *atg7[d77]/+* (85.1% vs. 85.8%; **Figure 2F**, lanes 5 and 9) and combining them resulted in a further reduction of neuronal survival to 77.2% (**Figure 2F**, lane 7). In contrast, combination with *atg7* did not significantly exacerbate the phenotype of *bchs17(M)/cl7* (**Figure 2F**, lanes 2 vs. 4). Another *atg7* deletion *atg7[d14]* was synthetic lethal when recombined with *cl7*, making it difficult to examine the effect of *atg7*- homozygosity on *bchs*.

Atg1 activity has previously been shown to rescue phenotypes that result from autophagic deficit by overexpression of a transgene (Scott et al., 2007). We attempted this in the background of *bchs* alleles, using two different available constructs (UAS-Atg1^{GS10797}, and UAS-Atg1(6A), a gift of T. Neufeld), but both of these resulted in nearly complete motor neuron death when expressed in the neurons to be assayed, alone and in combination with *bchs* alleles, and could therefore not be tested for rescue.

In summary, *bchs* alleles with or without BEACH products can be rescued substantially by enhancing a late autophagic step via Atg7 over-expression. Conversely, *bchs17(M)*, which removes both BEACH-containing isoforms, cannot be further exacerbated by disrupting autophagic activity via *Atg7* knockout. Both of these observations point to *atg7* acting in one functional pathway downstream of *bchs*, and its ability to override loss of BEACH isoforms.

Accumulation of Ubiquitinated Aggregates in *bchs* Motor Neuron Termini Accompanies Degeneration and Is Abolished by Augmenting Autophagy

Previous reports have demonstrated the accumulation of insoluble ubiquitinated protein aggregates in aged *bchs* adult heads and in photoreceptor axons of Bchs over-expressing late pupae (Finley et al., 2003; Simonsen et al., 2007). Larval motor neurons are ideally suited to examine the subcellular localization of such aggregates due to their clearly identifiable anatomy. Therefore, we investigated whether ubiquitinated aggregates accumulate in *bchs* motor neurons and where this occurs.

Aggregates appeared prominently in the dorsal-most synaptic arbors of motor neurons in third instar larval body walls of *bchs* animals (**Figure 3A**). There was no obvious accumulation of ubiquitinated conjugates in motor neuron axons and cell bodies in *bchs* mutants (data not shown). For quantification, aggregate area sizes were categorized into three groups: 0–1 μm^2 (small), 1.1–10 μm^2 (medium), and 10.1–50 μm^2 (large). While the smallest ubiquitinated aggregates were nearly always found in wild type termini, the frequency of medium- and large-sized aggregates was much higher in *bchs* mutants. The allele *bchsLL03462/cl7* had the highest occurrence of medium aggregates, whereas *bchs58(O)/cl7* had fewer overall (**Figure 3B**). Although this result was unexpected based on the severity of the alleles, it may be related to the possibly neomorphic nature of the *58(O)* allele.

We next investigated whether autophagy-modulating drugs affected the distribution of aggregates in termini, and whether this correlated with motor neuron viability. *bchs58(M)/cl7* and *bchs17(M)/cl7* fed 1 μM rapamycin showed significantly lower frequencies of medium and large ubiquitinated aggregates, while small aggregates increased significantly (**Figure 3C**; significance was calculated in comparison to frequency of a given aggregate size in the corresponding genotype without drug in **Figure 3A**).

In contrast to rapamycin feeding, Wortmannin and 3-MA did not affect the distribution of ubiquitinated aggregates in

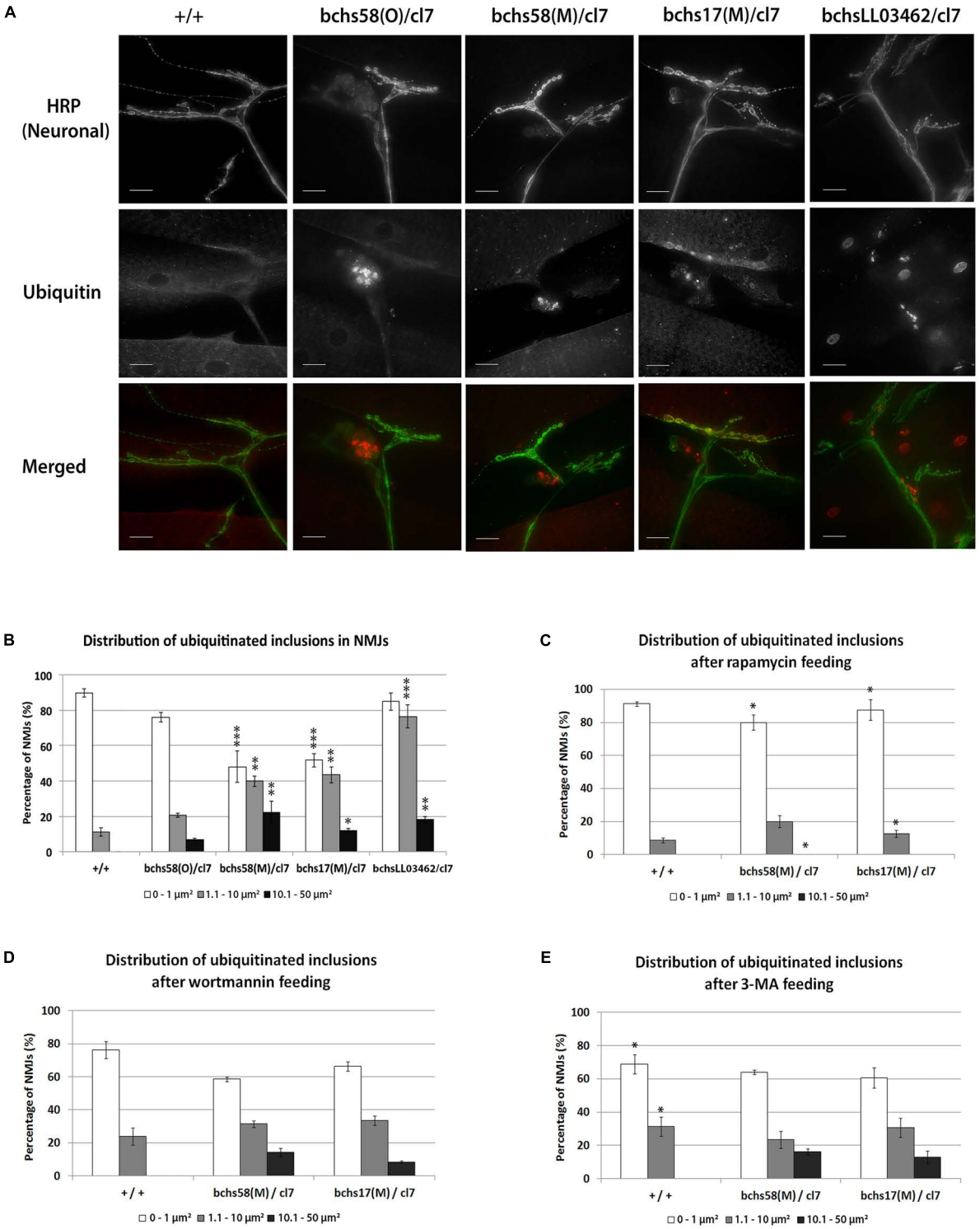

FIGURE 3 | Ubiquitinated aggregates accumulate in neuronal termini of *bchs* larval neuromuscular junctions and can be reduced by rapamycin feeding. **(A)** Third instar larvae were dissected and immunostained for anti-HRP (a pan-neuronal marker) and anti-poly-ubiquitin. Scale-bar = 20 μm. **(B)** Percentages of neuromuscular junctions with ubiquitinated inclusions in each of three size groups (see Materials and Methods) were calculated for the different genotypes. Experiments were performed in duplicate, and error bars represent S.E.M. Chi-square test was used to determine pairwise statistical significance between frequency of occurrence of a given aggregate class in *bchs* vs. the same class in the wild-type control. $*p < 0.05$, $**p < 0.01$, $***p < 0.001$. Larvae of the indicated genotypes were fed on **(C)** rapamycin, **(D)** Wortmannin, or **(E)** 3-methyladenine (see Materials and Methods) before repeating the same procedures as in **(B)** for analysis. Stars in **(A)** show significance of differences between classes in each of the genotypes and wild-type (+/+). Stars in **(C)** and **(E)** show significance for pairwise comparisons of numbers of ubiquitinated inclusions in the same genotype in **(B)** without drug.

bchs mutants (**Figures 3D,E**, compare to **B**). However, 3-MA feeding caused a significant shift toward the formation of medium (but absence of large) ubiquitinated aggregates in wild-type larvae (**Figure 3E**).

Early Autophagosomes Increase in *bchs* Primary Neurons and Bchs Expression Drives Progression to Late Autophagy

Since the observed accumulation of ubiquitinated aggregates in neuronal termini of *bchs* neuromuscular junctions suggests a blockage in the autophagy pathway, it was of interest to investigate where this blockage might be taking place. Because primary neurons prepared from third instar larval brains could be analyzed in much larger numbers than larval motor neurons, we used these to assess the number per cell and brightness of Atg5- and Atg8-positive compartments (**Figures 4A–H**). Atg5-positive compartments increased significantly in number and/or brightness in all *bchs* allelic combinations (**Figures 4A,B**), whereas Atg8-positive compartments were reduced, but only significantly in *bchs17(M)* mutants (**Figures 4E,F**) (cell images of additional *bchs* allelic combinations shown in **Supplementary Figure S2**). Ubiquitin-labeled inclusions were visible in all preparations, but appeared more prominent and vesicular rather than predominantly nuclear and cytoplasmic, in the neurons that were rescued by GFP-bchs-1 (**Figures 4C,G**).

Interestingly, expression of GFP-bchs-1 in *bchs* mutant backgrounds resulted in an increase in brightness of Atg5 in vesicles (**Figure 4B**, sample 3), but a reversal of the increase in Atg5 compartment number (**Figure 4A**, sample 3). Even more strikingly, GFP-bchs-1 expression also caused a very strong increase in both Atg8 compartment number and intensity over wild type (**Figures 4E,F**, sample 3; **Figure 4H**, panels 3, 5). Full multi-cell comparisons of Atg5 and Atg8 expression in the different genotypes are shown as montages in **Supplementary Figures S3–S6**. We also noted that both Atg5 and Atg8 accumulated detectably in the neurites of *bchs17(M)/cl7* compared to wild-type in neurons that had been allowed to differentiate further by aging for 4 additional days in culture (**Supplementary Figures S4B**, **S6B**). These neurons also showed notably more prominent ubiquitinated aggregates than the younger preparations (see enlarged insets, green in **Supplementary Figures S4B**, **S6B**).

In general, our findings with respect to Atg8 differ from those of Filimonenko et al. (2010), who reported no effect on starvation-induced LC3 expression in ALFY knockdowns. This discrepancy may be due to differences in methods of quantification, cell type, or presence vs. absence of autophagy induction. Surprisingly, the loss of *bchs* did not influence the localization of Huntingtin (Htt) Q93 ubiquitin aggregates with either Atg5 or Atg8 (**Supplementary Figure S7**), indicating that Bchs does not have an explicit role in guiding these aggregates to the nascent or fully formed autophagosome.

In order to discern whether *bchs*' effects on autophagic compartments were due to changes in flux, we treated control and *bchs*RNAi-treated primary neurons expressing mCherry-Atg8 with chloroquine in order to block auto-lysosomal degradation (**Supplementary Figures S8A–F**). Chloroquine reduced mCherry-Atg8 size and intensity significantly over controls, and this was strongly reversed by the presence of *bchs*RNAi. Additionally, we tested *bchs*' effects on another marker of autophagosomal maturation, Syntaxin 17 (Syx17), a vesicular synaptosome-associated protein receptor (SNARE) necessary for HOPS-mediated lysosomal-autophagosomal fusion (Takáts et al., 2014; **Supplementary Figures S8G–L**). Changes in expression and localization of Syx17 were evident: *bchs17(M)/cl7* appeared to increase the size of Syx17 compartments, while *bchs58(M)/cl7* neurons more often had smaller, more tightly localized Syx17 (**Supplementary Figure S8L**). Overexpression of GFP-bchs-1 notably resulted in large areas of Syx17 throughout the cell body and in the nucleus (**Supplementary Figures S8K,L**).

The functionality of Bchs-GFP isoform 1 —the most clearly autophagosome-associated isoform (see **Figure 1**)— which induced Atg8 compartment formation in the foregoing experiment (**Figure 4**), was assayed for its ability to rescue the motor neuron loss of different *bchs* loss of function alleles. To test this, GFP-bchs-1 was recombined onto the *cl7* deficiency chromosome, and crossed into the background of different *bchs* combinations. *bchsLL03462* by itself gave only ∼40% motor neuron survival, but was rescued by the transgene GFP-bchs-1 to ∼100% survival (**Figure 4I**). The ∼68% survival seen in *bchs17(M)* was mildly rescued to ∼80%, while *bchs58(M)* was not rescued (not shown). Expression of GFP-bchs-1 by itself resulted in extensive motor neuron loss, suggesting that particular levels or a balance of the three isoforms may be important.

We conclude from the above set of experiments that *bchs* neurons experience an autophagic block leading to an excess of early Atg5 compartments, which can be overcome by expression of the full-length Bchs isoform. Indeed, Bchs isoform1 appears to induce super-normal numbers and intensities of Atg8 vesicles (**Figures 4E,F**), as well as increasing the extent of Syx17 domains, which together reflect the mature autophagosome (**Supplementary Figure S8**). This indicates a likely function of the full-length Bchs protein in maturation of autophagosomal compartments.

Bchs Colocalizes Preferentially With Atg5 During Selective Autophagy and With Atg8 During Non-selective Autophagy

After autophagy stimulation by nutrient starvation, rapamycin treatment and Htt polyQ93 expression, it was observed generally that the size and number of individual Bchs, Atg5 and Atg8 compartments increased compared to non-treated controls (**Figures 5**, **6**). However, Bchs was homogeneously distributed throughout the primary neuron and colocalized only ∼20–25% with either marker, RFP-Atg5 or mCherry-Atg8a, under basal and induced autophagy (**Figures 5**, **6**), which is surprising in light of earlier findings with Alfy (Simonsen et al., 2004). We also note that in cases of overlap between Bchs and the respective markers, the punctae do not completely colocalize with each other (see merged images in **Figures 5**, **6**),

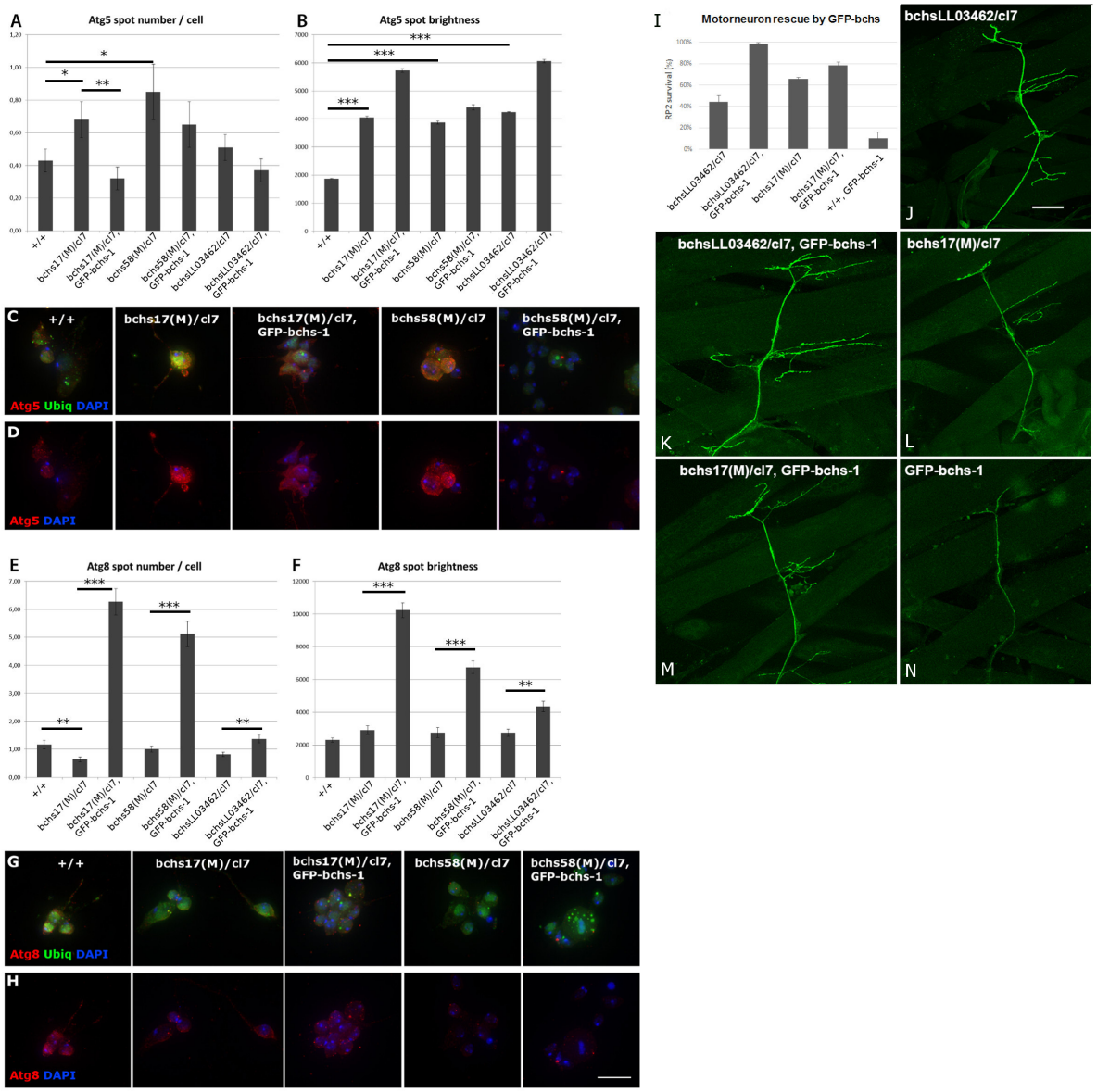

FIGURE 4 | Full-length Bchs drives an increase in transition of early Atg5-positive vesicles to Atg8-carrying autophagosomes, and full-length Bchs rescues *bchs* neuronal loss, but kills motor neurons in a wild-type background. **(A,B)** Early autophagic Atg5-positive vesicle number and brightness (fluorescence intensity per pixel within a spot) in primary larval neurons, with examples of neurons of individual genotypes **(C,D)**, also labeled with anti-poly-ubiquitin (green) and DAPI (blue) to show cell locations. $*p < 0.05$, $**p < 0.01$, $***p < 0.001$. **(E,F)** Late autophagic Atg8-positive vesicle number and brightness in the same genotypes as in **(A,B)**; examples shown in **(G,H)**. Atg5/Atg8 and DAPI are shown separately to make changes in abundance of the respective marker more visible. Scalebar = 10 μm. **(I–N)** RP2 motor neuron survival after GFP-bchs-1 expression via eve-Gal4 in *bchs* mutant backgrounds *bchsLL03462/cl7*, *bchs17(M)/cl7*, or in the control background (+/+). **(J–N)** Images of representative neuromuscular junctions in the larval body wall labeled with eve>GFP in the same *bchs* backgrounds, with or without GFP-bchs-1. Scalebar = 20 μm.

suggesting their localization on different compartments or sub-compartments.

The colocalization of endogenous Bchs with transgenically expressed compartmental markers in response to different stimuli was analyzed using Intensity Correlation Analysis (ICA) (Li et al., 2004; Schneider et al., 2012). The Manders' colocalization coefficient for the green channel (M2) (i.e., the proportion of the intensity in Bchs-positive (green) pixels overlapping with that in RFP-Atg5-positive (red) pixels), decreased during nutrient starvation, but not under rapamycin treatment (**Figures 5A,B,D**), indicating that dissociation from Atg5 compartments may be a specific response to starvation as opposed to general autophagic induction. In contrast, the expression of Htt Q93 (but not Q20) led to a significant increase in Rr, the Pearson's correlation coefficient, M1 (Manders' coefficient for the red channel) and M2 values with

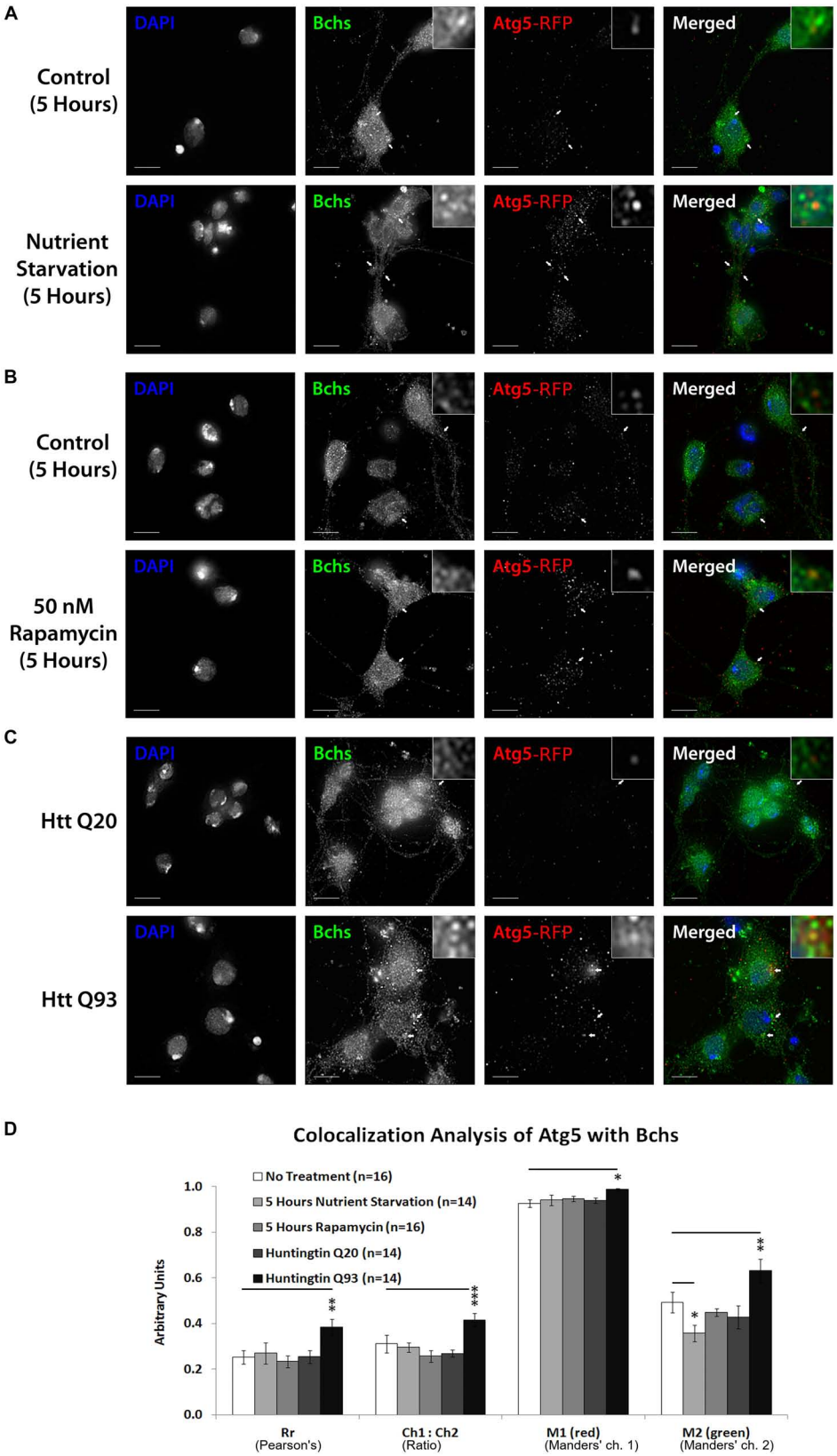

FIGURE 5 | Continued

FIGURE 5 | Bchs associates with RFP-Atg5 marked compartments during aggrephagy and dissociates from them during starvation-induced autophagy. Third instar larval primary neurons were immunostained for endogenous Bchs and transgenic RFP-Atg5 using anti-Bchs and anti-DsRed antibodies after different conditions of autophagy induction: **(A)** five hours of nutrient starvation by incubation with serum-free HL-3 buffer, **(B)** five hours of incubation with 50 nM rapamycin in complete medium, and **(C)** Htt normal (Q20) and expanded (Q93) polyQ expression. Scalebar = 5 μm. Arrowheads indicate regions of close association between Bchs and RFP-Atg5. The top-right inset shows a 10× magnification of one of the indicated regions. **(D)** Colocalization analysis was performed using ImageJ to obtain Rr (Pearson's correlation coefficient), Ch1:Ch2 ratio (red:green pixels ratio), thresholded M1 (Manders' colocalization coefficient for Channel 1) and M2 (Manders' colocalization coefficient for Channel 2). Error bars represent standard error of the mean for n = number of single-slice images. Unpaired Student's *t*-test was used for the statistical comparison between treatment and non-treatment groups. $*p < 0.05$, $**p < 0.01$, and $***p < 0.001$.

RFP-Atg5 (**Figures 5C,D**). The ratio of RFP-Atg5 intensity to endogenous Bchs intensity, expressed by Ch1:Ch2, also increased, although the transgenic RFP-tagged protein is expected to be expressed at constant levels. This may be due to the clearly visible increase in punctate localization of this marker upon autophagic induction, which would be expected to be enhanced by the colocalization algorithm during background subtraction. These results together suggest that Bchs may associate preferentially with early autophagosomal Atg5 compartments during aggrephagy, and at least partially dissociate from them during starvation-induced autophagy, moving toward an Atg8-associated compartment.

Selective Autophagy Lowers Bchs Colocalization With Rab11-GFP

Rab11 localizes onto recycling endosomes and is required for early endocytic membrane trafficking and recycling (Ullrich et al., 1996; Wilcke et al., 2000). Bchs colocalizes partially with Rab11-GFP in *Drosophila* embryonic motor neurons and Rab11 antagonizes Bchs function in synaptogenesis (Khodosh et al., 2006; Lim and Kraut, 2009). To look at how this interaction is affected by autophagy, the spatial relationship of Bchs with Rab11-GFP was investigated in primary neurons in response to autophagy induction by different conditions. After autophagy induction by all three methods – nutrient starvation, rapamycin treatment or Htt polyQ expression – there was a reduction in colocalization between Bchs and Rab11-GFP as measured by both the Pearson's correlation coefficient (Rr) and M1 (the proportion of Bchs intensity overlapping with Rab11-GFP), with Htt polyQ giving the strongest reduction (**Figures 7A–D**). These data show that Bchs associates less with Rab11 recycling compartments during the induction of selective (aggregate-induced) than under non-selective (starvation or rapamycin-induced) autophagy. However, the number of rab11-carrying compartments appeared not to be affected by autophagy induction, tested by using a YFP insertion in the rab11 gene [a gift of M. Brankatschk and S. Eaton (Dunst et al., 2015)] in primary neurons treated with rapamycin (not shown).

Live Imaging of GFP-Bchs With RFP-Atg5 or mCherry-Atg8a During Autophagy Induction Confirms Stimulus-Dependent Relocalization of Bchs

In order to study the dynamics of Bchs interaction with autophagic vesicles, primary neurons cultured from third instar larval brains expressing GFP-bchs-1 and RFP-Atg5 or mCherry-Atg8a were imaged live. GFP-bchs-1 punctae are localized adjacent to RFP-Atg5 punctae occasionally under basal autophagy (**Supplementary Figure S9** and **Supplementary Movie S1**). After nutrient starvation, GFP-Bchs and RFP-Atg5 appeared more distinct (**Supplementary Figure S9B** and **Supplementary Movie S2**), in agreement with the reduction in colocalization seen in fixed preparations (**Figure 5D**). RFP-Atg5 also re-locates nearer to the nuclear membrane after 40 min of starvation (**Supplementary Figure S9B**). These structures may correspond to the phagophore assembly sites, which are thought to form from omegasomes on the ER (Hayashi-Nishino et al., 2009; Ylä-Anttila et al., 2009).

After transfection of Htt Q15, occasional GFP-Bchs punctae adjacent to RFP-Atg5 punctae were observed (**Supplementary Figure S9C** and **Supplementary Movie S3**), similar to basal conditions. Htt Q128 transfection resulted in observable colocalization of GFP-bchs-1 and RFP-Atg5 in live neurons (**Supplementary Figure S9D** and **Supplementary Movie S4**). GFP-bchs-1 in these experiments was distributed mainly homogeneously throughout the cytosol, similarly to endogenous Bchs.

Under basal autophagy conditions, some mCherry-Atg8a punctae were adjacent to GFP-Bchs punctae (**Supplementary Figure S9E** and **Supplementary Movie S5**). After 2 h of nutrient starvation, however, there was a distinct enlargement of mCherry-Atg8a autophagosomes (**Supplementary Figure S9F** and **Supplementary Movie S6**). These doughnut-shaped punctae progressed to a bean-shaped forms, resembling the cross-section of vesicular compartments (visible in **Supplementary Figure S9F**).

When Htt Q15 or Q128 were expressed, there was little observable coincidence between mCherry-Atg8a and GFP-Bchs in live cells (**Supplementary Figures S9G,H** and **Supplementary Movies S7**, **S8**), similar to basal conditions and corroborating the colocalization analysis (**Figure 6D**). mCherry-Atg8a accumulated in a prominent focal swelling along the axon (left arrow in **Supplementary Figure S9H**), and an mCherry-Atg8a streak can be seen moving retrograde toward the focal swelling, but does not exit from it toward the cell soma, seeming to indicate a blockage of autophagosomal transport.

DISCUSSION

Physical interactions of the proposed aggrephagy adaptor and p62-binding BEACH domain protein (Nezis et al., 2008; Clausen et al., 2010) Bchs with other parts of the autophagic machinery have been demonstrated in biochemical studies. However, a convincing demonstration of how autophagic

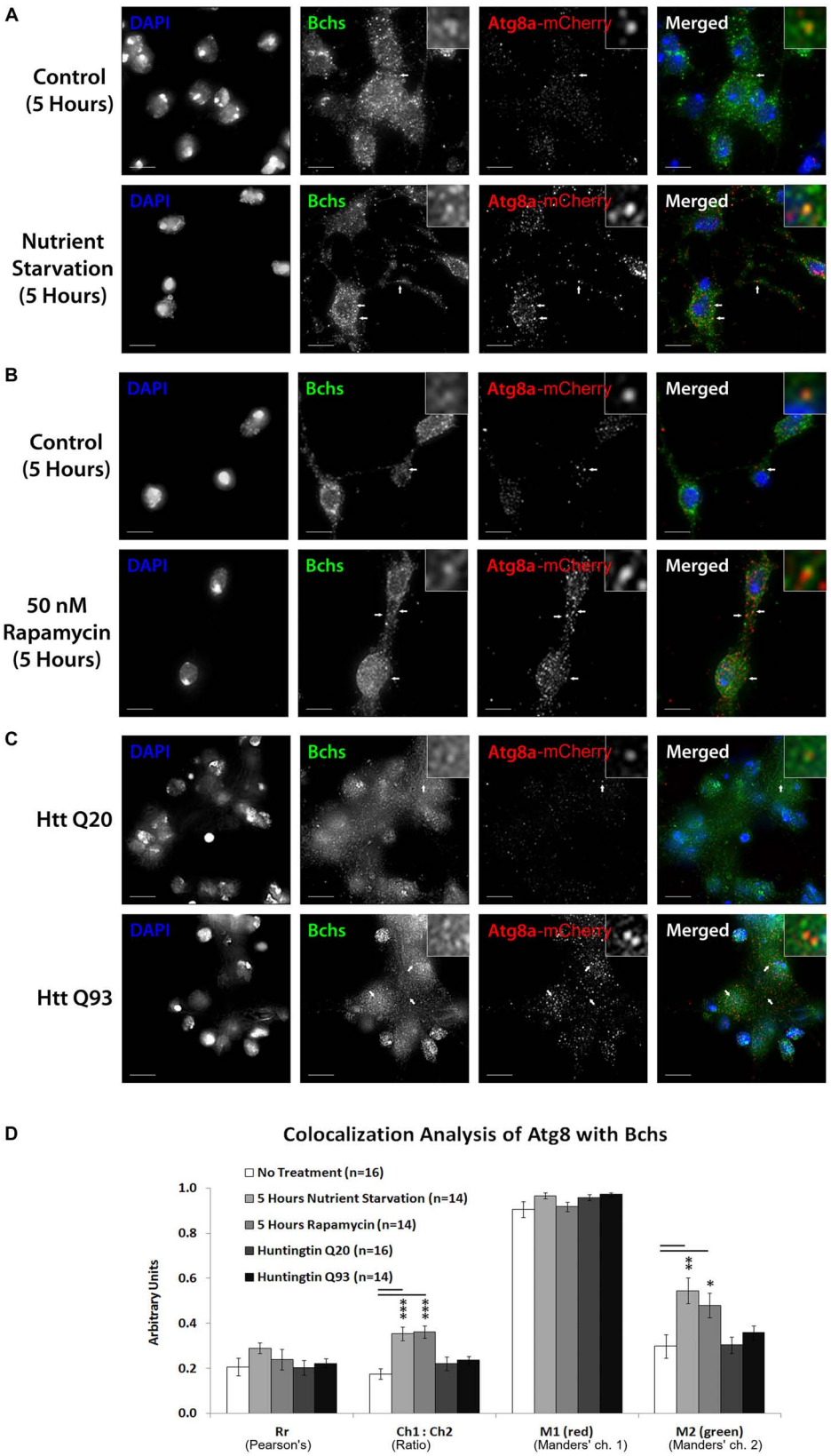

FIGURE 6 | Continued

FIGURE 6 | Nutrient starvation and rapamycin treatment gave a significant increase in the relative quantity of mCherry-Atg8a to Bchs (expressed by the Ch1:Ch2 value), likely explained by an increase in vesicular localization of the transgenically expressed tagged mCherry-Atg8a protein upon autophagy induction **(A,B,D)**. The amount of Bchs colocalizing with this mCherry-Atg8a (M2) also increased significantly **(D)**. In contrast, Htt Q93 expression did not increase M2 **(C,D)**, as it had with RFP-Atg5 (compare **Figure 5D**). These results show that Bchs increases its localization with mCherry-Atg8a-tagged compartments upon general (starvation-induced) autophagy, but not after aggregate induction.

manipulation might affect neurodegeneration in a *bchs* mutant phenotype has never been provided. This is important for two reasons: first, it is critical to examine effects on the intrinsic neuronal degeneration caused by loss of function of the gene, rather than relying solely on ectopic expression of aggregating proteins and over-expression of the Bchs product, or parts thereof (Finley et al., 2003; Simonsen et al., 2007; Clausen et al., 2010; Filimonenko et al., 2010). Second, modulating different steps in the autophagic pathway in the presence of mild vs. severe loss-of-function *bchs* alleles allows the placement of *bchs* in a hierarchical framework, thus giving clues to its possible function.

In this study, we carry out epistasis analyses by demonstrating that the degree of motor neuron loss in *bchs*, described in an earlier publication as representing a quantitative measure of degeneration, can be rescued by genetic and pharmacological autophagy induction, but only in *bchs* alleles that retain at least one of the three newly discovered BEACH-containing protein isoforms. Indeed, we observe that these isoforms are not equally or even predominantly associated with autophagosomes in primary larval brain neurons, and in fact the two shorter isoforms are often seen to be mutually exclusive with Atg5 and Atg8 expression in individual neurons (see **Figure 1**). Our autophagic interaction results suggest that the BEACH domain is essential for autophagic enhancement to be able to rescue neurons from degeneration. This was surprising, since Filimonenko et al. found that the WD40/FYVE region alone was responsible for binding Atg5 and could by itself mediate aggregate clearance (Filimonenko et al., 2010). One interpretation of this apparent contradiction is that aggregate non-clearance by itself may not be the sole or even primary cause of degeneration. Indeed, the most strongly degenerative loss of function allele, *bchs58(O)*, did not have the most severe aggregate accumulation.

Autophagy inhibiting drugs not only exacerbated neuronal death in the weaker *bchs* mutants but, importantly, also phenocopied *bchs*, showing that autophagy inhibition alone induces a similar extent of motor neuron death as is seen in *bchs* larvae. However, strong loss of function of *bchs* apparently impairs autophagy to such an extent that it is refractory to further exacerbation by these drugs. Consistent with this, strong *bchs* loss of function is only marginally significantly rescued by rapamycin, which triggers Atg1 activity, leading to the conclusion that Bchs functions downstream of Atg1 (Mizushima, 2010).

Epistatic relationships with *Atg7* are strikingly similar to the aforementioned with autophagy inhibitors. *Atg7* loss by itself phenocopies *bchs*, but only exacerbates weaker *bchs* alleles. Conversely, overexpression of Atg7, unlike rapamycin, is able to rescue even the loss of all BEACH domain Bchs isoforms. This would be surprising if Bchs were a strictly selective autophagy receptor for aggrephagy, and argues that a general boost in autophagy via Atg7 suffices to ameliorate neuronal death. These pieces of evidence suggest that Bchs acts upstream of Atg7 in the same pathway, and that the block in autophagy can be overcome by Atg7, although Atg7's function in conjugation of the Atg12-Atg5-Atg16 complex is nominally upstream of the step toward mature lipidated Atg8-carrying vesicles (schematized in **Figure 8**).

The accumulation of Atg5 compartments in *bchs* mutants, but a greatly increased number and intensity of Atg8-carrying vesicles after Bchs over-expression (**Figure 4**), indicate that Bchs may be involved in the progression from earlier steps of autophagy, wherein it associates with Atg5-positive phagophores during the induction of aggrephagy, to later Atg8-involving steps (schematized in **Figure 8**, top panel, left). Such a role for Bchs is also consistent with the greatly increased quantity of p62/Ref(2)p marker in *bchs* mutants, which we documented in an earlier publication (also see **Supplementary Figure S1D**; Hebbar et al., 2015).

Interestingly, and contrary to expectations based on earlier publications proposing a strictly aggrephagy-related role for Bchs (Filimonenko et al., 2010), we observe low overall colocalization in resting neurons with autophagy machinery in general (Rr is on the order of 0.2–0.25 for Atg5 and Atg8), and even anti-localization of the shorter 2nd and 3rd isoforms (see **Figure 1**). Moreover, the autophagosome-colocalizing population of Bchs associates with different vesicle populations, dependent on the autophagy-inducing agent. Our results support a scenario whereby aggregating proteins–Htt polyQ in this case– increase Bchs' association with (presumably early) Atg5-compartments, whereas starvation suppresses Atg5 localization in favor of mature Atg8 compartments. As indicated above, these observations may point to multiple Bchs functions, and different factors contributing to neuronal degeneration in addition to a strict role of aggrephagy (Lim and Kraut, 2009).

Low overall colocalization of Bchs with early and late autophagosomes contrasts with the high colocalization (Rr of ∼0.7) with Rab11, which is reduced by various forms of autophagic induction (see **Figure 7**). Bchs and Rab11 are postulated to perform antagonistic roles (Khodosh et al., 2006; Lim and Kraut, 2009), with Bchs promoting synaptogenesis while Rab11 inhibits it. Rab11 may antagonize Bchs through competitive routing of autophagosomal membrane sources under different autophagy stimuli (Longatti et al., 2012; Puri et al., 2013), for example under fed vs. starv conditions, although a change in rab11 vesicle number, size, or intensity was not apparent after autophagy induction (data not shown).

A previous study found Bchs enriched in vesicles at synaptic boutons of larval axon terminals (Khodosh et al., 2006). Notably, the initiation of autophagosome biogenesis occurs distally and

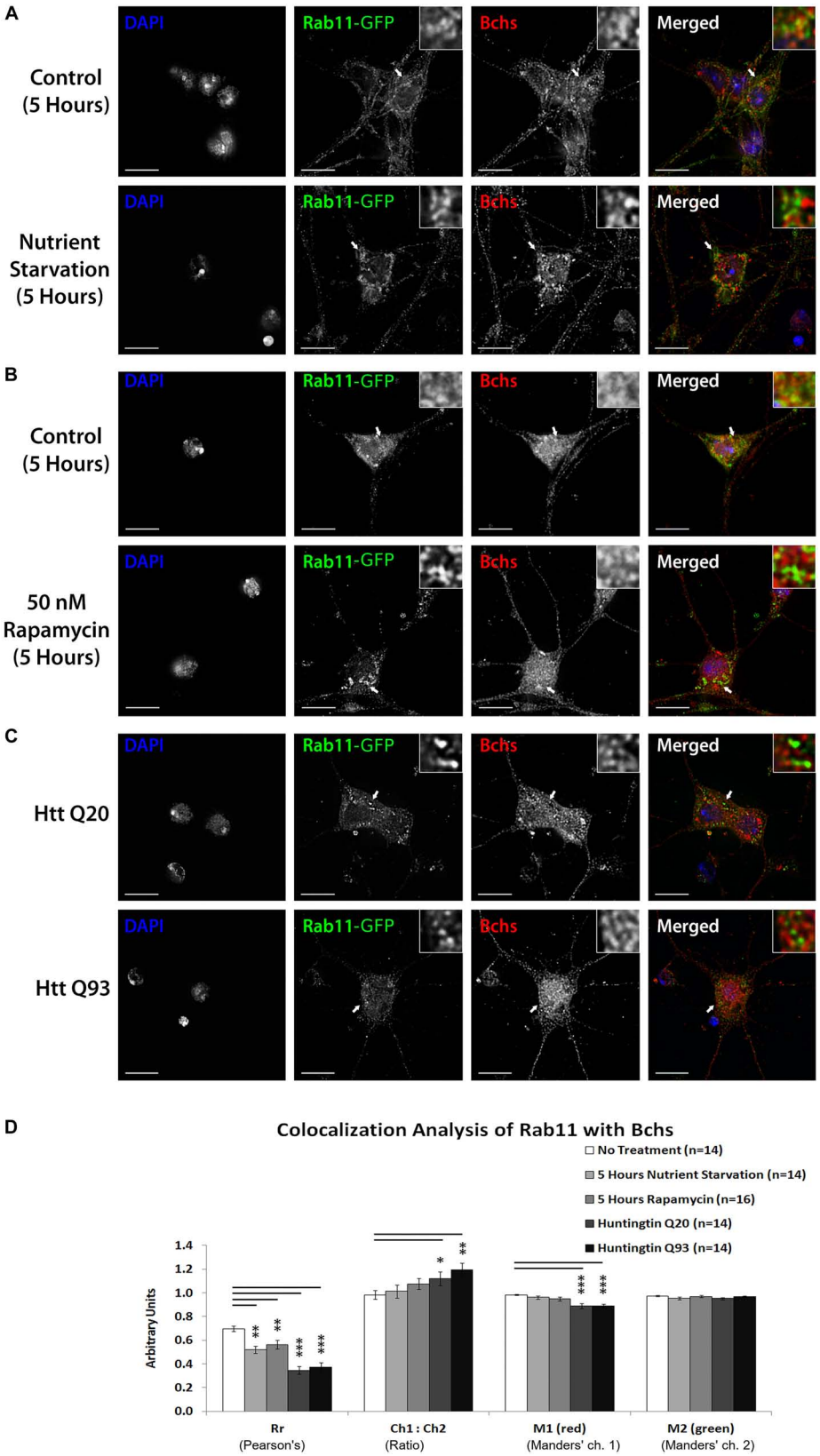

FIGURE 7 | Continued

FIGURE 7 | Bchs dissociates more from Rab11-GFP during selective autophagy than non-selective autophagy. Third instar larval primary neurons were immunostained for endogenous Bchs and transgenic Rab11-GFP using anti-Bchs and anti-GFP antibodies after different conditions of autophagy induction: **(A)** five hours of nutrient starvation by incubation with serum-free HL-3 buffer, **(B)** five hours of incubation with 50 nM rapamycin in complete medium, and **(C)** Htt normal (Q20) and expanded (Q93) polyQ expression. The top-right inset shows a 5× magnification of one of the indicated regions. Scalebar = 5 μm. **(D)** Colocalization analysis was performed using ImageJ to obtain Rr (Pearson's correlation coefficient), Ch1:Ch2 ratio (red:green pixels ratio), M1 and M2 (Manders' colocalization coefficients for channels 1 and 2). Error bars represent standard error of the mean for n = number of single-slice images. Unpaired Student's *t*-test was used for the statistical comparison between treatment and non-treatment groups. $*p < 0.05$, $**p < 0.01$, and $***p < 0.001$.

constitutively in the neurite tips of mouse primary neurons and these then mature as they are transported retrograde in a dynein-dependent manner toward the cell soma (Maday et al., 2012). Further, fusion between autophagosomes and late endosomes at neuronal termini is required for recruitment of the necessary motor proteins for retrograde transport of the fused compartment, the amphisome (Cheng et al., 2015). Given the role of BEACH domain proteins in vesicle fusion events, and Bchs' effects on transport of endolysosomes in motor neuron axons (Lim and Kraut, 2009), involvement in this early step of autophagic clearance in synaptic termini (Friedman et al., 2012) seems a likely scenario for its function.

A number of exocytic SNARE proteins are required at the step of autophagosome biogenesis to promote Atg9 recycling through tubulo-vesicular clustering and membrane fusion at phagophore assembly sites (Nair et al., 2011). In addition, the Q-SNARE Syx17 mediates the fusion of autophagosomes with late endosomes and lysosomes in mammalian cells and *Drosophila* (Itakura et al., 2012; Takáts et al., 2013). Intriguingly, the BEACH protein LYST binds to SNARE proteins (Tchernev et al., 2002), and we also detected Bchs-dependent changes in Syx17 distribution in neurons, raising the possibility of Bchs interacting with this or other SNAREs to promote vesicle fusion. On the other hand, our finding of increased numbers of Atg8 vesicles after over-expression of the large BEACH isoform is reminiscent of the increased numbers of lysosomes that were seen after LYST over-expression (Durchfort et al., 2012). This would be consistent with a similar role in vesicle fission (not fusion), as LYST and related proteins are thought to perform (Kypri et al., 2013), whereby BEACH proteins are implicated as accessories in both fission and fusion events of different vesicle populations (Cullinane et al., 2013). Bchs' possible role in vesicle trafficking and membrane dynamics, in the context of its recently reported genetic interactions with sphingolipid lipases (Hebbar et al., 2015) will be an interesting avenue to investigate in the future.

MATERIALS AND METHODS

Drosophila Stocks and Maintenance

Flies were raised on standard yeast/cornmeal agar food at 25°C. The fly lines used were *bchs58(O)*, *bchs58(M)*, *bchs17(M)*, *Df(2L)clot7*, *yw; EPgy2 Atg7[EY10058]* (Bloomington Drosophila Stock Center); *w; Atg7[d77]/CyO-GFP*, and *yw; UAS-mCherry-Atg8a* and UAS-Atg1(6A) were kindly provided by Thomas Neufeld. *yw;+; UAS-RFP-Atg5*, *w;+; UAS-Rab11-GFP*, and the Htt-polyQ expressing lines *w; UAS-Htt exon1-Q20* and *-Q93* were generous gifts of Katja Köhler, Sean Sweeney, Henry Chang, and Larry Marsh, respectively. The *bchsLL03462* and UAS-Atg1^{GS10797} stocks were obtained from Drosophila Genomics and Genetic Resources Stock Center in Kyoto Institute of Technology. *bchs* RNAi line #45028 was from the Vienna Drosophila Resource Center (VDRC). The eve-Gal4>UAS-CD8-GFP stock (an *even-skipped* driver combined with a membrane-bound GFP marker) was a kind gift of Miki Fujioka.

RT-PCR of *bchs* and *atg7* Transcripts and Generation of GFP-Bchs

Larval or adult brains were homogenized in 400 μL of TRIzol® reagent (Life Technologies, 15596-026), and total RNA was extracted with chloroform:TRIzol® 1:5. RT PCR was performed using Promega (A5000) M-MLV reverse transcriptase as per manufacturer's instructions, and PCR was carried out on each cDNA sample with GoTaq® polymerase (Promega, M3005). Gene specific primers used to amplify *bchs* splice isoform 2 were forward = GCAAACAGTTCAGACAATATAC and reverse = AAGATCCTTTATCAGCTGCTTGGC, and splice isoform 3 were forward = GATGGACAGAAAACGATGCTACC and reverse = TTCGCAGGATGAATTTCTCGTG. *atg7* specific primers were: forward = TCCGCAGACGGATTGATCTC and reverse = TGAACATCGATGACAGCCTTG; PCR primers for *rp49* were: forward = AGTCGGATCGATATGCTAAG and reverse = AGTAAACGCGGTTCTGCATG. *bchs* isoforms were cloned into pUAST vector containing a GFP tag at the 5′ end. Transgenic animals were generated by Best Gene (Chino Hills, CA, United States).

Motor Neuron Viability Assay

Third instar larvae were dissected, fixed 30 min in 4% paraformaldehyde (Sigma Aldrich, P6148), blocked 1 h in 5% bovine serum albumin (BSA) (PAA Laboratories, K41-001) in 0.1% Triton X-100 PBS (PBT), and incubated overnight at 4°C with primary antibodies: 1:500 anti-GFP (Clontech Laboratories, 632377), 1:10 1D4 anti-fasciclin II and 1:20 22C10 anti-futsch (Developmental Studies Hybridoma Bank), and washed in PBT. Secondary antibodies were 1:800 Cy2-conjugated goat anti-rabbit and 1:800 Cy3-conjugated goat anti-mouse (Jackson ImmunoResearch Laboratories, 111-225-144 and 115-165-146) in PBT. Motor neuron viability was scored by inspection. RP2 survival was scored as a percentage over total hemisegments and repeated in triplicate. Chi-square statistical test was performed.

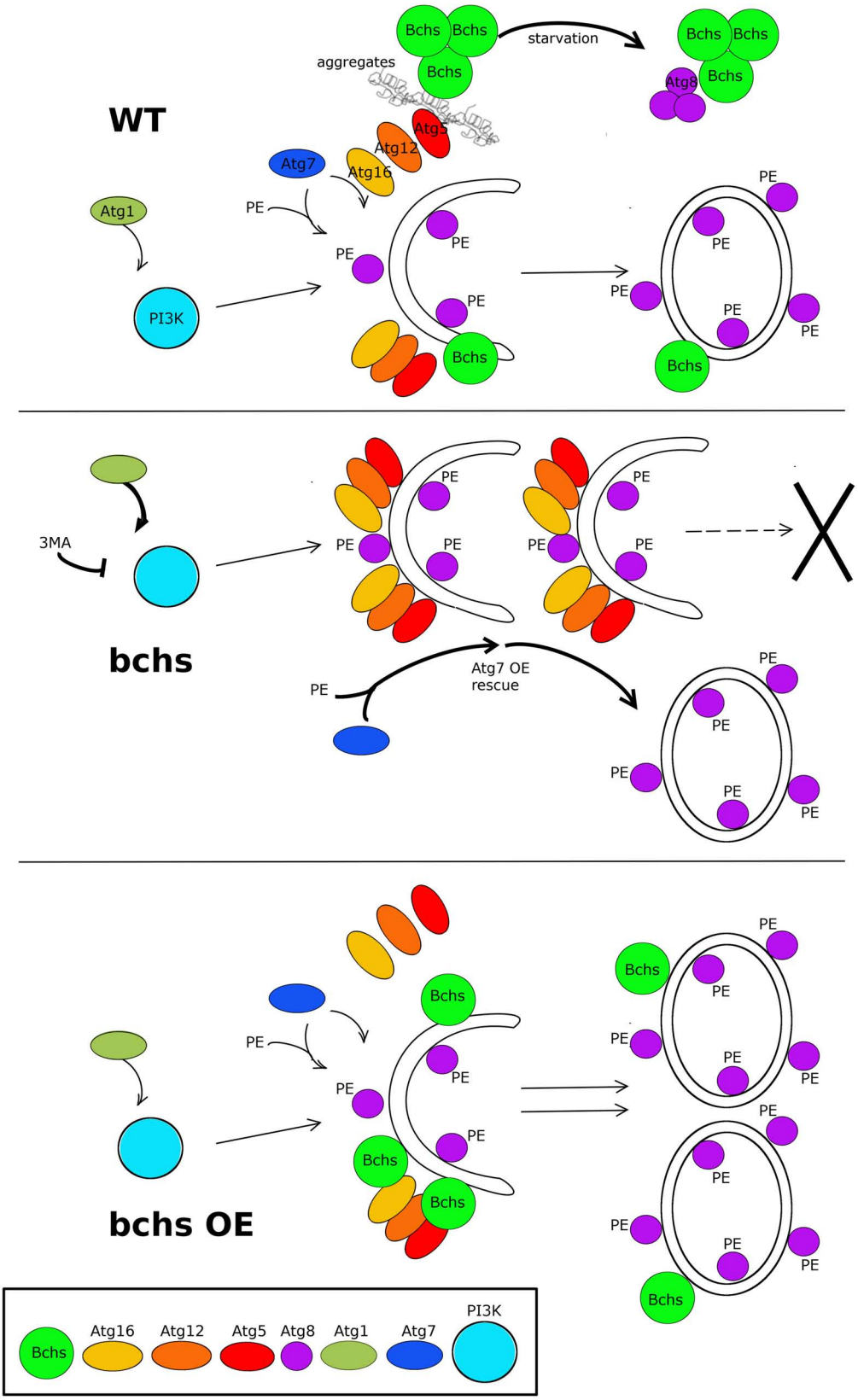

FIGURE 8 | Continued

FIGURE 8 | Schematic model of the possible relationship of Bchs and the autophagy pathway in the clearance of aggregated proteins and Atg8-carrying vesicle production. In the wild type situation (top), Bchs associates preferentially with Atg5 during the induction of aggrephagy (squiggly lines), and this association is suppressed by starvation-induced autophagy, wherein Bchs colocalizes more with Atg8. In the *bchs* case (middle), full maturation to Atg8-marked vesicles is reduced (−>X), and this is epistatic to upstream PI3K activation or inhibition by Atg1 or 3MA, but can be overcome by over-expressing Atg7 (thick arrows). Bchs over-expression (bchs OE; bottom) drives the maturation of autophagic vesicles to the Atg8-marked stage.

Drug Treatments and Western Analysis

Embryos were collected every 3 h on apple juice agar plates, and incubated at 25°C for 24 h; hatching first instar larvae were transferred into 2.0 mL Eppendorf tubes with food containing 0.05% (v/v) ethanol (vehicle control), 1 μM rapamycin (AG Scientific), 0.2 or 2 μM Wortmannin (AG Scientific; R-1018) or 5 mM 3-methyladenine (Calbioche®m, Merck Millipore, 189490), and dissected as third instar larvae. 10 μM Chloroquine was added to primary cultures for 2 h before fixation and staining with anti-mCherry. For Westerns, 5 third instar larval brains or 3 heads per treatment per lane were collected, frozen on dry ice, and ground with a pestle in RIPA lysis buffer (Thermo Fisher Scientific) with protease inhibitor cocktail. Rabbit anti-Bchs [for details see Lim and Kraut (2009)] or Rabbit anti-pS6K (Cell Signaling) were diluted 1:6000 and 1:1000, respectively, incubated on blots overnight at 4C, and detected with HRP-coupled secondary and SuperSignal West Pico plus reagent (Thermo Fisher Scientific).

Quantitative Size Analysis of Ubiquitinated Aggregates in Larval Neuromuscular Junctions

Aggregates were detected with 1:1000 mouse anti-poly-ubiquitin (clone FK2, Enzo Life Sciences, BML-PW8810) and 1:800 Cy5-goat anti-mouse and 1:500 Cy2-goat anti-horse radish peroxidase (Jackson ImmunoResearch Laboratories, 115-175-146 and 123-095-021). Image stacks were acquired under 40× objective lens with a DeltaVision OMX®microscope (Applied Precision) and deconvolved with softWoRx®5.0. To measure aggregate area, ImageJ particle analysis was used (Ullrich et al., 1996). The measurement scale (in microns) was defined on the image projection, adjusted to a segmentation threshold of 70, and converted to a binary image. A region of interest (ROI) was marked and 'Analyze Particles' used to measure the area of particles within the ROI. Particle size was categorized into 0–1, 1.1–10, and 10.1–50 μm^2. Percentages of neuromuscular junctions with aggregates in each of the three groups were calculated for each experimental set, which was repeated in triplicate, and a Chi-square statistical test was performed.

Primary Neuron Culture From Third Instar Larval Brains, and Imaging of GFP-Bchs-1

The protocol was modified from Kraft et al. (2006). Larvae were washed with 90% ethanol three times and sterile water twice to remove debris and contaminants. Four third instar larval brains were extracted in Shields and Sang, bacto-peptone and yeast extract (Sigma-Aldrich, S8398) medium containing penicillin-streptomycin and antibiotics-antimycotics (PAA Laboratories, P11-002), washed with sterile hemolymph-like 3 (HL-3) saline (70 mM NaCl, 115 mM sucrose, 5 mM trehalose, 5 mM KCl, 20 mM $MgCl_2$, 1 mM $CaCl_2$, 10 mM $NaHCO_3$, 5 mM HEPES, pH 7.4) three times, and incubated with 0.5 mg/mL collagenase type 1 (Sigma-Aldrich, C1639) in HL-3 1 h at room temperature. Brain tissue was then washed three times with complete medium with 10% heat-inactivated fetal bovine serum (HyClone, Thermo Fisher Scientific, SH30070.03), 20 μg/mL of bovine pancreas insulin (Sigma-Aldrich, I1882), penicillin-streptomycin and antibiotics-antimycotics. Brains were dissociated into a final volume of 150 μL as a single cell suspension by trituration and then aliquoted onto 22 mm^2 acid-washed cover-slips coated with 30 μg/mL of mouse laminin (BD Biosciences, 354232) and 167 μg/mL of concanavalin A (Sigma Aldrich, C0412) in 35 mm culture dishes and allowed to attach ∼12 h. 900 μL of complete medium was added to the culture dish and incubated for 1–4 days.

For the colocalization in **Figure 1**, live primary neurons from larval offspring of elav-Gal4>mCherry-Atg8a or elav-Gal4> UAS-RFP-Atg5 crossed with UAS-GFP-bchs-1, 2, or 3 were imaged at 60× magnification on the DeltaVision microscope as above, using Z-stack acquisition of 200 nm optical slices with interleaving green and red channels at 150 ms exposures. 100 image stacks for each colocalization were examined at each Z-level, and where vesicular localization of the Bchs isoform was detectable, the individual vesicle was then visually inspected in red/green image pairs for complete, non-, or partial overlap of Bchs with mCherry-Atg8a or RFP-Atg5. The colocalization algorithm used below was not applied here because of a high cytoplasmic expression level of the GFP-Bchs isoforms. Each vesicle expressing Bchs was only counted once. Standard error was calculated by averaging the percentages in each of the three categories ("yes," "no," or "partial") over the data separated into three equal batches of images.

Immunocytochemistry and Image Analysis of Compartments in *bchs* Primary Neurons

bchs and wild-type primary neurons were fixed with 4% paraformaldehyde in PBS for 15 min at room temperature and blocked with 5% normal goat serum (Life Technologies, 50-062Z) in 0.05% Triton X-100 PBS for 1 h. Antibody staining was performed as above with 1:1000 mouse anti-poly-ubiquitin (clone FK2, Enzo Life Sciences, BML-PW8810) and 1:500 rabbit anti-drAtg5 (Novus Biologicals, NB110-74818) or 1:500 rabbit anti-drAtg8a (a kind gift of Katja Köhler); anti-p62 (1:500) was kindly donated by Nezis et al. (2008). Samples were incubated with 1 μg/mL of 4′,6-diamidino-2-phenylindole (DAPI), dihydrochloride (Life Technologies, D1306) in PBS for

3 min, washed briefly with PBS, then water, and imaged at 60× magnification.

For the image analysis in **Figure 4**, images of primary neuron cultures were acquired as Z-stacks, with the step of 200 nm in between slices, using the same exposure, light intensity and filter settings for every condition. Collected stacks were then deconvolved as above, and converted into 16-bit TIFF stacks in FIJI[1] using LOCI BioFormats plug-in (Linkert et al., 2010). Each stack was then Z-projected using the maximum intensity method. Images were inspected under DAPI channel and only single cells, or small aggregates (<5 cells) with clearly separated cell nuclei were used for further spot counting. Because of varying spot intensity relative to cell body, and variable background signal, spots were counted manually, after setting the same display range of values. The cell number N used for calculations varied between conditions ($N_{average}$ ~100), but was not less than N_{min} = 50. The average spot number per cell and the standard error of the mean (SEM) were calculated. To measure spot characteristics, projected images were masked using the Maximum Entropy threshold method (Kapur et al., 1985). Brightness and size distribution and SEM of selected spots were measured using the Analyze Particles FIJI command.

Analysis of mCherry-Atg8 and Syx17 compartment size and brightness for **Supplementary Figure S8** was carried out on images acquired with a Yokogawa Spinning Disk confocal microscope with a 100×/1.4 NA Silicon immersion lens, using the Fiji plugin "find maxima" with the same manual threshold for all images, such that obvious spots of expression could be detected. All images were collected with identical exposure and laser power settings for the mCherry and Syx17 channels, and controls were processed in parallel for all experiments. For each condition, 80–100 individual images each with several neurons were assessed.

Quantitative Colocalization Analysis of Bchs With Different Compartmental Markers

Autophagy was induced in primary neurons by 5 h of nutrient starvation with HL-3, 5 h of 50 nM rapamycin in complete medium or Huntingtin Q93 expression. Controls (basal autophagy) were incubated in complete medium. Antibody staining was performed as above. For mCherry-Atg8a or RFP-Atg5, primary antibodies were 1:500 rabbit anti-Bchs and 1:100 mouse anti-DsRed (BD Pharmingen™, 551814). For Rab11-GFP, primary antibodies were rabbit anti-Bchs and 1:1000 mouse anti-GFP (Clontech Laboratories, 632375). Colocalization analysis was done with the ImageJ plugin 'Intensity Correlation Analysis' after channel splitting and background subtraction (Li et al., 2004). Rr (Pearson's correlation coefficient), Ch1:Ch2 ratios, M1 and M2 (Manders' colocalization coefficient for channel 1 and 2, with thresholding) were tabulated for each image. Unpaired Student's *t*-test was used to calculate *p*-values between treated and control groups.

[1]http://fiji.sc

Time-Lapse Imaging of GFP-Bchs With RFP-Atg5 or mCherry-Atg8a in Primary Neurons

Primary neurons expressing *GFP-Bchs* and *RFP-Atg5* or *mCherry-Atg8a* transgenes via elav-Gal4 were cultured on 35 mm glass bottom dishes (World Precision Instruments, FD35-100) coated as described above. For basal autophagy, cells were incubated in complete culture medium at room temperature and single focal-plane images were acquired for GFP-Bchs: green channel = 50% transmission, 800 ms; RFP-Atg5: red channel = 50% transmission, 800 ms; and mCherry-Atg8a: red channel = 32% transmission, 600 ms, every 10 min over 4 h, and deconvolved. For nutrient starvation, neurons were incubated in HL-3 saline at room temperature and immediately imaged as described. For transfection of Huntingtin 15Q or 128Q, 3 μL of FuGENE®HD transfection reagent (Promega, E2311) was used to couple 1 μg of pCINeoHtt1955.15Q.wt or pCINeoHtt1955.128Q.wt plasmid DNA (kind gift of Anat Yanai and Mahmoud Pouladi), respectively in a 3:1 ratio in a final volume of 50 μL complete culture medium without penicillin/streptomycin and antibiotics/antimycotics for 10 min at room temperature, and added to the cells with 1 mL of complete culture medium without penicillin/streptomycin and antibiotics/antimycotics for 48 h (without medium change).

AUTHOR CONTRIBUTIONS

JS, KO, and RK carried out experiments, interpreted results, and prepared figures. IAG carried out the experiments. AM carried out image analysis. JS drafted the manuscript and RK revised the manuscript.

FUNDING

This work was funded by the Biomedical Research Council of Singapore grant #09/1/22/19/610 and the Ministry of Education of Singapore grant #MOE2013-T1-002-229, a Bundesministerium für Bildung und Forschung (BMBF) Singapore–Germany cooperation grant to RK, and the Eleonore Trefftz Programme for visiting Women Professors at TU Dresden.

ACKNOWLEDGMENTS

We are very grateful to Prof. Michael Brand of the BIOTEC, TU Dresden and Prof. Eli Knust for support during manuscript revisions. We thank Catrin Hälsig for help in Western blots in **Figure 1A′**, Britta Schroth-Diez, Robert Haase, and Benoit Lombardot of the Laser Microscopic Imaging and Image Analysis Facilities for help in spinning disk imaging and Fiji analyses, all at the Max-Planck Institute of Molecular Cell Biology and Genetics (MPI-CBG) in Dresden. We would also like to

sincerely thank the final year project students Liyanah Mohd Zaffre, Hong Hwee Lim, Bruno Yip, and Weixin Xu, at the School of Biological Sciences, NTU Singapore, for contributing data to the live imaging analysis with GFP-bchs, and the Wortmannin and rapamycin studies.

SUPPLEMENTARY MATERIAL

The Supplementary Material for this article can be found online at: https://www.frontiersin.org/articles/10.3389/fcell.2019.00129/full#supplementary-material

REFERENCES

Bové, J., Martinez-Vicente, M., and Vila, M. (2011). Fighting neurodegeneration with rapamycin: mechanistic insights. *Nat. Rev. Neurosci.* 12, 437–452.

Cheng, X.-T., Zhou, B., Lin, M.-Y., Cai, Q., and Sheng, Z.-H. (2015). Axonal autophagosomes recruit dynein for retrograde transport through fusion with late endosomes. *J. Cell Biol.* 209, 377–386. doi: 10.1083/jcb.201412046

Clausen, T. H., Lamark, T., Isakson, P., Finley, K., Larsen, K. B., Brech, A., et al. (2010). p62/SQSTM1 and ALFY interact to facilitate the formation of p62 bodies/ALIS and their degradation by autophagy. *Autophagy* 6, 330–344. doi: 10.4161/auto.6.3.11226

Cuervo, A. M. (2008). Autophagy and aging: keeping that old broom working. *Trends Genet.* 24, 604–612. doi: 10.1016/j.tig.2008.10.002

Cullinane, A. R., Schäffer, A. A., and Huizing, M. (2013). The BEACH Is hot: a LYST of emerging roles for BEACH-domain containing proteins in human disease. *Traffic* 14, 749–766. doi: 10.1111/tra.12069

Dunst, S., Kazimiers, T., von Zadow, F., Jambor, H., Sagner, A., Brankatschk, B., et al. (2015). Endogenously tagged rab proteins: a resource to study membrane trafficking in drosophila. *Dev. Cell* 33, 351–365. doi: 10.1016/j.devcel.2015.03.022

Durchfort, N., Verhoef, S., Vaughn, M. B., Shrestha, R., Adam, D., Kaplan, J., et al. (2012). The enlarged lysosomes in beige(j) cells result from decreased lysosome fission and not increased lysosome fusion. *Traffic* 13, 108–119. doi: 10.1111/j.1600-0854.2011.01300.x

Filimonenko, M., Isakson, P., Finley, K. D., Anderson, M., Jeong, H., Melia, T. J., et al. (2010). The selective macroautophagic degradation of aggregated proteins requires the PI3P-binding protein Alfy. *Mol. Cell* 38, 265–279. doi: 10.1016/j.molcel.2010.04.007

Finley, K. D., Edeen, P. T., Cumming, R. C., Mardahl-Dumesnil, M. D., Taylor, B. J., Rodriguez, M. H., et al. (2003). Blue cheese mutations define a novel, conserved gene involved in progressive neural degeneration. *J. Neurosci.* 23, 1254–1264. doi: 10.1523/jneurosci.23-04-01254.2003

Friedman, L. G., Lachenmayer, M. L., Wang, J., He, L., Poulose, S. M., Komatsu, M., et al. (2012). Disrupted autophagy leads to dopaminergic axon and dendrite degeneration and promotes presynaptic accumulation of Î ± -synuclein and LRRK2 in the brain. *J. Neurosci.* 32, 7585–7593. doi: 10.1523/jneurosci.5809-11.2012

Ganley, I. G. (2013). Autophagosome maturation and lysosomal fusion. *Essays Biochem.* 55, 65–78. doi: 10.1042/bse0550065

Geng, J., and Klionsky, D. J. (2008). The Atg8 and Atg12 ubiquitin-like conjugation systems in macroautophagy. *EMBO Rep.* 9, 859–864. doi: 10.1038/embor.2008.163

Glickman, M. H., and Ciechanover, A. (2002). The ubiquitin-proteasome proteolytic pathway: destruction for the sake of construction. *Physiol. Rev.* 82, 373–428. doi: 10.1152/physrev.00027.2001

Hanada, T., Noda, N. N., Satomi, Y., Ichimura, Y., Fujioka, Y., Takao, T., et al. (2007). The Atg12-Atg5 conjugate has a novel E3-like activity for protein lipidation in autophagy. *J. Biol. Chem.* 282, 37298–37302. doi: 10.1074/jbc.c700195200

Hayashi-Nishino, M., Fujita, N., Noda, T., Yamaguchi, A., Yoshimori, T., and Yamamoto, A. (2009). A subdomain of the endoplasmic reticulum forms a cradle for autophagosome formation. *Nat. Cell Biol.* 11, 1433–1437. doi: 10.1038/ncb1991

Hebbar, S., Sahoo, I., Matysik, A., Argudo Garcia, I., Osborne, K. A., Papan, C., et al. (2015). ceramides and stress signalling intersect with autophagic defects in neurodegenerative drosophila blue cheese (bchs) mutants. *Sci. Rep.* 5:15926. doi: 10.1038/srep15926

Itakura, E., Kishi-Itakura, C., and Mizushima, N. (2012). The hairpin-type tail-anchored SNARE syntaxin 17 targets to autophagosomes for fusion with endosomes/lysosomes. *Cell* 151, 1256–1269. doi: 10.1016/j.cell.2012.11.001

Iwata, A., Riley, B. E., Johnston, J. A., and Kopito, R. R. (2005). HDAC6 and microtubules are required for autophagic degradation of aggregated huntingtin. *J. Biol. Chem.* 280, 40282–40292. doi: 10.1074/jbc.m508786200

Juhasz, G., Erdi, B., Sass, M., and Neufeld, T. P. (2007). Atg7-dependent autophagy promotes neuronal health, stress tolerance, and longevity but is dispensable for metamorphosis in Drosophila. *Genes Dev.* 21, 3061–3066. doi: 10.1101/gad.1600707

Kabeya, Y., Mizushima, N., Ueno, T., Yamamoto, A., Kirisako, T., Noda, T., et al. (2000). LC3, a mammalian homologue of yeast Apg8p, is localized in autophagosome membranes after processing. *EMBO J.* 19, 5720–5728. doi: 10.1093/emboj/19.21.5720

Kapur, J. N., Sahoo, P. K., and Wong, A. K. C. (1985). A new method for gray-level picture thresholding using the entropy of the histogram. *Comput. Vis. Graph. Image Process.* 29, 273–285. doi: 10.1016/0734-189x(85)90125-2

Khodosh, R., Augsburger, A., Schwarz, T. L., and Garrity, P. A. (2006). Bchs, a BEACH domain protein, antagonizes Rab11 in synapse morphogenesis and other developmental events. *Development* 133, 4655–4665. doi: 10.1242/dev.02650

Kraft, R., Escobar, M. M., Narro, M. L., Kurtis, J. L., Efrat, A., Barnard, K., et al. (2006). Phenotypes of drosophila brain neurons in primary culture reveal a role for fascin in neurite shape and trajectory. *J. Neurosci.* 26, 8734–8747. doi: 10.1523/jneurosci.2106-06.2006

Kuma, A., Mizushima, N., Ishihara, N., and Ohsumi, Y. (2002). Formation of the 350-kDa Apg12-Apg5·Apg16 multimeric complex, mediated by Apg16 oligomerization, is essential for autophagy in yeast. *J. Biol. Chem.* 277, 18619–18625. doi: 10.1074/jbc.m111889200

Kypri, E., Falkenstein, K., and Lozanne, A. D. (2013). Antagonistic control of lysosomal fusion by Rab14 and the Lyst-related protein LvsB. *Traffic* 14, 599–609. doi: 10.1111/tra.12058

Levine, B., and Klionsky, D. J. (2004). Development by self-digestion. *Dev. Cell* 6, 463–477. doi: 10.1016/s1534-5807(04)00099-1

Li, Q., Lau, A., Morris, T. J., Guo, L., Fordyce, C. B., and Stanley, E. F. (2004). A syntaxin 1, Gαo, and N-type calcium channel complex at a presynaptic nerve terminal: analysis by quantitative immunocolocalization. *J. Neurosci.* 24, 4070–4081. doi: 10.1523/jneurosci.0346-04.2004

Lim, A., and Kraut, R. (2009). The drosophila BEACH family protein, blue cheese, links lysosomal axon transport with motor neuron degeneration. *J. Neurosci.* 29, 951–963. doi: 10.1523/JNEUROSCI.2582-08.2009

Linkert, M., Rueden, C. T., Allan, C., Burel, J.-M., Moore, W., Patterson, A., et al. (2010). Metadata matters: access to image data in the real world. *J. Cell Biol.* 189, 777–782. doi: 10.1083/jcb.201004104

Longatti, A., Lamb, C. A., Razi, M., Yoshimura, S., Barr, F. A., and Tooze, S. A. (2012). TBC1D14 regulates autophagosome formation via Rab11- and ULK1-positive recycling endosomes. *J. Cell Biol.* 197, 659–675. doi: 10.1083/jcb.201111079

Lynch-Day, M. A., and Klionsky, D. J. (2010). The Cvt pathway as a model for selective autophagy. *Autophagy* 584, 1359–1366. doi: 10.1016/j.febslet.2010.02.013

Maday, S., Wallace, K. E., and Holzbaur, E. L. F. (2012). Autophagosomes initiate distally and mature during transport toward the cell soma in primary neurons. *J. Cell Biol.* 196, 407–417. doi: 10.1083/jcb.201106120

Mizushima, N. (2010). The role of the Atg1/ULK1 complex in autophagy regulation. *Cell Regul.* 22, 132–139. doi: 10.1016/j.ceb.2009.12.004

Mizushima, N., Ohsumi, Y., and Yoshimori, T. (2002). Autophagosome formation in mammalian cells. *Cell Struct. Funct.* 27, 421–429. doi: 10.1247/csf.27.421

Nair, U., Jotwani, A., Geng, J., Gammoh, N., Richerson, D., Yen, W.-L., et al. (2011). SNARE proteins are required for macroautophagy. *Cell* 146, 290–302. doi: 10.1016/j.cell.2011.06.022

Nedelsky, N. B., Todd, P. K., and Taylor, J. P. (2008). Autophagy and the ubiquitin-proteasome system: collaborators in neuroprotection. *Ubiquitin Proteasomes Dis.* 1782, 691–699. doi: 10.1016/j.bbadis.2008.10.002

Nezis, I. P., Simonsen, A., Sagona, A. P., Finley, K., Gaumer, S., Contamine, D., et al. (2008). Ref(2)P, the Drosophila melanogaster homologue of mammalian p62, is required for the formation of protein aggregates in adult brain. *J. Cell Biol.* 180, 1065–1071. doi: 10.1083/jcb.200711108

Ohsumi, Y. (2001). Molecular dissection of autophagy: two ubiquitin-like systems. *Nat. Rev. Mol. Cell Biol.* 2, 211–216. doi: 10.1038/35056522

Pandey, U. B., Nie, Z., Batlevi, Y., McCray, B. A., Ritson, G. P., Nedelsky, N. B., et al. (2007). HDAC6 rescues neurodegeneration and provides an essential link between autophagy and the UPS. *Nature* 447, 860–864. doi: 10.1038/nature05853

Powis, G., Bonjouklian, R., Berggren, M. M., Gallegos, A., Abraham, R., Ashendel, C., et al. (1994). Wortmannin, a potent and selective inhibitor of phosphatidylinositol-3-kinase. *Cancer Res.* 54, 2419–2423.

Puri, C., Renna, M., Bento, C. F., Moreau, K., and Rubinsztein, D. C. (2013). Diverse autophagosome membrane sources coalesce in recycling endosomes. *Cell* 154, 1285–1299. doi: 10.1016/j.cell.2013.08.044

Ravikumar, B., Vacher, C., Berger, Z., Davies, J. E., Luo, S., Oroz, L. G., et al. (2004). Inhibition of mTOR induces autophagy and reduces toxicity of polyglutamine expansions in fly and mouse models of Huntington disease. *Nat. Genet.* 36, 585–595. doi: 10.1038/ng1362

Rubinsztein, D. C., and Nixon, R. A. (2010). Rapamycin induces autophagic flux in neurons. *Proc. Natl. Acad. Sci. U.S.A.* 107, E181–E181.

Sarkar, S., Ravikumar, B., Floto, R. A., and Rubinsztein, D. C. (2008). Rapamycin and mTOR-independent autophagy inducers ameliorate toxicity of polyglutamine-expanded huntingtin and related proteinopathies. *Cell Death Differ.* 16, 46–56. doi: 10.1038/cdd.2008.110

Schneider, C. A., Rasband, W. S., and Eliceiri, K. W. (2012). NIH image to ImageJ: 25 years of image analysis. *Nat. Meth.* 9, 671–675. doi: 10.1038/nmeth.2089

Scott, R. C., Juhasz, G., and Neufeld, T. P. (2007). Direct induction of autophagy by Atg1 inhibits cell growth and induces apoptotic cell death. *Curr. Biol.* 17, 1–11. doi: 10.1016/j.cub.2006.10.053

Seglen, P. O., and Gordon, P. B. (1982). 3-methyladenine: specific inhibitor of autophagic/lysosomal protein degradation in isolated rat hepatocytes. *Proc. Natl. Acad. Sci. U.S.A.* 79, 1889–1892. doi: 10.1073/pnas.79.6.1889

Simonsen, A., Birkeland, H. C., Gillooly, D. J., Mizushima, N., Kuma, A., Yoshimori, T., et al. (2004). Alfy, a novel FYVE-domain-containing protein associated with protein granules and autophagic membranes. *J. Cell Sci.* 117, 4239–4251. doi: 10.1242/jcs.01287

Simonsen, A., Cumming, R. C., Lindmo, K., Galaviz, V., Cheng, S., Rusten, T. E., et al. (2007). Genetic modifiers of the drosophila blue cheese gene link defects in lysosomal transport with decreased life span and altered ubiquitinated-protein profiles. *Genetics* 176, 1283–1297. doi: 10.1534/genetics.106.065011

Takáts, S., Nagy, P., Varga, Á., Pircs, K., Kárpáti, M., Varga, K., et al. (2013). Autophagosomal syntaxin17-dependent lysosomal degradation maintains neuronal function in Drosophila. *J. Cell Biol.* 201, 531–539. doi: 10.1083/jcb.201211160

Takáts, S., Pircs, K., Nagy, P., Varga, Á., Kárpáti, M., Hegedűs, K., et al. (2014). Interaction of the HOPS complex with Syntaxin 17 mediates autophagosome clearance in *Drosophila*. *Mol. Biol. Cell* 25, 1338–1354. doi: 10.1091/mbc.E13-08-0449

Tchernev, V. T., Mansfield, T. A., Giot, L., Kumar, A. M., Nandabalan, K., Li, Y., et al. (2002). The chediak-higashi protein interacts with SNARE complex and signal transduction proteins. *Mol. Med.* 8, 56–64. doi: 10.1007/bf03402003

Ullrich, O., Reinsch, S., Urbé, S., Zerial, M., and Parton, R. G. (1996). Rab11 regulates recycling through the pericentriolar recycling endosome. *J. Cell Biol.* 135, 913–924. doi: 10.1083/jcb.135.4.913

Wilcke, M., Johannes, L., Galli, T., Mayau, V., Goud, B., and Salamero, J. (2000). Rab11 regulates the compartmentalization of early endosomes required for efficient transport from early endosomes to the trans-golgi network. *J. Cell Biol.* 151, 1207–1220. doi: 10.1083/jcb.151.6.1207

Ylä-Anttila, P., Vihinen, H., Jokitalo, E., and Eskelinen, E. (2009). 3D tomography reveals connections between the phagophore and endoplasmic reticulum. *Autophagy* 5, 1180–1185. doi: 10.4161/auto.5.8.10274

Conflict of Interest Statement: The authors declare that the research was conducted in the absence of any commercial or financial relationships that could be construed as a potential conflict of interest.

frontiers in Cell and Developmental Biology

ORIGINAL RESEARCH
published: 19 September 2019
doi: 10.3389/fcell.2019.00187

Coupling Phase Behavior of Fatty Acid Containing Membranes to Membrane Bio-Mechanics

*Arwen I. I. Tyler[1,2†], Jake L. Greenfield[1,3†], John M. Seddon[1], Nicholas J. Brooks[1] and Sowmya Purushothaman[4,5]**

[1] Department of Chemistry, Imperial College London, London, United Kingdom, [2] School of Food Science and Nutrition, University of Leeds, Leeds, United Kingdom, [3] Department of Chemistry, University of Cambridge, Cambridge, United Kingdom, [4] Department of Material Science, University of California, Davis, Davis, CA, United States, [5] Cavendish Laboratory, Cambridge, United Kingdom

OPEN ACCESS

Edited by:
Rachel Susan Kraut,
Max Planck Institute of Molecular Cell Biology and Genetics (MPI-CBG), Germany

Reviewed by:
James Alan Marrs,
Indiana University – Purdue University Indianapolis, United States
Ales Iglic,
University of Ljubljana, Slovenia
Cláudia Nunes,
LAQV Network of Chemistry and Technology, Portugal

***Correspondence:**
Sowmya Purushothaman
sowmya.purushothaman@gmail.com

[†]These authors have contributed equally to this work

Specialty section:
This article was submitted to Membrane Traffic, a section of the journal Frontiers in Cell and Developmental Biology

Received: 04 February 2019
Accepted: 22 August 2019
Published: 19 September 2019

Citation:
Tyler AII, Greenfield JL, Seddon JM, Brooks NJ and Purushothaman S (2019) Coupling Phase Behavior of Fatty Acid Containing Membranes to Membrane Bio-Mechanics. Front. Cell Dev. Biol. 7:187. doi: 10.3389/fcell.2019.00187

Biological membranes constantly modulate their fluidity for proper functioning of the cell. Modulation of membrane properties via regulation of fatty acid composition has gained a renewed interest owing to its relevance in endocytosis, endoplasmic reticulum membrane homeostasis, and adaptation mechanisms in the deep sea. Endowed with significant degrees of freedom, the presence of free fatty acids can alter the curvature of membranes which in turn can alter the response of curvature sensing proteins, thus defining adaptive ways to reconfigure membranes. Most significantly, recent experiments demonstrated that polyunsaturated lipids facilitate membrane bending and fission by endocytic proteins – the first step in the biogenesis of synaptic vesicles. Despite the vital roles of fatty acids, a systematic study relating the interactions between fatty acids and membrane and the consequent effect on the bio-mechanics of membranes under the influence of fatty acids has been sparse. Of specific interest is the vast disparity in the properties of *cis* and *trans* fatty acids, that only differ in the orientation of the double bond and yet have entirely unique and opposing chemical properties. Here we demonstrate a combined X-ray diffraction and membrane fluctuation analysis method to couple the structural properties to the biophysical properties of fatty acid-laden membranes to address current gaps in our understanding. By systematically doping pure dioleoyl phosphatidylcholine (DOPC) membranes with *cis* fatty acid and *trans* fatty acid we demonstrate that the presence of fatty acids doesn't always fluidize the membrane. Rather, an intricate balance between the curvature, molecular interactions, as well as the amount of specific fatty acid dictates the fluidity of membranes. Lower concentrations are dominated by the nature of interactions between the phospholipid and the fatty acids. *Trans* fatty acid increases the rigidity while decreasing the area per lipid similar to the properties depicted by the addition of saturated fatty acids to lipidic membranes. *Cis* fatty acid however displays the accepted view of having a fluidizing effect at small concentrations. At higher concentrations curvature frustration dominates, leading to increased rigidity irrespective of the type of fatty acid. These results are consistent with theoretical predictions as detailed in the manuscript.

Keywords: *cis*, *trans*, lipid, membrane, bending rigidity, diabetes, polyunsaturated fatty acid

INTRODUCTION

Biomembranes are composed of a wide variety of lipids, fatty acids, proteins, and cholesterol that play a crucial role in membrane-mediated processes. The composition of membranes is actively regulated to maintain membrane fluidity, structure, viscosity, and stress (Funari et al., 2003). Modulation of these biophysical properties can be monitored to understand membrane-associated processes like protein–lipid interactions, enzymatic activity, and regulation of surface receptors (Klausner et al., 1980).

One class of biomolecule that crucially affects membrane fluidity is fatty acids. Occurring as mono- or poly-unsaturated chains, fatty acids play a crucial role in various cellular processes (DeLong and Yayanos, 1985; Shaikh and Edidin, 2006; Mota et al., 2013; Picard and Daniel, 2013; Turk and Chapkin, 2013). For example, in neurodegenerative disorders like Alzheimer's disease and Huntington disease, disruptions in fatty acid biosynthesis have been closely associated with the progression of the disease. One theory suggests that Sterol Regulatory Element Binding protein (SREBP) regulates lipid homeostasis by sensing the level of cholesterol in the cell, and provides negative feedback in synthesizing more cholesterol. Upon activation, SREBP acts as a transcription factor and stimulates expression of enzymes that regulate the fatty acid biosynthesis pathway (Sameni et al., 2018). The reduced biosynthesis of cholesterol and fatty acids is one of the early events in Huntington disease. Similar roles of perturbation of membrane fluidity upon addition of fatty acids have been reported recently. Piezo1, a mechano-sensitive channel, regulates crucial cellular processes like vascular architecture, cell migration, and erythrocyte volume. A study revealed that membrane fluidity was sensitive to the type of fatty acids incorporated, which in turn affected the activation of Piezo1 (Romero et al., 2019). Understanding how fatty acids affect membrane fluidity thus poses a biologically relevant challenge. Coupling the bio-mechanical properties of membranes with structural reorganization taking place as a result of addition of biomolecules could act as a powerful bio-marker in identifying the onset of disease. One of the advantages of using membrane mechanics as a biomarker lies in delineating the need to map complex, less known biochemical events that alter membrane function.

Motivated by developing a complete structure – mechanics study of the effect of fatty acids on lipid membranes, we combined X-ray diffraction measurements (*structural information*) with bending energy measurements (*Bio-mechanical information*) on phospholipid membranes doped with fatty acids. As a proof-of-concept, we demonstrate the effect of two mono-unsaturated fatty acids, oleic acid (OA) and elaidic acid (EA) differing in the *cis–trans* configuration of the double bond (**Figure 1**), on dioleoylphosphatidylcholine (DOPC) bilayers. Both OA and EA have same molecular weight but the presence of a kink in OA makes them structurally different; EA has a more cylindrical shape and resembles saturated fatty acids. Here, we sought to understand how molecular conformations of EA and OA effect lipid bilayer membrane structure and mechanics.

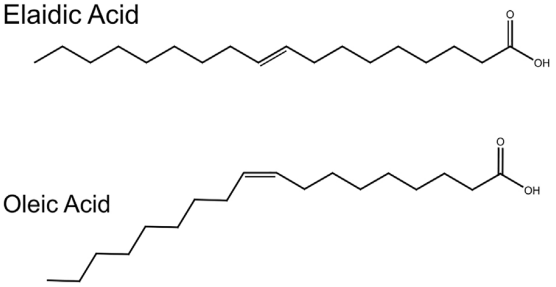

FIGURE 1 | Structures of oleic and elaidic acids. Oleic acid and elaidic acids are congeners with a double bond at the 9th carbon position. Oleic acid has a kink due to the *cis* double bond.

Both EA (*trans*) and OA (*cis*) have been shown to be associated with a variety of health conditions like coronary heart disease, atherosclerosis, Alzheimer's disease, diabetes, and cancer (Yang et al., 2011; Yaghmur et al., 2012; Turk and Chapkin, 2013). In the case of type 2 diabetes, it was reported that presence of *cis* fatty acids changes membrane flexibility which in turn causes a disruption in glucose transporter protein activity (Weijers, 2016). OA has also been associated with disruption of secretion of growth hormones associated with obesity by affecting the functioning of membrane proteins and proton flux across bilayers (Martin−Moreno et al., 1994; Hardman, 2004; Menendez et al., 2006; López-Miranda et al., 2010).

Given the importance of free fatty acids in cellular function, various biophysical studies have been carried out using artificial minimal systems. For example, structural changes in the bilayer membrane upon addition of fatty acids have been performed using X-ray diffraction and NMR techniques (Jilausner et al., 1980; Seddon et al., 1997; Templer et al., 1998; Inoue et al., 2001; Patel et al., 2001; Funari et al., 2003; Roach et al., 2004; Booth, 2005; Árnadóttir and Chalfie, 2010; Soubias et al., 2010; Yang et al., 2011; Vanni et al., 2014; Shaikh et al., 2015). X-ray diffraction studies by Seddon et al. (1997, 2006) revealed that addition of fatty acids influences membrane gel to L-alpha phase transitions and alters the lateral stress profile across the monolayer, favoring curved hexagonal and/or cubic phases. Upon addition of fatty acids to PC membranes the hydrophilic/hydrophobic balance is altered. This in turn affects the headgroup area to volume ratio which induces a curvature stress causing the transition to non-lamellar phases. In other studies (Mareš et al., 2008; Perutkova et al., 2009; Perutková et al., 2011), a closer look at the pivotal plane radius as a function of chain stiffness and internal curvature revealed that the increase in chain stiffness and internal curvature leads to a reduced pivotal plane radius favoring hexagonal phase transitions.

To obtain both structural as well as mechanical properties of bilayer membranes in response to the addition of EA and OA, we combined (a) vesicle fluctuation analysis on giant unilamellar vesicles (GUVs) for extracting the bending rigidity using our in-house algorithm, and (b) performed X-ray diffraction studies on simple DOPC/EA and DOPC/FA lipidic systems. Our results demonstrate that both EA and OA increase the bending rigidity

of the membrane. Structural studies using X-ray diffraction on fatty acid containing membranes show a topological transition to non-lamellar inverse hexagonal structures in both EA and OA containing membranes.

Based on the previous models described above, we expect an increase in the bending rigidity of GUVs upon addition of fatty acids owing to the increase in curvature frustration. Systematic addition of EA and OA to DOPC membranes, however, induced different effects on the bending rigidities, with EA containing DOPC vesicles showing a smaller increase compared to the OA containing vesicles. Interestingly, these results are consistent with theoretical predictions, as discussed below.

EXPERIMENTAL

Materials and Methods

1,2-Dioleoyl-*sn*-glycero-3-phosphocholine (DOPC), OA, and EA were bought from Sigma–Aldrich, Inc. (Gillingham, United Kingdom). The lipids had a purity of >99% and were used without further purification.

Sample Preparation for SAXS Measurements

Each lipid was freeze-dried individually, and samples were prepared by either mixing the desired amount of dry or stock solutions of lipids or dissolving them in chloroform. They were subsequently vortexed, dried under a steam of N_2 gas, and lyophilized for a minimum of 24 h. Samples were hydrated with 70 wt% HPLC grade water (VWR, United Kingdom) and subjected to a minimum of five freeze–thaw cycles in order to achieve reproducibility and sample homogeneity. Due to the lack of ions in the HPLC water, its pH couldn't be tested accurately using a pH meter but when tested with a pH universal indicator strip (Merck, Germany) it was shown to lie between 5 and 6. For the pH-dependent studies the pH of HPLC grade water was adjusted using HCl and NaOH to give a value of 3, 4, 5, 6, and 7 (±0.1) at 25°C as judged by a pH meter and universal indicator strips.

Preparation of GUVs

Bending rigidity measurements were performed on GUVs that were produced using the electroformation method (Miglena and Dimitrov, 1986; Angelova et al., 1992). Briefly, lipid mixtures were dissolved in 9:1 $CHCl_3$:CH_3OH solution at a concentration of 0.8 mg/ml. Two microliter drops of the solution were spread on ITO-coated glass plates and dried in a lyophilizer for 30 min. A 1 mm thick PDMS spacer was sandwiched between the two ITO plates to hold the solution used to hydrate the sample. The well was then filled with 100 mM sucrose solution. An AC voltage of 2.6 V at 10 Hz was applied to the plates for 3 h. The voltage was then increased to 4.6 V and the frequency reduced to 4.4 Hz for 15 min. The temperature was set so that the lipids were always below their chain melting temperature (24°C). GUVs were in the size range of 10–50 μm.

Giant unilamellar vesicles were re-suspended in 125 mM glucose solution. A visualization chamber was made using a 50 × 25 mm glass coverslip and an acrylic well. Around 80 μl of glucose solution was added into the well. Twenty microliters of GUVs were suspended into the glucose solution. The chamber was sealed with a cover slip to avoid air currents and reduce stray light due to scattering. The relaxation time scales of these fluctuations are in the range of a few milliseconds to a few seconds. The relaxation time decreases as the cubic power of the mode number. For example, the relaxation time scale τ_m is given by $\tau_m \sim 4\eta R^3/\kappa_c m^3$ where τ_m is the relaxation time for a given mode m, η is the viscosity of the medium, R is the radius of the vesicle, and κ_c the bending rigidity (Henriksen et al., 2004). This means that higher modes have shorter characteristic time scales. For video recording, a fast CMOS camera from Infinity (Lumenera, INFINITY 1-2 2.0 megapixel) was used. In order to capture the fluctuations, the camera integration time (exposure time) should be as short as possible. The exposure was kept to 1 ms and videos of approximately 1 min in time were recorded. All measurements were taken at 24°C.

Bending Rigidity

Vesicle fluctuation analysis (VFA) was used to extract the bending rigidity of the quasi spherical fluctuating vesicles (**Figure 2**). Briefly, the edges of the fluctuating vesicles were extracted using a fully automated LABVIEW routine based around the maximum intensity fitting of the bright edges. For a symmetric composition membrane, the spontaneous curvature vanishes. For small deformations in a membrane, the deviations from the mean shape are Fourier transformed and using the equipartition theorem, the mean square amplitude of each mode (q_x) is given by:

$$\langle h(q_x, y=0)^2 \rangle = \frac{1}{L}\frac{k_B T}{2\sigma}\left[\frac{1}{q_x} - \frac{1}{\sqrt{\frac{\sigma}{\kappa_c} + q_x^2}}\right] \quad (1)$$

where k_B is the Boltzmann constant, T is the temperature, σ is the membrane tension, κ_c is the bending rigidity, and L is the average circumference of the vesicle contours taken over all frames.

For bending dominated fluctuations, where $\frac{\sigma}{\left(\frac{q_x^2}{\kappa_c}\right)} \to 0$

We have

$$\langle h(q_x, y=0)^2 \rangle = \frac{1}{4L}\frac{k_B T}{\kappa_c q^3} \quad (2)$$

where $L = 2\pi <r>$ is the average circumference of the contour of all frames. Experimentally, it is required to calculate the Fourier transformation of the fluctuations about the mean radius of vesicle and relate it to the continuous Fourier transform $h(q)$. After finding the co-ordinates of the contour and representing them in polar coordinates, the mean radius of the vesicle $<r>$ is calculated for all $r(\theta_n)$, where n is the number of points on the circumference per frame, over all frames. The amplitude of fluctuation about the mean radius is given by $h_m = r(\theta_n) - <r>$. The FFT of the fluctuations is performed by using an inbuilt LabVIEW function.

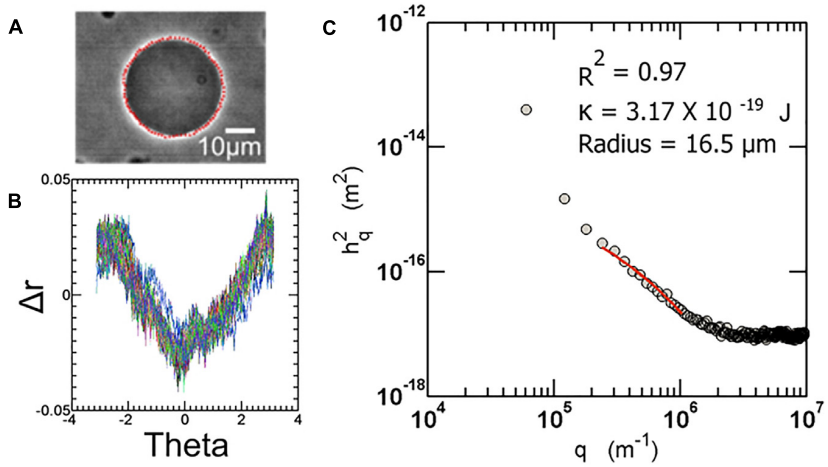

FIGURE 2 | (A) Sample image of a fluctuating vesicle at 23°C **(B)** The contour extracted is converted to *r*-theta which is further Fourier transformed to obtain a power spectrum as shown in **(C)**. All the automation routines are built in-house using LabVIEW software.

We consider only in-plane fluctuations since only these fluctuations can be captured with the microscope. Different modes depict regimes of the power spectrum governed by different parameters. The lower modes are mainly dominated by tension, or displacement factors of the vesicle. The intermediate regime (approx. between modes 6 and 20) represents the bending dominated region. This region is fit to the above equation to extract the bending rigidity. Detailed description of the method can be obtained from many excellent articles on the subject (Pécréaux et al., 2004; Yoon et al., 2010). The fluctuation analysis technique used here was developed in-house, and is described in depth in previous articles (see the Supplementary Information of Henriksen et al., 2004) (Elani et al., 2015; Purushothaman et al., 2015).

SAXS Measurements

X-ray experiments were carried out using a custom-built small angle X-ray beamline having a microsource X-ray generator (Bede Ltd., Durham, United Kingdom) producing X-rays with λ = 1.54 Å. A low divergence (2 mrad) X-ray beam is generated by monolithic poly-capillary optics (X-ray Optical Systems, Inc., United States). Diffraction patterns were recorded on a Gemstar intensified CCD X-ray detector (Photonic Science Ltd., Battle, United Kingdom). Sample capillaries were mounted in a custom-designed copper sample holder with Peltier temperature control (Melcor, United States), having an accuracy of ±0.1°C. The sample to detector distance was set to 200 mm, giving an accessible q range between 0.39 and 0.048 $Å^{-1}$. Samples were allowed to equilibrate for 10 min before each diffraction pattern was recorded.

Silver behenate (layer spacing d = 58.38 Å) was used to calibrate the low-angle X-ray diffraction data for all measurements. Diffraction images were analyzed using the IDL-based AXcess software package, developed in-house by Dr. A. Heron (Seddon et al., 2006). All the experiments were performed on three independent samples for each composition.

RESULTS AND DISCUSSION

We first performed small angle X-ray diffraction measurements to investigate the effect of compositional variation of fatty acids in DOPC membranes. The phase behavior of DOPC membranes with varying composition of fatty acids is presented below. Next, we describe the biomechanics of membranes containing *cis* and *trans* free fatty acids by extracting the bending rigidity of GUVs, using the fluctuation analysis developed in-house.

Phase Behavior

The phase behavior of DOPC:OA mixtures at limited hydration has recently been explored (Gillams et al., 2014). Here we investigate the phase behavior of DOPC:OA and DOPC:EA mixtures of up to 40 mol% fatty acid in excess (HPLC water, pH ∼5.5) water (70 wt%) at 25°C. DOPC:OA mixtures in HPLC water containing up to 20 mol% OA adopt a lamellar phase which slightly shrinks in layer spacing as the concentration of OA increases (**Figure 3**). At 30 mol% OA the lamellar phase is seen to coexist with a small broad hump under the first- and second-order reflections, and its lattice parameter is shifted to higher values (Gillams et al., 2014). Previous studies have shown that DOPC:OA mixtures at limited hydration form a lamellar phase coexisting with swollen Pn3m and Im3m cubic phases at 20 mol% OA. They also observed a hexagonal (H_{II}) phase coexisting with the swollen cubic phases at 30 mol% OA (Gillams et al., 2014). Due to the accessible q-range in our set-up we cannot determine whether the lamellar phase at 30 mol% OA is coexisting with swollen cubic phases. However, the similarity in phase behavior between the two studies indicates that it might be possible to attribute the broad hump to higher order reflections of swollen cubic phases, which are unresolved. At 40 mol% OA, the system transforms to a pure H_{II} phase with a layer spacing of 74.6 ± 0.05 Å.

The phase behavior of DOPC:EA mixtures is similar. Between 10 and 30 mol% EA a pure lamellar phase is formed which

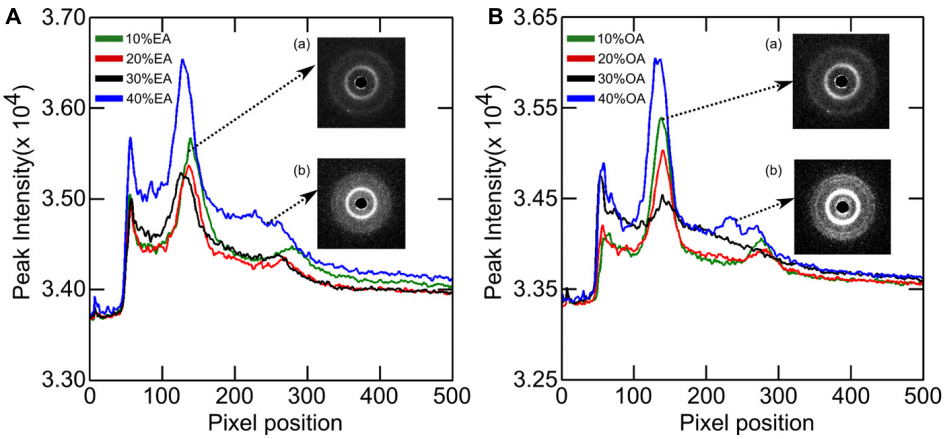

FIGURE 3 | X-ray diffraction images of **(A)** DOPC + Elaidic acid (EA) and **(B)** DOPC + Oleic acid (OA) mixtures. As the amount of fatty acids increase, peaks corresponding to inverse hexagonal phase starts appearing. See inset (b). Inset (a) represents the initial lamellar peaks.

transforms to a pure H_{II} phase at 40 mol% EA with a layer spacing of 74.9 Å (**Figure 4**). Here, the lattice parameter of the lamellar phase is seen to increase with increased EA concentration.

The pK_a of OA and EA has been reported to vary largely, with values ranging from 4.8 to 9.95 (Kanicky and Shah, 2002; Salentinig et al., 2010; Bennett et al., 2013). The reason for this large discrepancy is that the value depends on whether the pK_a has been measured for the fatty acid as a monomer in solution, in a micellar solution, or incorporated in a lipid bilayer. The pH of the water used in this study was ∼5.5. To test whether the change in the lattice parameter of the fatty acid containing DOPC mixtures used here was due to the electrostatic interactions of the fatty acids at pH 5.5 or due to the molecular structure of the fatty acid molecules, the effect of pH (3–6) on the phase behavior and resulting structures was also investigated. **Figure 4** shows that the phase behavior of the binary mixtures is unchanged with pH within this range. The layer spacing of the lamellar phase is relatively constant at different pH values for each mixture; however, the trend with increased fatty acid concentration is the same, indicating that the effect on the layer spacing is due to the molecular structure of the fatty acid molecules and not electrostatics, as the fatty acids should be fully protonated at pH 3. In order to confirm that the change in layer spacing is not related to protonation of the DOPC headgroup at low pH, the layer spacing of pure DOPC was also investigated between pH 3 and 6, and was found to be unchanged (**Figure 5**).

Bending Rigidity

The effect of mono-unsaturated fatty acids on the bending rigidity of the lipid membrane was studied by capturing membrane fluctuations of GUVs made from DOPC and fatty acid mixtures as described. **Figure 6** shows the bending rigidities of DOPC vesicles with varying amounts of OA and EA. The results are from the analysis of about 25–30 vesicles per sample. Addition of fatty acid to DOPC has different effects on the bending rigidity of the membrane depending on the fatty acid added. Addition of 10 mol% OA only marginally decreases the bending rigidity ($9.2 \times 10^{-20} \pm 1.1 \times 10^{-2}$ J) while 10 mol% EA increases it to $1.1 \times 10^{-19} \pm 1.3 \times 10^{-20}$ J compared to the bending rigidity of pure DOPC vesicles ($9.5 \times 10^{-20} \pm 0.8 \times 10^{-20}$ J). At 40 mol% of fatty acid, however, the bending rigidity of both OA and EA containing DOPC vesicles shows a large increase compared to 10 mol% fatty acid mixtures. It should be noted that this increase is less pronounced for EA compared to OA.

We will discuss the information obtained from X-ray diffraction measurements and couple the corresponding effect in the membrane mechanics. The differences in the effect on bending rigidities between the two fatty acids on DOPC membranes can be attributed to a number of factors, such as the phase behavior and the molecular structure of the individual fatty acid molecules.

Considering the lateral stress profile of a DOPC bilayer, addition of fatty acids should reduce the headgroup pressure. Consequently, this should be compensated by an increase in chain pressure. It is known that addition of fatty acids to phospholipids increases the negative spontaneous curvature of the lipid monolayer by increasing the hydrocarbon chain pressure, and curvature frustration then favors the formation of inverse phases (Zimmerberg and Gawrisch, 2006). The presence of a *cis* double bond in OA increases the splay of the hydrophobic chains more than its *trans* counterpart EA. For a given composition the effect of the presence of OA in bilayer forming lipids like DOPC will be greater in comparison to EA/DOPC mixtures. As a result, a lower concentration of OA is required to form inverse phases compared to EA. The observed phase behavior of the DOPC-EA and DOPC-OA systems supports this prediction.

Theoretical estimates made by Szleifer et al. (1990) on the dependence of bending rigidity on the average area per chain have shown that there is a dramatic decrease in bending rigidity as the area/molecule increases or when the curvature frustration is reduced, e.g., by addition of short chain amphiphiles (Figures 13, 14 of Salentinig et al., 2010). In our experiments, EA can be treated as a saturated amphiphile owing to its kinked structure at

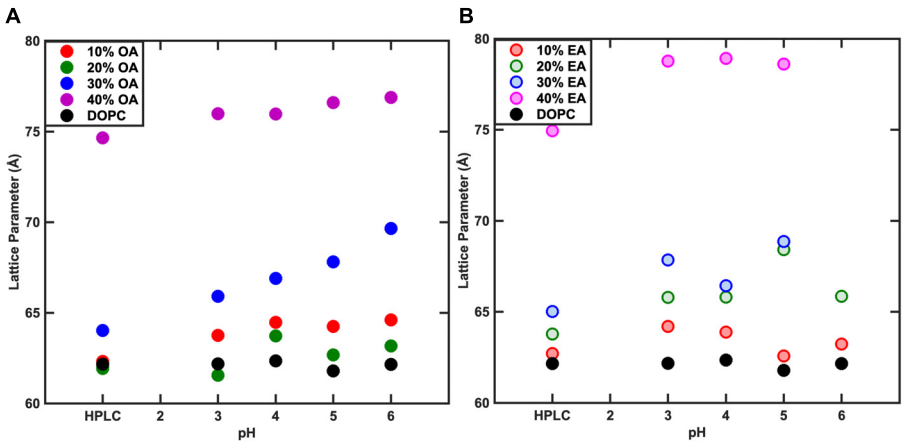

FIGURE 4 | Effect of pH on the phase behavior of fatty acid containing membranes. As the concentration of Fatty acid is changed, the lattice parameter changes however, the variation in the lattice parameter with pH is negligible. At 40% Fatty acid, both Oleic acid (OA) **(A)** and Elaidic acid (EA) **(B)** containing membrane systems adopt an H_{II} phase.

the double bond. Furthermore, studies (Leekumjorn et al., 2009) have shown that addition of *saturated* fatty acids to DOPC membranes decreases the average area per lipid linearly with concentration. On the contrary, addition of *unsaturated* fatty acids like OA has a less pronounced effect at low concentrations (up to 10 mol%). The area per lipid decreases less sharply upon further increase of *unsaturated* fatty acids. The average area per molecule of *saturated* fatty acid is low and unchanged upon increase in concentration in a DOPC bilayer. The area/molecule of *unsaturated* fatty acid like OA is higher and decreases as their concentration in the bilayer is increased. This has been attributed to the fact that the *saturated* fatty acid (EA) is relatively incompressible in the bilayer. The *unsaturated* fatty acids (OA), on the other hand, can order their chains by straightening their unsaturated chains. At high concentrations (>25 mol%) of fatty acid the area occupied by both saturated and unsaturated fatty acids is the same (**Figure 7**).

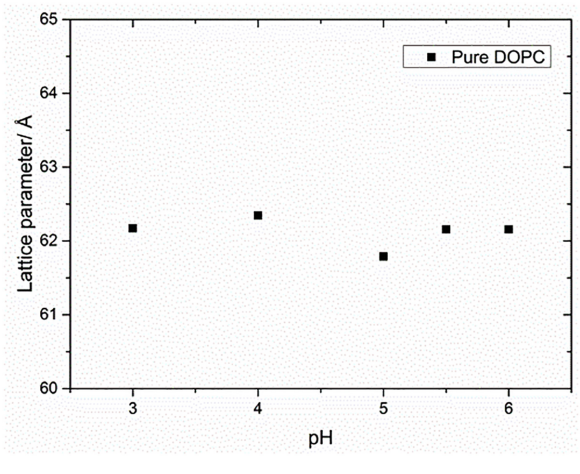

FIGURE 5 | Effect of pH on the lattice parameter of pure DOPC membranes. The lattice parameter remained constant for the range of pH values indicating that the effect of pH on lipid mixtures was negligible.

We look at the bending rigidities of vesicles containing fatty acid. Addition of 10% EA to DOPC membrane increases the lattice parameter which indicates a decrease in the area/lipid molecule (Leekumjorn et al., 2009). According to the theoretical predictions described above, a decrease in area/lipid causes an increase in the bending rigidity.

On the other hand, the addition of 10 mol% OA has very little effect on the lattice parameter of the lamellar phase compared to pure DOPC membranes. The bending rigidity of the binary mixture is slightly lower. OA increases membrane fluidity by decreasing the packing between phospholipids. This leads to increased fluctuations in the bilayer (Calder et al., 1994; Leekumjorn et al., 2009) which is reflected in the lowering of bending rigidity (**Figures 6**, **8**). One of the best ways to describe membrane fluidity is the lipid chain order parameter, which is a measure of the amplitude of the splay in the alkyl chains. An increase in order parameter indicates a decrease in chain conformational motion, tending to reduce membrane fluidity (Mills et al., 2008). The order parameter can be estimated using X-ray (Mills et al., 2008) diffraction measurements and NMR (Vameer et al., 2007) studies. It is expressed as:

$S = \frac{1}{2}\left(3\left\langle\cos^2\beta\right\rangle - 1\right)$, where S is the lipid chain average orientational order parameter and β is the average chain tilt angle from the bilayer normal.

At 20 mol% OA, there is a slight decrease in layer spacing at all pH measurements. Although a decrease in lattice parameter might imply a slight increase in area/molecule and hence a lower bending rigidity, we noted that the bending rigidity did not decrease, suggesting that the decrease in spacing is due to the water layers between the bilayers becoming slightly thinner.

At 30 mol% OA, however, the layer spacing of the lamellar phase increased. Consequently, the bending rigidity also rises consistent with the theoretical predictions.

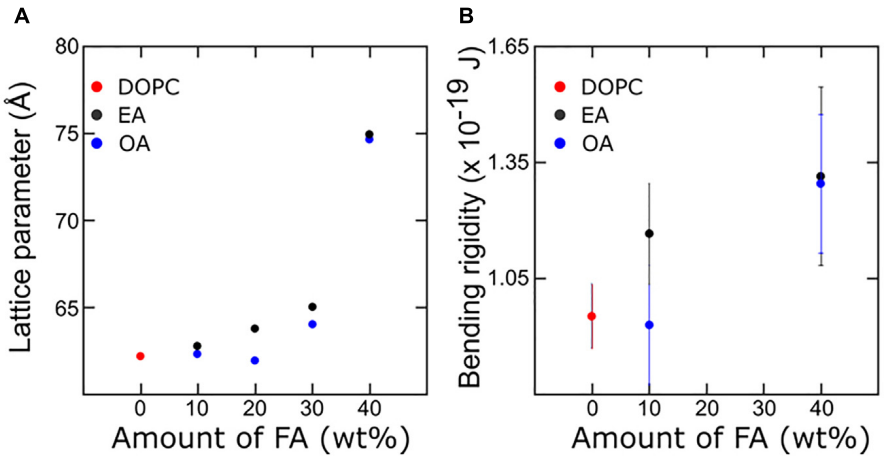

FIGURE 6 | Combined X-ray diffraction **(A)** and bending rigidity plot **(B)** describing membrane mechanics with respect to the corresponding change in molecular arrangement. The bulk 40% Fatty acid samples are in the H_{II} phase whereas in the GUVs they are confined to a bilayer structure.

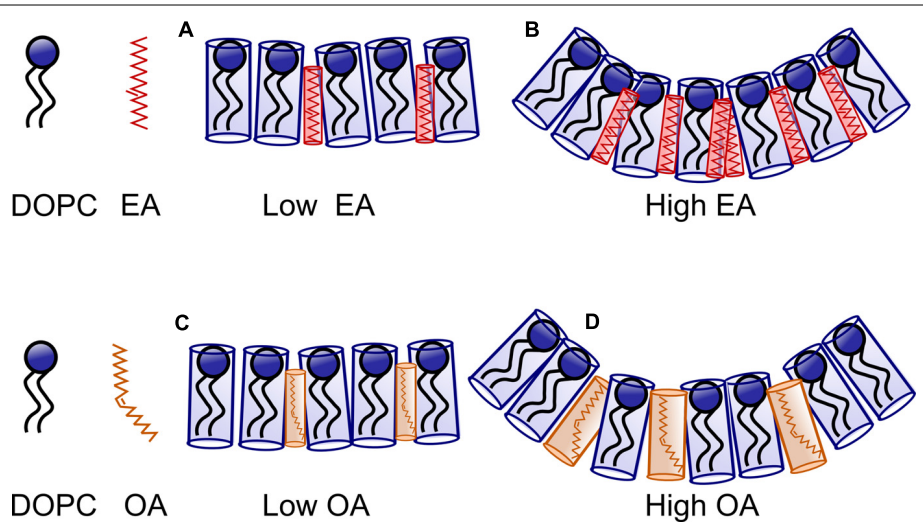

FIGURE 7 | Schematic representing the effect of Oleic acid (OA) and Elaidic Acid (EA) on DOPC membranes. At low concentration of EA/FA **(A)**, the effect of FA on the bilayer is small. At higher concentration curvature frustration dominates as the FA remain incompressible. However, more EA **(B)** is required to drive the system to a non-lamellar phase in comparison to OA. At low concentrations, OA containing membranes are similar to EA containing membranes. However, at high concentrations **(C)**, relatively less OA is required to induce curvature **(D)** owing to the kink in the structure of OA.

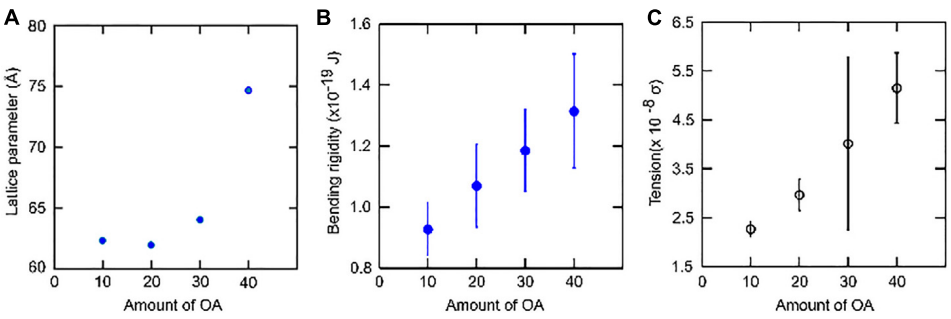

FIGURE 8 | Effect of systematic increase in the concentration of Oleic acid (OA) on DOPC membranes. **(A)** As the concentration increases, the lattice spacing increases. **(B)** The bending rigidity increases as the area per lipid decreases. **(C)** The tension in the membrane also increases. However, VFA gives bending rigidity values more reliably in comparison to tension measurements.

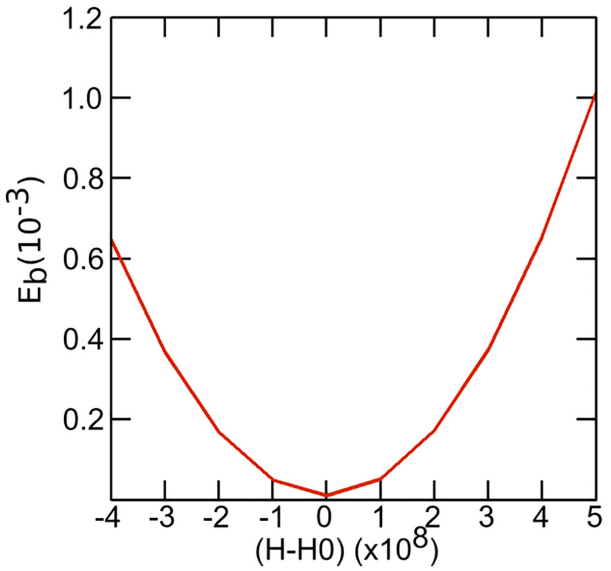

FIGURE 9 | Plot depicting the variation of bending rigidity as a function of spontaneous curvature. For fluctuations upto 100 nm we can see that the bending rigidity rises sharply if the system deviates from its preferred spontaneous curvature (H_0).

As mentioned earlier, the lamellar peak at 30 mol% OA is seen to coexist with a broad hump under the first-order reflection. We suggest that the origin of the broad hump might be poorly resolved higher order reflections of a cubic phase as seen by Gillams et al. (2014). If the system has a propensity to form a non-bilayer structure but is forced to remain in a bilayer arrangement in a vesicle then the bending rigidity will rise as the curvature elastic stress increases.

Taken together, at low OA concentrations, we believe that the forces dominating the bending rigidity are due to the effect of the molecular interactions between the OA and DOPC membrane, namely the increased fluidity of the bilayer, in contrast to the less "floppy" EA. As the concentration of fatty acid is increased, there is a decrease in area per (lipid + fatty acid) due to ordering of the unsaturated chains. This leads to an increase in the bending rigidity.

At 40 mol% fatty acid, however, the dominant force influencing the bending rigidity is curvature frustration for both the OA and EA systems. It has been shown that above 25 mol% fatty acid in DOPC, the area occupied by both saturated and unsaturated fatty acids is the same. As a result, the difference in the area occupied by the DOPC:OA and DOPC:EA membranes is less pronounced. Both fatty acids will thus have a similar effect on bending rigidity at higher concentrations.

As seen by SAXS, bulk DOPC:fatty acid systems at 40 mol% fatty acid adopt an inverse hexagonal phase. However, within a GUV they are forced to be in a bilayer state which leads to a sharp increase in the curvature frustration and a pronounced increase in the bending rigidity. Assuming the lipids are evenly distributed within the two leaflets, we can approximately estimate the effect on bending rigidity as the system deviates (or is forced to deviate) from its preferred radii of curvature. The fluctuation analysis studies show that fluctuations are in the order of 100 nm. Using this value as an estimated radius of curvature we can see that the bending rigidity rises sharply if the system deviates from its preferred spontaneous curvature (H_0) (**Figure 9**).

Mareš et al. (2008) detailed the relationship between intrinsic curvature and chain stiffness and the pivotal plane cross section radius to explain lamellar to hexagonal phase transitions. The model is based on anisotropic shape of lipid molecules described by principal intrinsic curvatures. The study demonstrated that as the chain stiffness and intrinsic curvature increase, the pivotal plane radius decrease leading to transition from lamellar to hexagonal phase. The decrease in the pivotal plane radius is thus a result of competition between the bending and interstitial energy. When the chain is stiff, there is propensity to curve toward the hexagonal corners to fill voids which leads to transition to hexagonal phase. This could explain the transition to inverted hexagonal phase at high fatty acid concentrations when the bending rigidity also increases.

CONCLUSION

In conclusion, the effect of *cis*- and *trans*-monounsaturated fatty acid on bilayer mechanics is studied using both X-ray diffraction and vesicle fluctuation analysis. Addition of fatty acids increases the bilayer bending rigidity. EA with its *trans* double bond behaves more like a saturated amphiphile, showing less change in area/molecule, and causing a smaller change in bending rigidity. The presence of *cis* double bonds in OA increases the probability of inducing negative curvature, increasing curvature frustration, and an increase in bending rigidity. Furthermore, higher concentrations show a dominant effect of curvature frustration, leading to higher bending rigidity, whereas at lower concentrations of fatty acids, several intermolecular interactions as well as the floppiness of the fatty acids dictate the thickness and rigidity of membranes. The theoretical model developed by Szleifer et al. (1990) to explain the curvature of lipidic membranes was useful in interpreting some of the findings reported here. Our observations show that the bending rigidity is sensitive to the type of fatty acids incorporated into DOPC membranes. The study demonstrates the potential application of bio-mechanical properties as unique bio-markers to identify membrane reorganization as a result of disruption in fatty acid biosynthesis as seen in certain neurodegenerative conditions.

AUTHOR CONTRIBUTIONS

JG performed all the bending rigidity measurements. AT performed all the X-ray diffraction and pH measurements. SP lead the project. JS provided guidance and helped in preparing the manuscript. NB was part of the project grant and provided funding support.

FUNDING

This work was supported by the Biotechnology and Biological Sciences Research Council Grant BB/F013167/1, Engineering and Physics Sciences Research Council Platform Grant EP/G00465X/1, and EPSRC Programme Grant EP/J017566/1.

ACKNOWLEDGMENTS

We would like to thank Prof. Oscar Ces, Imperial College London for supporting our work, and Prof. Atul N. Parikh, UC Davis, for providing the opportunity to present this work.

REFERENCES

Angelova, M. I., Soléau, S., Méléard, P., Faucon, F., and Bothorel, P. (1992). "Preparation of giant vesicles by external AC electric fields. Kinetics and applications," in *Trends in Colloid and Interface Science VI. Progress in Colloid & Polymer Science*, eds C. Helm, M. Lösche, and H. Möhwald (Berlin: Springer Verlag), 127–131. doi: 10.1007/bfb0116295

Árnadóttir, J., and Chalfie, M. (2010). Eukaryotic mechanosensitive channels. *Annu. Rev. Biophys.* 39, 111–137. doi: 10.1146/annurev.biophys.37.032807.125836

Bennett, W. F. D., Chen, A. W., Donnini, S., Groenhof, G., and Tieleman, D. P. (2013). Constant pH simulations with the coarse-grained MARTINI model — Application to oleic acid aggregates. *Can. J. Chem.* 91, 839–846. doi: 10.1139/cjc-2013-0010

Booth, P. (2005). Sane in the membrane: designing systems to modulate membrane proteins. *Curr. Opin. Struct. Biol.* 15, 435–440. doi: 10.1016/j.sbi.2005.06.002

Calder, P. C., Yaqoob, P., Harvey, D. J., Watts, A., and Newsholme, E. A. (1994). Incorporation of fatty acids by concanavalin A-stimulated lymphocytes and the effect on fatty acid composition and membrane fluidity. *Biochem. J.* 300, 509–518. doi: 10.1042/bj3000509

DeLong, E. F., and Yayanos, A. A. (1985). Adaptation of the membrane lipids of a deep-sea bacterium to changes in hydrostatic pressure. *Science* 228, 1101–1103. doi: 10.1126/science.3992247

Elani, Y., Purushothaman, S., Booth, P. J., Seddon, J. M., Brooks, N. J., Law, R. V., et al. (2015). Measurements of the effect of membrane asymmetry on the mechanical properties of lipid bilayers. *Chem. Commun.* 51, 6976–6979. doi: 10.1039/c5cc00712g

Funari, S. S., Barceló, F., and Escribá, P. V. (2003). Effects of oleic acid and its congeners, elaidic and stearic acids, on the structural properties of phosphatidylethanolamine membranes. *J. Lipid Res.* 44, 567–575. doi: 10.1194/jlr.m200356-jlr200

Gillams, R. J., Nylander, T., Plivelic, S., Dymond, M. K., and Attard, G. S. (2014). Formation of inverse topology lyotropic phases in dioleoylphosphatidylcholine/oleic acid and dioleoylphosphatidylethanolamine/oleic acid binary mixtures. *Langmuir* 30, 3337–3344. doi: 10.1021/la404275u

Hardman, W. E. (2004). (n-3) Fatty acids and cancer therapy. *J. Nutr.* 134, 3427S–3430S. doi: 10.1093/jn/134.12.3427S

Henriksen, J., Rowat, A. C., and Ipsen, J. H. (2004). Vesicle fluctuation analysis of the effects of sterols on membrane bending rigidity. *Eur. Biophys. J.* 33, 732–741. doi: 10.1007/s00249-004-0420-5

Inoue, T., Yanagihara, S. I., Misono, Y., and Suzuki, M. (2001). Effect of fatty acids on phase behavior of hydrated dipalmitoylphosphatidylcholine bilayer: saturated versus unsaturated fatty acids. *Chem. Phys. Lipids* 109, 117–133. doi: 10.1016/s0009-3084(00)00170-5

Jilausner, R. D., Kleinfeld, A. M., Hoover, R. L., and Karnovskys, M. J. (1980). Evidence derived from structurak perturbations induced by free fatty acids. *J. Biol. Chem.* 255, 1286–1295.

Kanicky, J. R., and Shah, D. O. (2002). Effect of degree, type, and position of unsaturation on the pKa of long-chain fatty acids. *J. Colloid Interface Sci.* 256, 201–207. doi: 10.1006/jcis.2001.8009

Klausner, R. D., Kleinfeld, A. M., Hoover, R. L., and Karnovsky, M. J. (1980). Evidence derived from structural perturbations induced by free fatty acids and lifetime heterogeneity analysis. *J. Biol. Chem.* 255, 1286–1295.

Leekumjorn, S., Cho, H. J., Wu, Y., Wright, N. T., Sum, A. K., Chan, C., et al. (2009). The role of fatty acid unsaturation in minimizing biophysical changes on the structure and local effects of bilayer membranes. *Biochim. Biophys. Acta* 1788, 1508–1516. doi: 10.1016/j.bbamem.2009.04.002

López-Miranda, J., Pérez-Jiménezа, F., Ros, E., De Caterina, R., Badimón, L., Covas, M. I., et al. (2010). Olive oil and health: summary of the II international conference on olive oil and health consensus report, Jaén and Córdoba (Spain) 2008. *Nutr. Metab. Cardiovasc. Dis.* 20, 284–294.

Mareš, T., Daniel, M., Perutkova, S., Perne, A., Dolinar, G., Iglic, A., et al. (2008). Role of phospholipid asymmetry in the stability of inverted haxagonal mesoscopic phases. *J. Phys. Chem. B* 112, 16575–16584. doi: 10.1021/jp805715r

Martin—Moreno, J. M., Willett, W. C., Gorgojo, L., Banegas, J. R., Rodriguez-Artalejo, F., et al. (1994). Dietary fat, olive oil intake and breast cancer risk. *Int. J. Cancer* 58, 774–780. doi: 10.1002/ijc.2910580604

Menendez, J. A., Papadimitropoulou, A., Vellon, L., and Lupu, R. A. (2006). Genomic explanation connecting "Mediterranean diet", olive oil and cancer: oleic acid, the main monounsaturated fatty acid of olive oil, induces formation of inhibitory "PEA3 transcription factor-PEA3 DNA binding site" complexes at the Her-2/neu (erbB-2. *Eur. J. Cancer* 42, 2425–2432. doi: 10.1016/j.ejca.2005.10.016

Miglena, A. I, and Dimitrov, D. S. (1986). Liposome electroformation. *Faraday Discuss. Chem. Soc.* 81, 303–311.

Mills, T. T., Toombes, G. E., Tristram-Nagle, S., Smilgies, D. M., Feigenson, G. W., Nagle, J. F., et al. (2008). Order parameters and areas in fluid-phase oriented lipid membranes using wide angle X-ray scattering. *Biophys. J.* 95, 669–681. doi: 10.1529/biophysj.107.127845

Mota, M. J., Lopes, R. P., Delgadillo, I., and Saraiva, J. A. (2013). Microorganisms under high pressure–adaptation, growth and biotechnological potential. *Biotechnol. Adv.* 31, 1426–1434. doi: 10.1016/j.biotechadv.2013.06.007

Patel, A. J., Lazdunski, M., and Honoré, E. (2001). Lipid and mechano-gated 2P domain K + channels. *Curr. Opin. Cell Biol.* 13, 422–428. doi: 10.1016/s0955-0674(00)00231-3

Pécréaux, J., Döbereiner, H. G., Prost, J., Joanny, J. F., and Bassereau, P. (2004). Refined contour analysis of giant unilamellar vesicles. *Eur. Phys. J. E. Soft Matter* 13, 277–290. doi: 10.1140/epje/i2004-10001-9

Perutková, Á, Matej, D., Michael, R., Gregor, P., Veronika, K. I, Aleš, I., et al. (2011). Elastic deformations in hexagonal phases studied by small-angle X-ray diffraction and simulations. *Phys. Chem. Chem. Phys.* 13, 3100–3107. doi: 10.1039/c0cp01187h

Perutkova, S., Daniel, M., Dolinar, G., Rappolt, M., and Kralj-iglic, V. (2009). Stability of the inverted hexagonal phase. *Adv. Planar Lipid Bilayers Liposomes* 9, 237–278. doi: 10.1016/s1554-4516(09)09009-7

Picard, A., and Daniel, I. (2013). Pressure as an environmental parameter for microbial life–a review. *Biophys. Chem.* 183, 30–41. doi: 10.1016/j.bpc.2013.06.019

Purushothaman, S., Cicuta, P., Ces, O., and Brooks, N. J. (2015). Influence of high pressure on the bending rigidity of model membranes. *J. Phys. Chem. B* 119, 9805–9810. doi: 10.1021/acs.jpcb.5b05272

Roach, C., Feller, S. E., Ward, J. A., Shaikh, S. R., Zerouga, M., Stillwell, W., et al. (2004). Comparison of cis and trans fatty acid containing phosphatidylcholines on membrane properties. *Biochemistry* 43, 6344–6351. doi: 10.1021/bi049917r

Romero, L. O., Massey, A. E., Mata-Daboin, A. D., Sierra-Valdez, F., Chauhan, S. C., Cordero-Morales, J. F., et al. (2019). Dietary fatty acids fine-tune Piezo1 mechanical response. *Nat. Commun.* 10:1200. doi: 10.1038/s41467-019-09055-7

Salentinig, S., Sagalowicz, L., and Glatter, O. (2010). Self-assembled structures and pKa value of oleic acid in systems of biological relevance. *Langmuir* 26, 11670–11679. doi: 10.1021/la101012a

Sameni, S., Malacrida, L., Tan, Z., and Digman, M. A. (2018). Alteration in fluidity of cell plasma membrane in huntington disease revealed by spectral phasor analysis. *Sci. Rep. Nat. Publ. Gr.* 8:6060.

Seddon, J. M., Squires, A. M., Conn, C. E., Ces, O., Heron, A. J., Mulet, X., et al. (2006). Pressure-jump X-ray studies of liquid crystal transitions in lipids. *Philos. Trans. A Math. Phys. Eng. Sci.* 364, 2635–2655. doi: 10.1098/rsta.2006.1844

Seddon, J. M., Templer, R. H., Warrender, N. A., Huang, Z., Cevc, G., Marsh, D., et al. (1997). Phosphatidylcholine–fatty acid membranes: effects of headgroup hydration on the phase behaviour and structural parameters of the gel and inverse hexagonal (HII) phases. *Biochim. Biophys. Acta Biomembr.* 1327, 131–147. doi: 10.1016/s0005-2736(97)00047-3

Shaikh, S. R., and Edidin, M. (2006). Polyunsaturated fatty acids, membrane organization, T cells, and antigen presentation. *Am. J. Clin. Nutr.* 84, 1277–1289. doi: 10.1093/ajcn/84.6.1277

Shaikh, S. R., Kinnun, J. J., Leng, X., Williams, J. A., and Wassall, S. R. (2015). How polyunsaturated fatty acids modify molecular organization in membranes: insight from NMR studies of model systems. *Biochim. Biophys. Acta* 1848, 211–219. doi: 10.1016/j.bbamem.2014.04.020

Soubias, O., Teague, W. E., Hines, K. G., Mitchell, D. C., and Gawrisch, K. (2010). Contribution of membrane elastic energy to rhodopsin function. *Biophys. J.* 99, 817–824. doi: 10.1016/j.bpj.2010.04.068

Szleifer, I., Kramer, D., Ben-Shaul, A., Gelbart, W. M., and Safran, S. A. (1990). Molecular theory of curvature elasticity in surfactant films. *J. Chem. Phys.* 92:6800. doi: 10.1063/1.458267

Templer, R. H., Seddon, J. M., Warrender, N. A., Syrykh, A., and Huang, Z. (1998). Inverse bicontinuous cubic phases in 2: 1 fatty acid / phosphatidylcholine mixtures . the effects of chain length, hydration, and temperature. *J. Phys. Chem. B* 5647, 7251–7261. doi: 10.1021/jp972835a

Turk, H. F., and Chapkin, R. S. (2013). Membrane lipid raft organization is uniquely modified by n-3 polyunsaturated fatty acids. *Prostaglandins. Leukot. Essent. Fatty Acids* 88, 43–47. doi: 10.1016/j.plefa.2012.03.008

Vameer, L. S., De Groot, B. L., Reat, V., Milon, A., and Czaplicki, J. (2007). Acyl chain order parameter profiles in phospholipid bilayers: computation from molecular dynamics simulations and comparison with 2 H NMR experiments. *Eur. Biophys. J.* 36, 919–931. doi: 10.1007/s00249-007-0192-9

Vanni, S., Hirose, H., Barelli, H., Antonny, B., and Gautier, R. (2014). A sub-nanometre view of how membrane curvature and composition modulate lipid packing and protein recruitment. *Nat. Commun.* 5:4916. doi: 10.1038/ncomms5916

Weijers, R. N. M. (2016). Membrane flexibility, free fatty acids, and the onset of vascular and neurological lesions in type 2 diabetes. *J. Diabetes Metab. Disord.* 15:13. doi: 10.1186/s40200-016-0235-9

Yaghmur, A., Sartori, B., and Rappolt, M. (2012). Self-assembled nanostructures of fully hydrated monoelaidin-elaidic acid and monoelaidin-oleic acid systems. *Langmuir* 28, 10105–10119. doi: 10.1021/la3019716

Yang, X., Sheng, W., Sun, G. Y., and Lee, J. C. M. (2011). Effects of fatty acid unsaturation numbers on membrane fluidity and α-secretase-dependent amyloid precursor protein processing. *Neurochem. Int.* 58, 321–329. doi: 10.1016/j.neuint.2010.12.004

Yoon, Y. Z., Hale, J. P., Petrov, P. G., and Cicuta, P. (2010). Mechanical properties of ternary lipid membranes near a liquid-liquid phase separation boundary. *J. Phys. Condens. Matter* 22:062101. doi: 10.1088/0953-8984/22/6/062101

Zimmerberg, J., and Gawrisch, K. (2006). The physical chemistry of biological membranes. *Comp. Biochem. Physiol. Part A Physiol.* 2, 564–567. doi: 10.1038/nchembio1106-564

Conflict of Interest Statement: The authors declare that the research was conducted in the absence of any commercial or financial relationships that could be construed as a potential conflict of interest.

frontiers in Cell and Developmental Biology

ORIGINAL RESEARCH
published: 10 October 2019
doi: 10.3389/fcell.2019.00206

Selective Phosphorylation of Akt/Protein-Kinase B Isoforms in Response to Dietary Cues

Laura Christin Trautenberg[1], *Elodie Prince*[1], *Cornelia Maas*[1], *Nora Beier*[1], *Freya Honold*[1], *Michal Grzybek*[2,3]* *and Marko Brankatschk*[1*†]

[1] TU Dresden (BIOTEC), Dresden, Germany, [2] Paul Langerhans Institute Dresden of the Helmholtz Zentrum München at the University Hospital and Faculty of Medicine Carl Gustav Carus of TU Dresden, Technische Universität Dresden, Dresden, Germany, [3] German Center for Diabetes Research (DZD e.V.), Oberschleissheim, Germany

A calorie-rich diet is one reason for the continuous spread of metabolic syndromes in western societies. Smart food design is one powerful tool to prevent metabolic stress, and the search for suitable bioactive additives is a continuous task. The nutrient-sensing insulin pathway is an evolutionary conserved mechanism that plays an important role in metabolism, growth and development. Recently, lipid cues capable to stimulate insulin signaling were identified. However, the mechanistic base of their activity remains obscure to date. We show that specific Akt/Protein-kinase B isoforms are responsive to different calorie-rich diets, and potentiate the activity of the cellular insulin cascade. Our data add a new dimension to existing models and position *Drosophila* as a powerful tool to study the relation between dietary lipid cues and the insulin-induced cellular signal pathway.

Keywords: *Drosophila*, *Saccharomyces cerevisiae*, *Cystobasidium oligophagum*, Akt, PKB, Akt phosphorylation, insulin signaling, yeast lipids

OPEN ACCESS

Edited by:
Guillaume Thibault, Nanyang Technological University, Singapore

Reviewed by:
Hua Bai, Iowa State University, United States
Marc Tatar, Brown University, United States

***Correspondence:**
Michal Grzybek
michal.grzybek@tu-dresden.de
Marko Brankatschk
marko.brankatschk@tu-dresden.de

†Leading author

Specialty section:
This article was submitted to Membrane Traffic, a section of the journal Frontiers in Cell and Developmental Biology

Received: *26 April 2019*
Accepted: *06 September 2019*
Published: *10 October 2019*

Citation:
Trautenberg LC, Prince E, Maas C, Beier N, Honold F, Grzybek M and Brankatschk M (2019) Selective Phosphorylation of Akt/Protein-Kinase B Isoforms in Response to Dietary Cues. Front. Cell Dev. Biol. 7:206. doi: 10.3389/fcell.2019.00206

INTRODUCTION

Food composition is instructive for the metabolic response of organisms and recent studies demonstrate an important role of lipid cues including dietary lipids in modulating systemic insulin signaling. The identity and mechanism of such metabolically active lipids remains obscure; however, their regulating function is restricted to calorie-rich nutritional settings and is second to the role of sugars (Migrenne et al., 2006; Oh et al., 2010; Brankatschk et al., 2014). It is suggested that circulating fatty acids bind to cellular receptors and that way, induce the secretion of metabolic regulators (Nolan et al., 2006; Oh et al., 2010; Hauke et al., 2018). On the other hand, absorbed lipids are re-integrated into cellular membranes and therefore, can change biophysical membrane properties (Abbott et al., 2012). Variables like membrane fluidity and thickness possibly modulate the amount and activity of membrane proteins such as the Insulin receptor (Ginsberg et al., 1981; Murphy, 1990; Gutmann et al., 2018). The Insulin receptor (InR) is a dimeric type-I membrane protein that belongs to the tyrosine-kinase receptor family (Fernandez et al., 1995). Bound to insulin, the InR recruits adapter proteins and activates the PI-3 kinase (Böhni et al., 1999). The PI-3 kinase converts the inner leaflet membrane lipid $PI(4,5)P_2$ into $PI(3,4,5)P_3$, which attracts the Protein kinase B/Akt (Scanga et al., 2000). Different Akt isoforms have been identified in vertebrates and invertebrates. For instance, mice or fruit flies express three different protein versions (Andjelković et al., 1995; Gonzalez and McGraw, 2009a). In *Drosophila*, the presence of individual Akt isoforms (dAkt's) is stage-dependent. Adult flies express two dAkt proteins, which are

different in size: the smaller $dAkt^{66}$ and the larger $dAkt^{85}$, close to 66 and 85 kDa, respectively (Andjelković et al., 1995). The structure of Akt shows high molecular and functional conservation; this kinase possesses multiple regulatory phosphorylation sites and the positions $dAkt^{Ser505}$ and $dAkt^{Thr342}$ are characterized (Manning and Toker, 2017). The functional relevance of the vertebrate $Akt1^{Ser473}$ (which corresponds to the $dAkt^{Ser505}$) is well-studied (Alessi et al., 1996); however, the biological role of $Akt1^{Thr308}$ (which corresponds to the $dAkt^{Thr342}$) is more obscure. It is widely accepted that the enzyme reaches full activity once phosphorylated on both positions (Alessi et al., 1996; Scheid et al., 2002). Akt is a negative regulator of the transcription factor FOXO (Calnan and Brunet, 2008). When insulin signaling levels are low, FOXO translocates from the cell cytoplasm into the nucleus (Puig, 2003). Whereas, high Akt activity prevents FOXO from entering the nucleus, and the cells predominantly switch to anabolic reactions building stocks of storage molecules such as fatty acids (Xu et al., 2012). Taken together, circulating lipids are potentially capable to modulate the insulin-signaling cascade at multiple levels. If so, what pressures could possibly favor lipids as regulators of the insulin signaling?

Drosophila feed preferentially on rotting fruits, a diet composed by plant material and microbes such as yeast. Fruits are the main source for carbohydrates while microbes provide dietary amino acids. It was shown that a calorie-rich diet supplemented with yeast lipids increases circulating *Drosophila* insulin-like peptides (dILPs) and facilitates high systemic insulin signaling levels (Brankatschk et al., 2014). High insulin signaling stimulates the proliferation and developmental rate of flies. On the other hand, the fly dietary lipid composition is dependent on the consumed yeast species, microbial growth stage and available carbon source, and environmental temperature (Chandler et al., 2012; Klose et al., 2012). Decomposing plant material is rich in sugars and proteins, which are degraded to smaller molecules (monosaccharides and amino acids) prior to intestinal absorption. Although it is shown that extreme quantities or the absence of individual compounds in experimental conditions can change the activity of metabolic circuits, such nutritional settings are not likely found in the wild.

The structure of fatty acids and other lipid species is defined by their origin. For instance, plants produce more unsaturated and long fatty acids, as well as phytosterols which are structurally different from fungal or mammalian counterparts. If microbial lipid cues convey dietary signals to flies, then two principal questions arise. First, do all microbes associated with *Drosophila* promote the proliferation of fruit flies? Second, is the growth dependent microbial lipid composition instructive for the generative cycle of flies?

Here, we report the isolation of *Cystobasidium oligophagum*, a ubiquitous *Basidiomycota*, from *Drosophila* droppings. Although *C. oligophagum* attracts adult flies, we show that these yeasts do not promote fruit fly oviposition or development. Compared to baker's yeast (*Saccharomyces cerevisiae*), *C. oligophagum* produce similar amounts of protein and sugar but differ in their lipid composition. Calorie-rich food based on either yeast type supports the generative cycle of *Drosophila*; however, only diet manufactured from stationary *S. cerevisiae* accelerates its developmental rate and increases egg production. Moreover, we demonstrate that flies kept on food prepared from stationary *S. cerevisiae* upregulate selectively the $dAkt^{85}$-isoform, and that the enzyme is highly phosphorylated. Thus, we speculate that lipid cues derived from stationary *S. cerevisiae* stimulate the accumulation of $PI(3,4,5)P_3$ at the inner plasma-membrane leaflet of *Drosophila* cells. $dAkt^{85}$ binds to $PI(3,4,5)P_3$ and as such is accessible for the phosphoinositide-dependent Protein kinase 1 (PDK1) or the Rictor-mammalian target of rapamycin complex 2 (mTorC2) (Cho et al., 2001; Sarbassov et al., 2005).

RESULTS

Cystobasidium oligophagum and *Saccharomyces cerevisiae* Have Different Lipid Qualities

On rotting plant material, yeast are predominant microbes preferred by *Drosophila*. To investigate which fungi are associated with flies, we have analyzed microbial isolates from fly droppings of wild type *OregonR* flies kept on plant food in an open cage. Fly poo positioned on plant food at 20°C contained *C. oligophagum*; but not *S. cerevisiae*, which is the preferred yeast used in experimental *Drosophila* research. To compare the caloric value of each yeasts, we have cultivated *C. oligophagum* or *S. cerevisiae* at 20°C in a lipid-free, defined medium. We harvested the fungi in their exponential (EP) and stationary growth phases (SP), and measured their protein and trehalose content using commercial detection assays (**Supplementary Figure 1**). Remarkably, both fungi produce very similar amounts of protein and trehalose (**Supplementary Figures 1B,D**). To evaluate the fungal lipidomes, we extracted lipids from all four yeast samples and adjusted their total lipid amounts. Subsequently, we separated individual lipid classes by using reverse phase Thin-Layer Chromatography (2D-TLC). As expected, we confirmed that *S. cerevisiae* lipid profiles depend on growth stages (**Figures 1C,D** in black and **Supplementary Figure 1E**; Klose et al., 2012). Interestingly, lipids from *C. oligophagum* show minimal growth-dependent quality changes (**Figures 1C,D** in red and **Supplementary Figure 1E**). To estimate relative lipid quantities, we have adjusted the lipid amounts to phosphate levels measured in our samples. Like reported, the lipidome of *C. oligophagum* is overrepresented by lipids with properties shown by free fatty acids with respect to *S. cerevisiae* (Vyas and Chhabra, 2017). Furthermore, we found that the relative amounts of individual lipid classes do not vary between EP and SP stages. In contrast, proliferating *S. cerevisiae* have less triacylglycerids (TAGs) and sterol-esters with respect to stationary cells (data not shown). To visualize the lipid distribution in fungal cells, we stained live yeasts with Bodipy-505. The dye is capable to penetrate the plasma membrane and preferentially accumulates in lipid-rich regions such as lipid droplets. As expected, in *S. cerevisiae* cells, Bodipy-505 is enriched in lipid droplets and we noted that SP yeast cells contain a higher number of such organelles (**Figures 1A,B**). Taken together, we have confirmed that lipid extract qualities and membrane organizations of

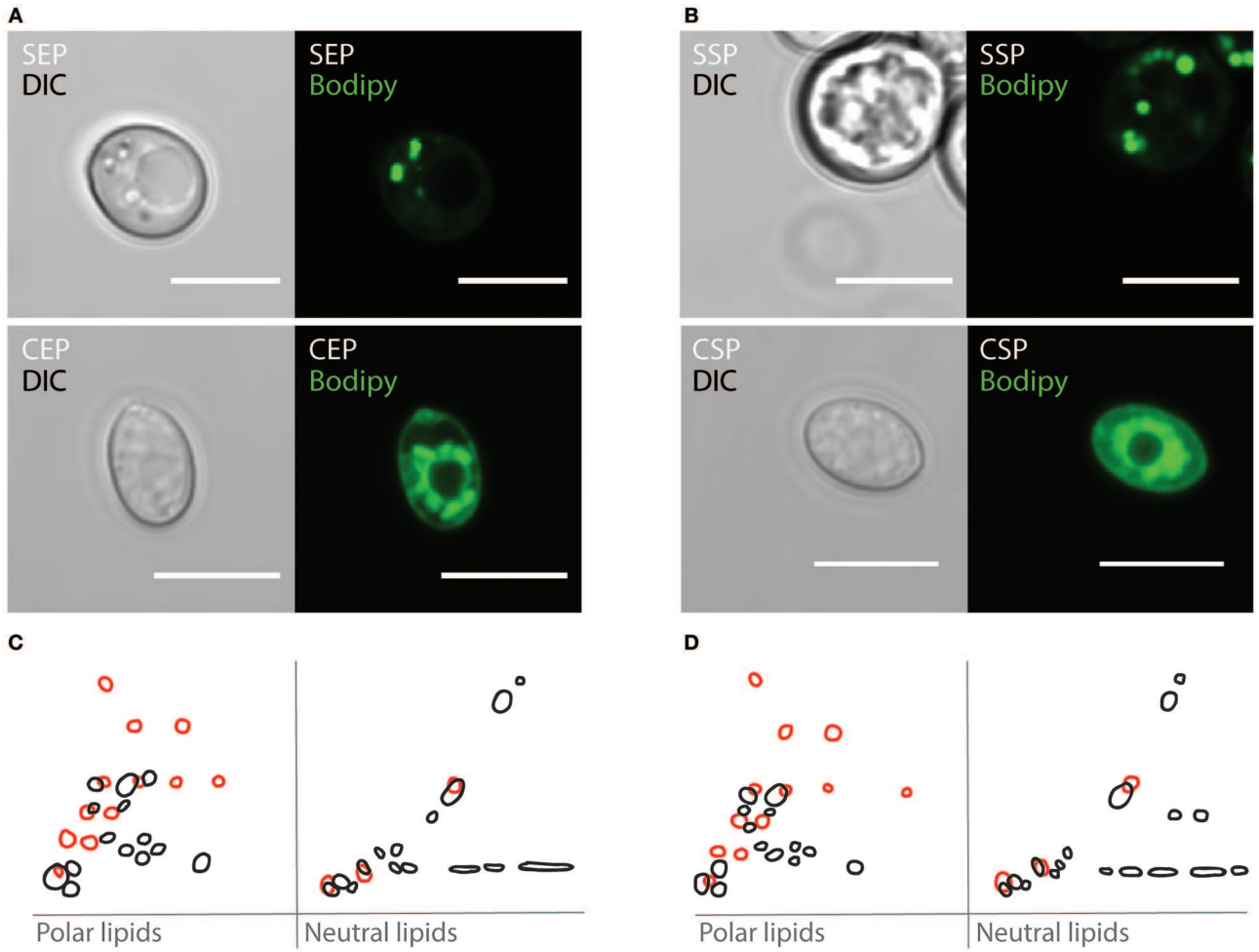

FIGURE 1 | *Cystobasidium oligophagum* and *Saccharomyces cerevisiae* have different lipid profiles. **(A,B)** Photographs of yeast harvested at specific growth stages probed with BODIPY-505. Shown are *S. cerevisiae* (S) or *C. oligophagum* (C) in exponential (EP) in **(A)** or stationary growth phase (SP) in **(B)**. Scale bar = 5μm. **(C,D)** Shown are 2D-TLC profiles of polar and neutral lipids. Lipid signatures from *S. cerevisiae* (black) or *C. oligophagum* (red) from exponential **(C)** and stationary **(D)** growth stages.

S. cerevisiae depend on growth; whereas *C. oligophagum* lipid profiles appear remarkably static throughout the generative cycle.

Designed Yeast Food Mimics the Biological Activity of the Respective Yeast

To test if *C. oligophagum* attract adult flies, we placed wild-type *OregonR* in feeding chambers and video-recorded their feeding behavior. Already after a short adaptation time, all tested animals started to feed and females positioned their eggs close to the provided yeast bait (**Figures 2A–C**, **Movies 1–3**). Interestingly, we noted that flies feeding on *S. cerevisiae* produced reproducibly higher egg numbers compared to flies feeding on *C. oligophagum* or plant material only ($n = 5$, total egg number: *C. oligophagum* = 299, *S. cerevisiae* = 578, and plant material = 184 eggs, each assay plate with 20–30 females and 15 males at 20°C). The oviposition rate of females is one readout for their metabolic activity. Since both yeast types do not show gross differences in their sugar or protein amounts, we speculated either that flies feed less on *C. oligophagum* or that dietary lipid profiles are instructive for the fly metabolism.

To neglect possible caloric differences or problems with the intestinal accessibility of nutrients we designed fly food recipes based on our cultured yeast. All four diets are equi-caloric (∼550 kcal/l), enriched in plant proteins and sugars to prevent carbon or amino acid shortages, and feature approximately identical carbohydrate: protein ratios (2:1). Moreover, the nature of our recipes minimizes the proportion of native yeast sugars and proteins (native yeast sugar and proteins are ∼0.0002% w/v while added sugar and proteins are ∼0.11% w/v in food). On the other hand, the fungal lipidomes are the only lipid source. To estimate the quantity of lipids, we weighted the dry mass of each food type and measured phosphate amounts present in respective lipid extracts. Food (F) produced from *C. oligophagum* (C) or *S. cerevisiae* (S) show similar phospholipid

mass (n = 3, CEP-F = 0.6; CSP-F = 0.5, SEP-F = 0.3, and SSP-F = 0.4 mg phospholipids/g food). Of note, the assay is unable to capture neutral lipids such as fatty acids and sterols. In addition, the unavoidable heat treatment during food preparation could break or modify some yeast products. Therefore, we have analyzed the phosphate-standardized lipid extracts using TLC. We found that heat treatment is changing the TLC profile of yeast. Especially some hydrophobic compounds produced by *C. oligophagum* with properties similar to neutral lipids (e.g., fatty acids, diacylglycerids, TAGs) are degraded at 110°C; whereas lipids from *S. cerevisiae* proof to be more heat stable (**Supplementary Figure 2**). At this point, we are not able to identify the heat-sensitive molecules. Taken together, the lipid profiles of the designed diets differ from respective yeast lipidomes.

To test if the created yeast food recipes induce similar physiological changes in feeding *Drosophila*, we have repeated the feeding-behavior experiments. Given a choice between plant material and yeast-based diets, adult flies tended to feed on the latter. Moreover, feeding was indifferent between two tested wild type genotypes irrespective of the provided yeast-food type (**Figures 2E,F**). Female flies kept on SSP-F

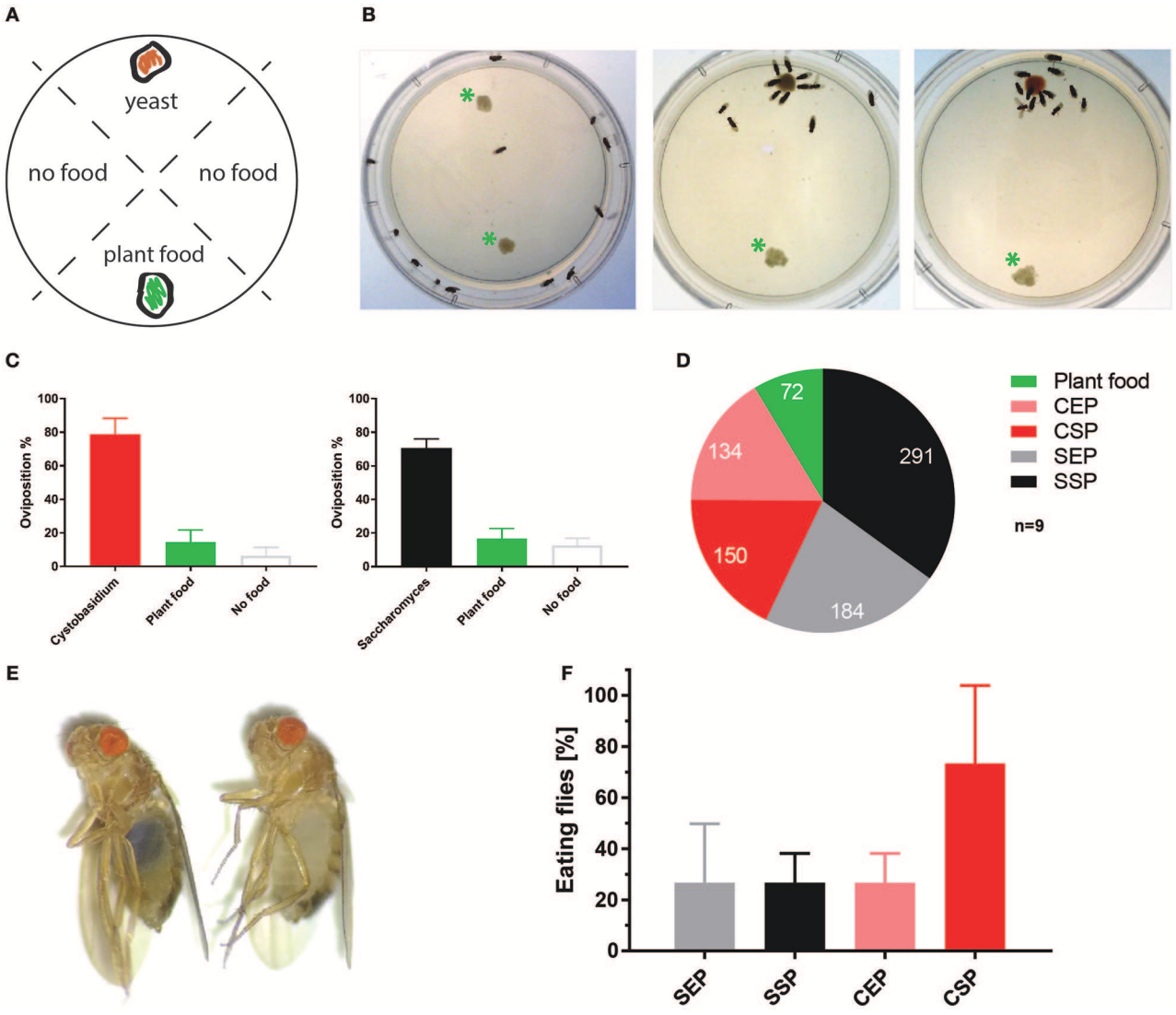

FIGURE 2 | *Cystobasidium oligophagum* attracts *Drosophila melanogaster.* **(A)** Scheme that depicts our quantification approach. Assay plates are divided into four sectors loaded with food (yeast or plant food) or without a bait (no food). **(B)** Shown are screenshots from movies that show the feeding behavior of wild type flies. Photograph with control plate (left), plates testing *S. cerevisiae* (middle), or *C. oligophagum* (right). *Plant food bait. **(C)** Plotted are percentages of eggs positioned in different food sectors: *S. cerevisiae* (black), *C. oligophagum* (red), plant food (yellow), or no food (gray). **(D)** Depicted are total egg numbers (n = 9/food type) from flies fed with plant food, exponentially (EP), and stationary (SP) grown *S. cerevisiae* (S) or *C. oligophagum* (C). **(E)** Shown is a photograph of a fly feeding on blue-stained food (left) and a not feeding fly kept on the identical diet (right). **(F)** Plotted is the percentage of feeding wild type flies (n = 3, total of 15 mated females/food type) kept on different blue stained diets. Note, there is no significant difference between CSP and other samples (Dunn's multiple comparisons test: $p > 0.05$).

produced more eggs than siblings kept on the other food types, thus mirroring the activity of live *S. cerevisiae* (**Figure 2D**, **Movies 4–7**). To investigate if food or fly-associated microbes convey the biological activity of SSP-F, we created microbe-free (axenic) larvae and tracked their growth and survival rates, both indicators for metabolic activity. Axenic animals rely entirely on provided food compositions and show a direct response to nutritional settings. Interestingly, only larvae kept on SSP-F were able to match the developmental speed and success of their microbe-bearing counterparts. All other axenic cultures developed slower and with lower survival rates (**Figure 3**).

Taken together, the designed food types are indifferent in their caloric content, their carbohydrate: protein ratios are identical, and the diets are rich in amino acids and monosaccharides. In consequence, the quality and quantity of the respective dietary lipid load is modulating the response of flies.

Dietary Lipid Extracts Regulate the Cellular Insulin Signal Cascade

Animals fed with high-fat diet or kept on chow-food show very different lipidomes (Carvalho et al., 2012). We have shown that the lipid extract composition of the different yeast foods varies. Thus, we wondered if the nutritional lipid quality in the experimental setups would induce endogenous lipid changes in feeding *Drosophila* (Carvalho et al., 2012). To do so, we transferred adults reared on normal food and kept the animals for 7 or 14 days on our yeast diets. Lipid extracts from larvae or adult fly heads did not reveal changes in the composition of complex endogenous lipids at 1D-TLC resolution (**Supplementary Figure 3**). It remains possible that structural qualities of absorbed and integrated dietary fatty acids, only visible by mass spectroscopy, regulate the fecundity and developmental rate. In addition, it was shown that *S. cerevisiae* are able to facilitate systemic insulin signaling in fruit flies (Brankatschk et al., 2014). Thus, we decided to probe for the localization of the transcription factor dFOXO (**Figure 4**). dFOXO is the most downstream target of the insulin pathway and resides in the nucleus at low metabolic rates. We found that only microbe-infested larvae kept on CSP-F show a predominant nuclear dFOXO localization. In stark contrast, dFOXO in axenic CSP-F-feeding siblings is mainly cytoplasmic (**Figure 4B**, ANOVA test between CSP and ax CSP: $p < 0.0001$). In addition, we found that microbes do not change dFOXO activity in larval cultures thriving on SEP-F, SSP-F, or CEP-F (**Figure 4B**, ANOVA test between food type and its axenic counterpart: $p > 0.05$). Taken together, associated microbes block dFOXO activity in animals feeding on CSP-F. However, only axenic cultures kept on SSP-F match the developmental success shown by their microbe-infested counterparts (**Figure 3**).

Many different dILPs regulate the larval development and thus, mimic the function of vertebrate insulin-like growth factors (IGFs; Brogiolo et al., 2001). Moreover, invertebrate dILPs probably represent an ancestral regulative network that channels IGFs and insulin-like signaling to one receptor (Barbieri et al., 2003; Grönke et al., 2010). Therefore, developmental dILPs blur metabolic aspects of the insulin circuit. To circumvent the problem, we decided to analyse dAkt activity in adult fly-head samples since dILPs expressed only in the larval

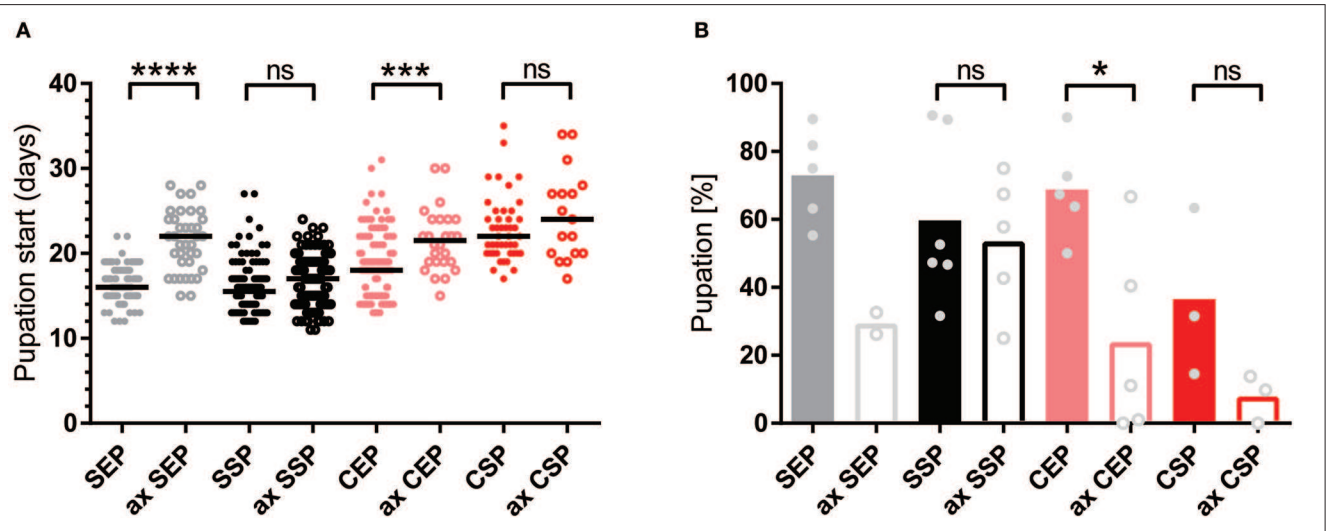

FIGURE 3 | Stationary yeast food rescues the metabolic syndrome of axenic larvae. **(A,B)** Plotted is the larval developmental speed **(A)** and survival rate **(B)** of axenic (ax) and microbe-associated larvae kept on food based on exponential (EP) and stationary (SP) *S. cerevisiae* (S) or *C. oligophagum* (C). Each spot represents one tracked individual **(A)** or one experimental cohort of minimum 20 individuals **(B)**. Differences between the mean values of experimental groups were compared with Dunn's multiple comparisons test for developmental speed and Tukey's multiple comparison test for survival rate data. n.s., none significant; $^{*}p < 0.05$, $^{***}p < 0.001$, $^{****}p < 0.0001$. *P*-values: **(A)** CEP vs. ax CEP $p = 0.0009$, CEP vs. CSP $p < 0.0001$, CEP vs. ax CSP $p = 0.0001$, CEP vs. SEP $p = 0.0091$, CEP vs. ax SEP $p = 0.0001$, CEP vs. SSP $p < 0.0001$, ax CEP vs. SEP $p < 0.0001$, ax CEP vs. SSP $p < 0.0001$, ax CEP vs. ax SSP $p < 0.0001$, CSP vs. SEP $p < 0.0001$, CSP vs. SSP $p < 0.0001$, CSP vs. ax SSP $p < 0.0001$, ax CSP vs. SEP $p < 0.0001$, ax CSP vs. SSP $p < 0.0001$, ax CSP vs. ax SSP $p < 0.0001$, SEP vs. ax SEP $p < 0.0001$, ax SEP vs. SSP $p < 0.0001$, ax SEP vs. ax SSP $p < 0.0001$; (B) CEP vs. ax CEP $p = 0.0336$, CEP vs. ax CSP $p = 0.008$, ax CEP vs. SEP $p = 0.0158$, ax CSP vs. SEP $p = 0.004$, ax CSP vs. SSP $p = 0.0261$.

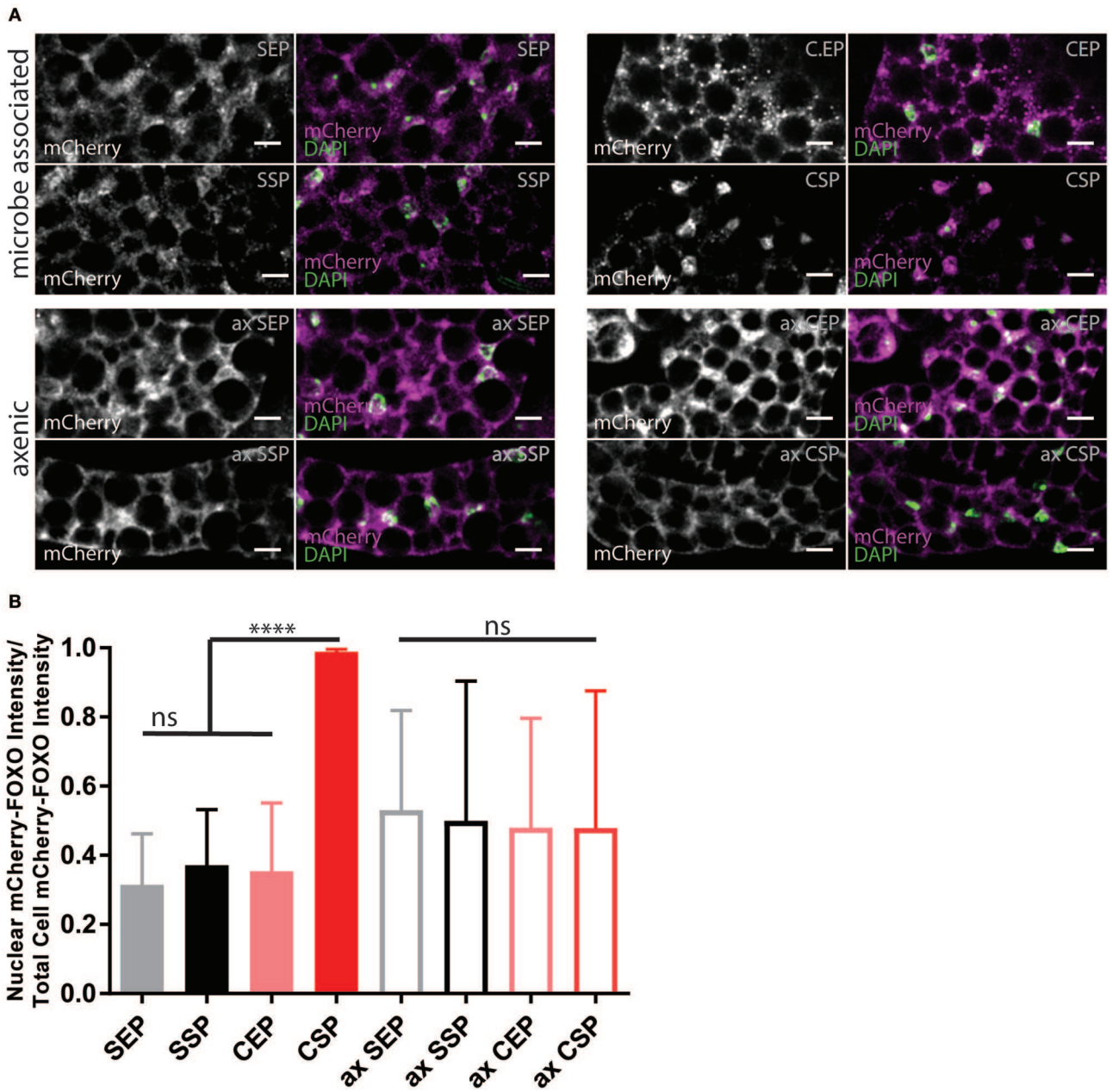

FIGURE 4 | Yeast food quality and microbial load modulate dFOXO activity. **(A)** Photographs from larval fat bodies (early 3rd instar larvae). Samples were probed for mCherry-FOXO (magenta, white) and DAPI (green). Shown are samples from microbe associated (upper two panels) or axenic (ax, lower two panels) individuals kept on food based on stationary (SP) or exponentially (EP) grown *S. cerevisiae* (S) or *C. oligophagum* (C). Scale bars = 10μm. **(B)** Plotted is the quantification of mCherry-FOXO fluorescent intensity in nuclei of fat body cells ($n \geq 3$ with ≥15 cells/sample). Differences between the mean values of groups were compared with Tukey's multiple comparisons test. n.s., none significant; ****$p < 0.0001$. *P*-values: SEP vs. CSP $p < 0.0001$, SEP vs. ax SEP $p = 0.0019$, SEP vs. ax SSP $p = 0.0275$, SSP vs. CSP $p < 0.0001$, CEP vs. CSP $p < 0.0001$, CEP vs. ax SEP $p = 0.0192$, CSP vs. ax SEP $p < 0.0001$, CSP vs. ax SSP $p < 0.0001$, CSP vs. ax CEP $p < 0.0001$, CSP vs. ax CSP $p < 0.0001$.

and pupal stage are not present anymore (Zhang et al., 2009; Grönke et al., 2010). Phosphorylated active dAkt deactivates dFOXO (Calnan and Brunet, 2008). Therefore, we speculated with reference to the shown oviposition preference of mated females (**Figure 2D**) that only flies kept on SSP-F will show high dAkt phosphorylation levels. To test our hypothesis, we raised adults on normal food and then transferred the animals onto different yeast-based diets for 7 or 14 days at 20°C. We found that early into our experiment dFOXO levels do not change in flies kept on different diets (**Figure 5A**). Interestingly,

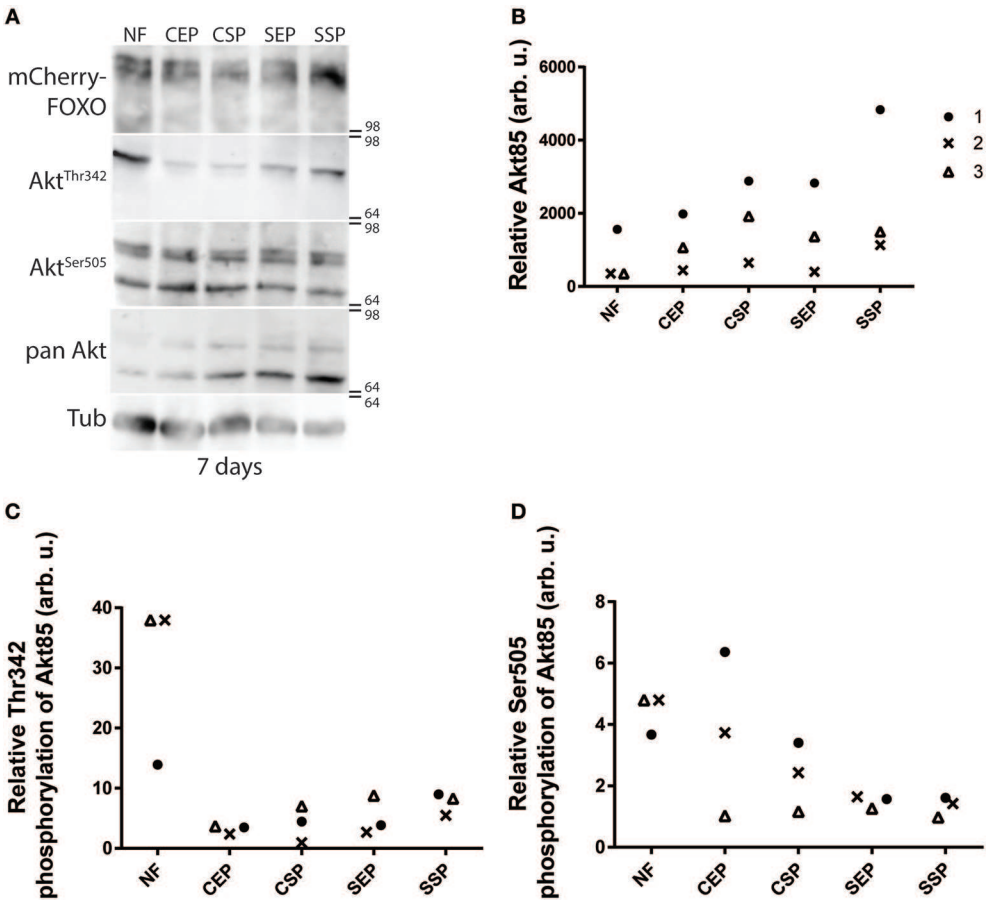

FIGURE 5 | Individual dAkt isoforms facilitate dInR induced cellular insulin signaling. **(A)** Protein samples from flies kept on normal food (NF), and food from stationary (SP), or exponentially (EP) grown *S. cerevisiae* (S) or *C. oligophagum* (C). Shown is a photograph from a Western-Blot membrane of adult head-samples from flies taken 7 days after transfer from normal food (NF) to the respective yeast diet probed for mCherry (mCherry-FOXO), phosphorylated dAkt (Akt^{Thr342} or Akt^{Ser505}), pan-dAkt protein (pan Akt), and Tubulin (Tub). **(B–D)** Quantification of three independent Western-Blot replica from head-samples (9 heads per sample) of adult flies taken 7 days after transfer from normal food (NF) to the respective yeast diet (SSP, SEP, CSP, or CEP). Shown are relative ratios of pan-$dAkt^{85}$/Tubulin **(B)**, phosphorylated $dAkt^{85-Thr342}$/pan-$dAkt^{85}$ **(C)**, and $dAkt^{85-Ser505}$/pan-$dAkt^{85}$ **(D)**.

compared with normal food-fed specimen, flies kept on our yeast-food types upregulate $dAkt^{85}$ protein levels after 7 days (**Figures 5A,B**). Later, at the 14-day time point, only flies on SSP-F maintain higher or similar $dAkt^{85}$ amounts with respect to normal food feeding animals (**Supplementary Figures 4A,B**). Interestingly, during the early upregulation of $dAkt^{85}$, the relative phosphorylation levels at $Akt^{85-Ser505}$ and $Akt^{85-Thr342}$ drop with increasing protein amounts (**Figures 5C,D**). This trend is not continued; after 2 weeks, relative $dAKT^{85}$ phosphorylation stabilizes close to levels shown by animals kept on normal food (**Supplementary Figures 4C,D**). Of note, $dAkt^{66}$ is phosphorylated at its $dAkt^{66-Ser505}$ position, but never detectable at $dAkt^{66-Thr342}$ (**Figure 5A**, **Supplementary Figure 4A**). We conclude that in adult differentiated cells, $dAkt^{85}$ is the predominant metabolically active dAkt isoform; and we propose that dietary lipids present in stationary *S. cerevisiae* elevate or stabilize $dAkt^{85}$ amounts to facilitate cellular insulin signaling.

DISCUSSION

Environmental factors drive the spread and the dynamic behavior of insect populations as well as the quality and abundance of accessible food sources. Recent findings add another dimension to this simple equation, the identity and state of food-associated microbes (Nicholson et al., 2012). *Drosophila* are attracted by volatile yeast cues and prefer to feed on calorie-rich rotting plant material infested by yeast and other microbes (Becher et al., 2012). Such microbes share often the optimal temperature range of fruit flies (Watson, 1987; Petavy et al., 2001; Tsuji et al., 2017). Hence, available rotting fruits or other decomposing plant materials, in a given area, are infested by different yeast species (Chandler et al., 2012). We have isolated the yeast *Cystobasidium oligophagum* from wild type *OregonR* flies kept outside of the laboratory, a ubiquitous fungus known to degrade plant material. Is *C. oligophagum* a likely candidate associated with fruit flies? We show that *C. oligophagum* attracts flies

and that *Drosophila* consume these yeasts. The fact that we have found this fungus in fly droppings indicates that some cells survive the intestinal passage (**Supplementary Figure 5**). However, to what proportion *C. oligophagum* is present on rotting fruits remains unclear and it remains to be shown if these type of yeast is found on wild flies (Chandler et al., 2012). In the laboratory, *Saccharomyces cerevisiae* is widely used to cultivate *Drosophila*. Recently, it was reported that lipid extracts from *S. cerevisiae* accelerate the generative cycle of flies by increasing the systemic insulin signaling rate (Brankatschk et al., 2014). However, *S. cerevisiae* are not predominant in regional natural habitats and it is likely that the interaction between fruit flies and their microbial surrounding is more complex (Hoang et al., 2015). In consequence, several questions arise in our quest to understand how microbes modulate the physiology and evolutionary conserved metabolic circuits of fruit flies. At first, we attempt to answer the question if all food-associated yeast provide factors that enhance the generative cycle of *Drosophila*.

At this point, it is not possible to estimate how natural variations of the genetic configuration in wild fly populations change the metabolic response of individuals. Therefore, we kept wild type flies (e.g., *OregonR* or *mCherry-FOXO*), harboring a defined genotype, on plant material supplemented with either *S. cerevisiae* or *C. oligophagum*. Interestingly, females feeding on *C. oligophagum* show low egg numbers compared to flies feeding on *S. cerevisiae*. Our finding allows for different explanations, either *C. oligophagum* is a poor diet or *C. oligophagum* products do not stimulate the metabolism of *Drosophila*. To exclude variables [including protein/sugar ratio, nutritional caloric load (Fanson et al., 2012), intestinal resorption (Diamond, 1991), microbial growth stage (Klose et al., 2012), or the immune response to microbes (Hoffmann, 2003)], we have created artificial food from both yeast. The resultant diets are enriched in protein and sugars to dwarf yields of respective fungal compounds. Of note, we found that the heat-treatment step in our food preparation protocols is changing the profile of hydrophobic yeast compounds detected by TLC. Reverse phase thin layer chromatography separates molecules based on their hydrophobicity and charge. Therefore, compounds like heat-sensitive vitamins containing fatty acid residues are well-detectable on TLC (Mohammad et al., 2012). To ensure the biological activity of our diets, we decided to repeat the egg-laying experiments performed earlier with living yeast. We observed that adult flies prefer *S. cerevisiae* food, especially produced from stationary cells. In addition, the same diet promoted development. Our results fit well with earlier experiments based on yeast food prepared from commercially available dry Baker's yeast from the grocery store (Carvalho et al., 2012; Brankatschk et al., 2014, 2018). Such dry yeast are composed from stationary cells grown in a fermenter. We speculate that the short reactivation time of dry yeast prior to our experiments (food preparation protocols, experiments with live yeast) is not sufficient to change their nutritional profile and therefore, *S. cerevisiae* harvested in their exponential growth phase nor any *C. oligophagum* culture accelerated *Drosophila* development.

Fly-associated microbes can modulate the nutritional input and, in some cases, promote directly or indirectly the insulin pathway. For instance, *Acetobacter pomorum* secrete metabolites capable to induce insulin signaling (Shin et al., 2011). In poor nutritional conditions, *Lactobacterium* replenish amino acid shortages and thus, restore the metabolic activity of the host (Storelli et al., 2011). To exclude the microbial variable in our experiments, we decided to test the development of microbe-free (axenic) larvae. Axenic animals tend to develop a metabolic syndrome, similar to insulin resistance, resulting in lower survival and slower developmental rates (Shin et al., 2011; Ridley et al., 2012). Therefore, we decided to run microbe-bearing and microbe-free cultures in parallel. Astonishingly, only axenic cultures thriving on stationary *S. cerevisiae* food matched the developmental parameters from siblings kept on the respective microbe-infested diet. We assume stationary yeast produce a heat-stable biological active compound capable to accelerate the development of *Drosophila*. We propose two possibilities; first, that lipid extracts from stationary yeast change the lipidome of the host leading to increased cellular insulin responsiveness. Although we did not detect any changes of endogenous complex lipids in response to the provided diets, our TLC-based analyses may not be sensitive enough. A better view could be provided by lipid mass spectroscopy (Carvalho et al., 2012) and the functional tests of biophysical membrane properties (Brankatschk et al., 2018). Second, it was shown that lipid extracts from stationary *S. cerevisiae* hyper-activate insulin-producing cells (Brankatschk et al., 2014). The consequent high circulating levels of insulin-like peptides stimulate the InR regulated cellular signal cascade (Brankatschk et al., 2014). We found that the transcription factor dFOXO changes its nuclear localization in response to the microbial load associated with the animals. It is widely accepted that the mTor-like signaling, one integral component of the *Drosophila* immune system, is modulating Akt and hence, changing FOXO activity (Pourrajab et al., 2015). Our cultivation protocol mildly stimulates the larval digestive system and food-associated microbes likely induce an immune response. Therefore, it is fair to speculate that developmental differences between axenic and non-axenic animals are not purely based on nutritional/metabolic factors (Slack et al., 2015).

Larval development includes the expression of many different dILPs that control the growth rate and morphological appearance of tissues irrespective of the metabolic input. To disentangle developmental from metabolic aspects, we resolved to study the phosphorylation of Akt, a central enzyme of the InR-controlled signal cascade, in adult flies. It is widely accepted that phosphorylated Akt is active, and that active Akt is responsible for the negative regulation of FOXO (Calnan and Brunet, 2008). Vertebrates express different Akt isoforms; for instance mice or humans express three different Akt proteins. Of note, the different isoforms are not equally expressed in all cell types (Gonzalez and McGraw, 2009a,b). Surprisingly, knock-out mice with only one functional copy of Akt1 are viable but show some physiological changes and are sensitive to dietary sugar loads (Dummler et al., 2006). However, most studies presume a parallel activity of all Akt isoforms and value the contribution of individual Akt isoforms in the insulin signal cascade based

on their present levels (Gonzalez and McGraw, 2009a; Santi and Lee, 2010). Alike vertebrates, fruit flies express three different isoforms of the kinase Akt (Andjelković et al., 1995). As reported, we have detected two isoforms in our adult head-samples, $dAkt^{66}$ and $dAkt^{85}$. However, we found that $dAkt^{85}$ is predominantly regulated in response to dietary cues and that $dAkt^{66}$ is hardly phosphorylated at the $dAkt^{66-Thr342}$ site. We conclude that individual dAkt isoforms in adult flies are differently addressed in response to dietary cues. In sum, we predict that lipid extracts from stationary *S. cerevisiae* increase circulating dILP levels and more insulin peptides bind to their receptor (Brankatschk et al., 2014). The insulin-bound dInR recruit additional PI3 kinases, which induce the production of Phosphoinositol-(3,4,5)-phosphate (PIP_3) by conversion of membrane integrated Phosphoinositol-(4,5)-phosphate (PIP_2) (Scanga et al., 2000). Therefore, the PIP2:PIP3 ratio is shifted and more cytoplasmic $dAkt^{85}$ associates with PIP3 and is phosphorylated by local kinases. Further, phosphorylated $dAkt^{85}$ regulates the downstream transcription factor dFOXO; this would implicate that $dAkt^{85}$, similar to vertebrate Akt2 (Garofalo et al., 2003), is responsible for the insulin-mediated glucose disposal. In addition, since $dAkt^{66}$ is never phosphorylated at its Thr342 position, we reinforce the idea that $dAkt^{66}$, like vertebrate Akt3, fulfills more developmental roles (Andjelković et al., 1995; Santi and Lee, 2010) or is rather required to amplify signals from none-metabolic pathways (Weichhart and Saemann, 2008; Grootjans et al., 2016).

In sum, we add, to the complexity of microbe-host interactions, the variable of microbial growth stage; and we spotlight the differential phosphorylation and expression of dAkt isoforms as a versatile tool to facilitate the cellular insulin signal cascade. In addition, our work positions nutritional lipids as important metabolic modulators within a high-caloric environment; therefore, the quality of dietary lipids may represent a suitable target to define bioactive food.

MATERIALS AND METHODS

Fly Stocks

If not stated otherwise, flies were kept at RT in a day/night cycle. *mCherry::foxo* from S. Eaton lab, *CantonS* from J.-C. Billeter's lab and *OregonR* were purchased from Bloomington stock center.

Yeast

Saccharomyces cerevisiae (BY4741) was obtained from K. Ostermann and *Cystobasidium oligophagum* are wild isolates identified by M. Kaltenpoth.

Food Recipes

Normal food (https://bdsc.indiana.edu/information/recipes/bloomfood.html) and plant food (Carvalho et al., 2012) were produced following published protocols, using dry-yeast purchased from the grocery discounter Kaufland. *Saccharomyces cerevisiae* (BY4741) and *C. oligophagum* foods were produced based on pelleted yeast obtained from SCP-medium (1.9 g/L yeast nitrogen base, 5 g/L ammonium sulfate, 20 g/L glucose, 20 g/L peptone) cultures grown at 20°C (v = 100 ml; wet yeast-pellet = 9.04 g, glucose = 6 g, soy peptone = 2 g, sucrose = 3 g, agar-agar = 1 g, and nipagin = 0.4 g). The Exponential Growth Phase (EP) is defined at the optical density $OD_{600}{}^{EP} = 2–3$ for *S. cerevisiae* or a $mass^{EP}$ of 0.02 g/ml for *C. oligophagum* and the Stationary Growth Phase (SP) at $OD_{600}^{SP} > 5$ (*S. cerevisiae*) and a $mass^{SPof} > 0.04$ g/ml (*C. oligophagum*). Of note, *C. oligophagum* cells tend to aggregate preventing a conventional optical density measurement.

Cystobasidium oligophagum Isolation

OregonR were kept in an open cage on plant food without resistance factors for 2 weeks at 20°C, and subsequently transferred onto apple-juice plates. Deposited droppings were resolved in water and plated onto YPD-culture media plates. After 72 h at 20°C, microbial colonies were picked, cultivated in YPD media and samples send for 18S ribosomal sequencing.

Behavior Assays

CantonS flies were raised on normal food, adults were transferred for 6 h on apple juice plates at 22°C, and subsequently placed on assay plates (20% apple juice, 1% agar, each plate with 3 males and 9 mated females) fitted with food baits opposing each other. Fly behavior was recorded for 3 h at 22°C and afterwards plates were kept for 24 h at 20°C. Subsequently, flies were removed, and deposed eggs counted.

Larval Developmental Tracking

Eggs from *OregonR* collected from apple juice-agar plates were washed with tap water, bleached with Sodiumhypochloride (10%) and transferred onto apple juice plates. Later, hatched first-instar larvae were placed onto food and kept at 20°C.

Axenic Animals

Eggs from *OregonR* collected from apple juice agar plates were washed with tap water, bleached with Sodiumhypochloride (10%) and transferred onto sterile apple juice plates (treated with hard UV light). Later, hatched first instar larvae were placed under sterile conditions onto microbe-free food using aseptic tools and kept at 20°C.

Trehalose Measurements

Samples were autoclaved and processed like recommended by manufacturer (Trehalose Kit, Megazyme).

Protein Estimation

Samples were autoclaved and processed like recommended by manufacturer (BCA Kit, Pierce).

Lipid Extraction and TLC

Tissue samples were thawed on ice, homogenized in HBS using an IKA ULTRA-TURRAX disperser (level 5, 1 min), and lipid-extracted by the BUME method (Löfgren et al., 2012). Extracted lipids were stored in chloroform/methanol (2:1) solution at −80°C.

Feeding Assay

Food intake measurements on dyed food was performed as described elsewhere (Deshpande et al., 2014). The food was stained with 1% w/v bromophenol blue solution. *mCherry::foxo* flies (one male and five mated females, 0 to 7-days old) were transferred on respective diets at 20°C. After 4 h, feeding was interrupted by freezing flies in liquid nitrogen. Only females were used to quantify blue stained fly guts.

Biochemistry

Western Blot Analysis

mCherry::foxo flies were raised on normal food and 0 to 3-day-old adults were transferred for 14 days on respective diets at 20°C (male to female ratio 1:3; food renewal in regular intervals). Adults were snap-frozen with liquid nitrogen and fly heads removed. Fly heads were homogenized with a pestle in sample buffer (loading buffer, please see https://openwetware.org) and subsequently heat-inactivated for 10 min. Homogenates were centrifuged and supernatants used for TRIS-SDS-PAGE. Separated proteins were transferred by Tank-Blotting to nitrocellulose membrane. Membranes were blocked for 1 h with 5% BSA in 0.1% Triton X-100/PBS and then incubated with antibodies in blocking solution overnight. Polyclonal antibodies used to probe were Akt-pSer505 (Cell Signaling, 4054S), Akt-pThr308 (Invitrogen, 44-602G), Akt (Invitrogen, MAS14916), mCherry (Invitrogen, PAS-34974), and Tubulin (Cell Signaling, 2144S). After washing, membranes were incubated with HRP conjugated antibodies (Thermo Fischer, 31466) for 1 h and then bands detected with chemiluminescence.

Quantification

Samples were taken after 7 days ($n = 3$) and 14 days ($n = 2$) after specimen were transferred from normal food to respective yeast diets. Signals from Western blot membranes were photographed using an ImageQuant L4000 reader and photographs were analyzed using FIJI software (Schindelin et al., 2012). Each signal-band region of interest was selected with the "rectangle"-selection tool and the mean of fluorescence intensity was calculated. The intensity values have been normalized to the signals of the membrane background and of the tubulin signal from the same blots. Plotted are signal ratios between: $dAKT^{85}$/Tubulin (**Figure 5B**, **Supplementary Figure 4B**), phospho-$dAKT^{85-Thr342}$/$dAKT^{85}$ (**Figure 5C**, **Supplementary Figure 4C**), and phospho-$dAKT^{85-Ser505}$/$dAKT^{85}$ (**Figure 5D**, **Supplementary Figure 4D**).

Immunohistochemistry

Microscopy Analysis

mCherry::foxo and *CantonS* first instar larvae were transferred on respective food and kept at 20°C. After 5 days, larvae were fixed and dissected in 4% PFA, blocked for 1 h in blocking solution (5% native goat serum, 0.1% Triton X-100 in PBS, pH = 7.2) and incubated with anti-mCherry antibody (Invitrogen, PAS-34974) over night at 4°C. After washing, samples were incubated with goat-anti-rabbit-Alexa Fluor 555 (Thermo Fisher) and stained with DAPI for 2 h at room temperature. *mCherry*-FOXO signal in larval fat body was detected using confocal microscopy (Zeiss LSM700, 20x objective, respective Bandpass filters).

Quantification

The quantification of the mCherry signal has been performed on individual cells (cells) of larval fat bodies from several biological replicates (n). The densities of the fluorescence intensity (IntDen) were measured with Fiji Image J (Schindelin et al., 2012) (SEP: $n = 8$, cells = 41; SSP: $n = 9$, cells = 43; CEP: $n = 9$, cells = 45; CSP: $n = 9$, cells = 47; ax SEP: $n = 9$, cells = 48; ax SSP: $n = 9$, cells = 40; ax CEP: $n = 3$, cells = 15; ax CSP: $n = 5$, cells = 23). The IntDen values have been normalized to the IntDen signal values of *CantonS* fat bodies ($n = 3$–5, cells = 3–5). For each cell, the mCherry IntDen value of the whole cell ($IntDen_{cell}$) and the nucleus ($IntDen_{nucleus}$) have been measured by using FIJI and the "freehand"-selection tool; while the cytoplasm IntDen ($IntDen_{cyto}$) signal has been calculated as following: $IntDen_{cyto} = IntDen_{cell}$-$IntDen_{nucleus}$ Then, the ratio $IntDen_{nucleus}/(IntDen_{nucleus} + IntDen_{cyto})$ have been calculated for each cell.

Yeast lipid droplets were stained with Bodipy 505/515 (Thermo Fisher) on ice for 2 h, and later life yeast were imaged using fluorescent-confocal microscopy (Zeiss LSM780, 63x oil objective, respective DIC, and Bandpass filters).

Yeast Digestion Assay

OregonR third-instar larvae were transferred for 2 h into a tube containing Bodipy 505/515 stained *S. cerevisiae* or *C. oligophagum* (both harvested in stationary growth phase, grown at 20°C). Guts from feeding larvae were dissected in ice-cold PBS, and subsequently imaged using confocal microscopy (Zeiss LSM780, 10x objective, respective DIC, and Bandpass filters). Composite gut images were stitched together from overlapping single two-channel image tiles using the Fiji Plug in Preibisch et al. (2009).

Statistics

Statistical analyses were performed with GraphPad Prism 7. Sample sizes are listed above or in figure legends. Difference between the mean ranks of blue stained food eating fly samples were calculated using Dunn's multiple comparisons test. Difference between the experimental groups for pupation speed and survival rate were calculated using Dunn's and Tukey's multiple comparisons test, respectively. Tukey's multiple comparisons test was also used to assess differences in nuclear mCherry-FOXO localization in fat body cells between groups.

DATA AVAILABILITY STATEMENT

All datasets generated for this study are included in the manuscript/**Supplementary Files**.

AUTHOR CONTRIBUTIONS

Experimental work by LT, EP, CM, NB, FH, and MG. Manuscript concept by LT, EP, MG, and MB.

FUNDING

This work was supported by the German research council (DFG) by grants to MB, EP, FH, NB, and LT (BR5492, BR5493–FOG2682) and MG (Project Number 251981924–TRR 83 and Project Number 347368302–FOG2682) and the Open Access Funding by the Publication Fund of the TU Dresden.

ACKNOWLEDGMENTS

We are thankful to Martin Kaltenpoth (University Mainz) for identifying *Cystobasidium oligophagum*.

SUPPLEMENTARY MATERIAL

The Supplementary Material for this article can be found online at: https://www.frontiersin.org/articles/10.3389/fcell.2019.00206/full#supplementary-material

Supplementary Figure 1 | Yeast growth state is important for lipid quality in *S. cerevisiae.* **(A,C)** Plotted are the growth curves of *S. cerevisiae* **(A)** or *C. oligophagum* in **(C)**. R^2 indicates goodness of fit to the non-linear sigmoidal regression model. **(B,D)** Plotted are the protein and trehalose content of samples based on exponential (EP) and stationary (SP) *S. cerevisiae* (S) in **(B)** or *C. oligophagum* (C) in **(D)**. Lipid profiles **(E)** of polar and neutral lipids based on exponential (EP) and stationary (SP) *S. cerevisiae* (S) (SEP, SSP) or *C. oligophagum* (C) (CEP, CSP) were analyzed by 2-D Thin-layer chromatography.

Supplementary Figure 2 | Heat-treatment changes the lipid profile of yeast. Shown is the lipid profile of yeast and yeast food lipid extract samples by separation with 1-D Thin-layer chromatography. Samples are based on sole stationary (SP) *S. cerevisiae* (S) or *C. oligophagum* (C) and respective foods (food), before and after autoclaving (aut.). Lipid markers include: CE, cholesterol esters; Cer-PE, ceramide phosphorylethanolamine; DAG, diacylglycerol; Erg, ergosterol; FA, fatty acid; MAG, monoacylglycerols; TAG, triacylglycerol.

Supplementary Figure 3 | Fly endogenous lipid composition is not altered by nutritional lipids. **(A,B)** Shown is the separation of larval **(A)** and adult head **(B)** lipid extract samples by 1-D Thin-layer chromatography. Samples from animals kept on food based on exponential (EP) and stationary (SP) *S. cerevisiae* (S) or *C. oligophagum* (C). Samples were analyzed in triplicates (1–3). Lipid markers include: Card, cardiolipin; CE, cholesterol esters, Cer, ceramide; Ch-Ac, cholesterol-acetate; Chol, cholesterol; CPE, ceramide phosphorylethanolamine; DAG, diacylglycerol; Erg, ergosterol; FA, fatty acid; Gb3, globotriaosylceramide; GC, glucosylceramide; GM1-3, ganglioside; Lan, lanosterol; LC, lactosylceramide; PA, phosphatidic acid; PC, phosphatidylcholine; PE, phosphatidylethanolamine; PG, phosphatidylglycerol; PI, phosphatidylinositol; POPG, 2-Oleoyl-1-palmitoyl-sn-glycero-3-phospho-rac-(1-glycerol); PS, phosphatidylserine; Sit, sitosterol; SM, sphingomyelin; TAG, triacylglycerol.

Supplementary Figure 4 | Individual dAkt isoforms facilitate dInR induced cellular insulin signaling. **(A)** Protein samples from flies kept on normal food (nf), and food from stationary (sp) or exponentially (ep) grown *S. cerevisiae* (s) or *C. oligophagum* (c). Shown is a photograph from a Western-Blot membrane of adult head-samples from flies taken 14 days after transfer from normal food (NF) to the respective yeast diet probed for mCherry-dFOXO, p-dAkt (Akt^{Thr342} or Akt^{Ser505}), pan-dAkt protein (Akt), and Tubulin (Tub). **(B–D)** Quantification of two independent Western-Blot replica from head-samples ($n = 9$ heads each sample) of adult flies taken 14 days (14d_n) after transfer from normal food (NF) to the respective yeast diet (SSP, SEP, CSP, or CEP). Shown are relative ratios of pan-$dAkt^{85}$/Tubulin **(B)**, phosphorylated $dAkt^{85-Thr342}$/pan-$dAkt^{85}$ **(C)**, and $dAkt^{85-Ser505}$/pan-$dAkt^{85}$ **(D)** with respect to samples from specimen kept on normal food.

Supplementary Figure 5 | Some *Cystobasidium* cells might survive the larval intestinal passage. **(A,B)** Third instar larvae were fed with stained (Bodipy) *S. cerevisiae* **(A)** or *C. oligophagum* **(B)**. Guts from feeding larvae were dissected and imaged. Shown is a stitched whole gut image and two distinct magnified sections, part of the anterior midgut (1) and hindgut (2). Black scale bars = 500 μm, white scale bars = 50 μm.

Supplementary Movies | Exemplary movies show the behavior of adult flies on plates. Food samples are based on exponential (EP) and stationary (SP) *S. cerevisiae* (SEP, SSP) or *C. oligophagum* (CEP, CSP).

Movie 1 | Testing plant food vs. plant food.

Movie 2 | Testing *S. cerevisiae* vs. plant food.

Movie 3 | Testing *C. oligophagum* vs. plant food.

Movie 4 | Testing SEP vs. plant food.

Movie 5 | Testing SSP vs. plant food.

Movie 6 | Testing CEP vs. plant food.

Movie 7 | Testing CSP vs. plant food.

REFERENCES

Abbott, S. K., Else, P. L., Atkins, T. A., and Hulbert, A. J. (2012). Fatty acid composition of membrane bilayers: importance of diet polyunsaturated fat balance. *Biochim. Biophys. Acta* 1818, 1309–1317. doi: 10.1016/j.bbamem.2012.01.011

Alessi, D. R., Andjelkovic, M., Caudwell, B., Cron, P., Morrice, N., Cohen, P., et al. (1996). Mechanism of activation of protein kinase B by insulin and IGF-1. *EMBO J.* 15, 6541–6551. doi: 10.1002/j.1460-2075.1996.tb01045.x

Andjelković, M., Jones, P. F., Grossniklaus, U., Cron, P., Schier, A. F., Dick, M., et al. (1995). Developmental regulation of expression and activity of multiple forms of the *Drosophila* RAC protein kinase. *J. Biol. Chem.* 270, 4066–4075. doi: 10.1074/jbc.270.8.4066

Barbieri, M., Bonafè, M., Franceschi, C., and Paolisso, G. (2003). Insulin/IGF-I-signaling pathway: an evolutionarily conserved mechanism of longevity from yeast to humans. *Am. J. Physiol. Endocrinol. Metab.* 285, E1064–E1071. doi: 10.1152/ajpendo.00296.2003

Becher, P. G., Flick, G., Rozpedowska, E., Schmidt, A., Hagman, A., Lebreton, S., et al. (2012). Yeast, not fruit volatiles mediate *Drosophila* melanogaster attraction, oviposition and development. *Funct. Ecol.* 26, 822–828. doi: 10.1111/j.1365-2435.2012.02006.x

Böhni, R., Riesgo-Escovar, J., Oldham, S., Brogiolo, W., Stocker, H., Andruss, B. F., et al. (1999). Autonomous control of cell and organ size by CHICO, a *Drosophila* homolog of vertebrate IRS1–4. *Cell* 97, 865–875. doi: 10.1016/S0092-8674(00)80799-0

Brankatschk, M., Dunst, S., Nemetschke, L., and Eaton, S. (2014). Delivery of circulating lipoproteins to specific neurons in the *Drosophila* brain regulates systemic insulin signaling. *Elife* 3:e02862. doi: 10.7554/eLife.02862

Brankatschk, M., Gutmann, T., Knittelfelder, O., Palladini, A., Prince, E., Grzybek, M., et al. (2018). A temperature-dependent switch in feeding preference improves *Drosophila* development and survival in the cold. *Dev. Cell* 47, 257–259. doi: 10.1016/j.devcel.2018.10.010

Brogiolo, W., Stocker, H., Ikeya, T., Rintelen, F., Fernandez, R., and Hafen, E. (2001). An evolutionarily conserved function of the *Drosophila* insulin receptor and insulin-like peptides in growth control. *Curr. Biol.* 11, 213–221. doi: 10.1016/S0960-9822(01)00068-9

Calnan, D. R., and Brunet, A. (2008). The FoxO code. *Oncogene* 27, 2276–2288. doi: 10.1038/onc.2008.21

Carvalho, M., Sampaio, J. L., Palm, W., Brankatschk, M., Eaton, S., and Shevchenko, A. (2012). Effects of diet and development on the *Drosophila* lipidome. *Mol. Syst. Biol.* 8:600. doi: 10.1038/msb.2012.29

Chandler, J. A., Eisen, J. A., and Kopp, A. (2012). Yeast communities of diverse *Drosophila* species: comparison of two symbiont groups in the same hosts. *Appl. Environ. Microbiol.* 78, 7327–7336. doi: 10.1128/AEM.01741-12

Cho, K. S., Lee, J. H., Kim, S., Kim, D., Koh, H., Lee, J., et al. (2001). *Drosophila* phosphoinositide-dependent kinase-1 regulates apoptosis and growth via the phosphoinositide 3-kinase-dependent signaling pathway. *Proc. Natl. Acad. Sci. U.S.A.* 98, 6144–6149. doi: 10.1073/pnas.101596998

Deshpande, S. A., Carvalho, G. B., Amador, A., Phillips, A. M., Hoxha, S., Lizotte, K. J., et al. (2014). Quantifying *Drosophila* food intake: comparative analysis of current methodology. *Nat. Methods* 11, 535–540. doi: 10.1038/nmeth.2899

Diamond, J. (1991). Evolutionary design of intestinal nutrient absorption: enough but not too much. *Physiology* 6, 92–96. doi: 10.1152/physiologyonline.1991.6.2.92

Dummler, B., Tschopp, O., Hynx, D., Yang, Z.-Z., Dirnhofer, S., and Hemmings, B. A. (2006). Life with a single isoform of Akt: mice lacking Akt2 and Akt3 are viable but display impaired glucose homeostasis and growth deficiencies. *Mol. Cell. Biol.* 26, 8042–8051. doi: 10.1128/MCB.00722-06

Fanson, B. G., Yap, S., and Taylor, P. W. (2012). Geometry of compensatory feeding and water consumption in *Drosophila* melanogaster. *J. Exp. Biol.* 215, 766–773. doi: 10.1242/jeb.066860

Fernandez, R., Tabarini, D., Azpiazu, N., Frasch, M., and Schlessinger, J. (1995). The *Drosophila* insulin receptor homolog: a gene essential for embryonic development encodes two receptor isoforms with different signaling potential. *EMBO J.* 14, 3373–3384. doi: 10.1002/j.1460-2075.1995.tb07343.x

Garofalo, R. S., Orena, S. J., Rafidi, K., Torchia, A. J., Stock, J. L., Hildebrandt, A. L., et al. (2003). Severe diabetes, age-dependent loss of adipose tissue, and mild growth deficiency in mice lacking Akt2/PKB beta. *J. Clin. Invest.* 112, 197–208. doi: 10.1172/JCI16885

Ginsberg, B. H., Brown, T. J., Simon, I., and Spector, A. A. (1981). Effect of the membrane lipid environment on the properties of insulin receptors. *Diabetes* 30, 773–780. doi: 10.2337/diab.30.9.773

Gonzalez, E., and McGraw, T. E. (2009a). The Akt kinases: isoform specificity in metabolism and cancer. *Cell Cycle* 8, 2502–2508. doi: 10.4161/cc.8.16.9335

Gonzalez, E., and McGraw, T. E. (2009b). Insulin-modulated Akt subcellular localization determines Akt isoform-specific signaling. *Proc. Natl. Acad. Sci. U.S.A.* 106, 7004–7009. doi: 10.1073/pnas.0901933106

Grönke, S., Clarke, D.-F., Broughton, S., Andrews, T. D., and Partridge, L. (2010). Molecular evolution and functional characterization of *Drosophila* insulin-like peptides. *PLoS Genet.* 6:e1000857. doi: 10.1371/journal.pgen.1000857

Grootjans, J., Kaser, A., Kaufman, R. J., and Blumberg, R. S. (2016). The unfolded protein response in immunity and inflammation. *Nat. Rev. Immunol.* 16, 469–484. doi: 10.1038/nri.2016.62

Gutmann, T., Kim, K. H., Grzybek, M., Walz, T., and Coskun, Ü. (2018). Visualization of ligand-induced transmembrane signaling in the full-length human insulin receptor. *J. Cell Biol.* 217, 1643–1649. doi: 10.1083/jcb.201711047

Hauke, S., Keutler, K., Phapale, P., Yushchenko, D. A., and Schultz, C. (2018). Endogenous fatty acids are essential signaling factors of pancreatic β-cells and insulin secretion. *Diabetes* 67, 1986–1998. doi: 10.2337/db17-1215

Hoang, D., Kopp, A., and Chandler, J. A. (2015). Interactions between *Drosophila* and its natural yeast symbionts—Is *Saccharomyces cerevisiae* a good model for studying the fly-yeast relationship? *PeerJ* 3:e1116. doi: 10.7717/peerj.1116

Hoffmann, J. A. (2003). The immune response of *Drosophila*. *Nature* 426, 33–38. doi: 10.1038/nature02021

Klose, C., Surma, M. A., Gerl, M. J., Meyenhofer, F., Shevchenko, A., and Simons, K. (2012). Flexibility of a eukaryotic lipidome – insights from yeast lipidomics. *PLoS ONE* 7:e35063. doi: 10.1371/journal.pone.0035063

Löfgren, L., Ståhlman, M., Forsberg, G.-B., Saarinen, S., Nilsson, R., and Hansson, G. I. (2012). The BUME method: a novel automated chloroform-free 96-well total lipid extraction method for blood plasma. *J. Lipid Res.* 53, 1690–1700. doi: 10.1194/jlr.D023036

Manning, B. D., and Toker, A. (2017). AKT/PKB signaling: navigating the network. *Cell.* 169, 381–405. doi: 10.1016/j.cell.2017.04.001

Migrenne, S., Cruciani-Guglielmacci, C., Kang, L., Wang, R., Rouch, C., Lefevre, A.-L., et al. (2006). Fatty acid signaling in the hypothalamus and the neural control of insulin secretion. *Diabetes* 55(Suppl. 2), S139–S144. doi: 10.2337/db06-S017

Mohammad, A., Moheman, A., and El-Desoky, G. (2012). Amino acid and vitamin determinations by TLC/HPTLC: review of the current state. *Cent. Eur. J. Chem.* 10, 731–750. doi: 10.2478/s11532-012-0019-0

Murphy, M. G. (1990). Dietary fatty acids and membrane protein function. *J. Nutr. Biochem.* 1, 68–79. doi: 10.1016/0955-2863(90)90052-M

Nicholson, J. K., Holmes, E., Kinross, J., Burcelin, R., Gibson, G., Jia, W., et al. (2012). Host-gut microbiota metabolic interactions. *Science* 336, 1262–1267. doi: 10.1126/science.1223813

Nolan, C. J., Madiraju, M. S. R., Delghingaro-Augusto, V., Peyot, M.-L., and Prentki, M. (2006). Fatty acid signaling in the -cell and insulin secretion. *Diabetes* 55(Suppl. 2), S16–S23. doi: 10.2337/db06-S003

Oh, D. Y., Talukdar, S., Bae, E. J., Imamura, T., Morinaga, H., Fan, W., et al. (2010). GPR120 is an omega-3 fatty acid receptor mediating potent anti-inflammatory and insulin-sensitizing effects. *Cell* 142, 687–698. doi: 10.1016/j.cell.2010.07.041

Petavy, G., David, J. R., Gibert, P., and Moreteau, B. (2001). Viability and rate of development at different temperatures in *Drosophila*: a comparison of constant and alternating thermal regimes. *J. Therm. Biol.* 26, 29–39. doi: 10.1016/S0306-4565(00)00022-X

Pourrajab, F., Yazdi, M. B., Zarch, M. B., Zarch, M. B., and Hekmatimoghaddam, S. (2015). Cross talk of the first-line defense TLRs with PI3K/Akt pathway, in preconditioning therapeutic approach. *Mol Cell Ther* 3:4. doi: 10.1186/s40591-015-0041-7

Preibisch, S., Saalfeld, S., and Tomancak, P. (2009). Globally optimal stitching of tiled 3D microscopic image acquisitions. *Bioinformatics* 25, 1463–1465. doi: 10.1093/bioinformatics/btp184

Puig, O. (2003). Control of cell number by *Drosophila* FOXO: downstream and feedback regulation of the insulin receptor pathway. *Genes Dev.* 17, 2006–2020. doi: 10.1101/gad.1098703

Ridley, E. V., Wong, A. C.-N., Westmiller, S., and Douglas, A. E. (2012). Impact of the resident microbiota on the nutritional phenotype of *Drosophila* melanogaster. *PLoS ONE* 7:e36765. doi: 10.1371/journal.pone.0036765

Santi, S. A., and Lee, H. (2010). The Akt isoforms are present at distinct subcellular locations. *Am. J. Physiol. Cell Physiol.* 298, C580–C591. doi: 10.1152/ajpcell.00375.2009

Sarbassov, D. D., Guertin, D. A., Ali, S. M., and Sabatini, D. M. (2005). Phosphorylation and regulation of Akt/PKB by the rictor-mTOR complex. *Science* 307, 1098–1101. doi: 10.1126/science.1106148

Scanga, S. E., Ruel, L., Binari, R. C., Snow, B., Stambolic, V., Bouchard, D., et al. (2000). The conserved PI3'K/PTEN/Akt signaling pathway regulates both cell size and survival in *Drosophila*. *Oncogene* 19, 3971–3977. doi: 10.1038/sj.onc.1203739

Scheid, M. P., Marignani, P. A., and Woodgett, J. R. (2002). Multiple phosphoinositide 3-kinase-dependent steps in activation of protein kinase B. *Mol. Cell. Biol.* 22, 6247–6260. doi: 10.1128/MCB.22.17.6247-6260.2002

Schindelin, J., Arganda-Carreras, I., Frise, E., Kaynig, V., Longair, M., Pietzsch, T., et al. (2012). Fiji: an open-source platform for biological-image analysis. *Nat. Methods* 9, 676–682. doi: 10.1038/nmeth.2019

Shin, S. C., Kim, S.-H., You, H., Kim, B., Kim, A. C., Lee, K.-A., et al. (2011). *Drosophila* microbiome modulates host developmental and metabolic homeostasis via insulin signaling. *Science* 334, 670–674. doi: 10.1126/science.1212782

Slack, C., Alic, N., Foley, A., Cabecinha, M., Hoddinott, M. P., and Partridge, L. (2015). The Ras-Erk-ETS-signaling pathway is a drug target for longevity. *Cell* 162, 72–83. doi: 10.1016/j.cell.2015.06.023

Storelli, G., Defaye, A., Erkosar, B., Hols, P., Royet, J., and Leulier, F. (2011). *Lactobacillus plantarum* promotes *Drosophila* systemic growth by modulating hormonal signals through TOR-dependent nutrient sensing. *Cell Metab.* 14, 403–414. doi: 10.1016/j.cmet.2011.07.012

Tsuji, M., Tsujimoto, M., and Imura, S. (2017). *Cystobasidium tubakii* and *Cystobasidium ongulense*, new basidiomycetous yeast species isolated from East Ongul Island, East Antarctica. *Mycoscience* 58, 103–110. doi: 10.1016/j.myc.2016.11.002

Vyas, S., and Chhabra, M. (2017). Isolation, identification and characterization of *Cystobasidium oligophagum* JRC1: a cellulase and lipase producing oleaginous yeast. *Bioresour. Technol.* 223, 250–258. doi: 10.1016/j.biortech.2016.10.039

Watson, K. (1987). "Temperature relations," in *The Yeasts*, eds A. H. Rose and J. S. Harrison (London: Academic Press). 41–71.

Weichhart, T., and Saemann, M. D. (2008). The PI3K/Akt/mTOR pathway in innate immune cells: emerging therapeutic applications. *Ann. Rheum. Dis.* 67(Suppl. 3), iii70–iii74. doi: 10.1136/ard.2008.098459

Xu, X., Gopalacharyulu, P., Seppänen-Laakso, T., Ruskeepää, A.-L., Aye, C. C., Carson, B. P., et al. (2012). Insulin signaling regulates fatty acid catabolism at the level of CoA Activation. *PLoS Genet.* 8:e1002478. doi: 10.1371/journal.pgen.1002478

Zhang, H., Liu, J., Li, C. R., Momen, B., Kohanski, R. A., and Pick, L. (2009). Deletion of *Drosophila* insulin-like peptides causes growth defects and metabolic abnormalities. *Proc. Natl. Acad. Sci. U.S.A.* 106, 19617–19622. doi: 10.1073/pnas.0905083106

Conflict of Interest: The authors declare that the research was conducted in the absence of any commercial or financial relationships that could be construed as a potential conflict of interest.

Advantages of publishing in Frontiers

OPEN ACCESS
Articles are free to read for greatest visibility and readership

FAST PUBLICATION
Around 90 days from submission to decision

HIGH QUALITY PEER-REVIEW
Rigorous, collaborative, and constructive peer-review

TRANSPARENT PEER-REVIEW
Editors and reviewers acknowledged by name on published articles

Frontiers
Avenue du Tribunal-Fédéral 34
1005 Lausanne | Switzerland

Visit us: www.frontiersin.org
Contact us: info@frontiersin.org | +41 21 510 17 00

REPRODUCIBILITY OF RESEARCH
Support open data and methods to enhance research reproducibility

DIGITAL PUBLISHING
Articles designed for optimal readership across devices

FOLLOW US
@frontiersin

IMPACT METRICS
Advanced article metrics track visibility across digital media

EXTENSIVE PROMOTION
Marketing and promotion of impactful research

LOOP RESEARCH NETWORK
Our network increases your article's readership